NASA TECHNICAL MEMORANDUM

NASA TM X-3234

LONGITUDINAL AERODYNAMIC CHARACTERISTICS OF A DEFLECTED-THRUST PROPULSIVE-LIFT TRANSPORT MODEL

Danny R. Hoad

Langley Directorate
U.S. Army Air Mobility R&D Laboratory
Hampton, Va. 23665

NATIONAL AERONAUTICS AND SPACE ADMINISTRATION • WASHINGTON, D. C. • NOVEMBER 1975

1. Report No.	2. Government Accession No.	3. Recipient's Catalog No.
NASA TM X-3234		

4. Title and Subtitle	5. Report Date
LONGITUDINAL AERODYNAMIC CHARACTERISTICS OF A DEFLECTED-THRUST PROPULSIVE-LIFT TRANSPORT MODEL	November 1975
	6. Performing Organization Code

7. Author(s)	8. Performing Organization Report No.
Danny R. Hoad, Langley Directorate, U.S. Army Air Mobility R&D Laboratory	L-10106
	10. Work Unit No.
9. Performing Organization Name and Address	505-10-41-03
NASA Langley Research Center Hampton, Va. 23665	11. Contract or Grant No.
	13. Type of Report and Period Covered
12. Sponsoring Agency Name and Address	Technical Memorandum
National Aeronautics and Space Administration Washington, D.C. 20546	14. Sponsoring Agency Code

15. Supplementary Notes

16. Abstract

A wind-tunnel investigation has been conducted to determine the effect of deflecting the engine exit of a four-engine double-slotted flap transport to provide STOL performance. Longitudinal aerodynamic data were obtained at various engine exit positions and deflections. The data were obtained at three flap deflections representing cruise, take-off, and landing conditions for a range of angles of attack and various thrust coefficients. Downwash angles at the location of the horizontal tail were measured. The data are presented without analysis or discussion.

17. Key Words (Suggested by Author(s))	18. Distribution Statement
STOL Propulsive lift Deflected thrust Transport	Unclassified – Unlimited Subject Category 02

19. Security Classif. (of this report)	20. Security Classif. (of this page)	21. No. of Pages	22. Price*
Unclassified	Unclassified	184	$7.00

*For sale by the National Technical Information Service, Springfield, Virginia 22161

LONGITUDINAL AERODYNAMIC CHARACTERISTICS OF A DEFLECTED-THRUST PROPULSIVE-LIFT TRANSPORT MODEL

Danny R. Hoad
Langley Directorate, U.S. Army Air Mobility R&D Laboratory

SUMMARY

A wind-tunnel investigation has been conducted to determine the effect of deflecting the engine exit of a four-engine double-slotted flap transport to provide STOL performance. Longitudinal aerodynamic data were obtained at various engine exit positions and deflections. The data were obtained at three flap deflections representing cruise, take-off, and landing conditions for a range of angles of attack and various thrust coefficients. Downwash angles at the location of the horizontal tail were measured. The data are presented without analysis or discussion.

INTRODUCTION

Many concepts have been considered to provide propulsive lift for jet-powered transport aircraft. These concepts include externally blown flap, upper surface blown flap, internally blown flap, augmentor wing, and deflected thrust. (See refs. 1 to 6.) A comparison of several of these concepts, investigated on a geometrically similar model, is presented in reference 7. One of the concepts compared was a configuration utilizing deflected thrust coupled with mechanical flaps. The present paper presents the results of an investigation conducted to determine the longitudinal aerodynamic characteristics of a deflected-thrust concept with double-slotted flaps.

The model used in this investigation was one of those used in reference 7 and was built by the National Aeronautics and Space Administration. It was a four-engine short take-off and landing (STOL) transport whose engine configurations were designed to simulate three specific chordwise engine exit positions and various exit deflection angles. At each engine exit position, up to five different deflection angles were available. The engine deflectors were built by the U.S. Air Force Flight Dynamics Laboratory.

The investigation was conducted in the Langley V/STOL tunnel. Tests were conducted with three flap deflections and various engine exit deflection angles, corresponding to cruise, take-off, and landing configurations. Each configuration was tested through an

angle-of-attack range for several different values of engine thrust coefficients. Force and moment data were recorded at each angle of attack and downwash was measured for several configurations. These data are presented without analysis. No lateral-directional data are presented.

SYMBOLS

The longitudinal aerodynamic data in this report are referred to the stability axes. (See fig. 1.) The origin of the axes was located on the fuselage center line longitudinally at 0.40 mean geometric chord and vertically at the center line of the engines.

The units for the physical quantities defined in this paper are given in the International System of Units (SI) and the U.S. Customary Units. Equivalent dimensions were determined by using the conversion factors given in reference 8.

b wing span, m (ft)

c local wing chord, m (ft)

$\bar{c}$ mean geometric chord, m (ft)

C_D drag coefficient, $\frac{\text{Drag}}{q_\infty S}$

C_L lift coefficient, $\frac{\text{Lift}}{q_\infty S}$

C_m pitching-moment coefficient, $\frac{\text{Pitching moment}}{q_\infty S\bar{c}}$

C_μ thrust coefficient, $\frac{\text{Thrust}}{q_\infty S}$

i_t horizontal-tail incidence angle (positive, trailing edge down), deg

q_∞ free-stream dynamic pressure, N/m^2 (lb/ft^2)

S wing area, m^2 (ft^2)

T thrust, N (lbf)

X, Z body reference axes (see fig. 1)

α angle of attack, deg

δ_f wing trailing-edge flap deflection (positive when deflected down), deg

δ_j engine exit deflection angle (positive when deflected down), deg

$\delta_{j,T}$ jet-exhaust deflection angle (positive when deflected down), $\tan^{-1} \frac{\text{Normal force}}{\text{Axial force}}$, deg

ϵ downwash angle at horizontal tail (positive down from horizontal), deg

MODEL AND APPARATUS

A three-view drawing of the model with dimensional characteristics is presented in figure 2. This model was identical to the model used in reference 2 and was very similar to the models used in reference 4. Photographs of the model are presented in figure 3.

The model had a 9.3-percent-thick supercritical airfoil wing with a nominal 30° quarter-chord sweep. The 20-percent-chord wing-leading-edge slat extended from the fuselage to the wing tip with a deflection of 50°. The span of the leading-edge slats was broken only to allow space for the engine pylons. The 35-percent-wing-chord double-slotted flap system extended from the fuselage to the 70.8-percent semispan station. The flap elements were deflected to 35° and 65° from the flap chord zero position for the various tests. The flap chord zero position is deflected -1.6° relative to the wing reference chord. Flap, vane, and leading-edge slat details are shown schematically in figure 4.

The horizontal tail had a 11.0-percent-thick symmetrical supercritical airfoil with an incidence range of $\pm 20^\circ$ in 5° increments. It had a 15-percent-chord leading-edge slat set at -40°.

The cruise configuration was defined as the model with 0° flaps, no wing-leading-edge slats, and no horizontal-tail leading-edge slats. The take-off configuration was defined as the model with the double-slotted flap system set at 35°, wing-leading-edge slat deployed at 50°, and horizontal-tail leading-edge slat deployed at -40°. The landing configuration was defined as the model with the flap system set at 65°, wing-leading-edge slat deployed at 50°, and horizontal-tail leading-edge slat deployed at -40°.

Four air-powered ejector engine simulators were used to represent each fan-jet propulsion system. Each engine simulator was a two-part ejector with individual air-supply lines and control valves designed to provide efflux of the fan and gas-generator stages similar to that shown in figure 5(a). To simplify calibration and tunnel testing, it was decided to use only the fan stage ejector to provide the engine exhaust. Each ejector

was fitted with a series of cowl assemblies to provide a desired engine exit location and deflection. The "basic engine" cowl assembly (fig. 5(b)) was designed so that the fan-exit location was at the -13 percent chord for the inboard engines and the -17 percent chord for the outboard engines. (Negative values denote positions forward of the leading edge.) The exit was not deflected from the horizontal for the basic engine. The other cowl assemblies are presented in figure 5, and the nomenclature for each is presented in the following table:

Cowl assembly		Nomenclature	Figure
Exit location, percent c	δ_j, deg		
10	45	10-45	5(c)
10	90	10-90	5(d)
75	0	75-0	5(e)
75	25	75-25	5(f)
75	45	75-45	5(g)
75	65	75-65	5(h)
75	90	75-90	5(i)
110	25	110-25	5(j)
110	45	110-45	5(k)
110	65	110-65	5(l)
110	90	110-90	5(m)

For some of the tests a flat plug was placed in the engine inlets to determine the effect caused by flow through the nacelle and deflected at the engine exit for power-off conditions.

For most of the tests, a rake (figs. 3 and 6) was fastened to the sting. The rake consisted of seven yaw-pitch probes calibrated to determine the flow direction at each probe tip. The rake was offset from the fuselage in the vicinity of the horizontal tail so that the downwash angle could be determined. (See fig. 6.) Most of the rake data were taken with the horizontal and vertical tail removed; however, one series of tests was made with the vertical tail in place.

The model was mounted in the Langley V/STOL tunnel on a sting-supported six-component strain-gage balance for measurements of the total forces and moments.

TESTS AND CORRECTIONS

This investigation was conducted in the Langley V/STOL tunnel at a free-stream dynamic pressure of 574 Pa (12 lb/ft^2). The Reynolds number (based on wing mean aerodynamic chord $\bar{c}$ and free-stream velocity) was approximately 0.579×10^6. The data presented in this report have been corrected for wind-tunnel wall effects by using the method described in reference 9.

Calibrations were made to determine the thrust, inlet mass-flow rate, and primary mass-flow rate of the fan stage of each engine cowl assembly separately as a function of its plenum pressure. These data were run at zero airspeed and reflect the static thrust only. The values of thrust coefficient are based on this static-thrust calibration and are presented as the conventional thrust coefficient, that is, static thrust nondimensionalized by the product of free-stream dynamic pressure and wing area $\left(C_\mu = \frac{T}{q_\infty S}\right)$.

Jet-deflection angles $\delta_{j,T}$ and static-thrust recovery efficiency were determined from measurements of the normal and axial forces made in the static-thrust condition with flaps deflected and leading-edge slat deployed. The engine simulator assemblies using engine exit deflectors to turn the flow achieved jet-deflection angles equal to their respective deflector angles. The flap static turning effectiveness parameters for those engine simulator assemblies which used the flap system to turn the engine flow simulating an externally blown flap configuration are presented.

The various engine deflections and model configurations tested were chosen to represent a cruise, take-off, and landing configuration. The cruise configuration was tested only with the basic engine. The engine simulators tested with each configuration were as follows:

Engine simulator assembly for –	
Take-off configuration	Landing configuration
Basic engine	Basic engine
10-45 engine	10-45 engine
75-0 engine	10-90 engine
75-25 engine	75-0 engine
75-45 engine	75-45 engine
110-25 engine	75-65 engine
110-45 engine	75-90 engine
	110-45 engine
	110-65 engine
	110-90 engine

The seven-probe yaw-pitch rake measured the downwash angle at the horizontal tail. The accuracy of each probe is $\pm 1^{o}$ in flow angle. The data presented were machine faired. A more liberal fairing could be applied to these data by considering the degree of accuracy. Wall corrections were not applied to the probe data for correction to the local angle of attack of the tail. Calculations indicate that the maximum local angle-of-attack change is 1^{o} when the method described in reference 10 is used. A sample of the downwash angles for one configuration $(75\text{-}0,\ C_{\mu} = 0)$ and engine inlets closed and open is presented. Since the differences are slight, and the other configurations with power off are typical, only the one figure is presented.

PRESENTATION OF RESULTS

Results of the present investigation are presented in the following figures without analysis or discussion:

Langley Research Center
National Aeronautics and Space Administration
Hampton, Va. 23665

August 1, 1975

REFERENCES

1. Hoad, Danny R.: Longitudinal Aerodynamic Characteristics of an Externally Blown Flap Powered-Lift Model With Several Propulsive System Simulators. NASA TN D-7670, 1974.

2. Johnson, William G., Jr.: Aerodynamic Characteristics of a Powered, Externally Blown Flap STOL Transport Model With Two Engine Simulator Sizes. NASA TN D-8057, 1975.

3. Phelps, Arthur E., III; and Smith, Charles C., Jr.: Wind-Tunnel Investigation of an Upper Surface Blown Jet-Flap Powered-Lift Configuration. NASA TN D-7399, 1973.

4. Sleeman, William C., Jr.; and Hohlweg, William C.: Low-Speed Wind-Tunnel Investigation of a Four-Engine Upper Surface Blown Model Having a Swept Wing and Rectangular and D-Shaped Exhaust Nozzles. NASA TN D-8061, 1975.

5. Koenig, David G.; Corsiglia, Victor R.; and Morelli, Joseph P.: Aerodynamic Characteristics of a Large-Scale Model With an Unswept Wing and Augmented Jet Flap. NASA TN D-4610, 1968.

6. Henderson, Robert L.: Low-Speed Wind-Tunnel Investigation of a Semispan STOL Jet Transport Wing With Deflected Thrust and Blowing Boundary-Layer Control. NASA TN D-6256, 1971.

7. STOL Technology. NASA SP-320, 1972.

8. Mechtly, E. A.: The International System of Units – Physical Constants and Conversion Factors (Second Revision). NASA SP-7012, 1973.

9. Heyson, Harry H.: Linearized Theory of Wind-Tunnel Jet-Boundary Corrections and Ground Effect for VTOL-STOL Aircraft. NASA TR R-124, 1962.

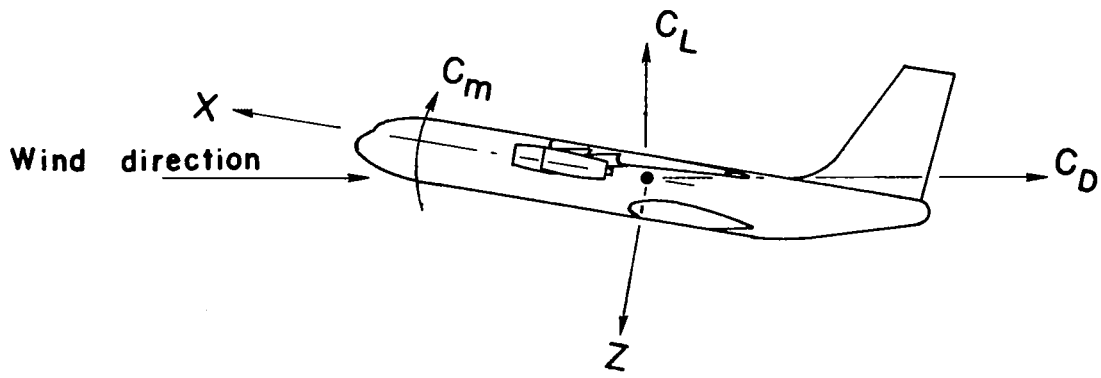

Figure 1.- Axis system used in presentation of data. Arrows indicate positive direction of forces and moments.

Wing:

Airfoil section: 9.3% thick supercritical	
Area, sq m (sq ft)	.483 (5.202)
Mean geometric chord, m (ft)	.290 (.950)
Span, m (ft)	1.902 (6.240)
Aspect ratio	7.48

Horizontal tail:

Airfoil section: 11.0% thick supercritical	
Area, sq m (sq ft)	.156 (1.682)
Mean geometric chord, m (ft)	.213 (.699)
Span, m (ft)	.796 (2.613)
Aspect ratio	4.06

Vertical tail:

Airfoil section: 11.0% thick supercritical	
Area, sq m (sq ft)	.138 (1.488)
Mean geometric chord, m (ft)	.294 (.964)
Span, m (ft)	.488 (1.600)

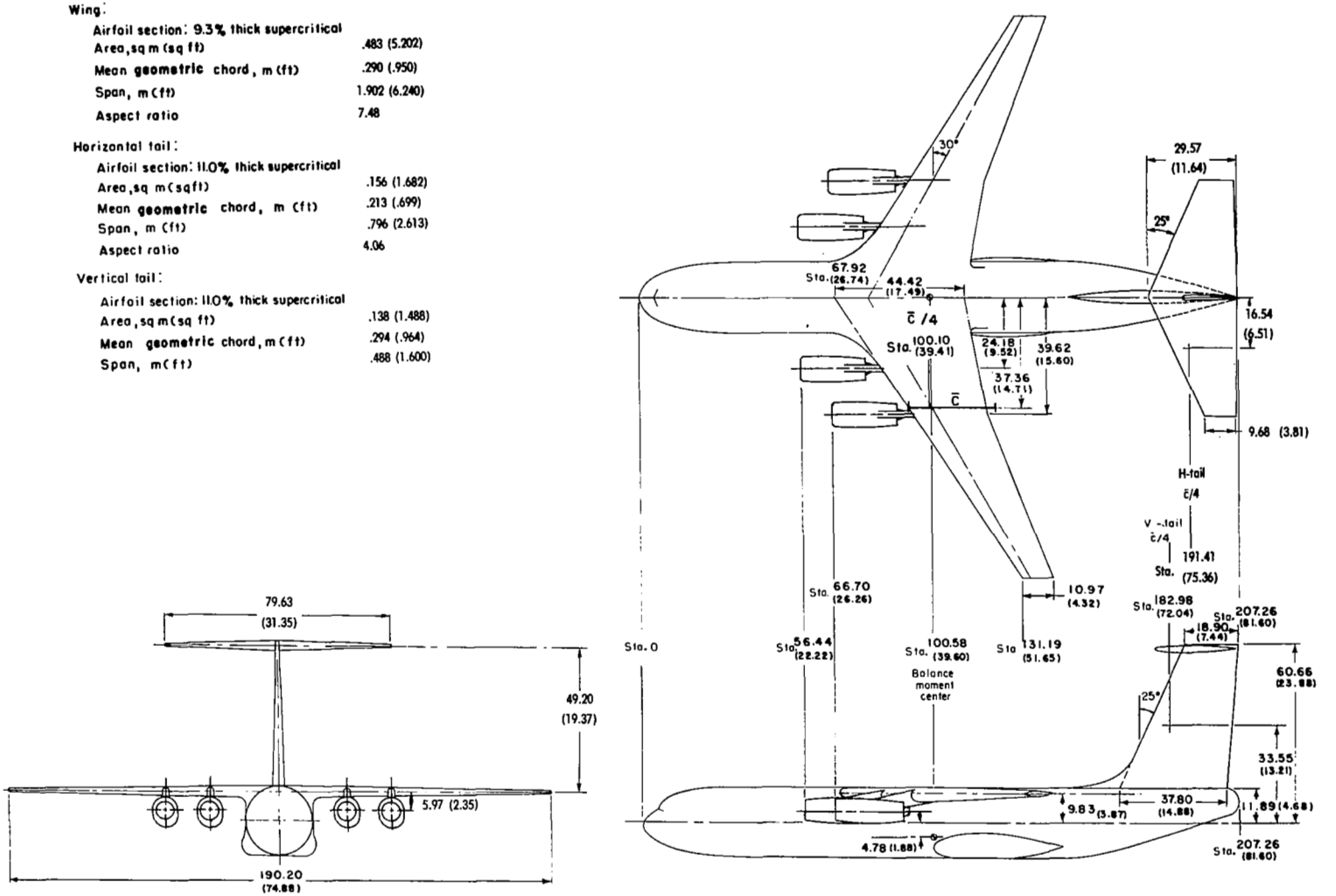

Figure 2.- Dimensions and characteristics of the model. Dimensions are in centimeters (in.) unless otherwise noted.

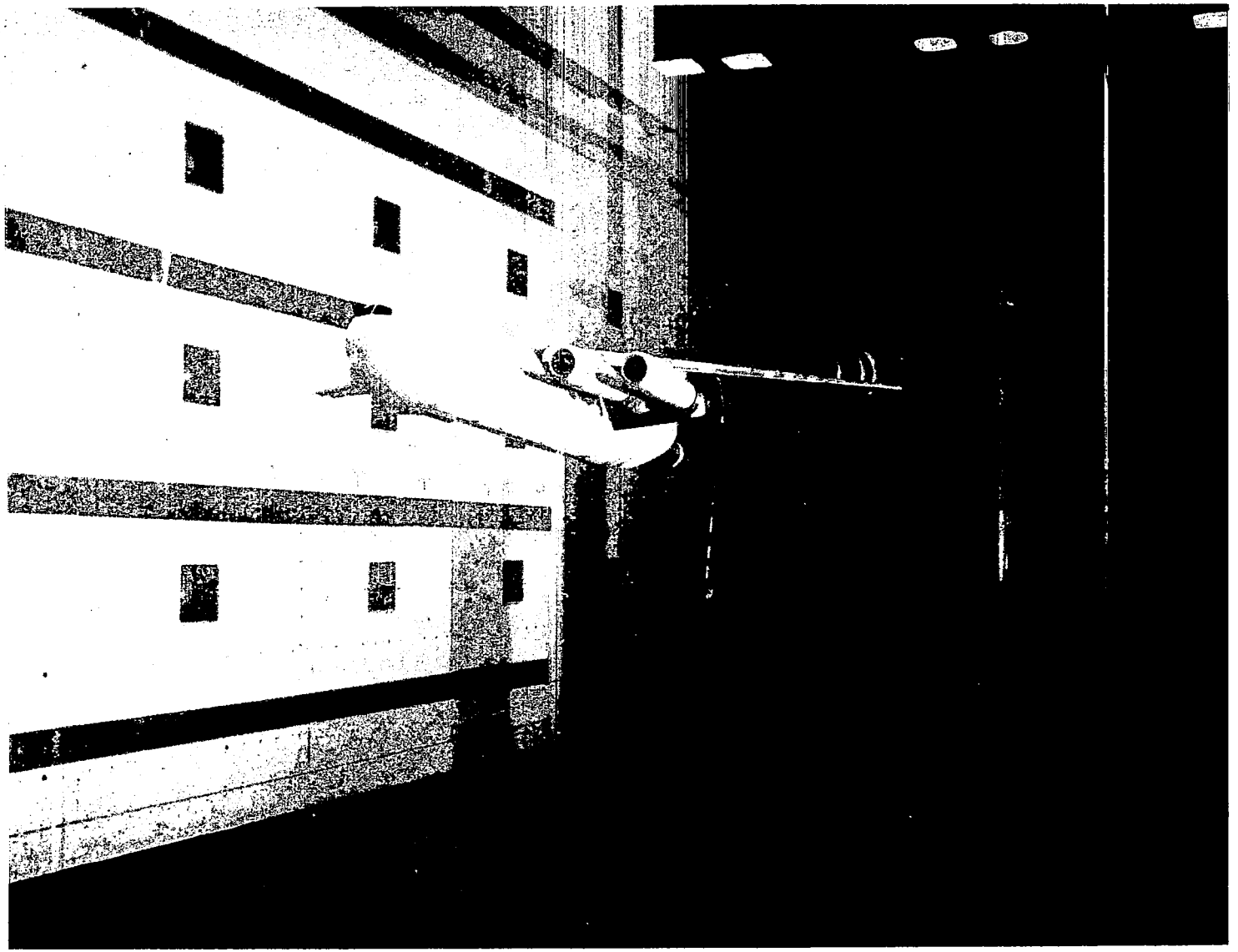

L-72-5502

(a) Front view of model with 75-65 engine and yaw-pitch rake installed.

Figure 3.- Model installed in Langley V/STOL tunnel.

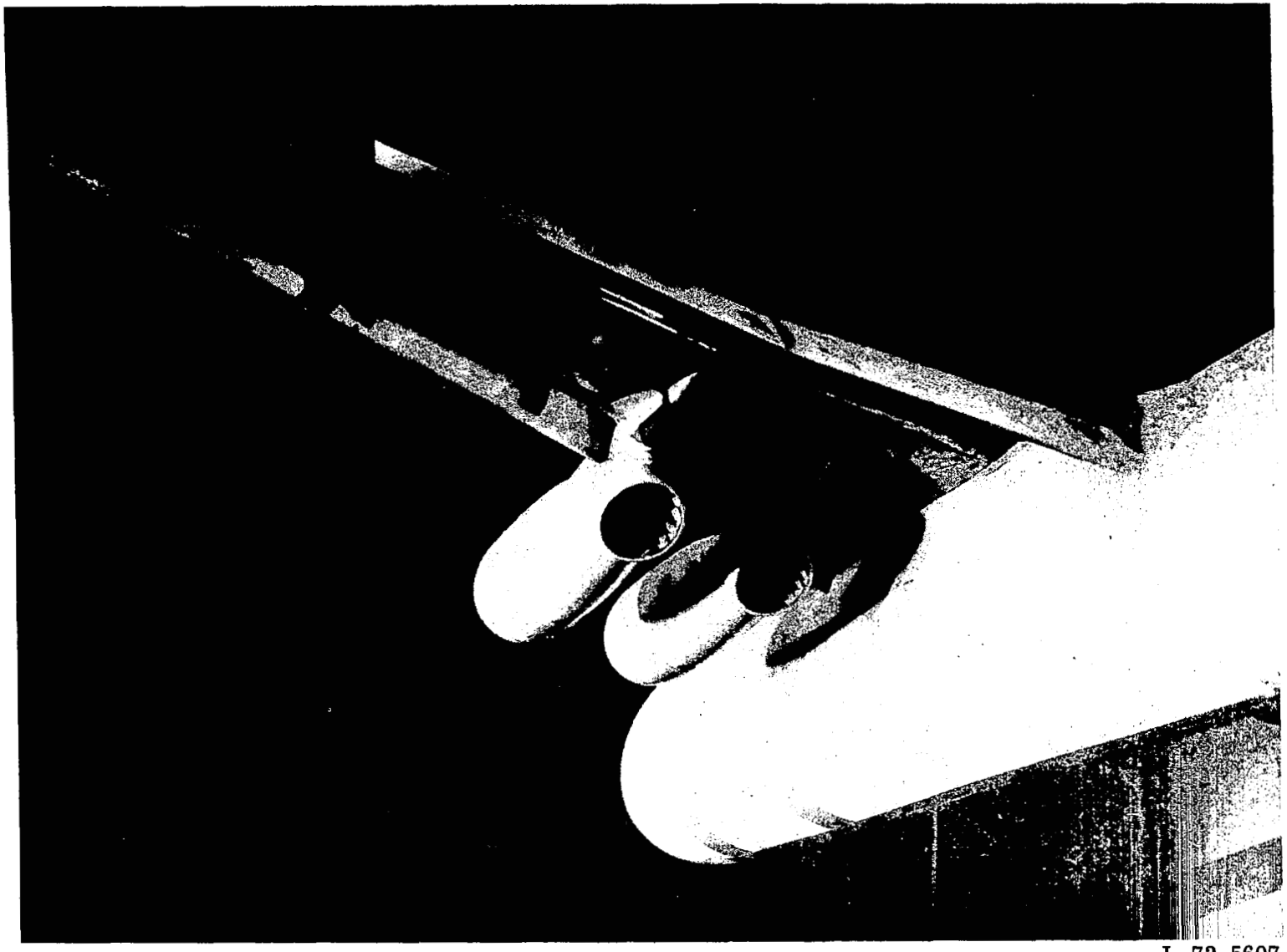

L-72-5607

(b) Rear view of model showing details of 10-45 engines and flap system.

Figure 3.- Concluded.

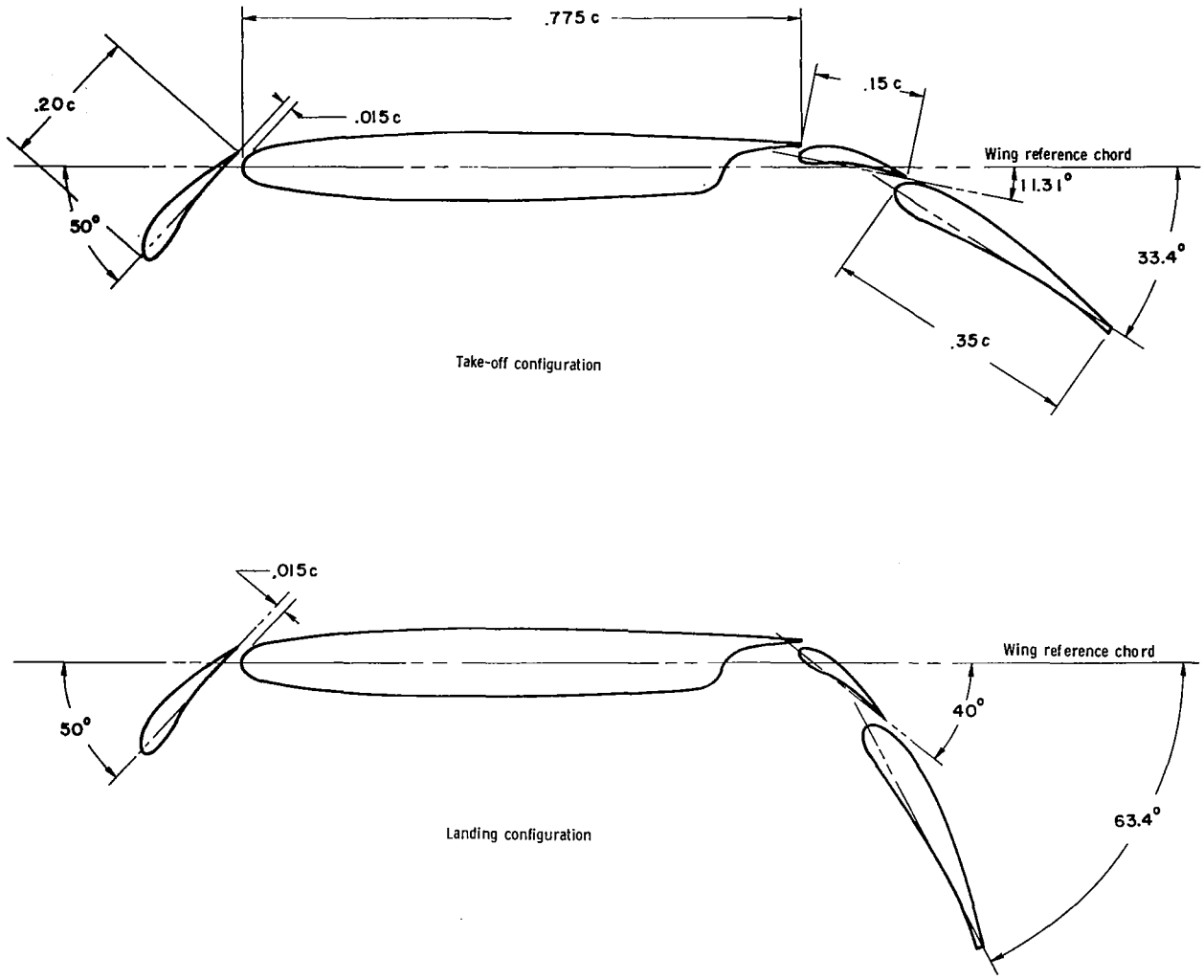

Figure 4.- Wing details in take-off and landing configuration. Dimensions are given in fraction of local chord.

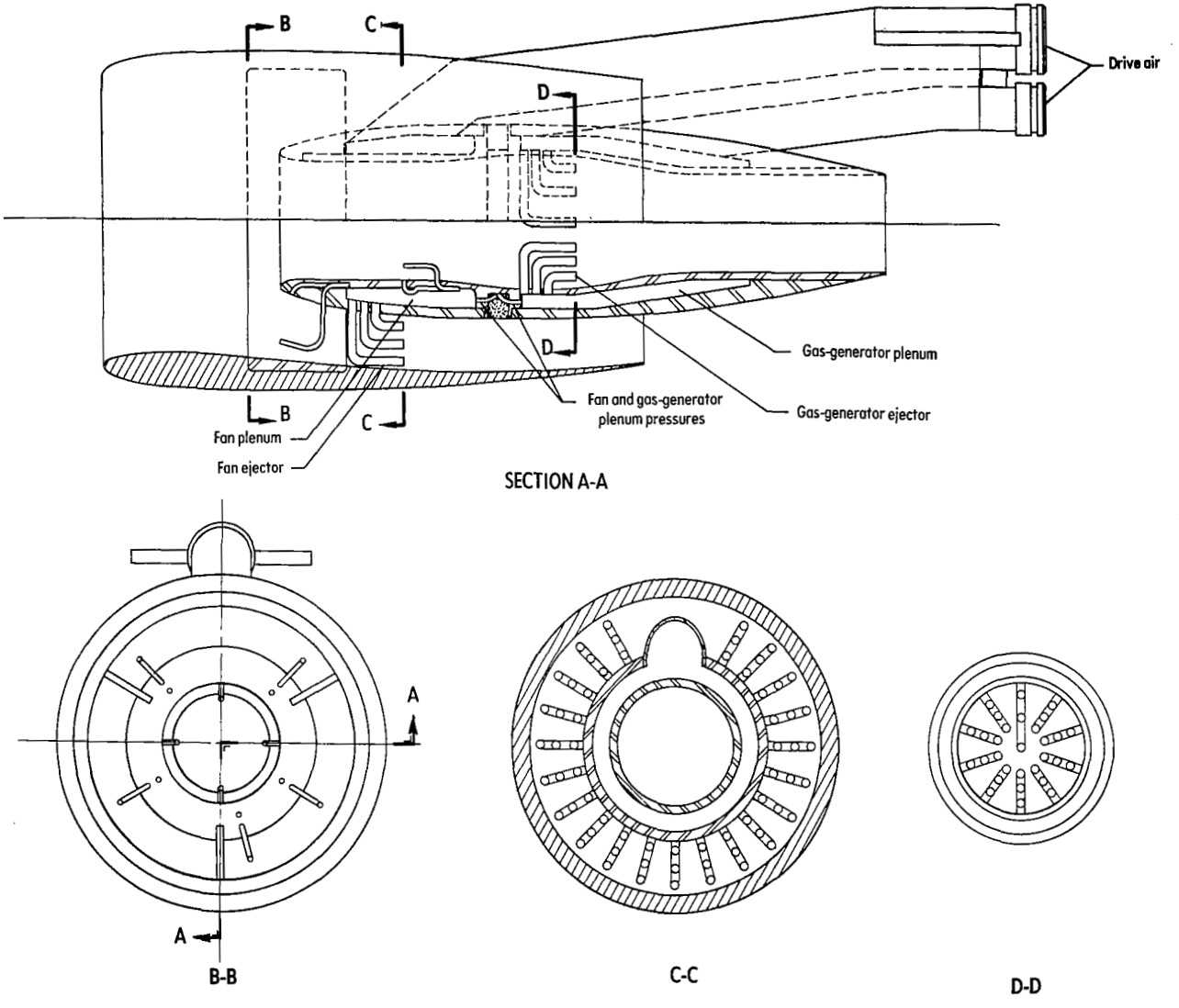

(a) Ejector details.

Figure 5.- Details of engine simulators installed in outboard position on model. Dimensions are in centimeters (in.).

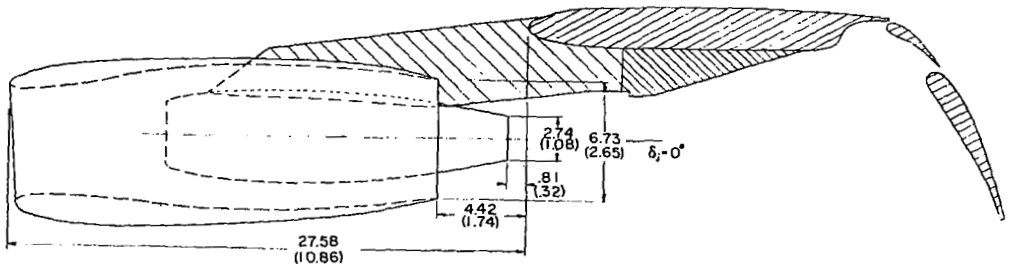

(b) Basic engine.

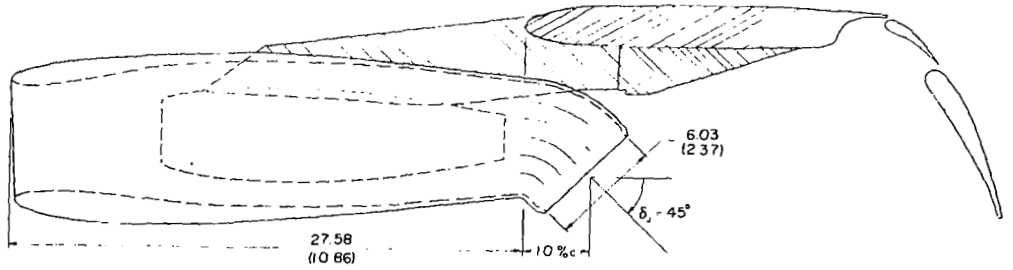

(c) 10-45 engine.

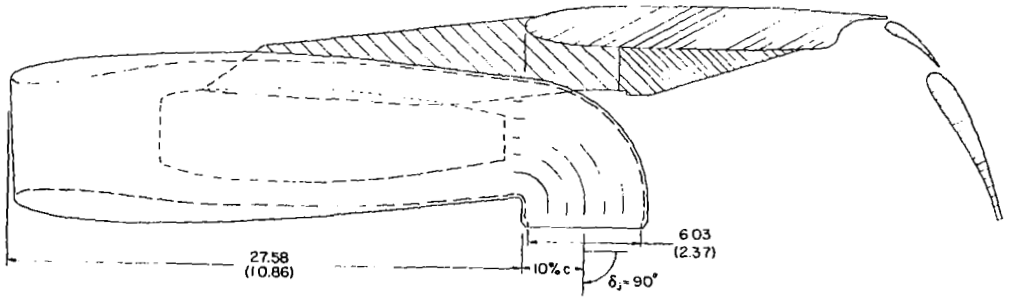

(d) 10-90 engine.

Figure 5.- Continued.

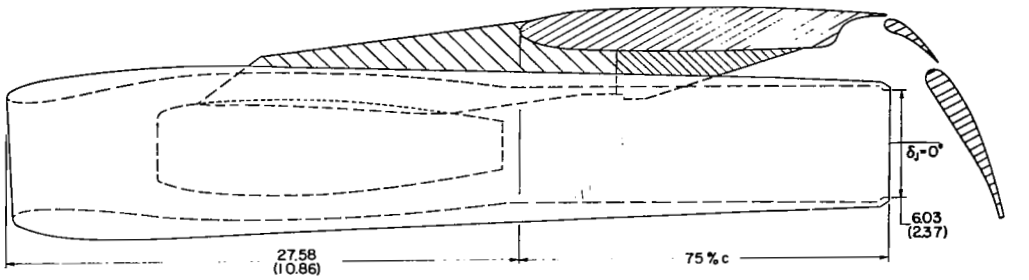

(e) 75-0 engine.

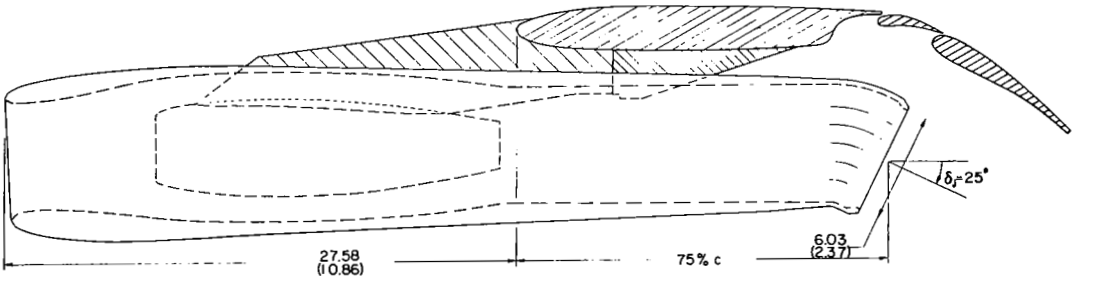

(f) 75-25 engine.

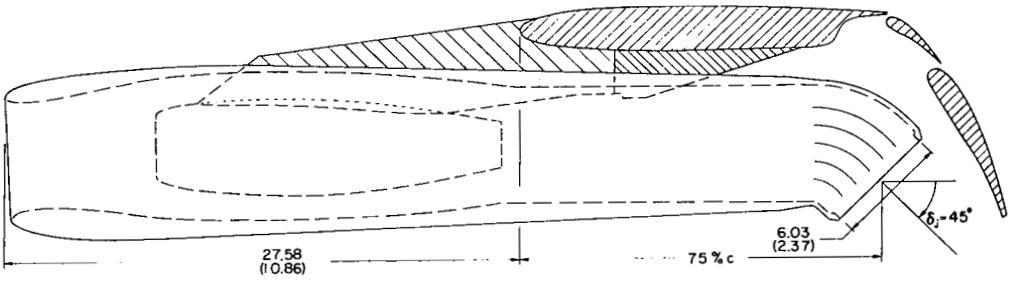

(g) 75-45 engine.

Figure 5.- Continued.

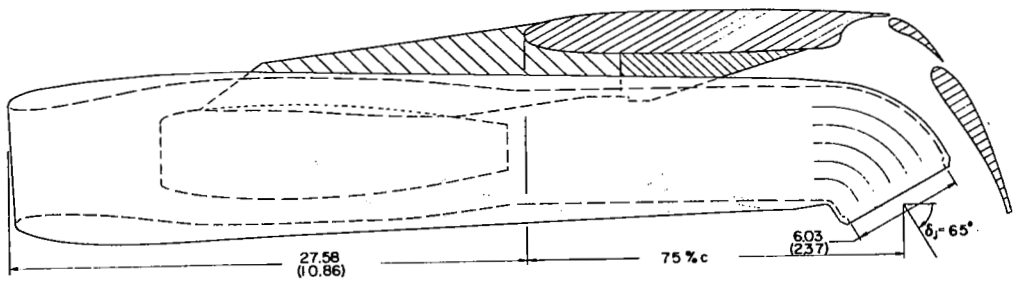

(h) 75-65 engine.

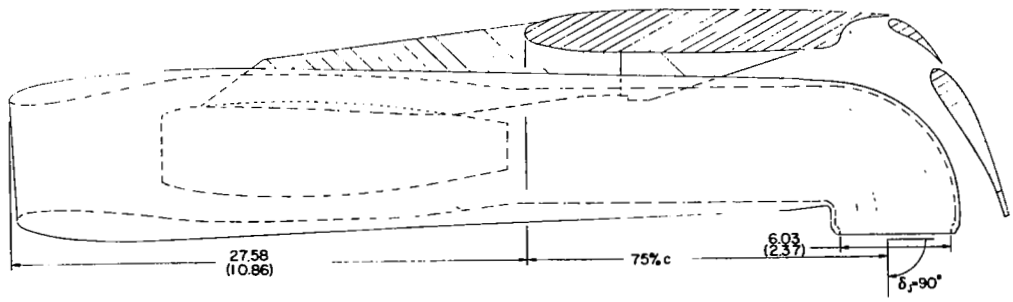

(i) 75-90 engine.

Figure 5.- Continued.

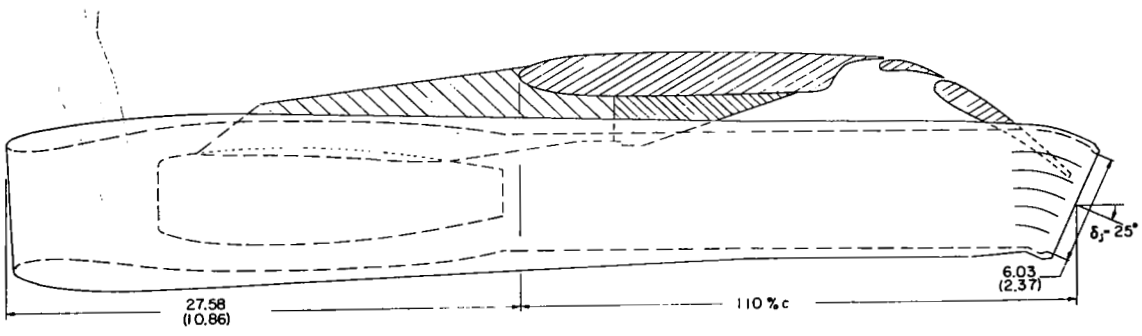

(j) 110-25 engine.

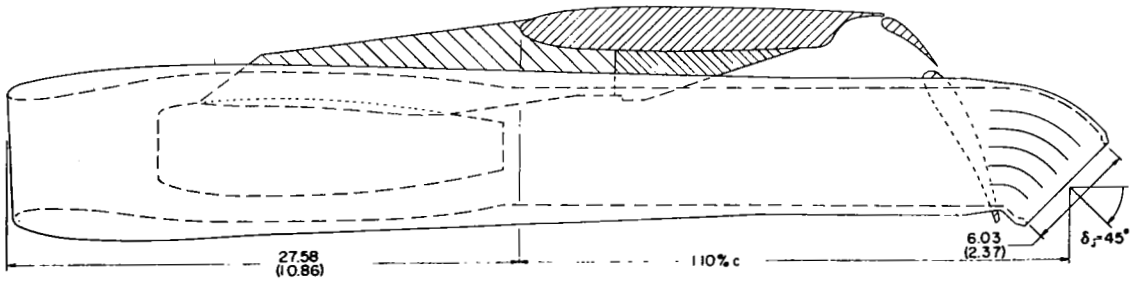

(k) 110-45 engine.

Figure 5.- Continued.

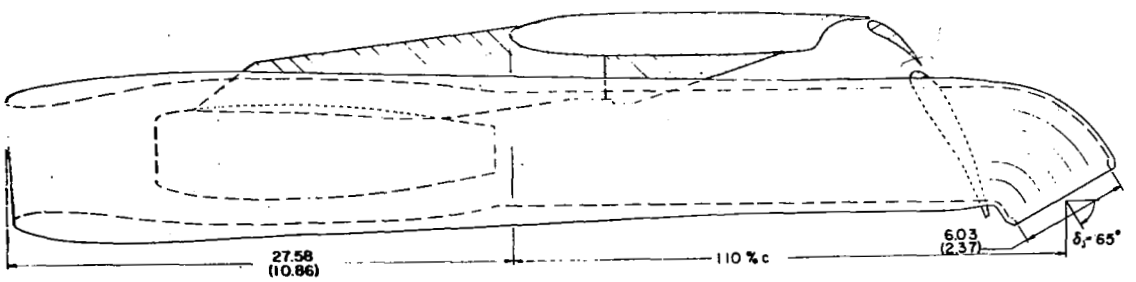

(l) 110-65 engine.

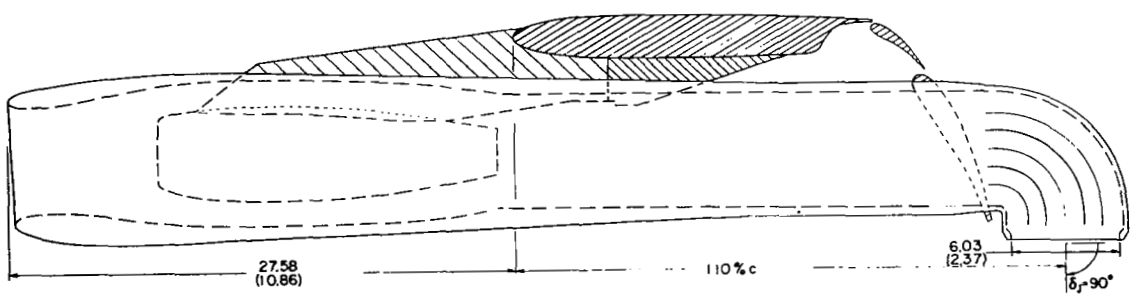

(m) 110-90 engine.

Figure 5.- Concluded.

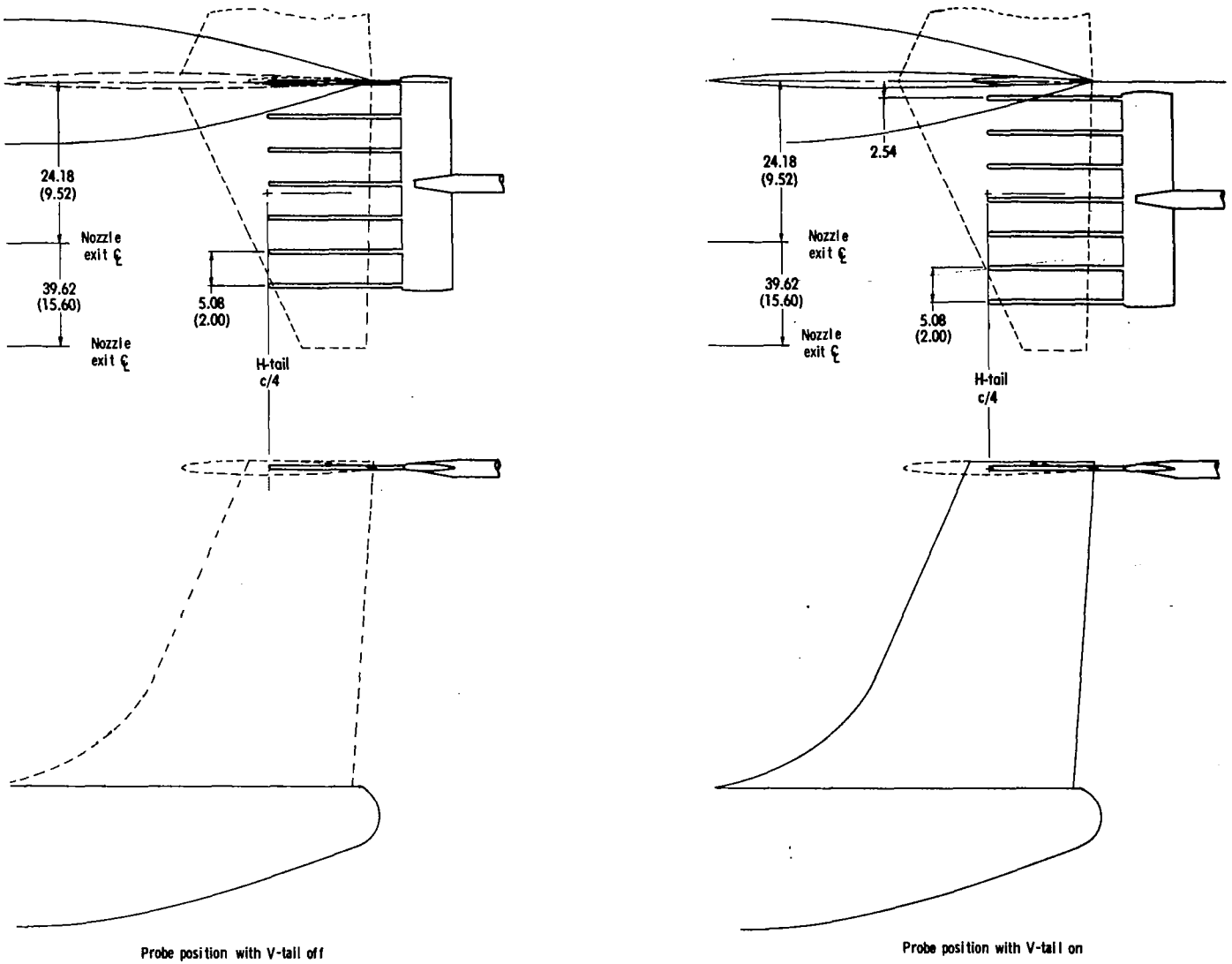

Figure 6.- Details of yaw-pitch rake position. Dimensions are in centimeters (in.).

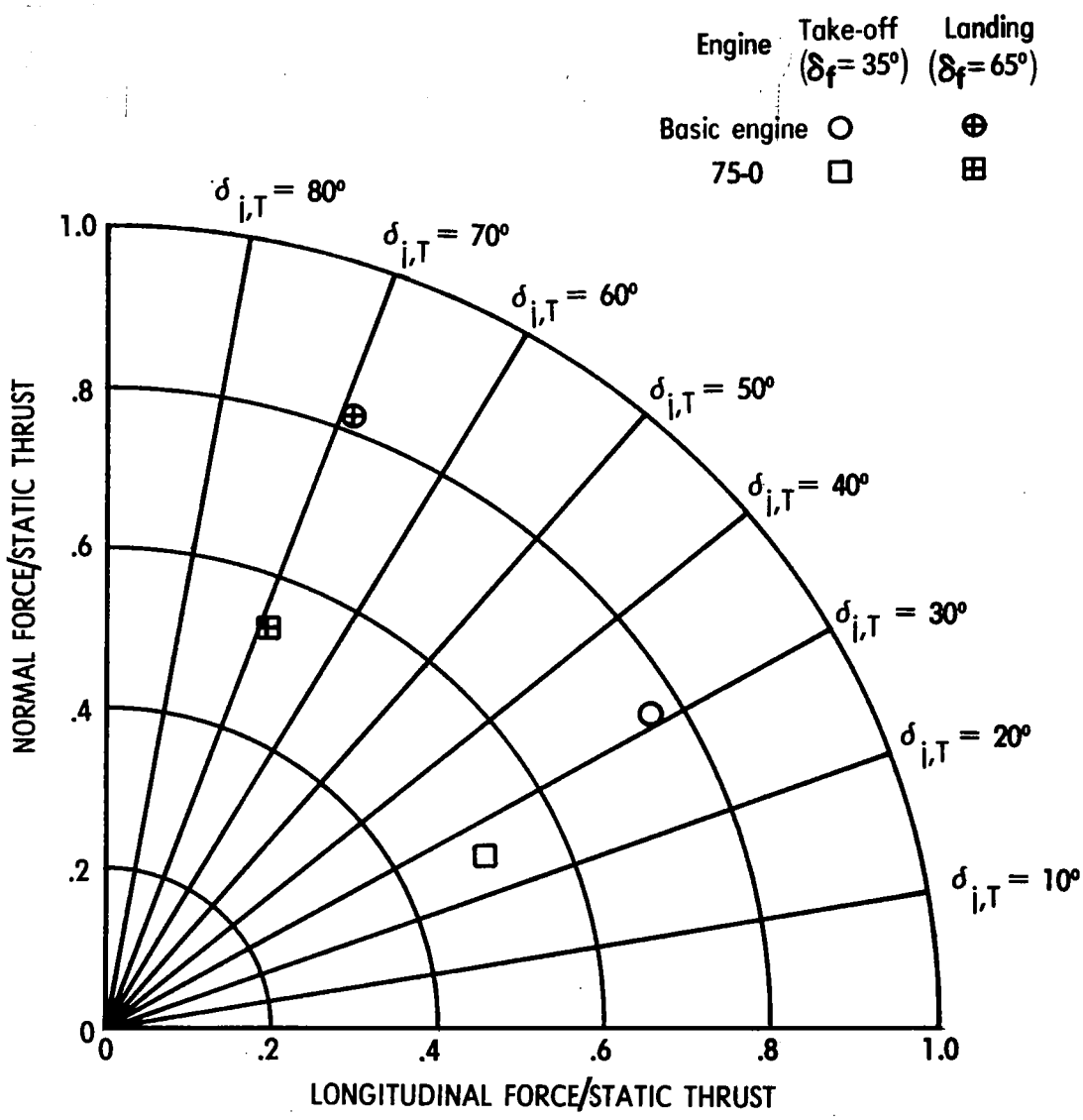

Figure 7.- Flap static turning effectiveness for externally blown flap configurations. Tail off; $q_\infty = 0$, T = 832 N (187 lb).

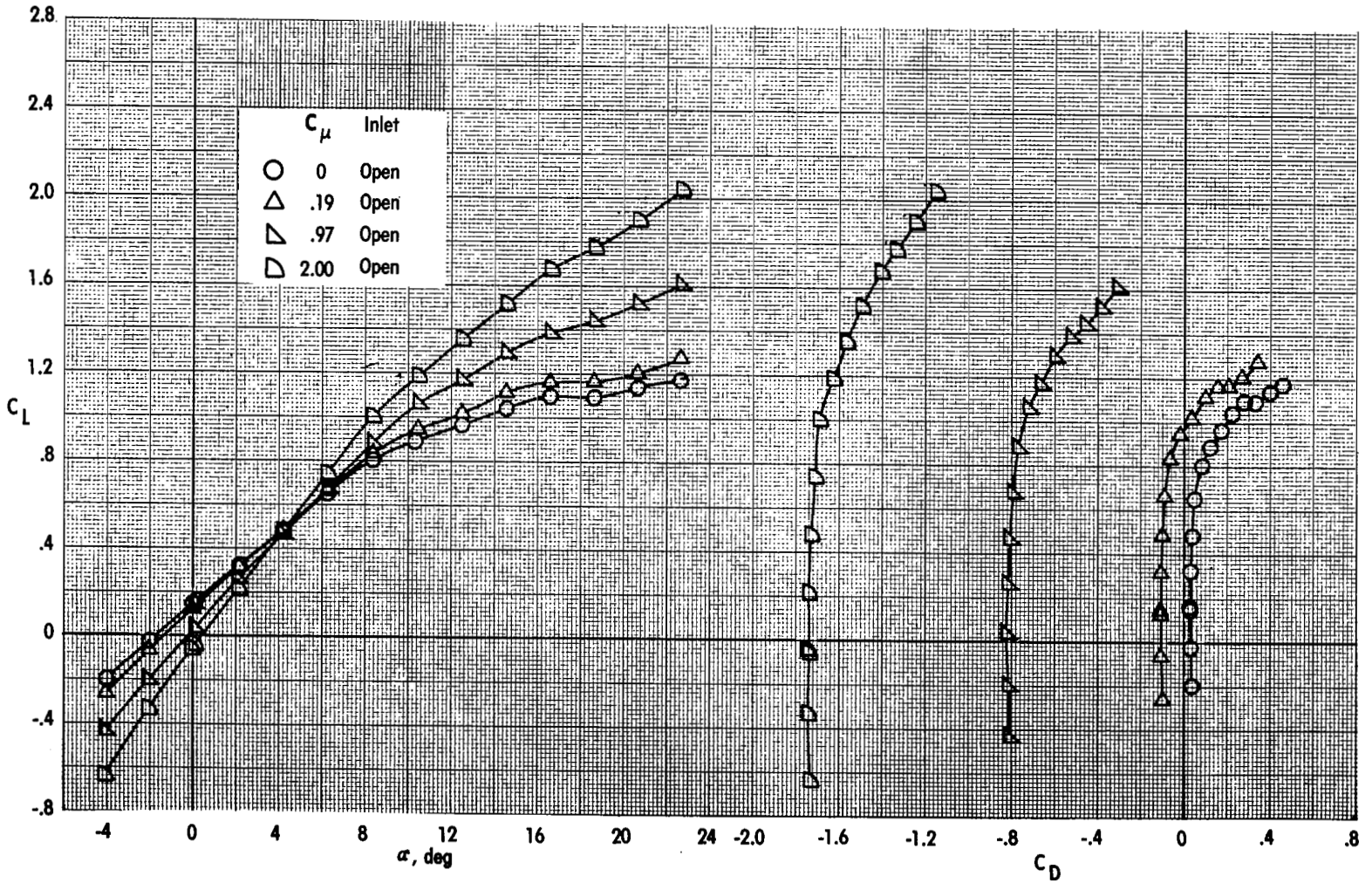

Figure 8.- Effect of thrust coefficient on longitudinal aerodynamic characteristics. Cruise configuration; basic engine; tail off.

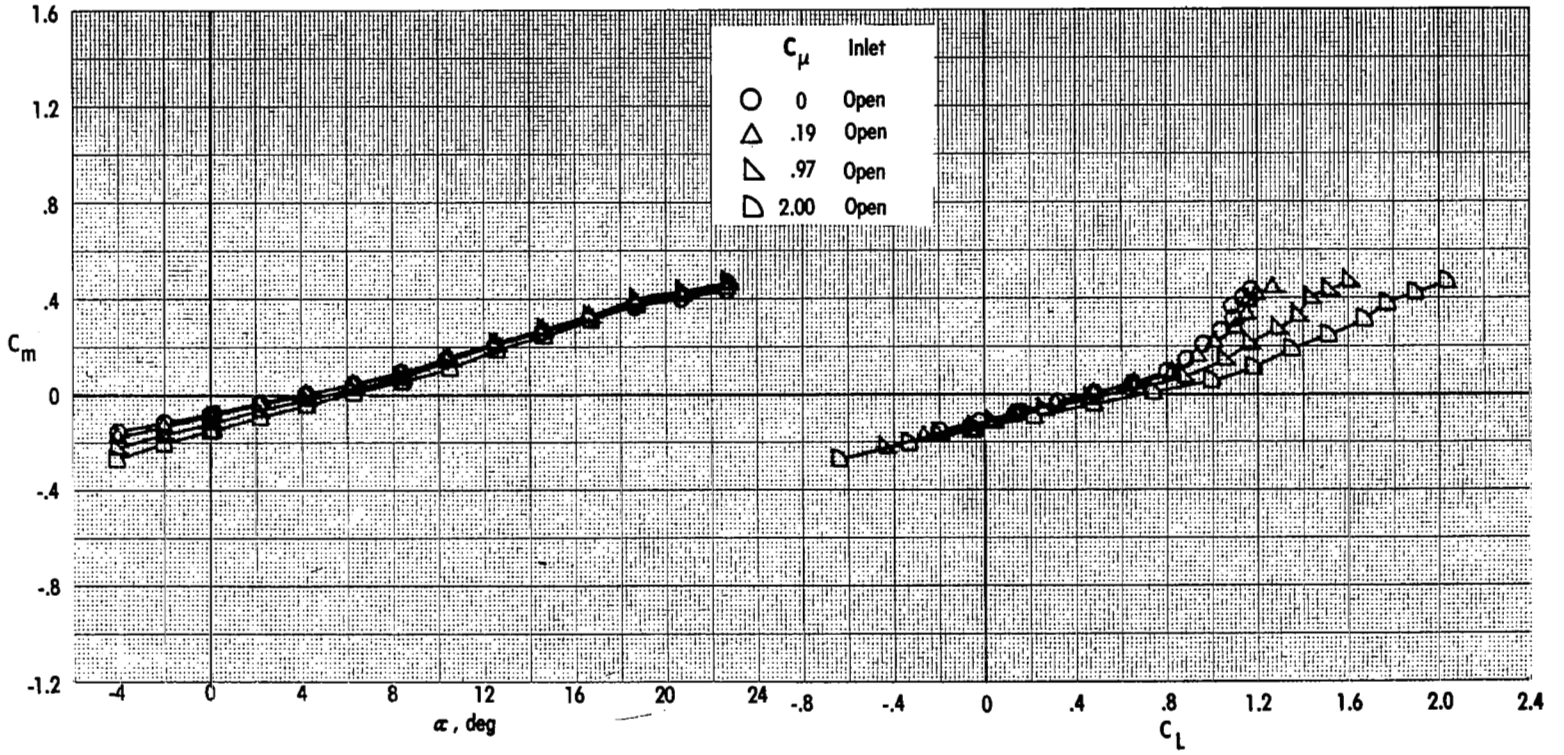

Figure 8.- Concluded.

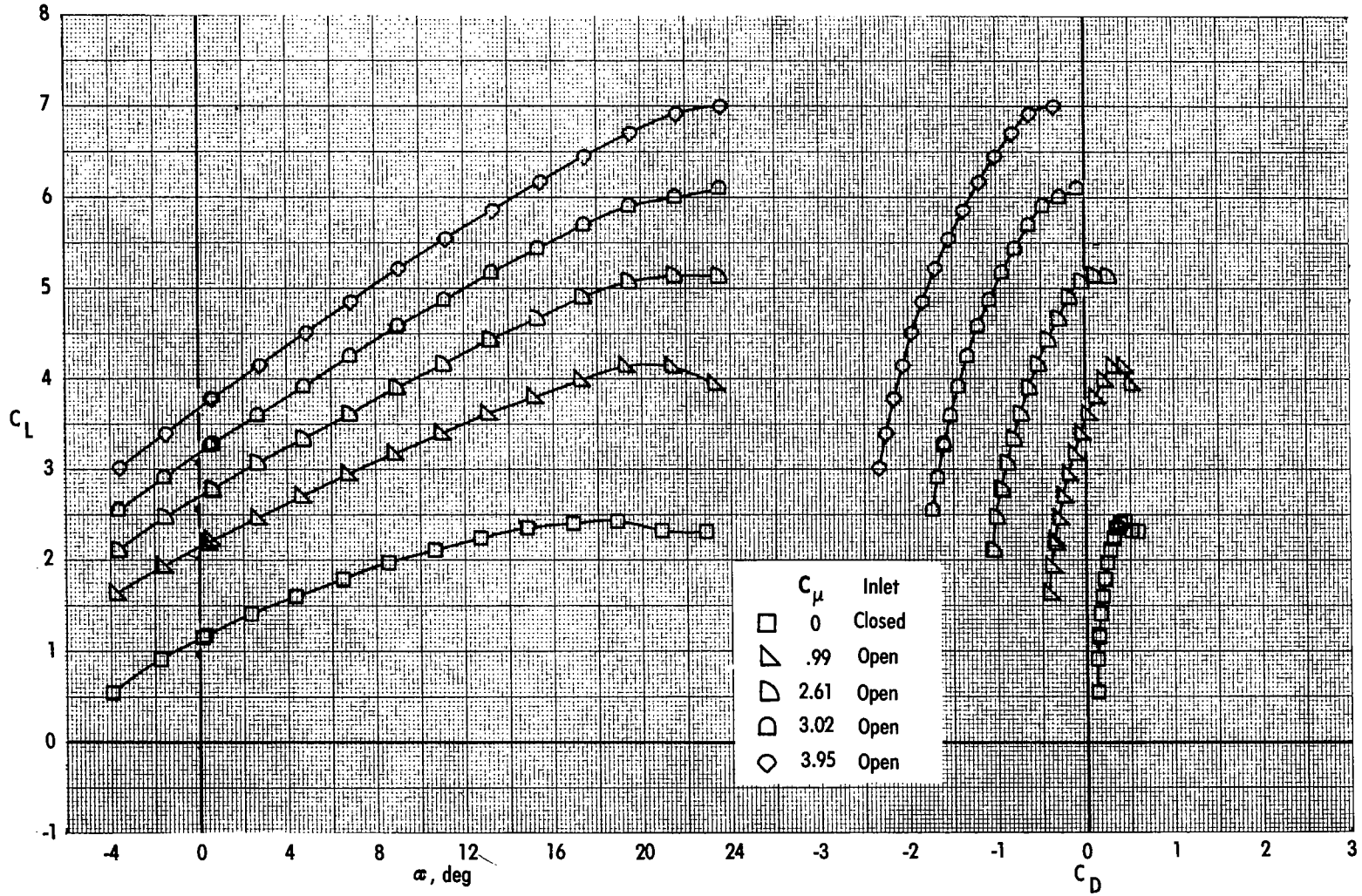

Figure 9.- Effect of thrust coefficient on longitudinal aerodynamic characteristics. Take-off configuration; basic engine; tail off.

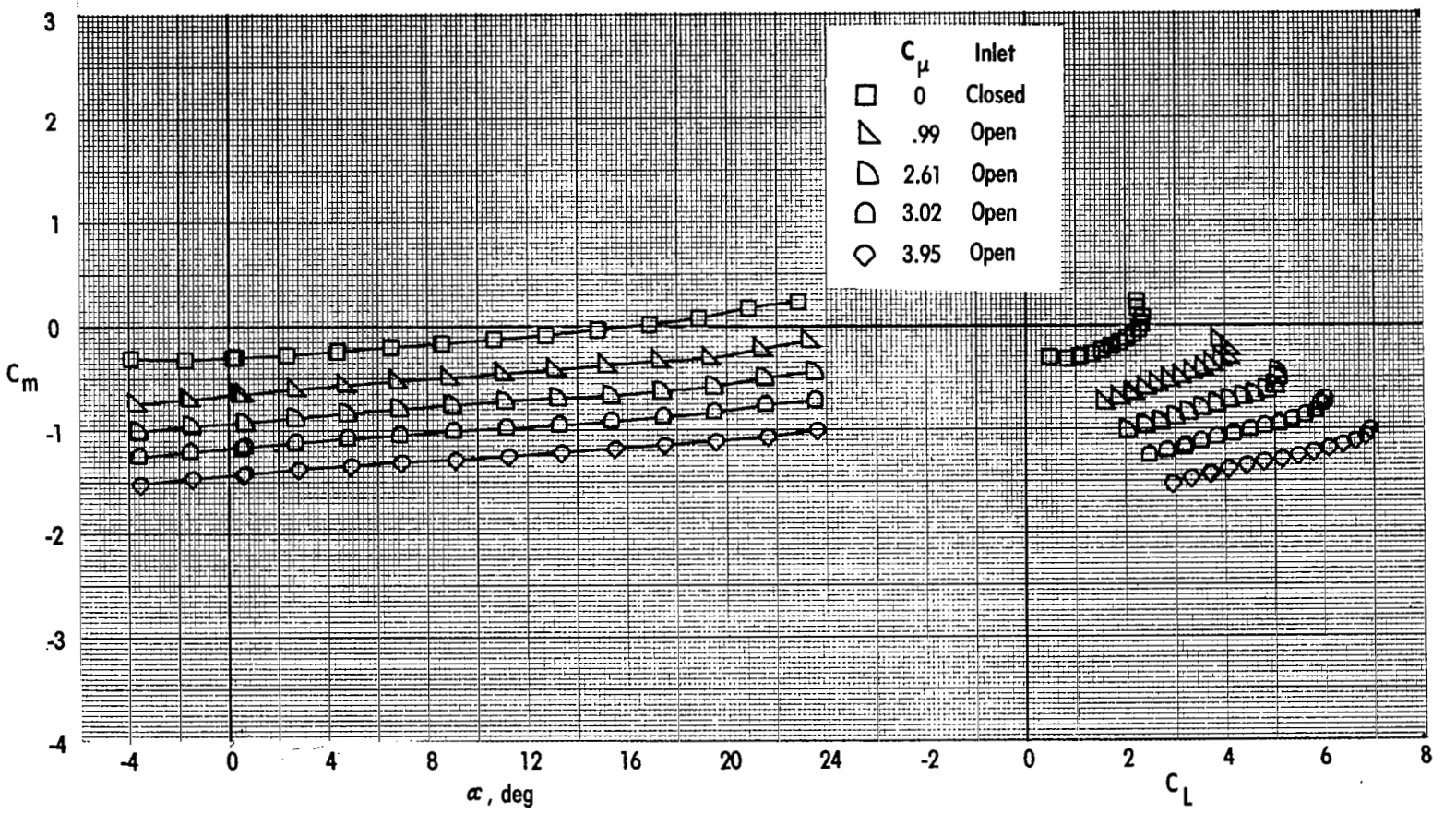

Figure 9.- Concluded.

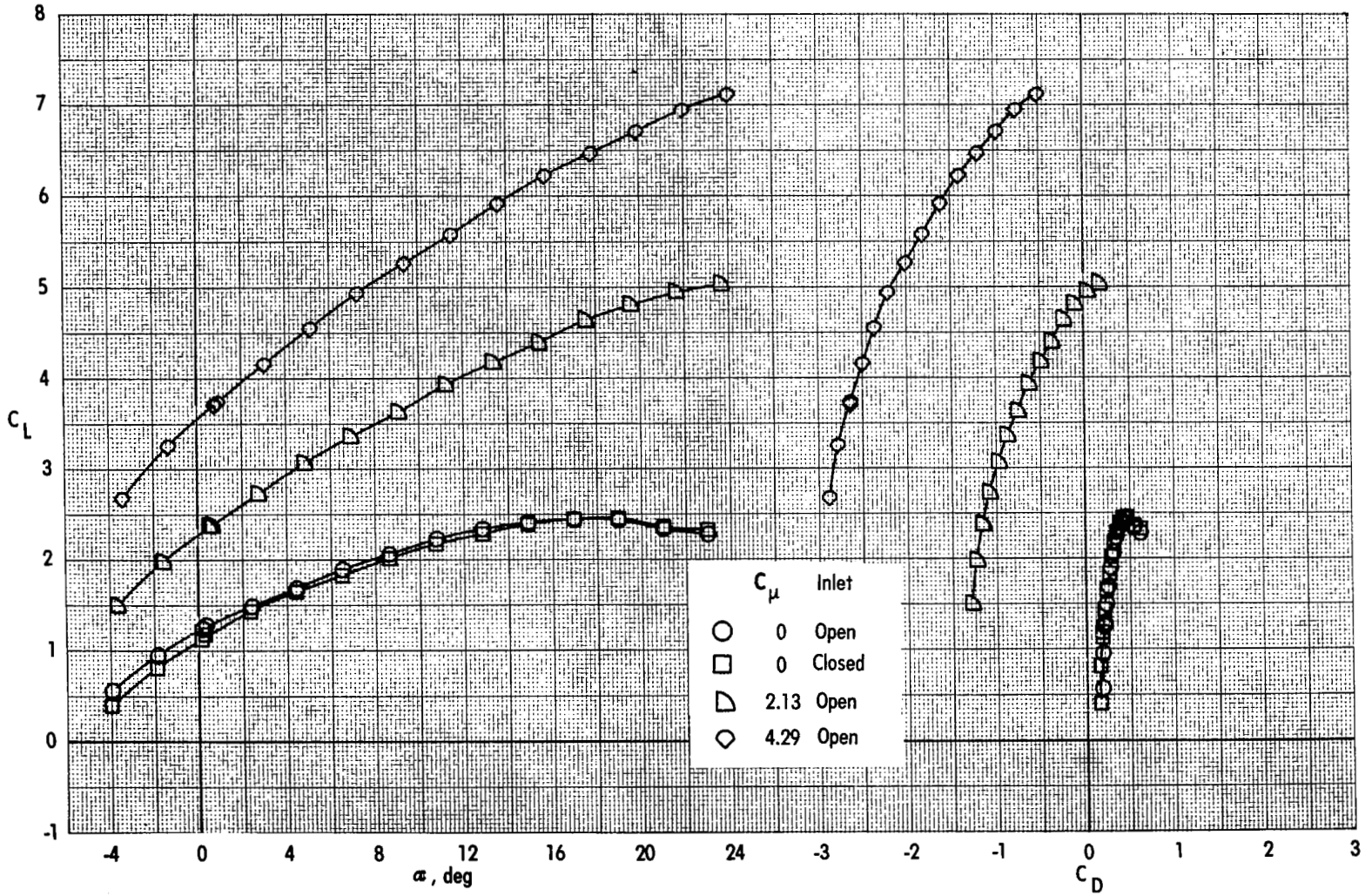

Figure 10.- Effect of thrust coefficient on longitudinal aerodynamic characteristics. Take-off configuration; engine 10-45; tail off.

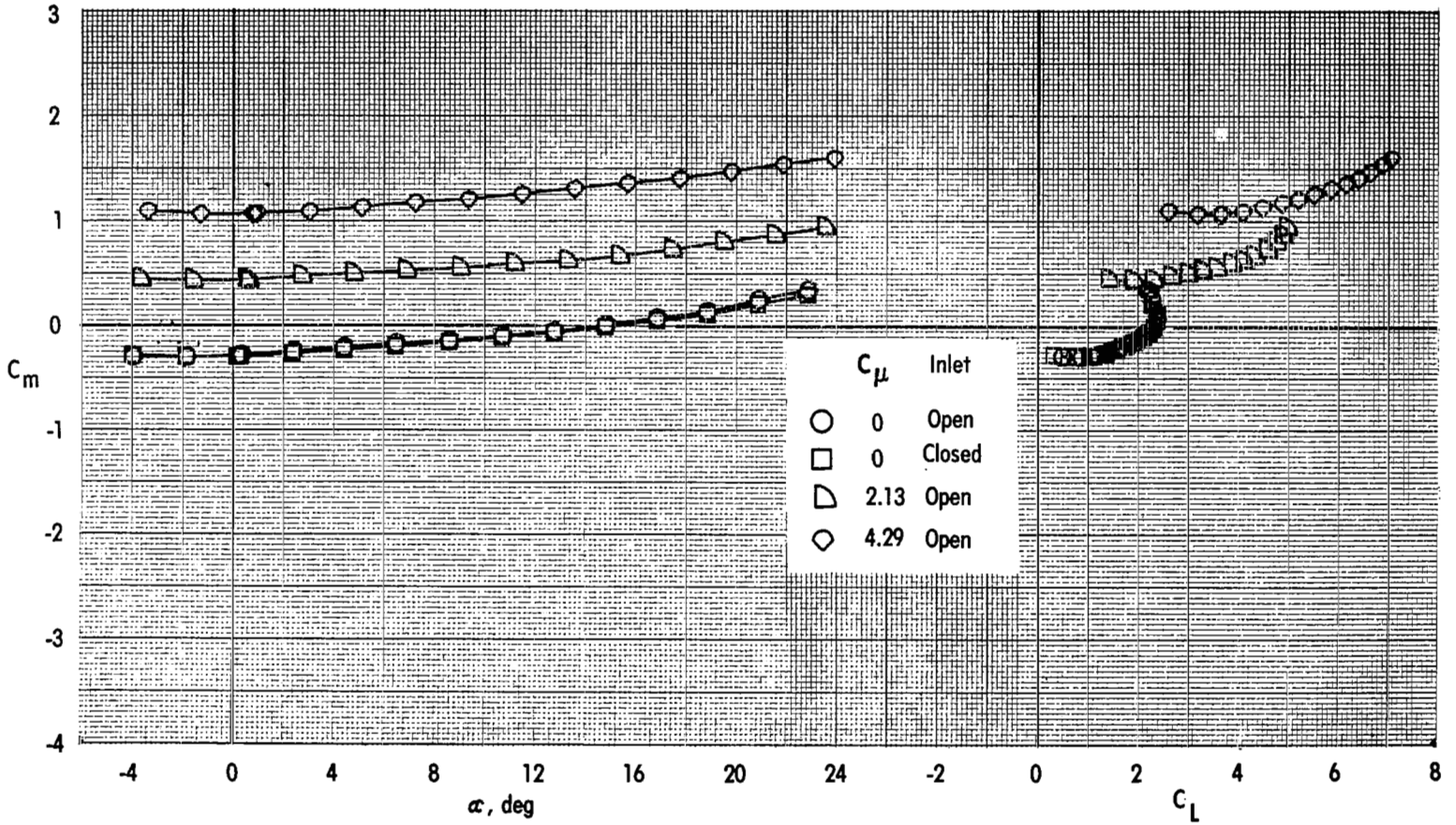

Figure 10.- Concluded.

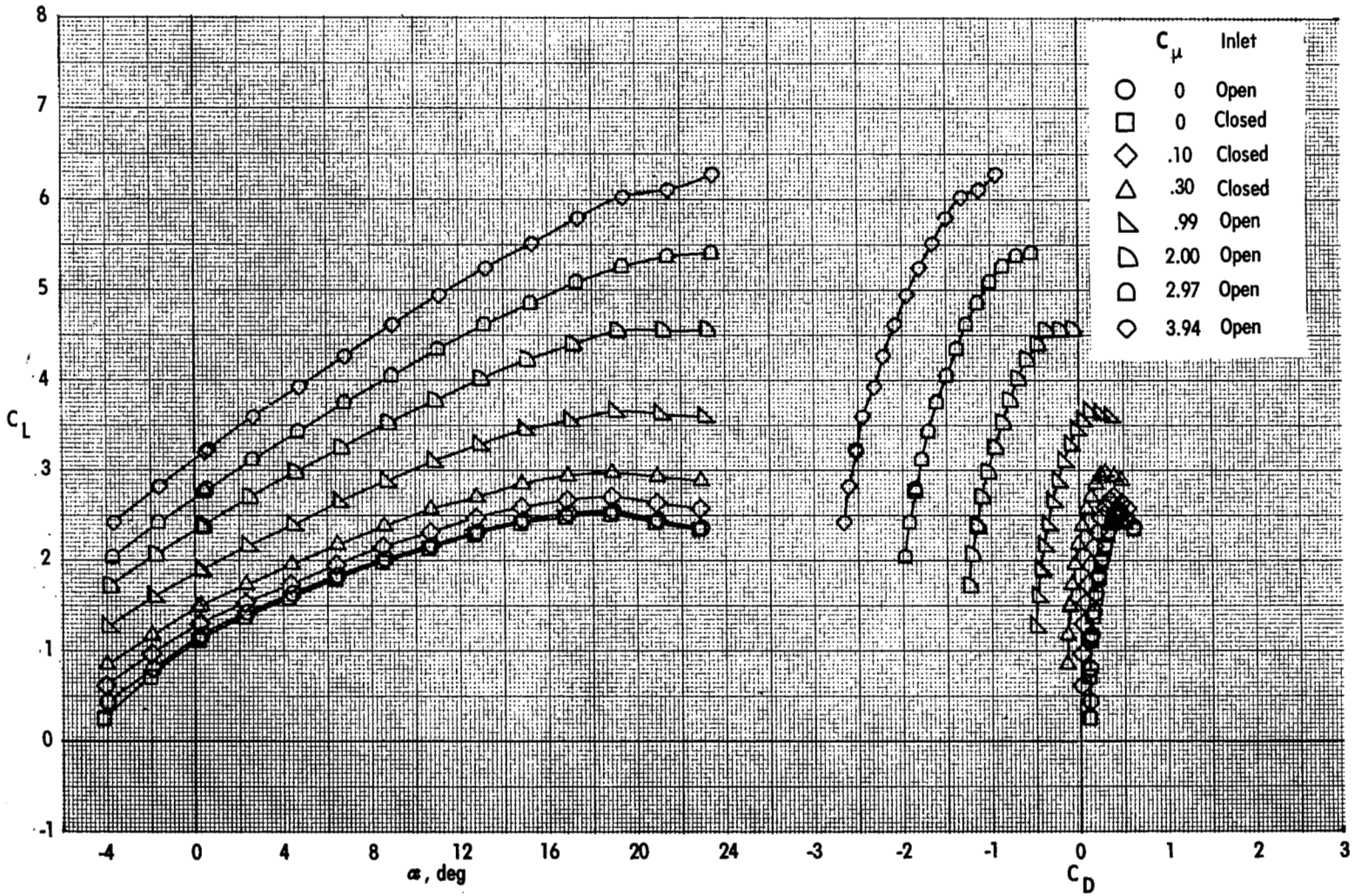

Figure 11.- Effect of thrust coefficient on longitudinal aerodynamic characteristics. Take-off configuration; engine 75-0; tail off.

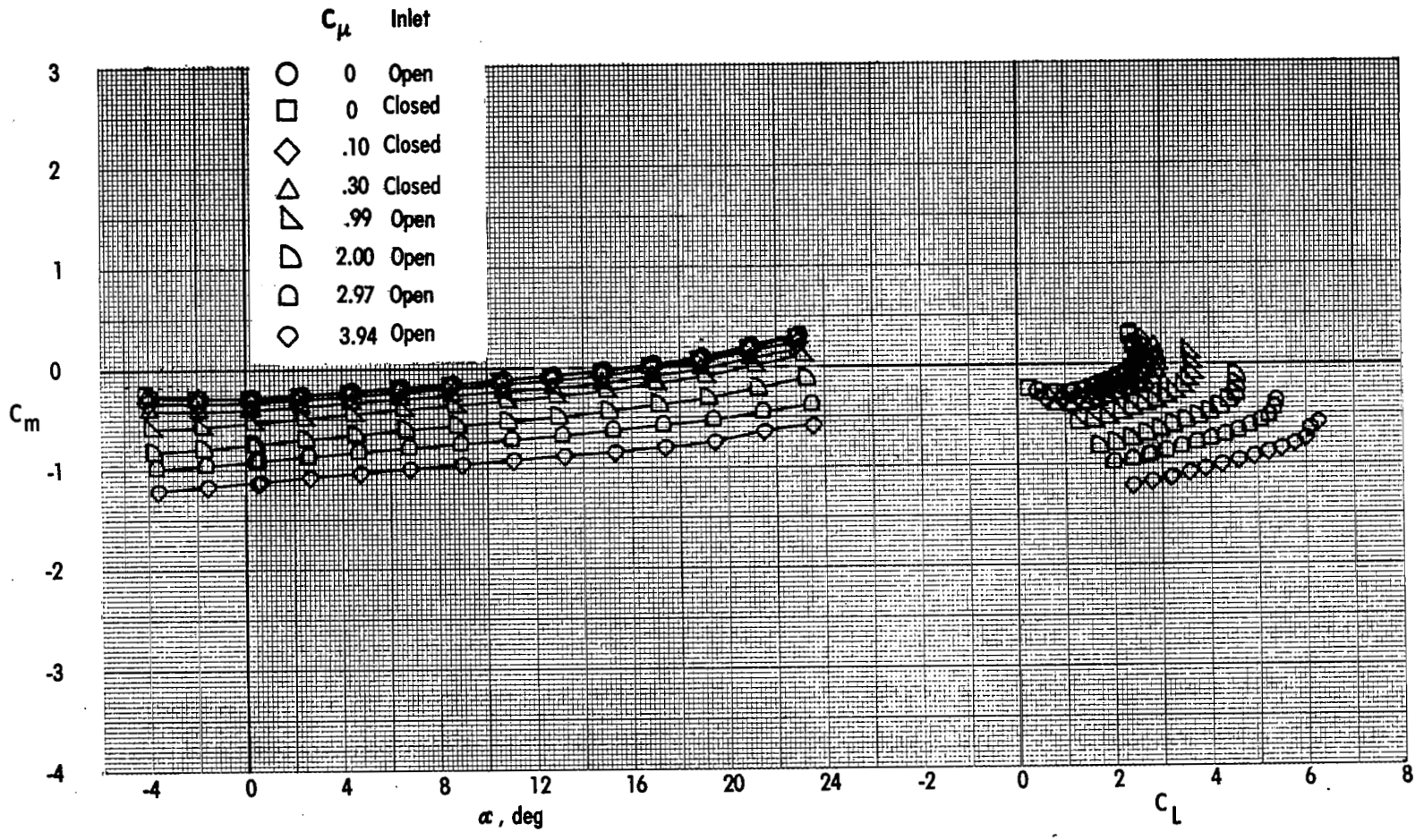

Figure 11.- Concluded.

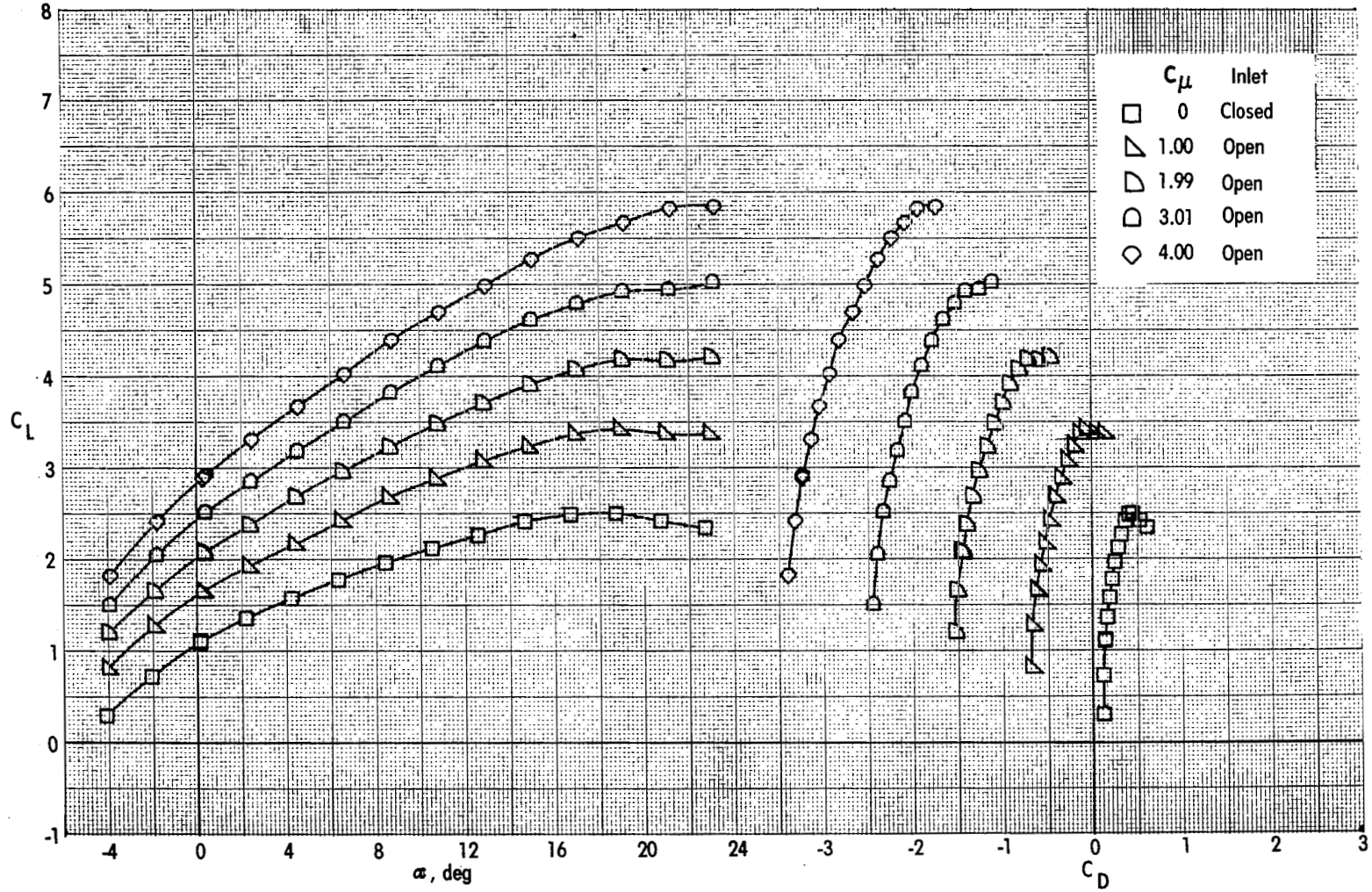

Figure 12.- Effect of thrust coefficient on longitudinal aerodynamic characteristics. Take-off characteristics; engine 75-25; tail off.

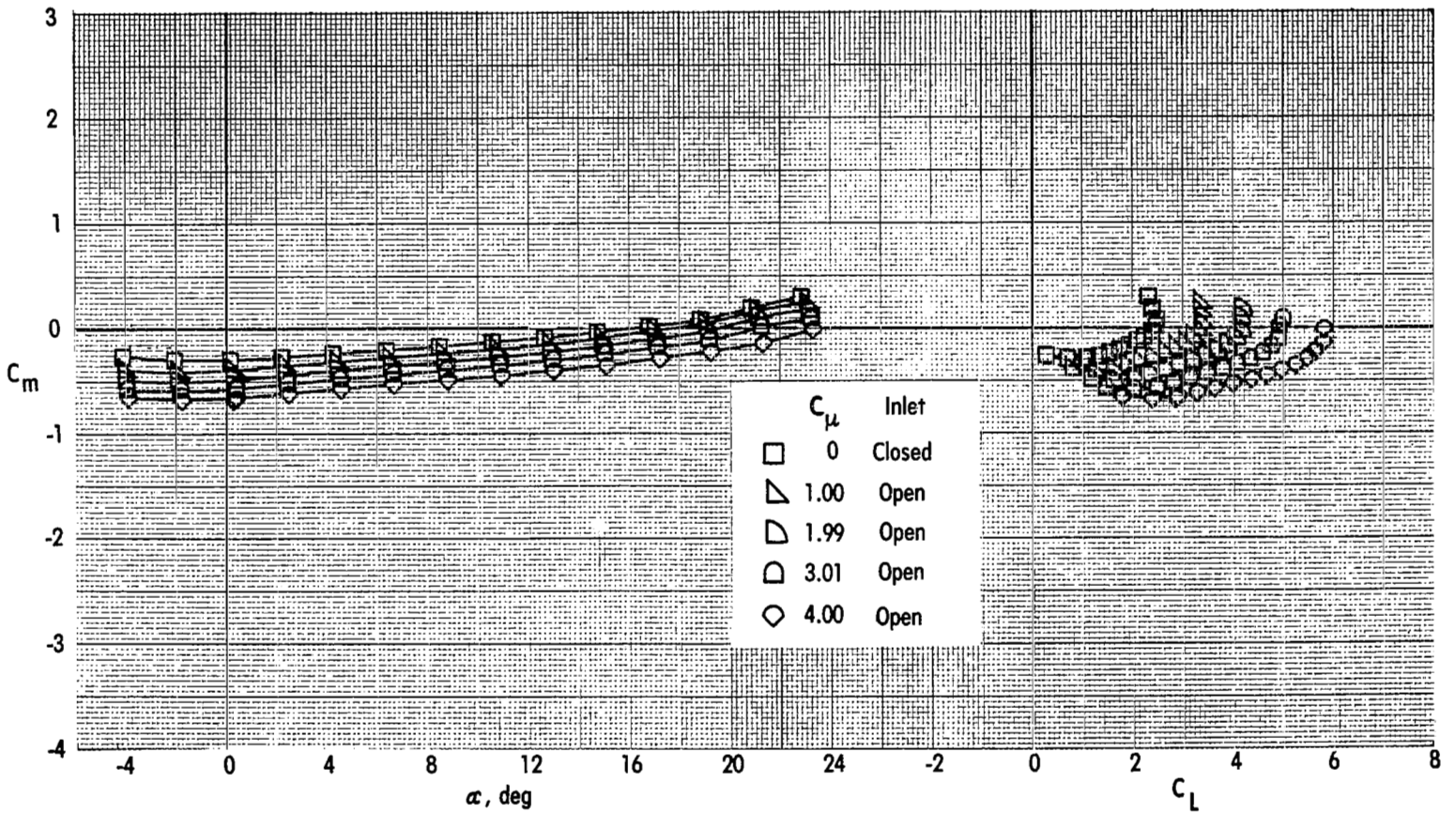

Figure 12.- Concluded.

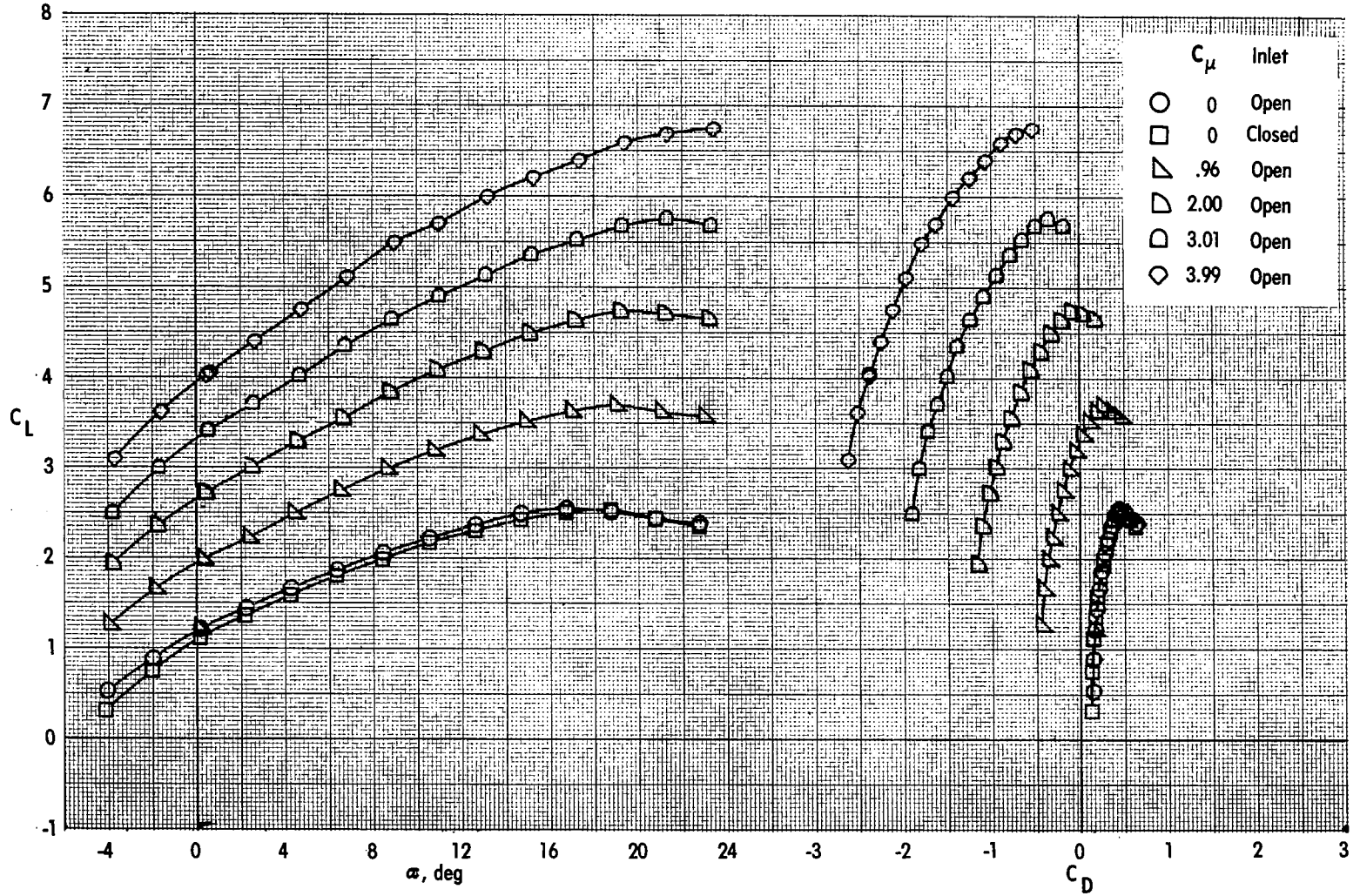

Figure 13.- Effect of thrust coefficient on longitudinal aerodynamic characteristics. Take-off configuration; engine 75-45; tail off.

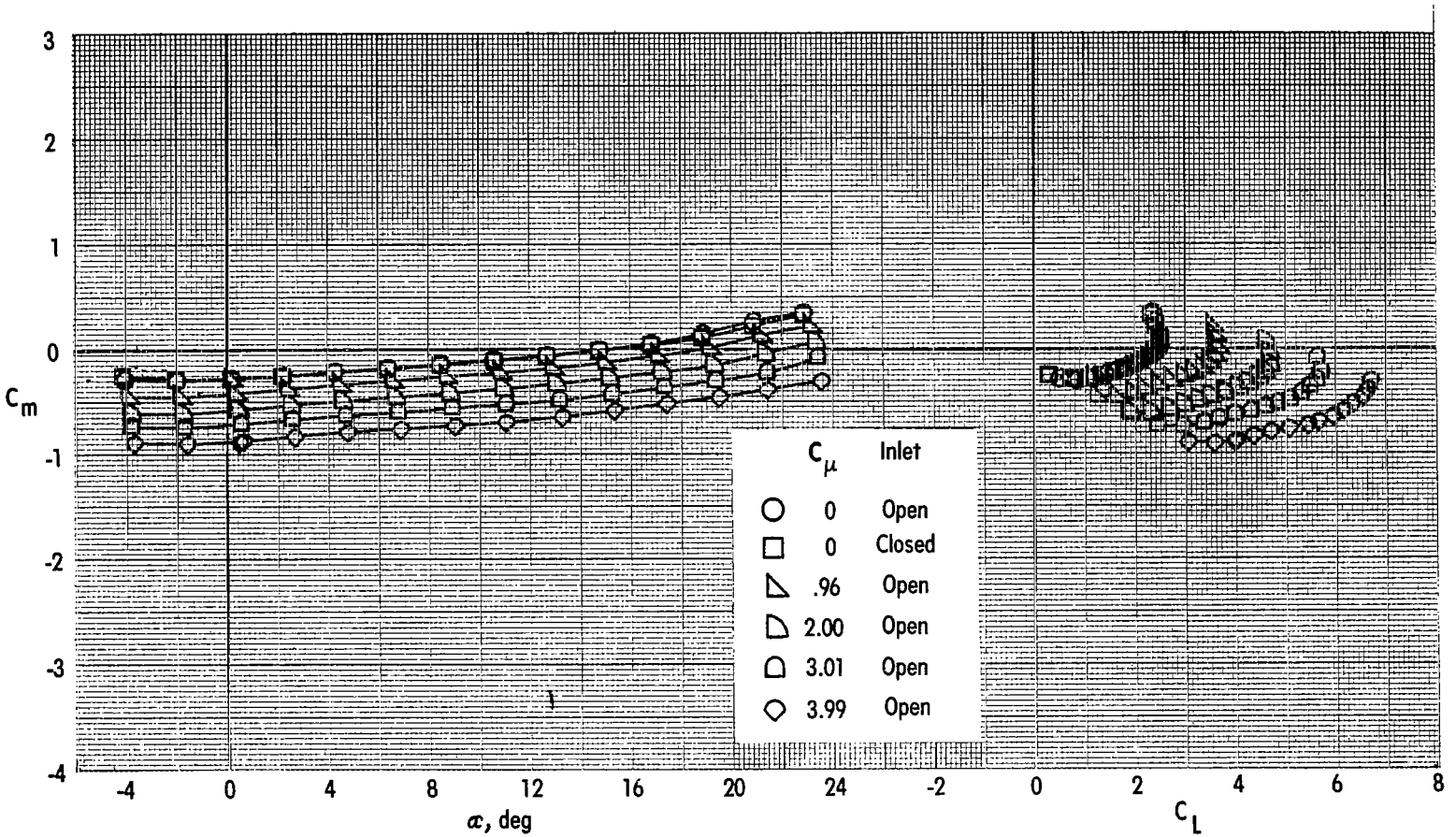

Figure 13.- Concluded.

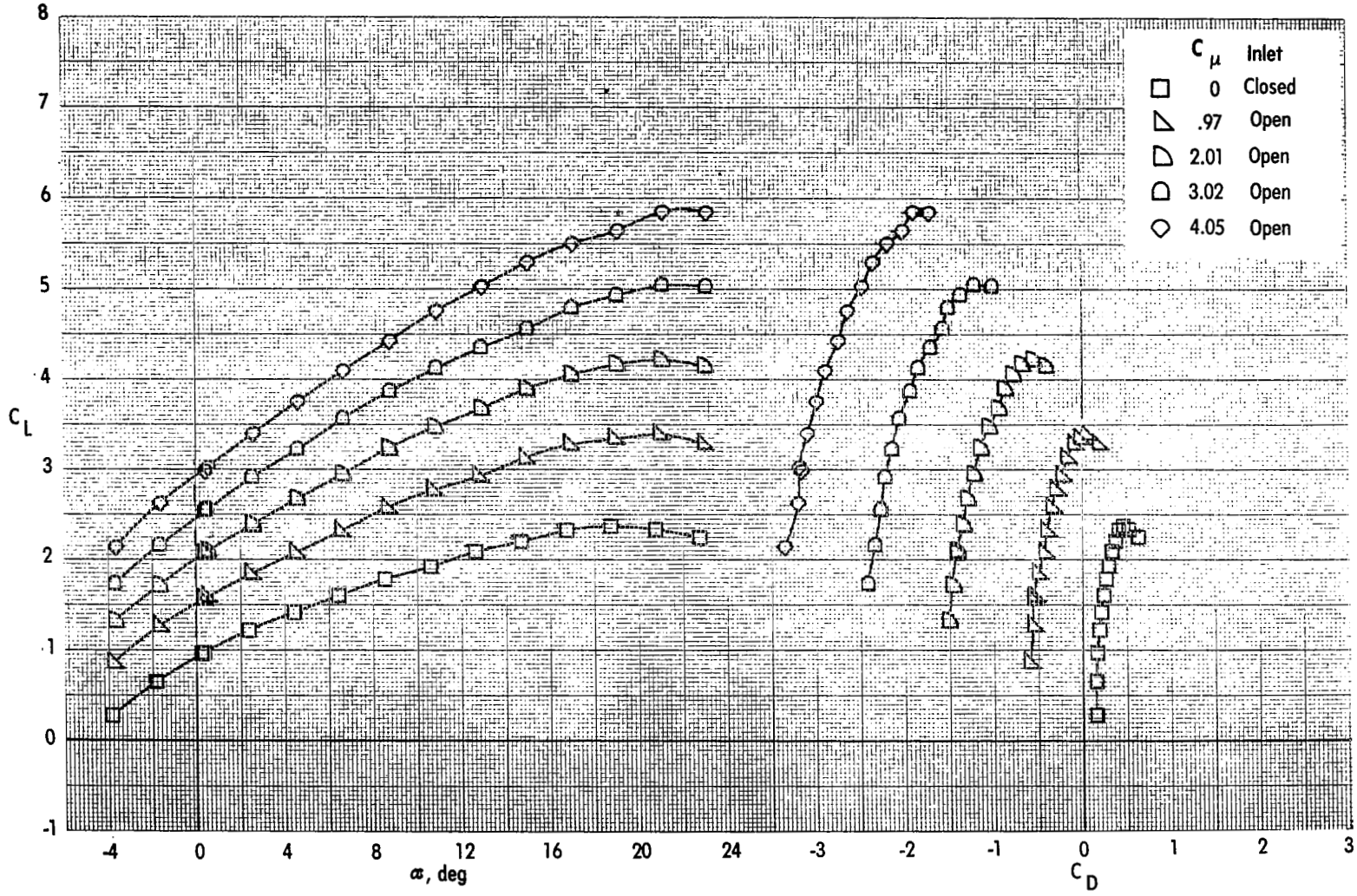

Figure 14.- Effect of thrust coefficient on longitudinal aerodynamic characteristics. Take-off configuration; engine 110-25; tail off.

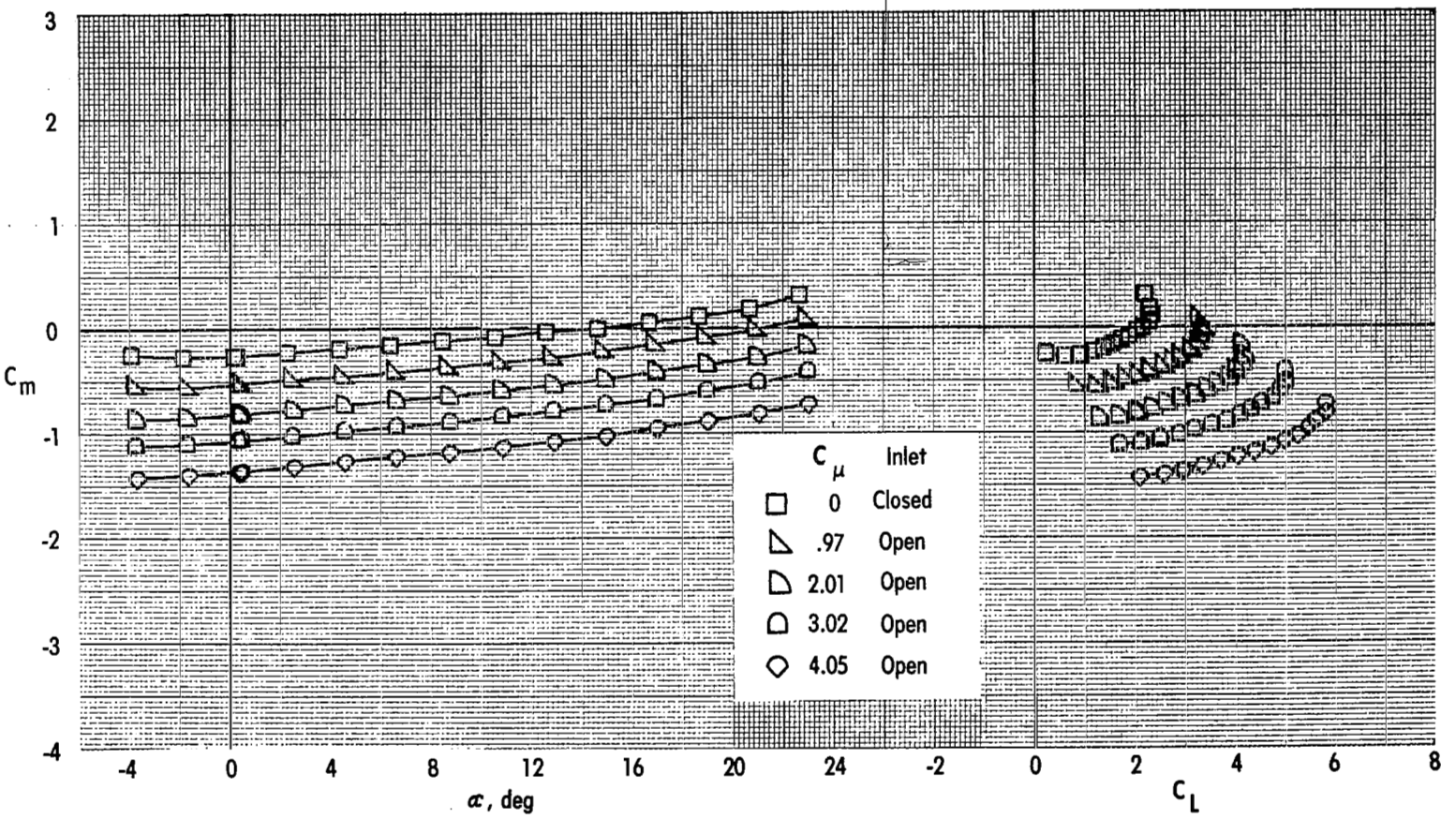

Figure 14.- Concluded.

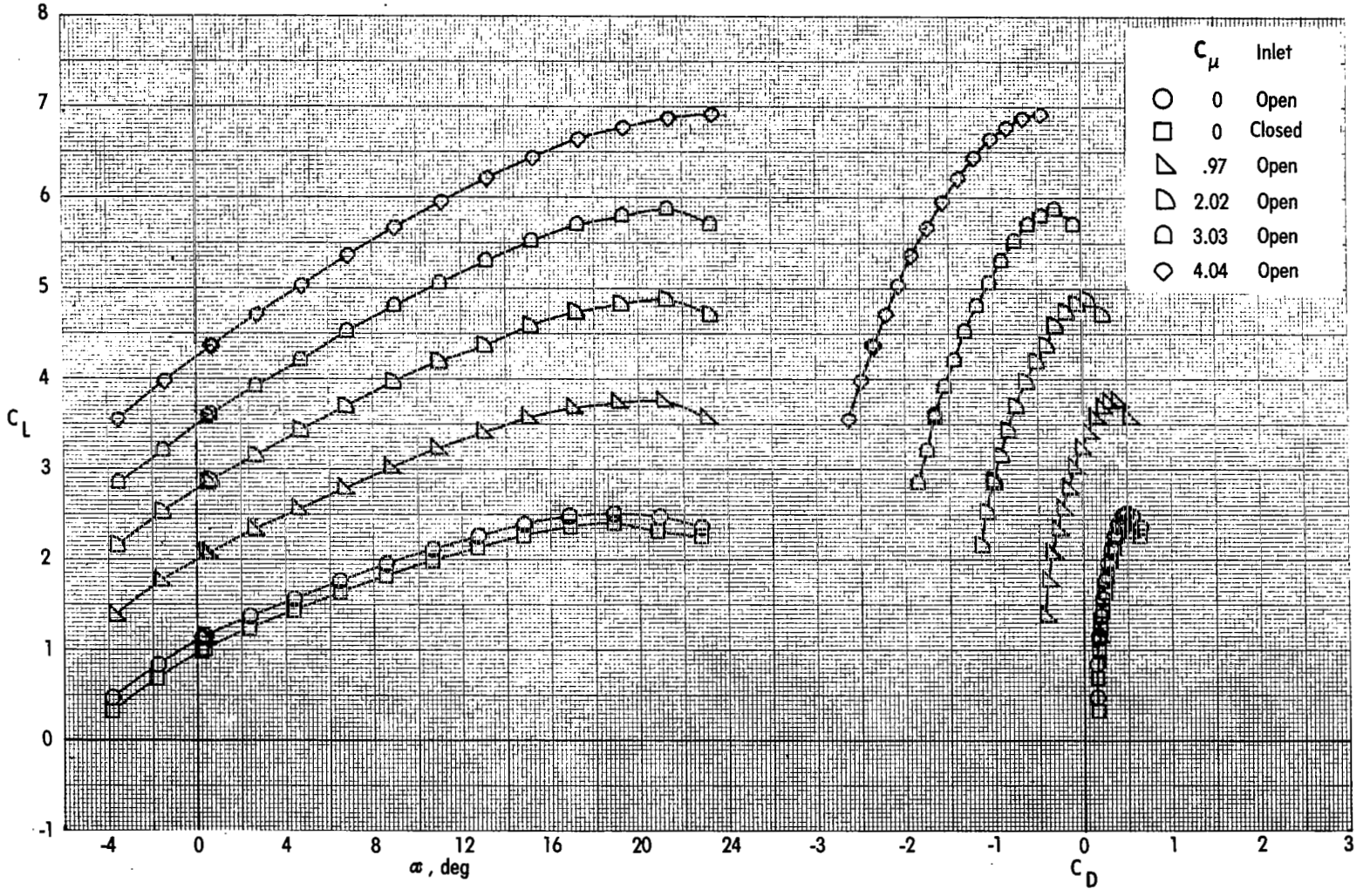

Figure 15.- Effect of thrust coefficient on longitudinal aerodynamic characteristics. Take-off configuration; engine 110-45; tail off.

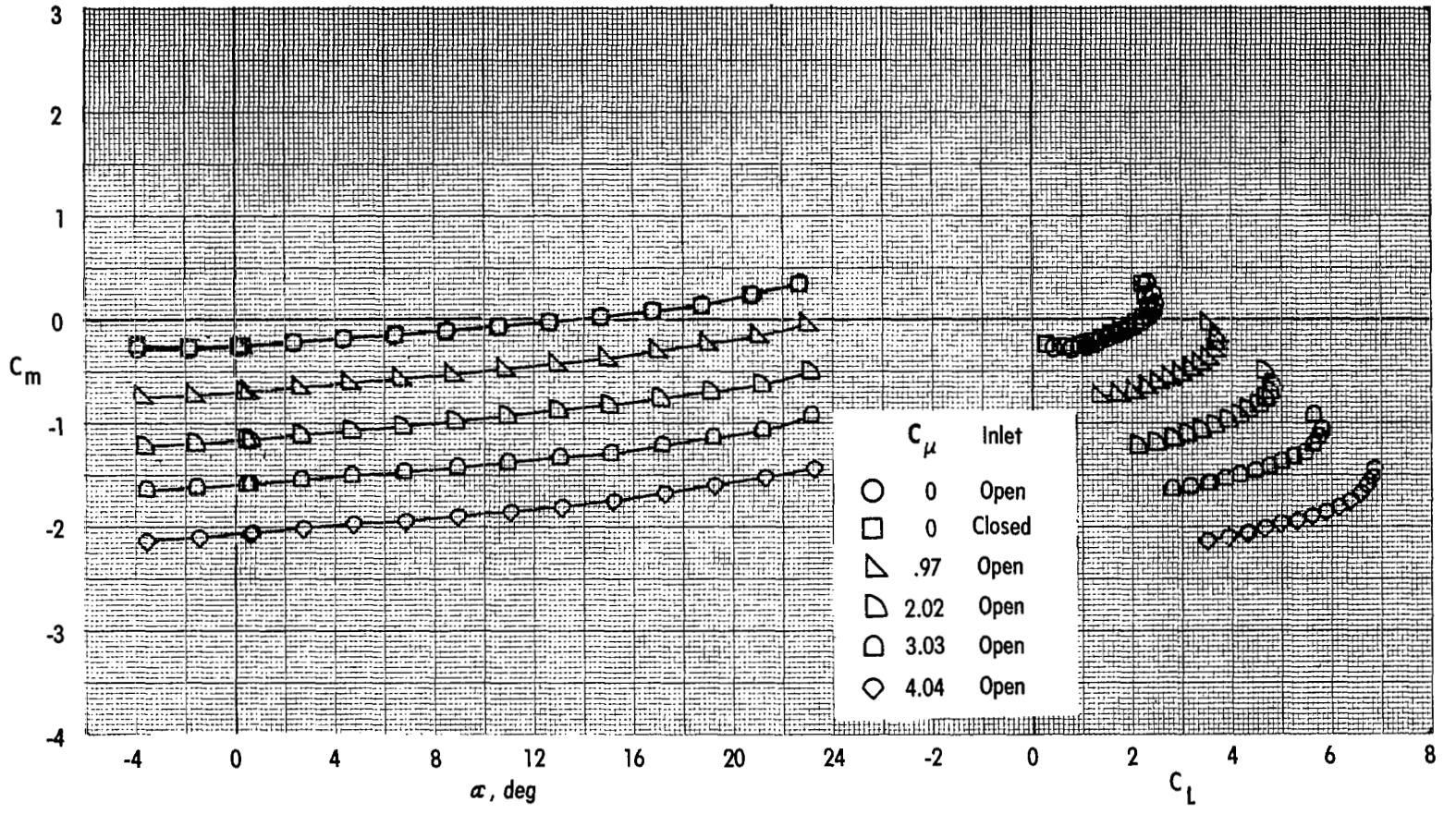

Figure 15.- Concluded.

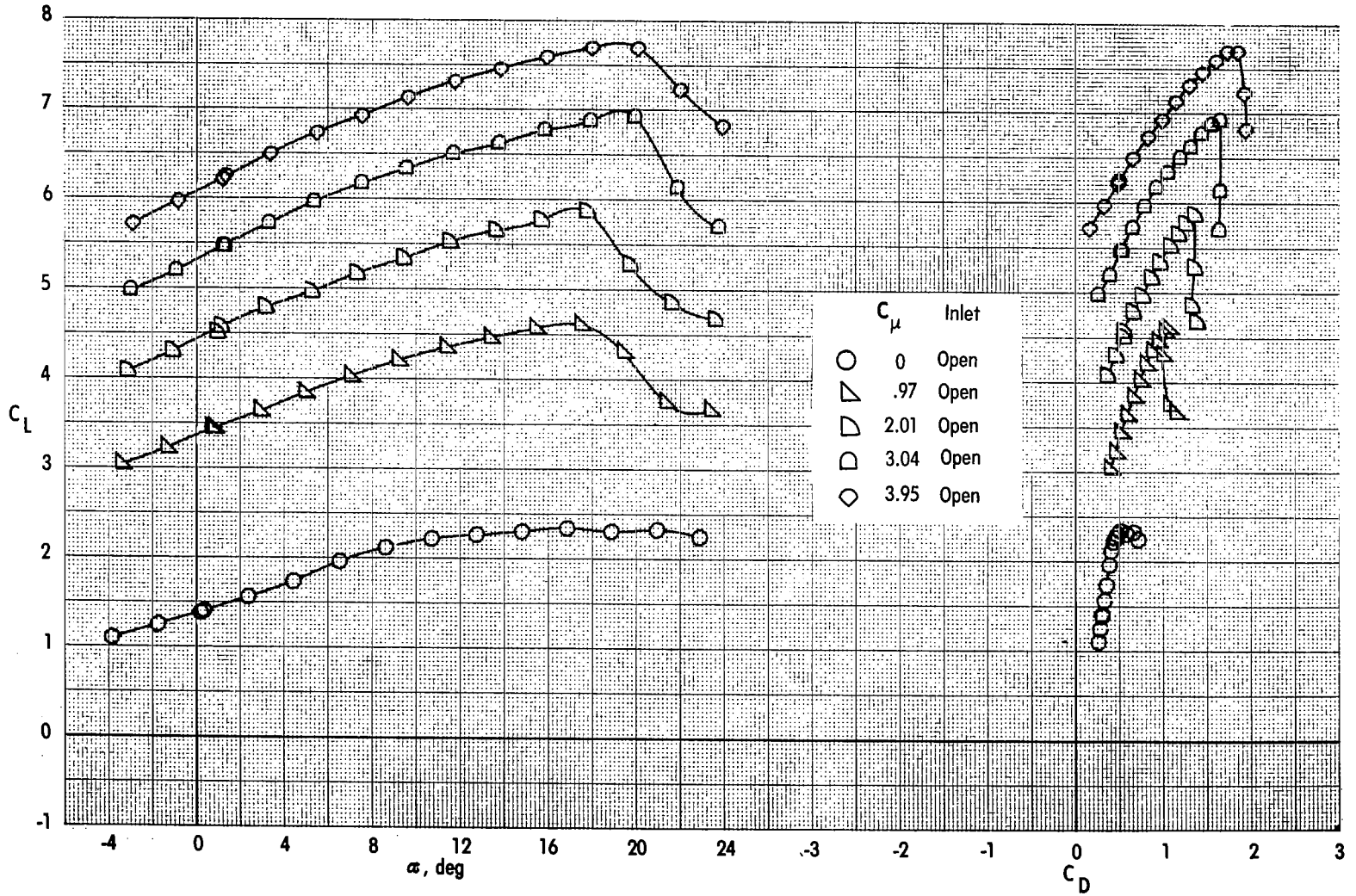

Figure 16.- Effect of thrust coefficient on longitudinal aerodynamic characteristics. Landing configuration; basic engine; tail off.

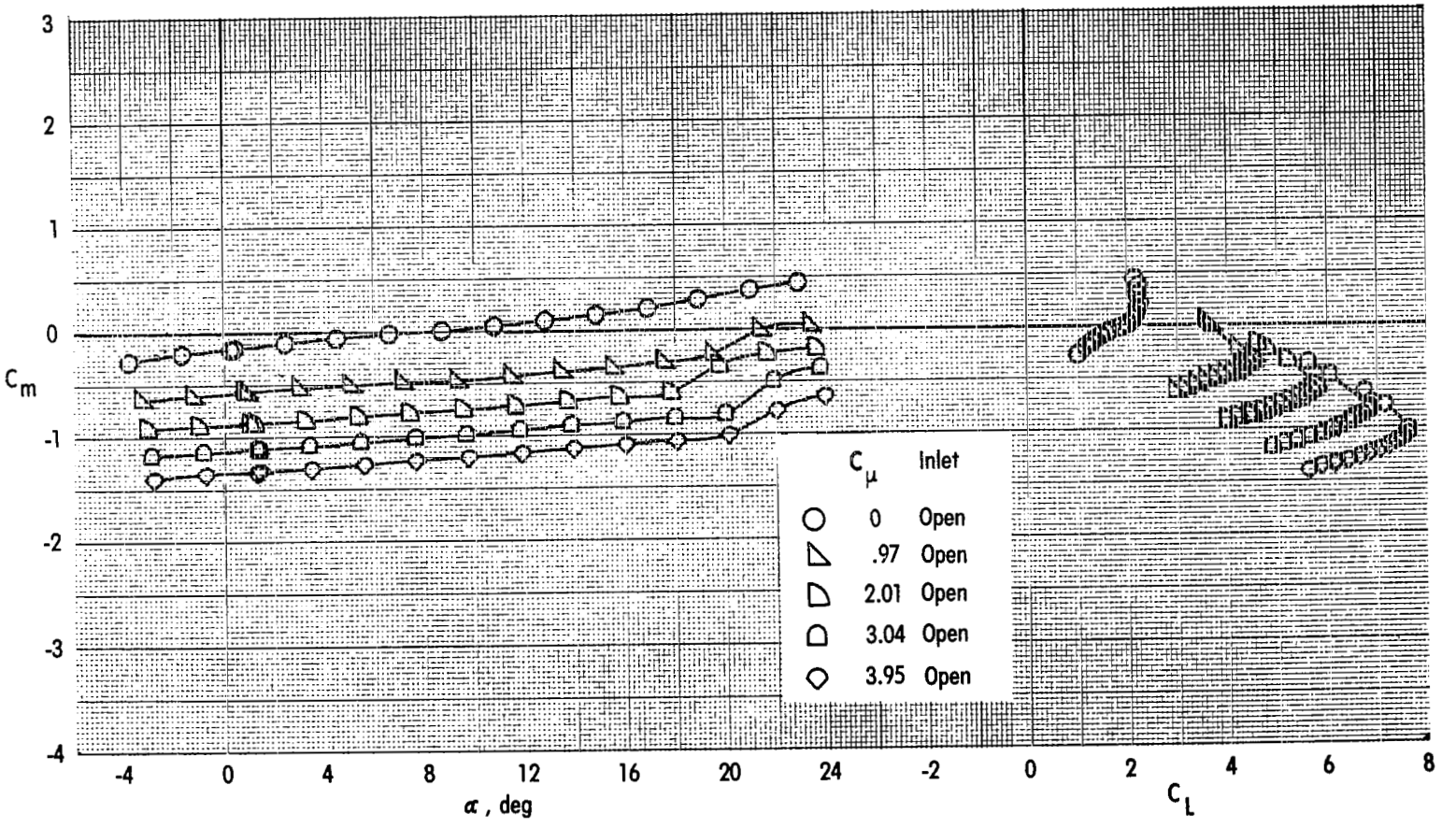

Figure 16.- Concluded.

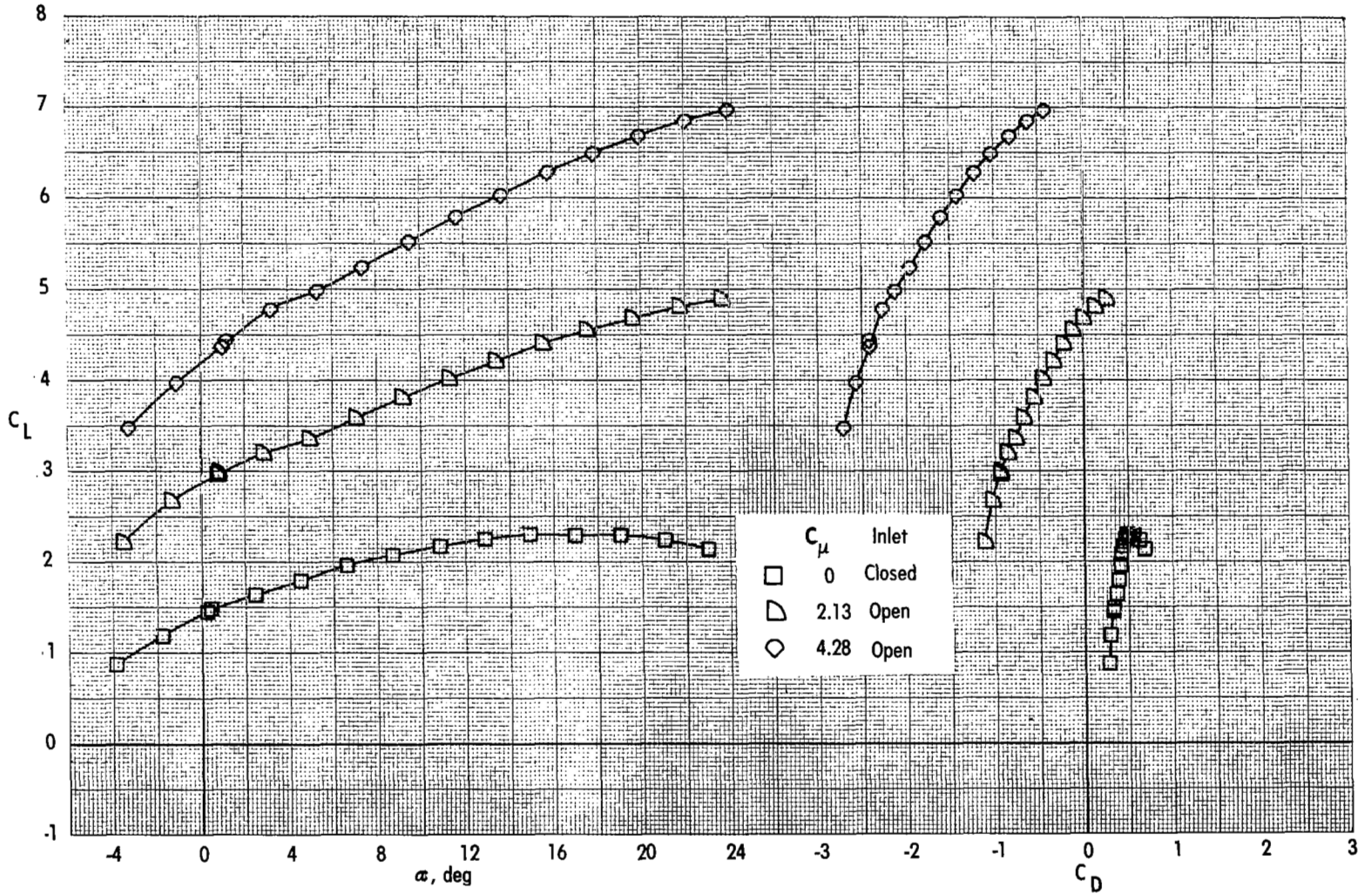

Figure 17.- Effect of thrust coefficient on longitudinal aerodynamic characteristics. Landing configuration; engine 10-45; tail off.

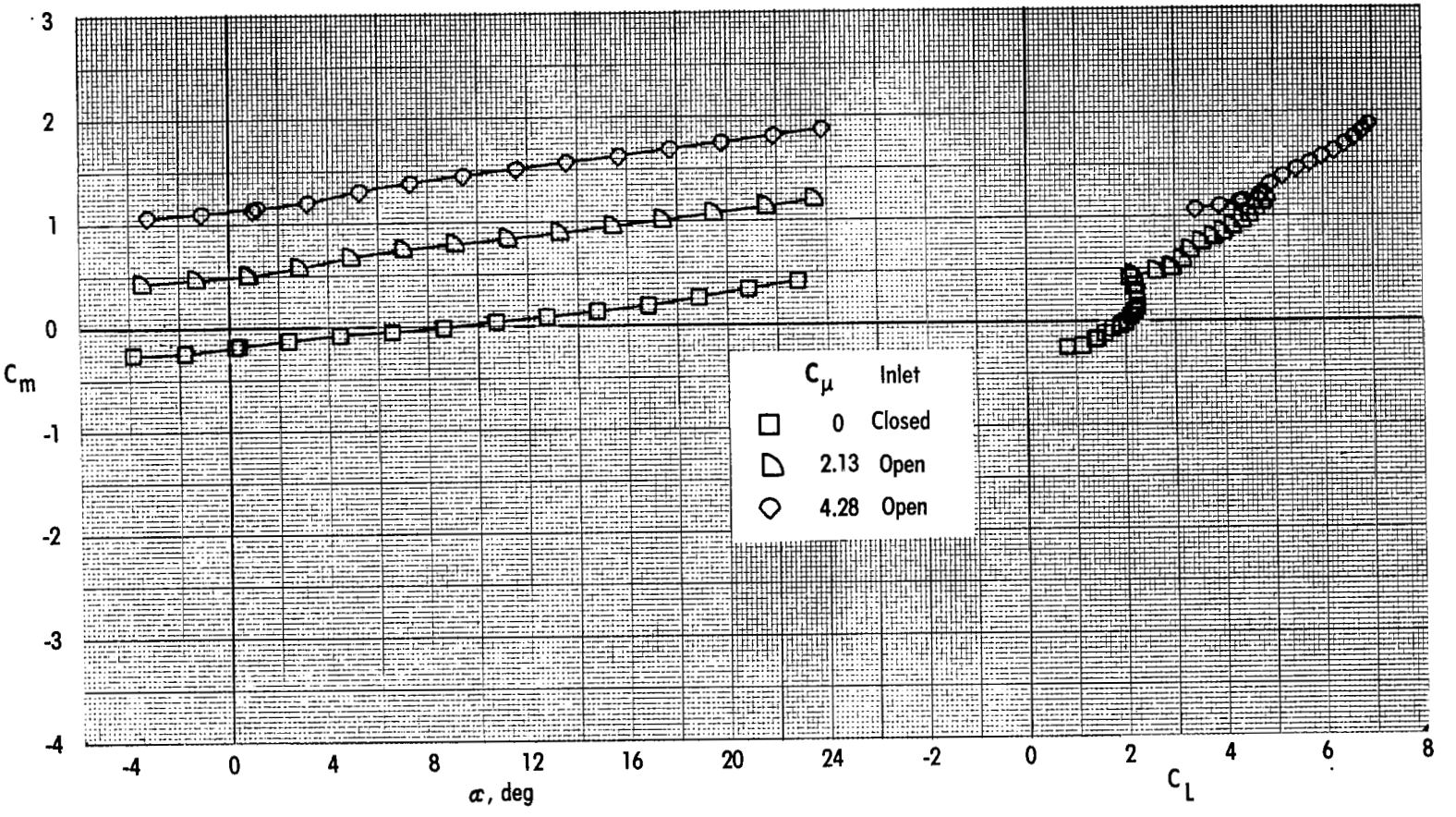

Figure 17.- Concluded.

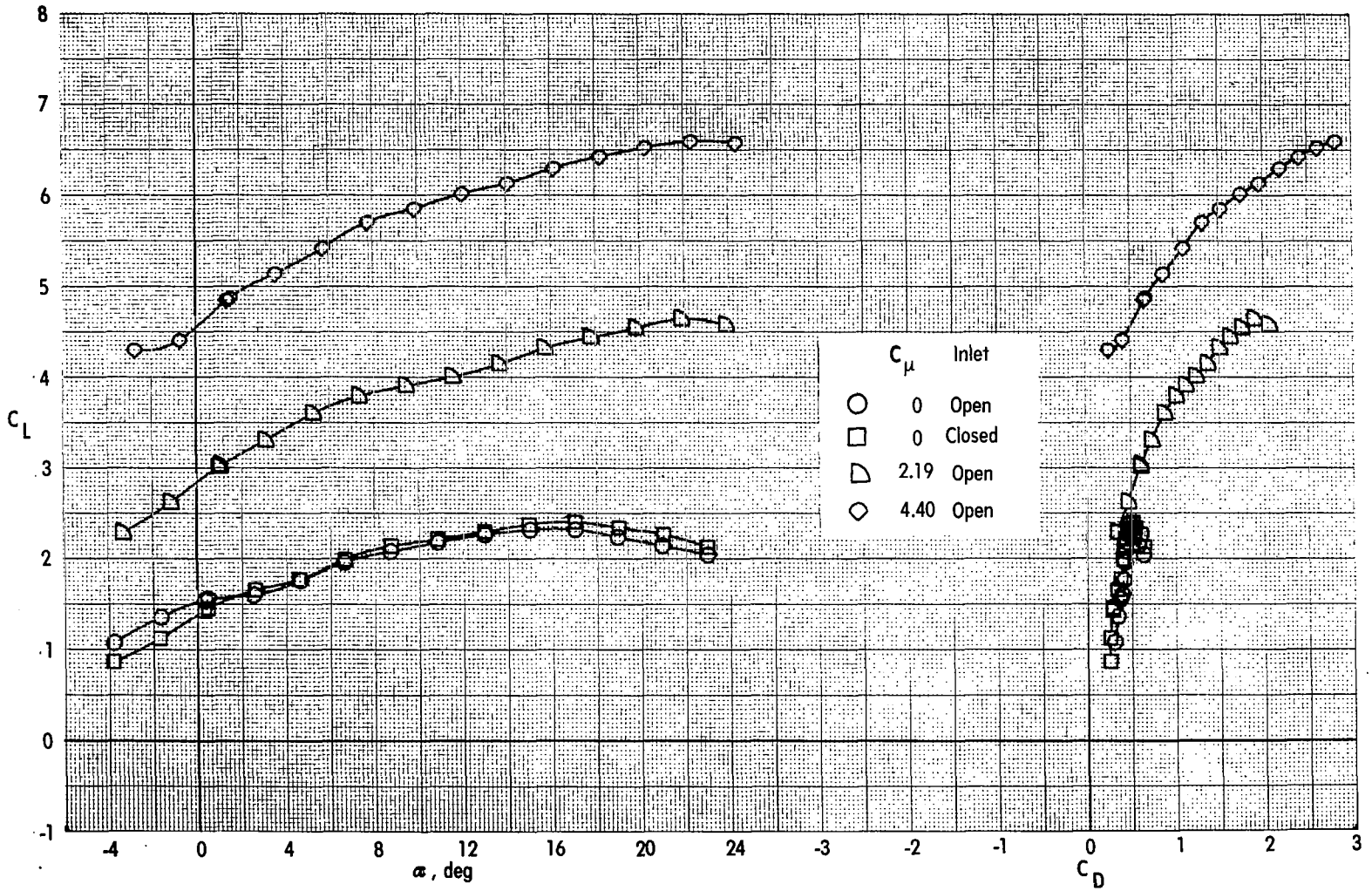

Figure 18.- Effect of thrust coefficient on longitudinal aerodynamic characteristics. Landing configuration; engine 10-90; tail off.

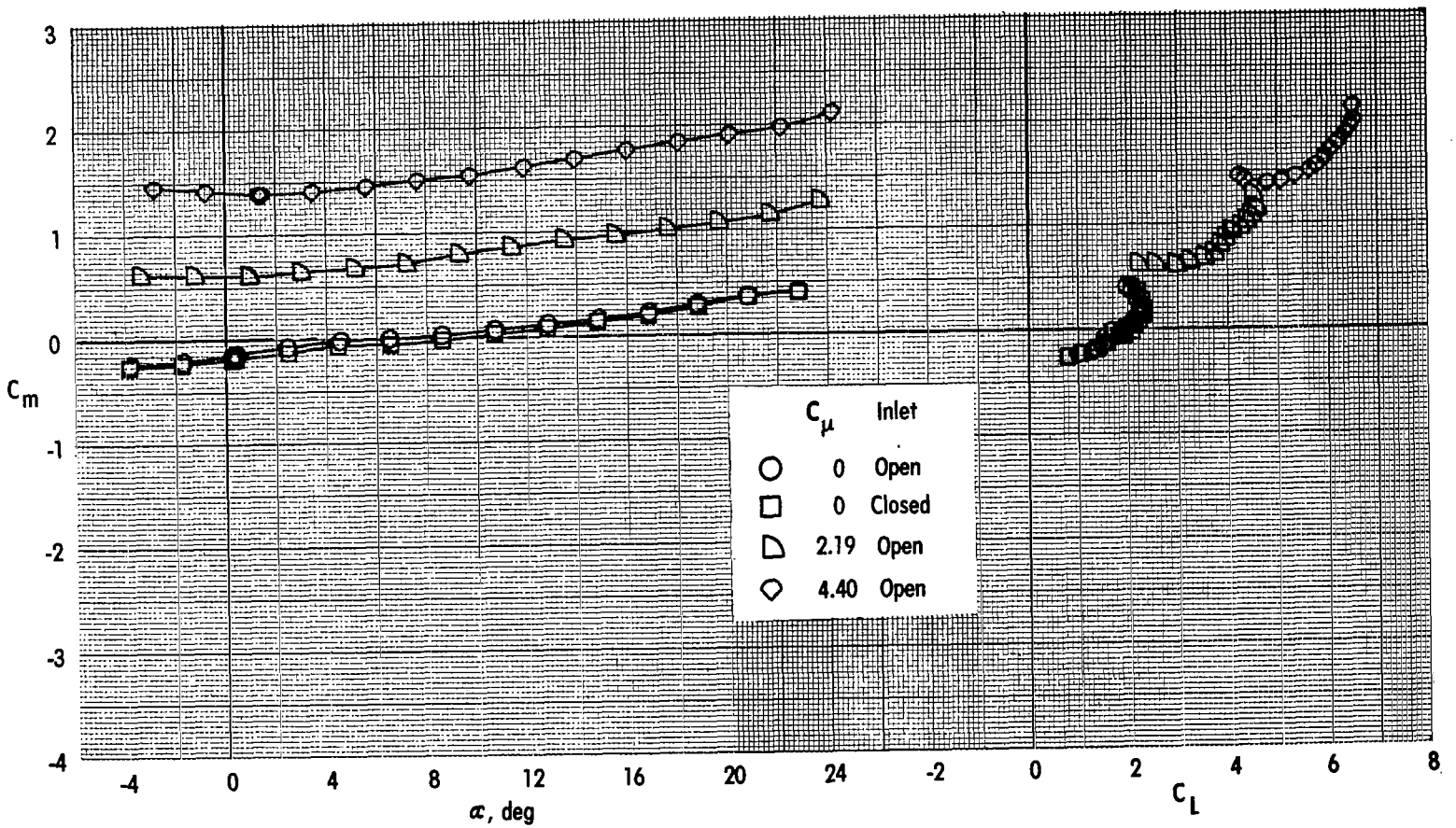

Figure 18.- Concluded.

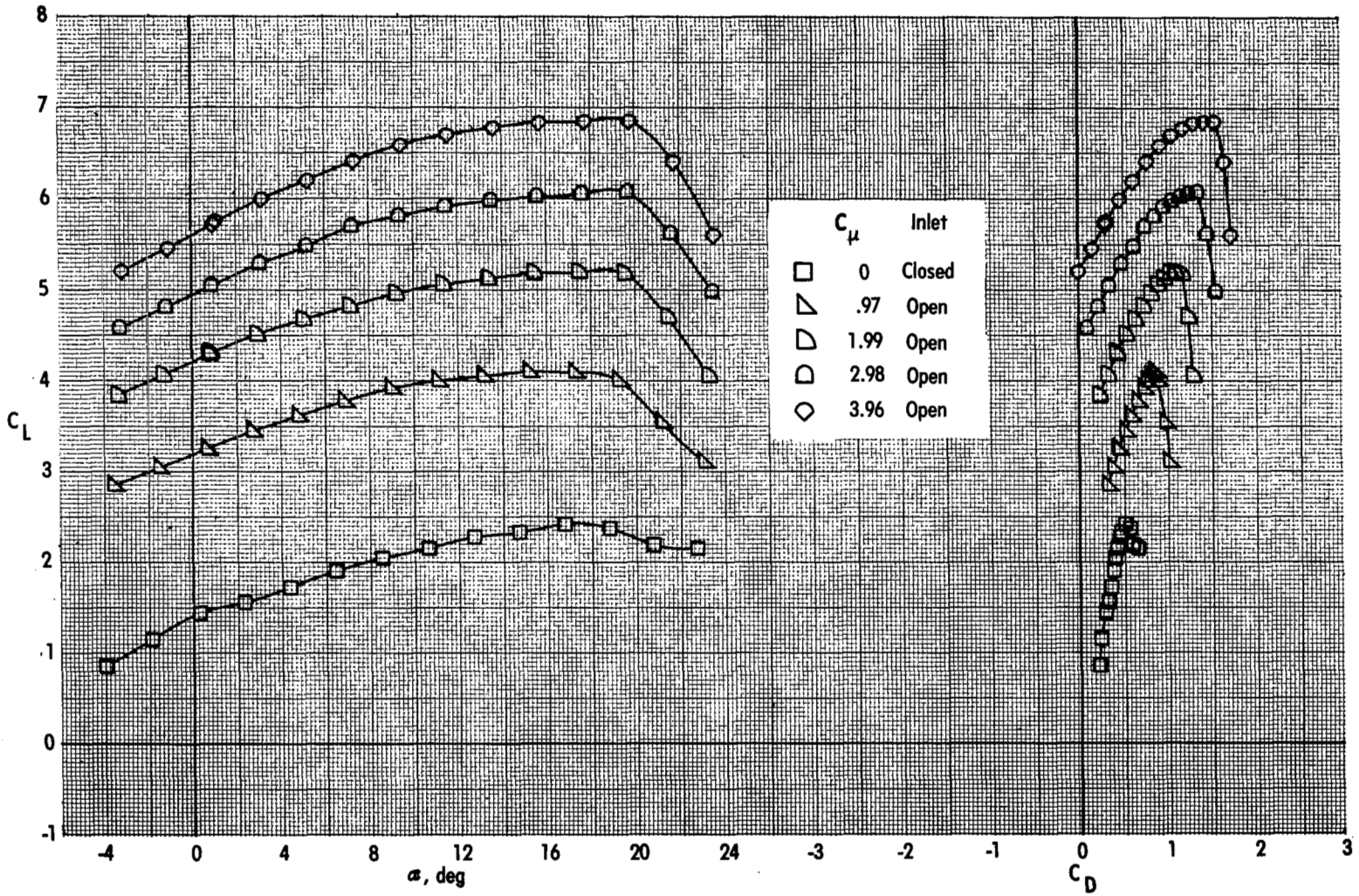

Figure 19.- Effect of thrust coefficient on longitudinal aerodynamic characteristics. Landing configuration; engine 75-0; tail off.

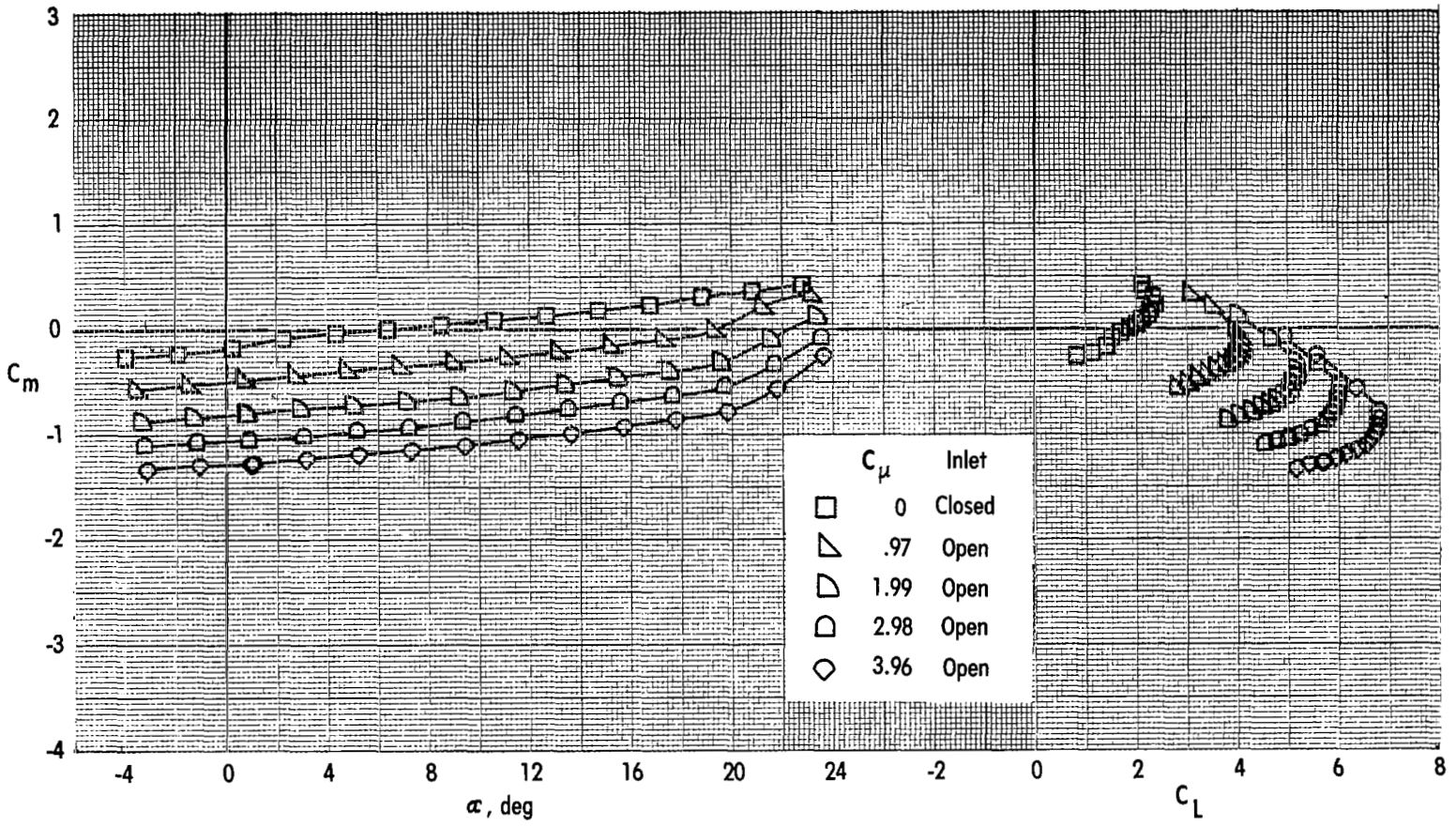

Figure 19.- Concluded.

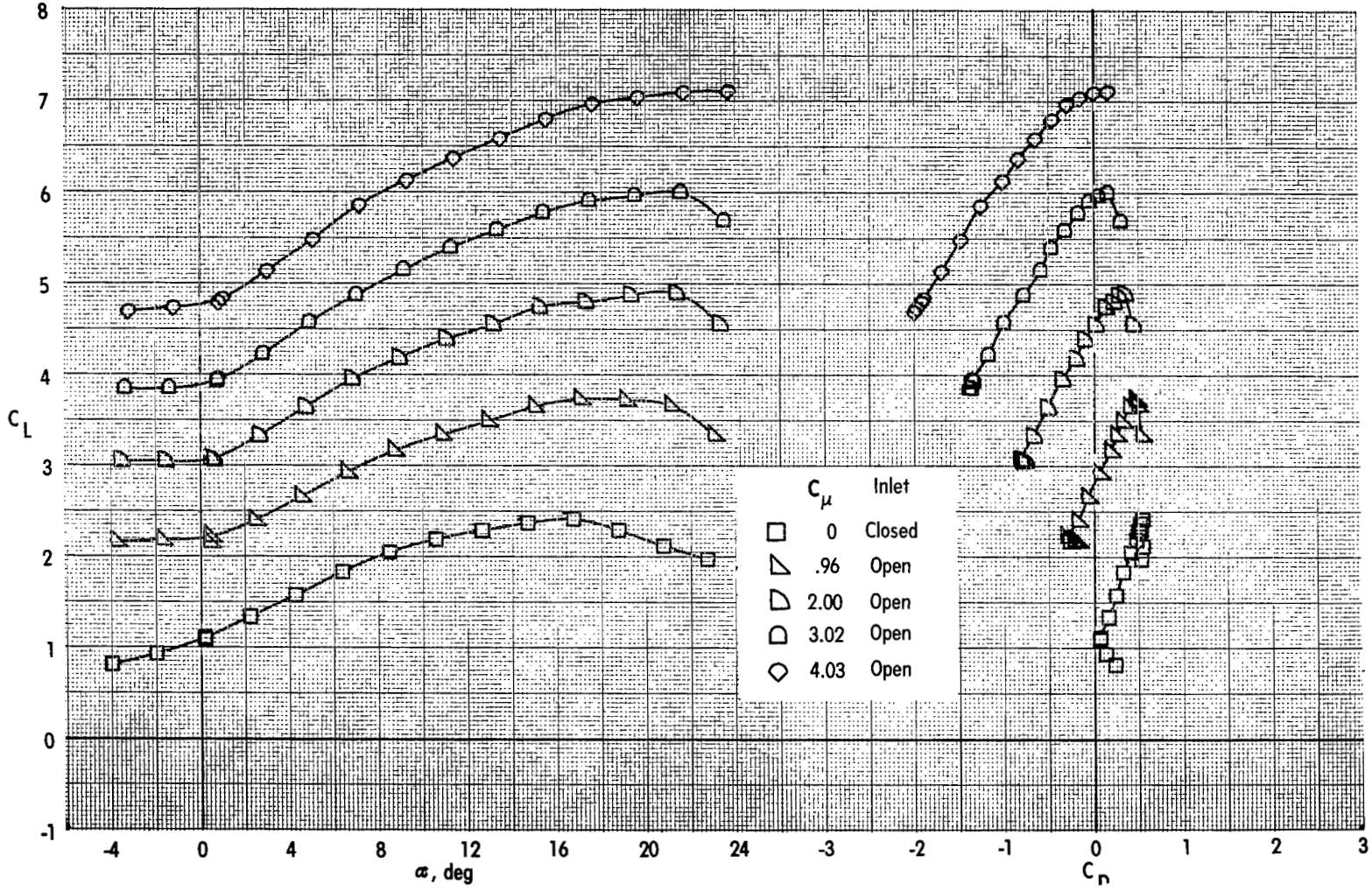

Figure 20.- Effect of thrust coefficient on longitudinal aerodynamic characteristics. Landing configuration; engine 75-45; tail off.

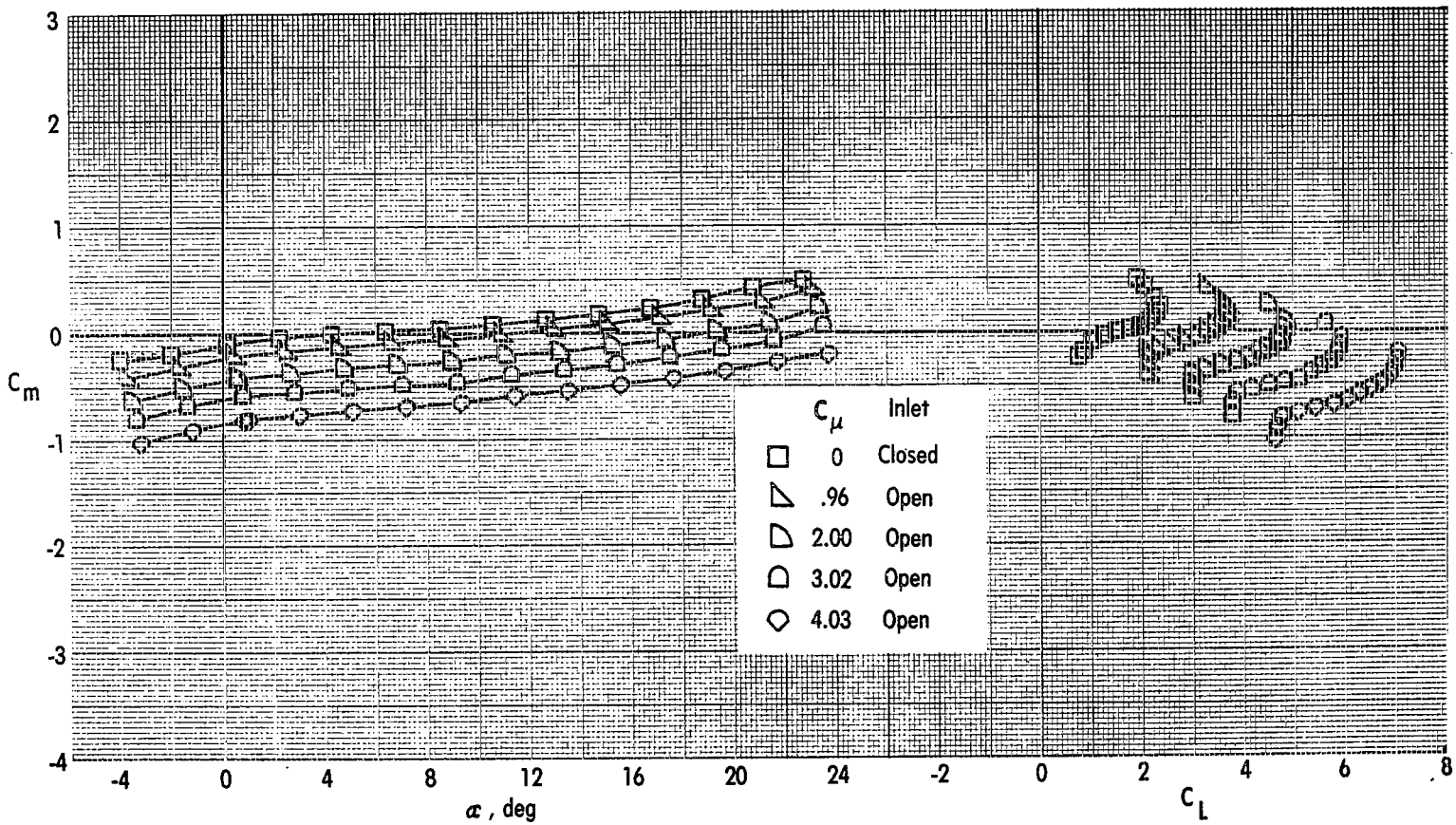

Figure 20.- Concluded.

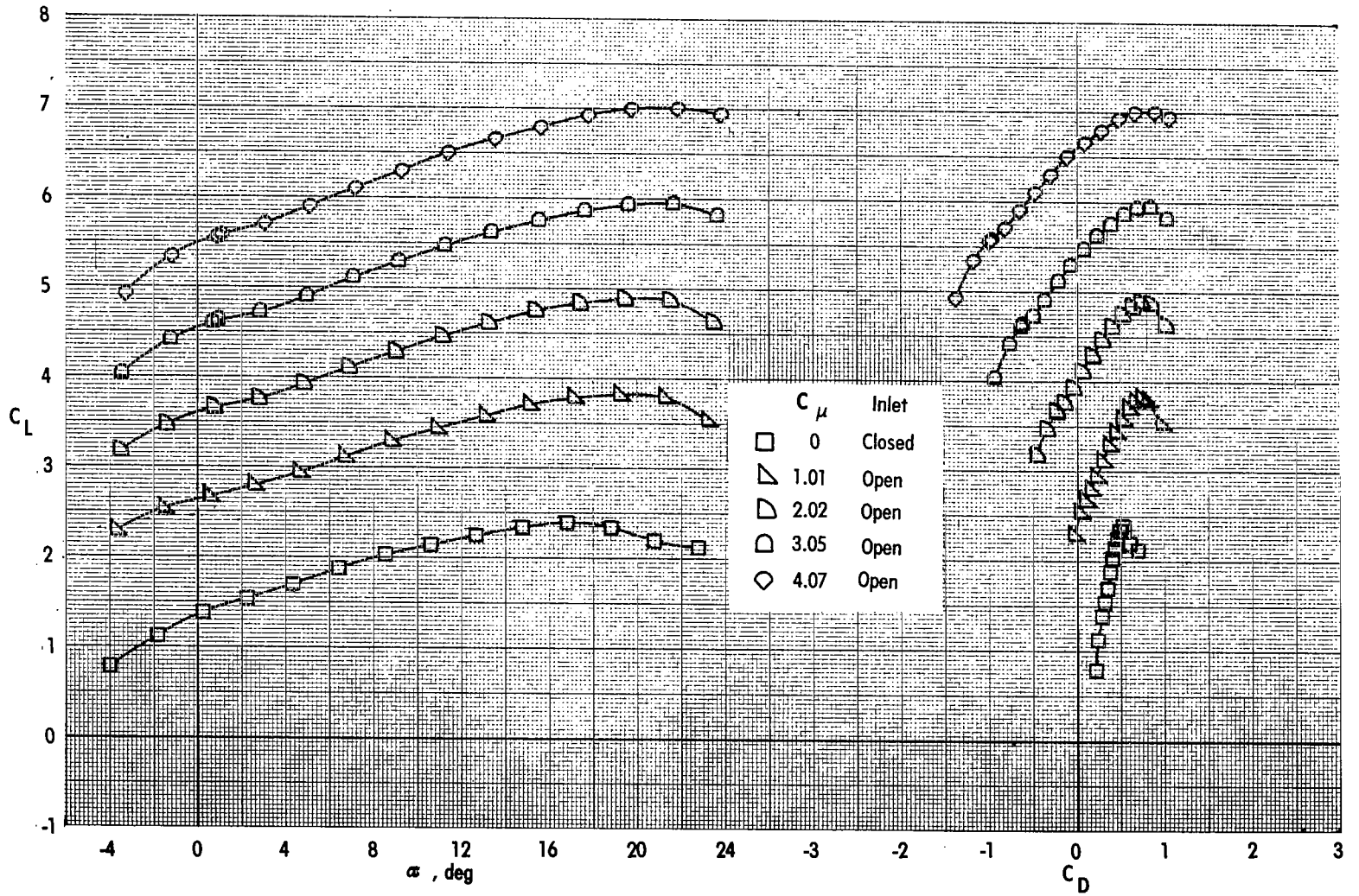

Figure 21.- Effect of thrust coefficient on longitudinal aerodynamic characteristics. Landing configuration; engine 75-65; tail off.

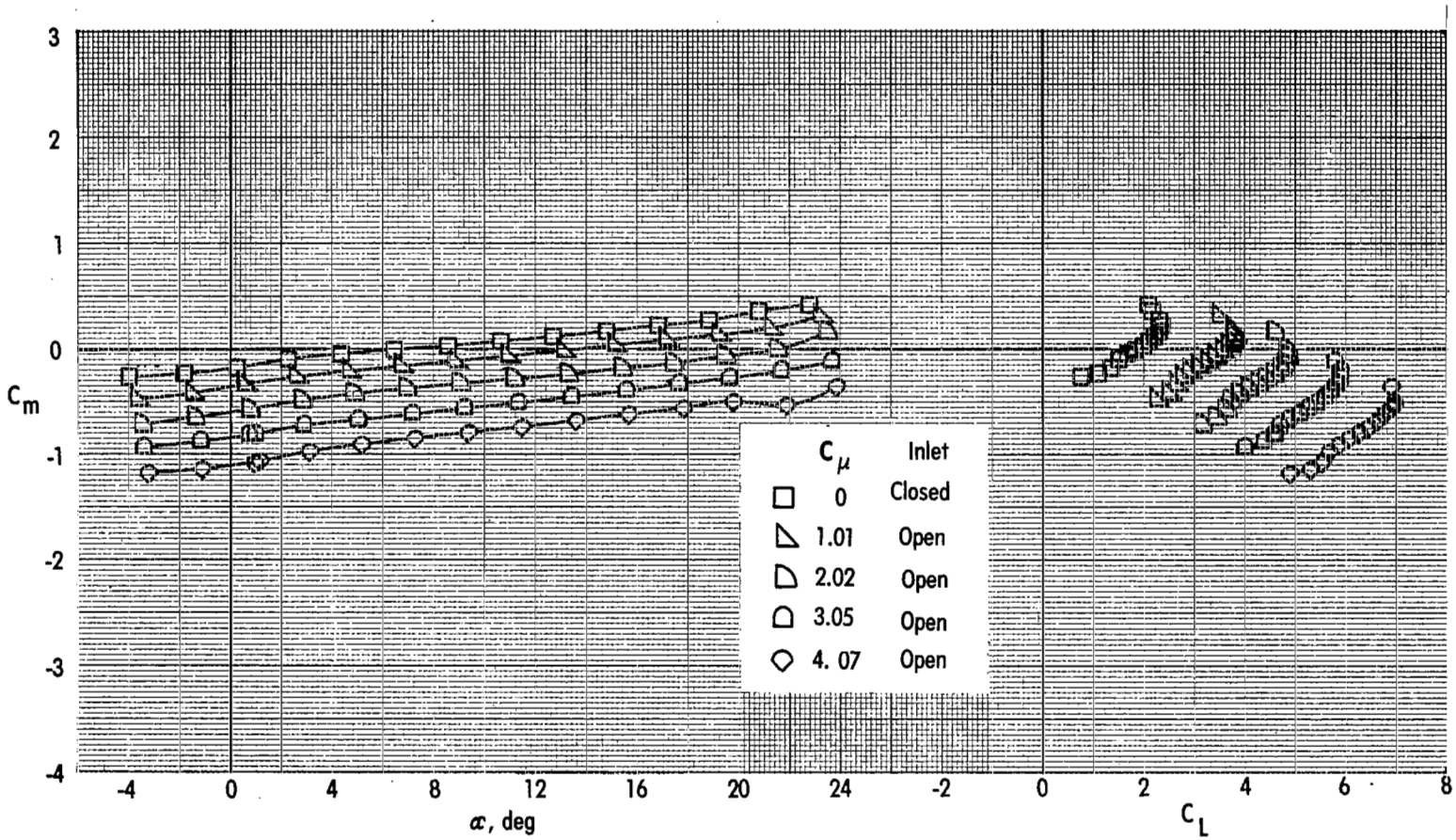

Figure 21.- Concluded.

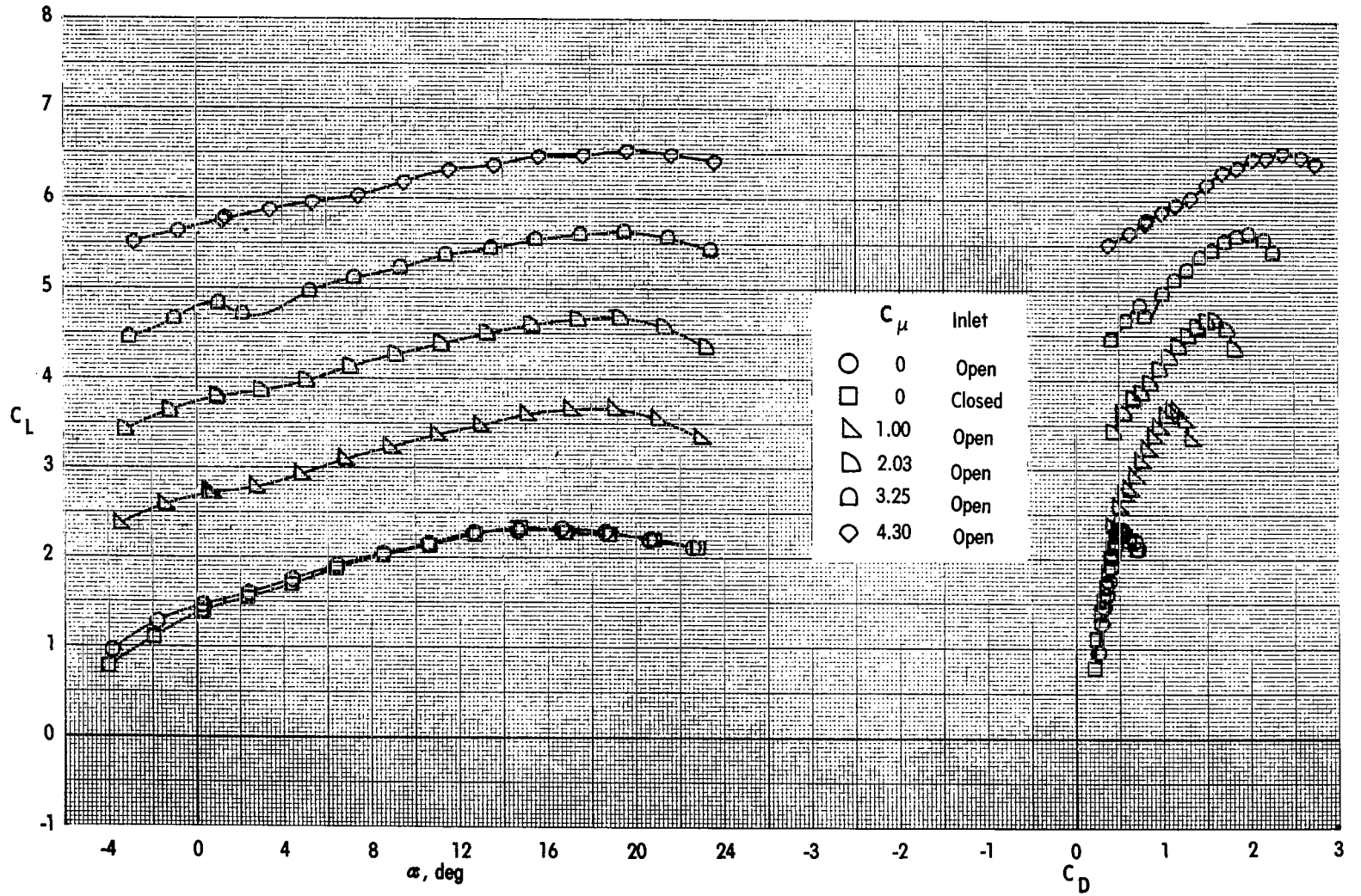

Figure 22.- Effect of thrust coefficient on longitudinal aerodynamic characteristics. Landing configuration; engine 75-90; tail off.

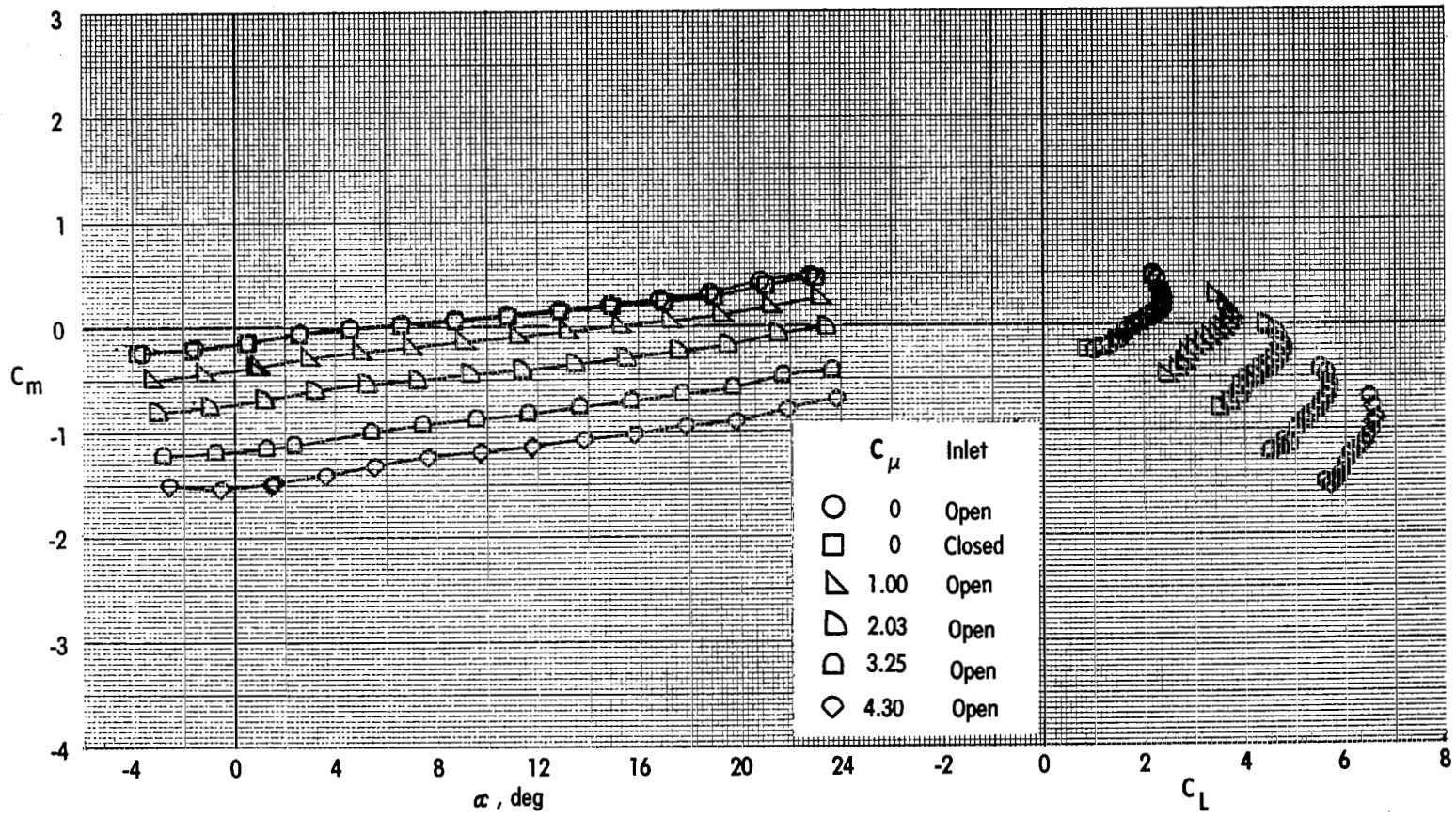

Figure 22.- Concluded.

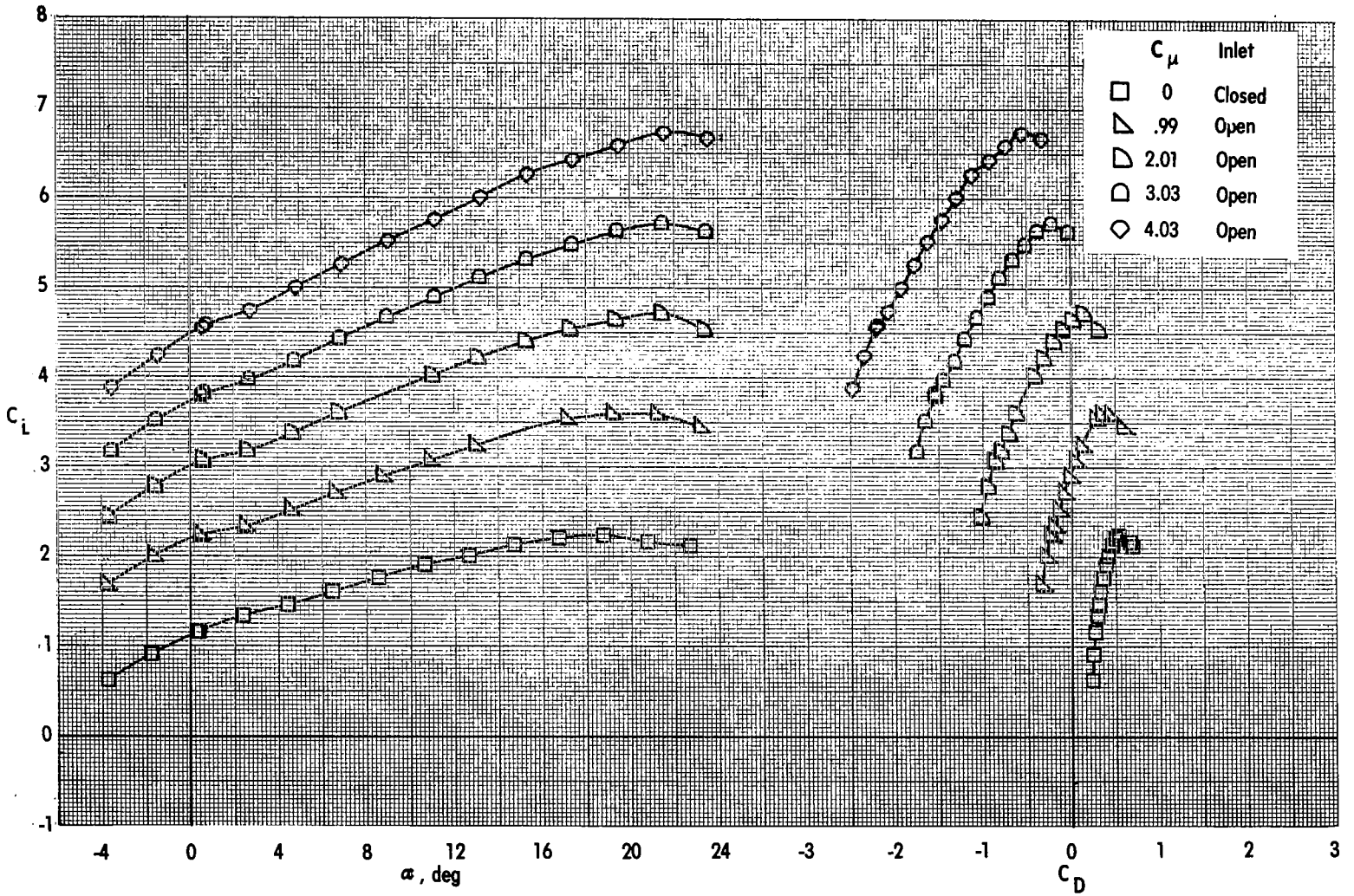

Figure 23.- Effect of thrust coefficient on longitudinal aerodynamic characteristics. Landing configuration; engine 110-45; tail off.

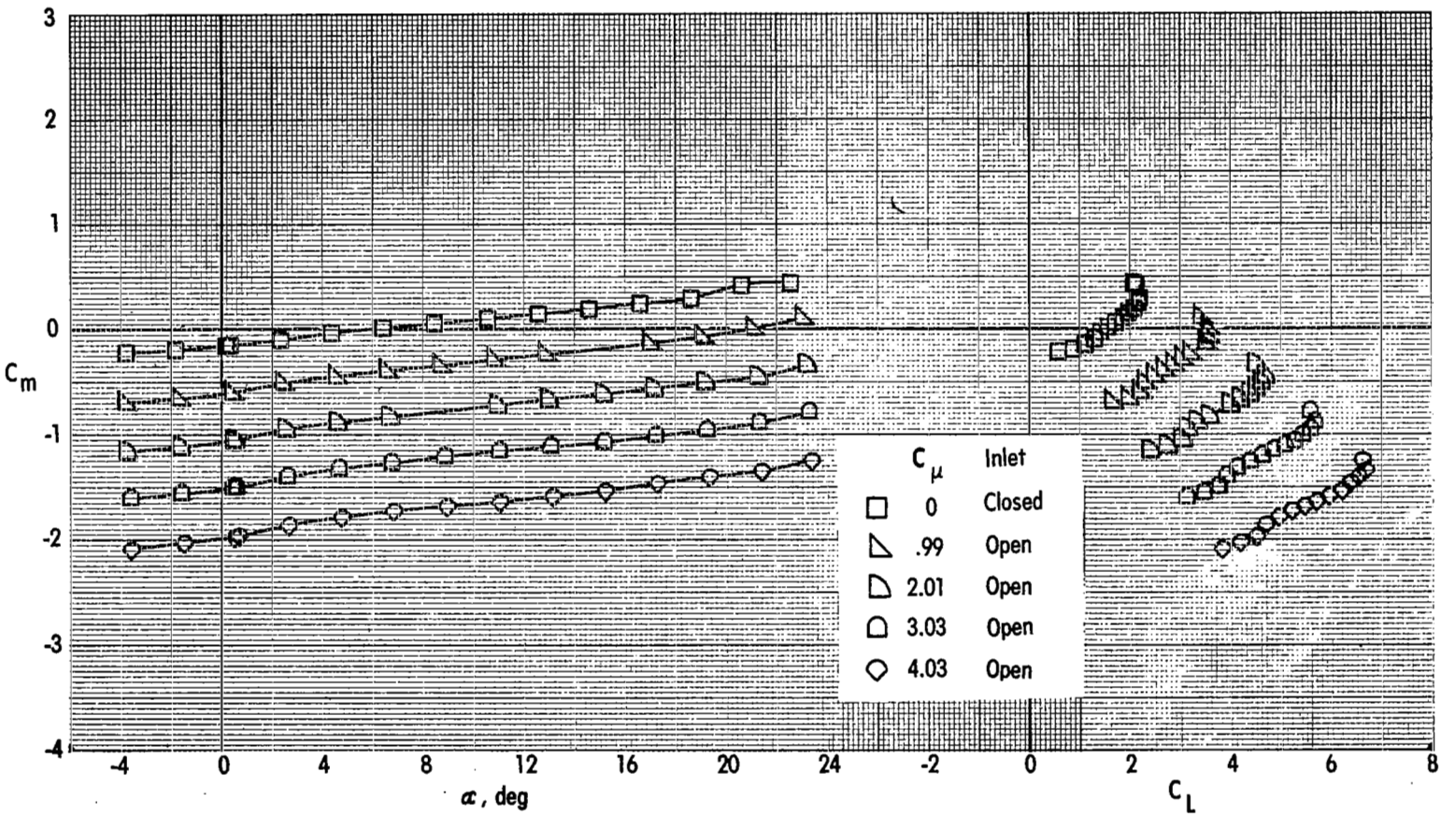

Figure 23.- Concluded.

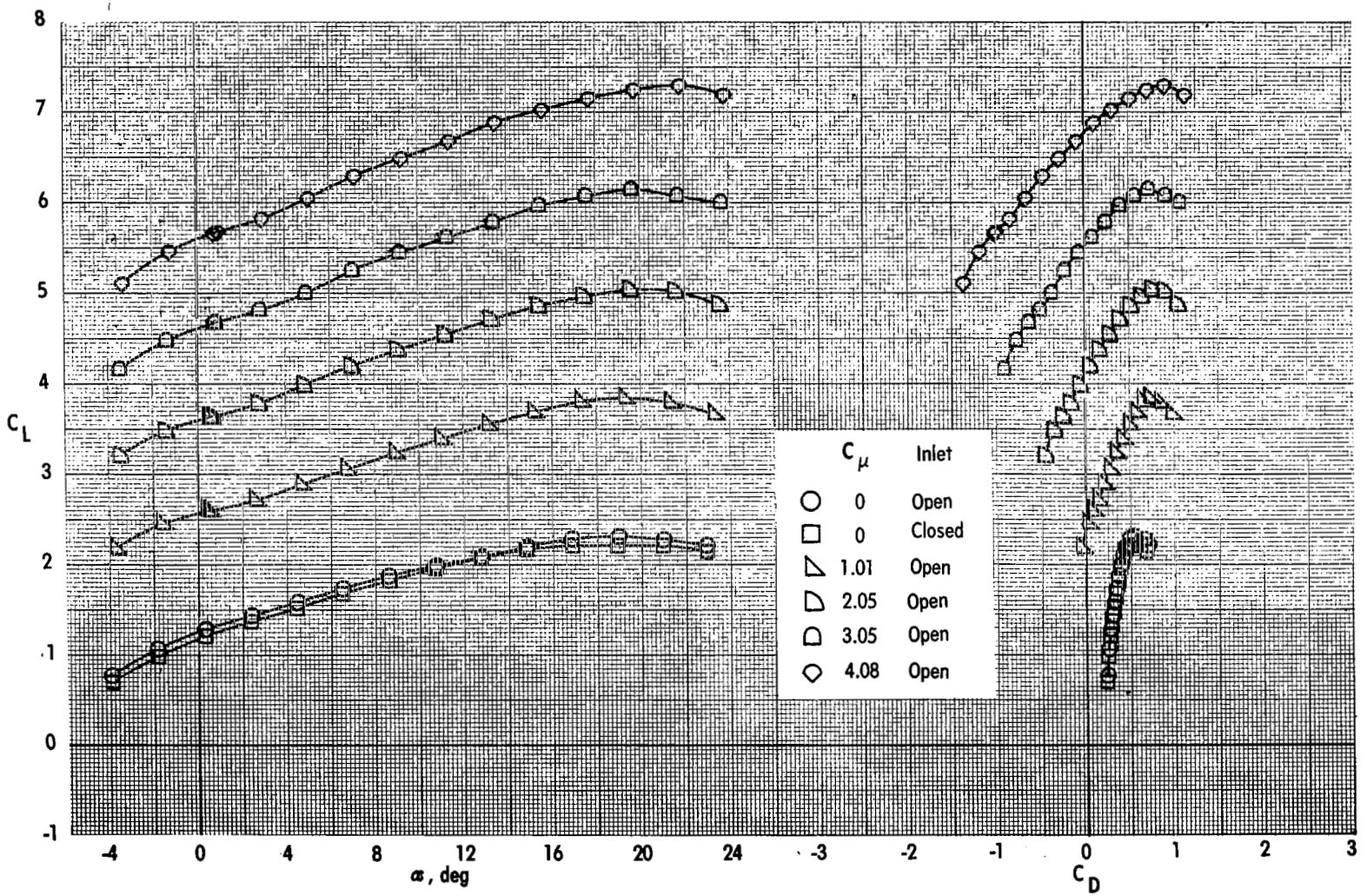

Figure 24.- Effect of thrust coefficient on longitudinal aerodynamic characteristics. Landing configuration; engine 110-65; tail off.

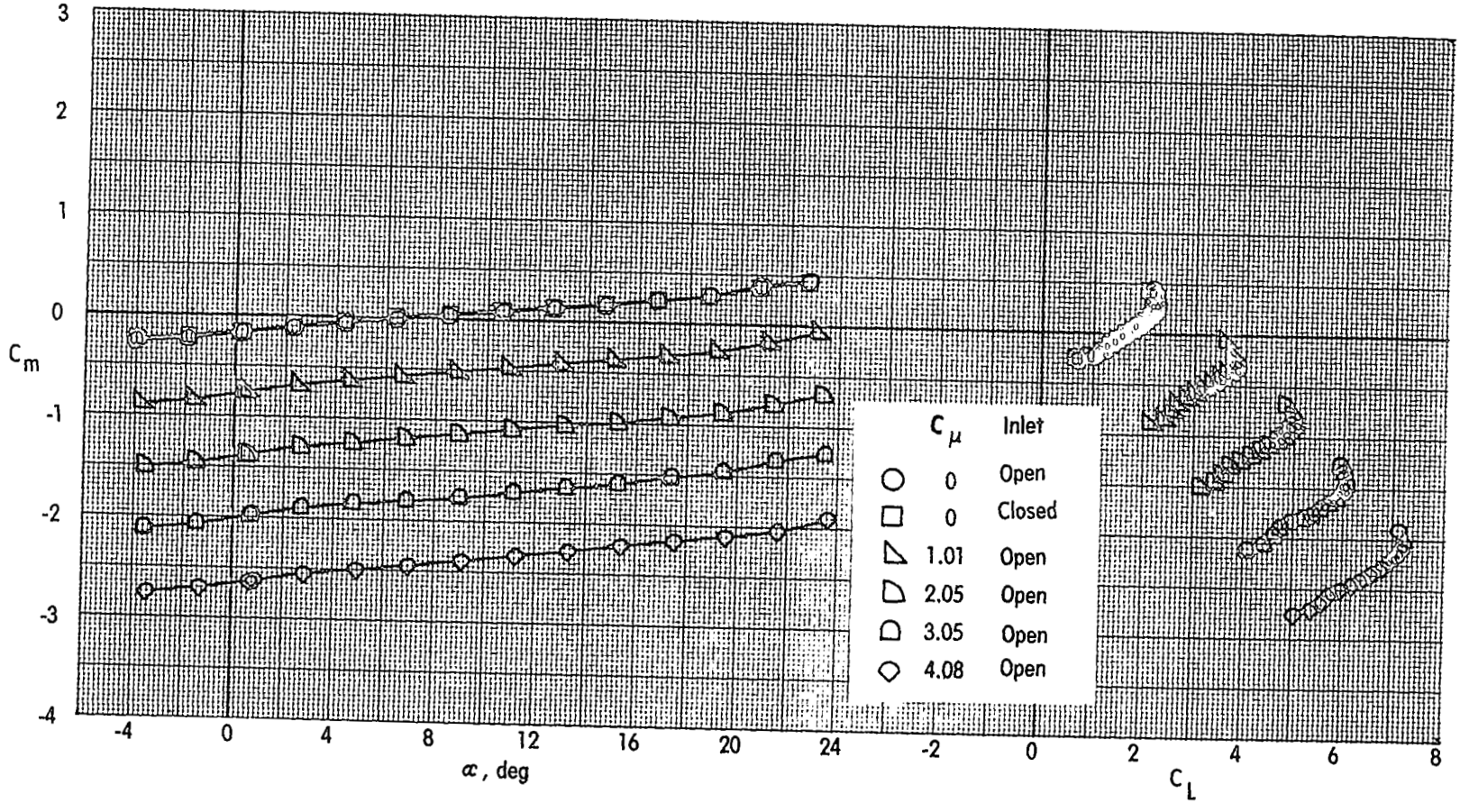

Figure 24.- Concluded.

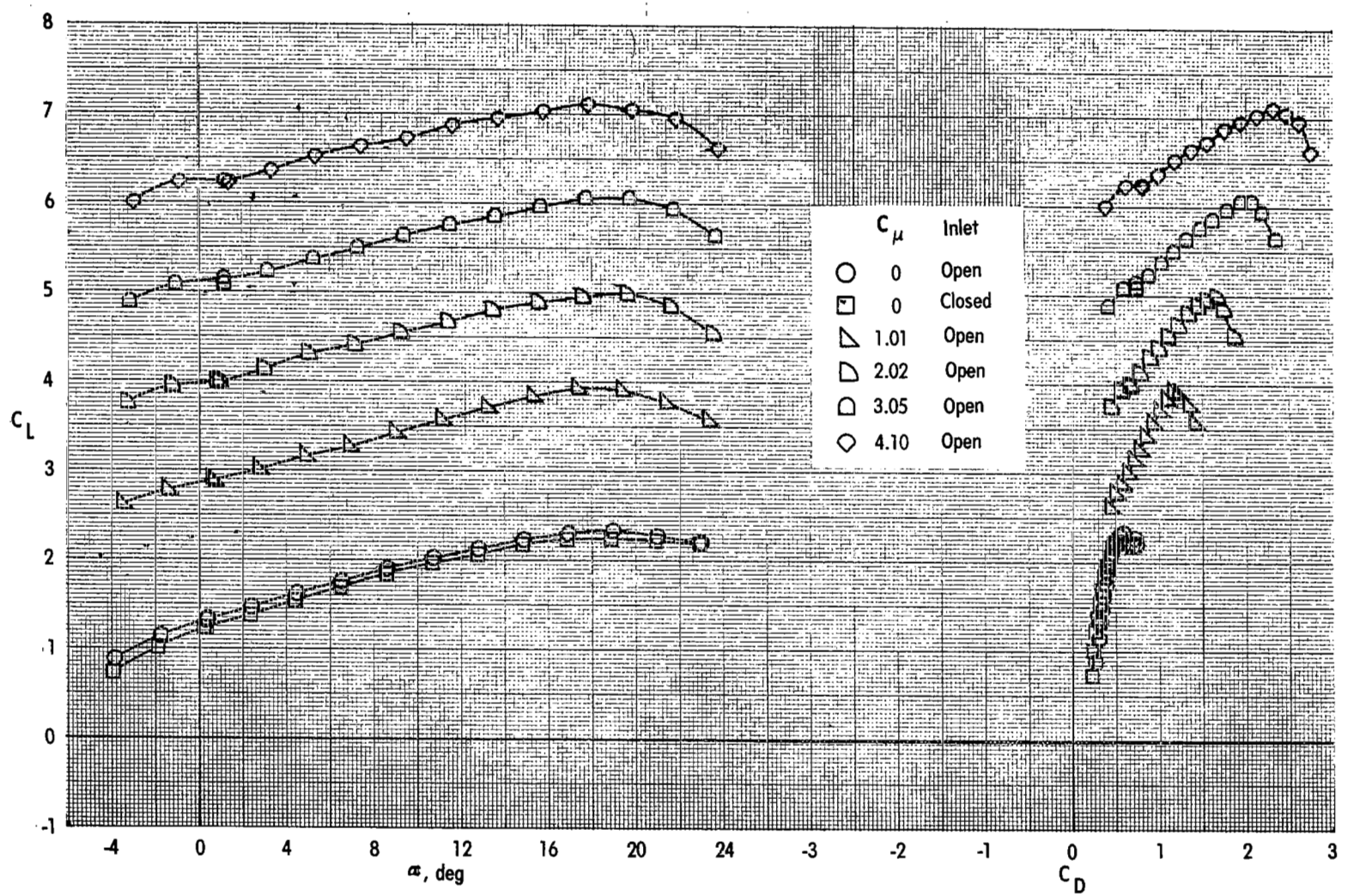

Figure 25.- Effect of thrust coefficient on longitudinal aerodynamic characteristics. Landing configuration; engine 110-90; tail off.

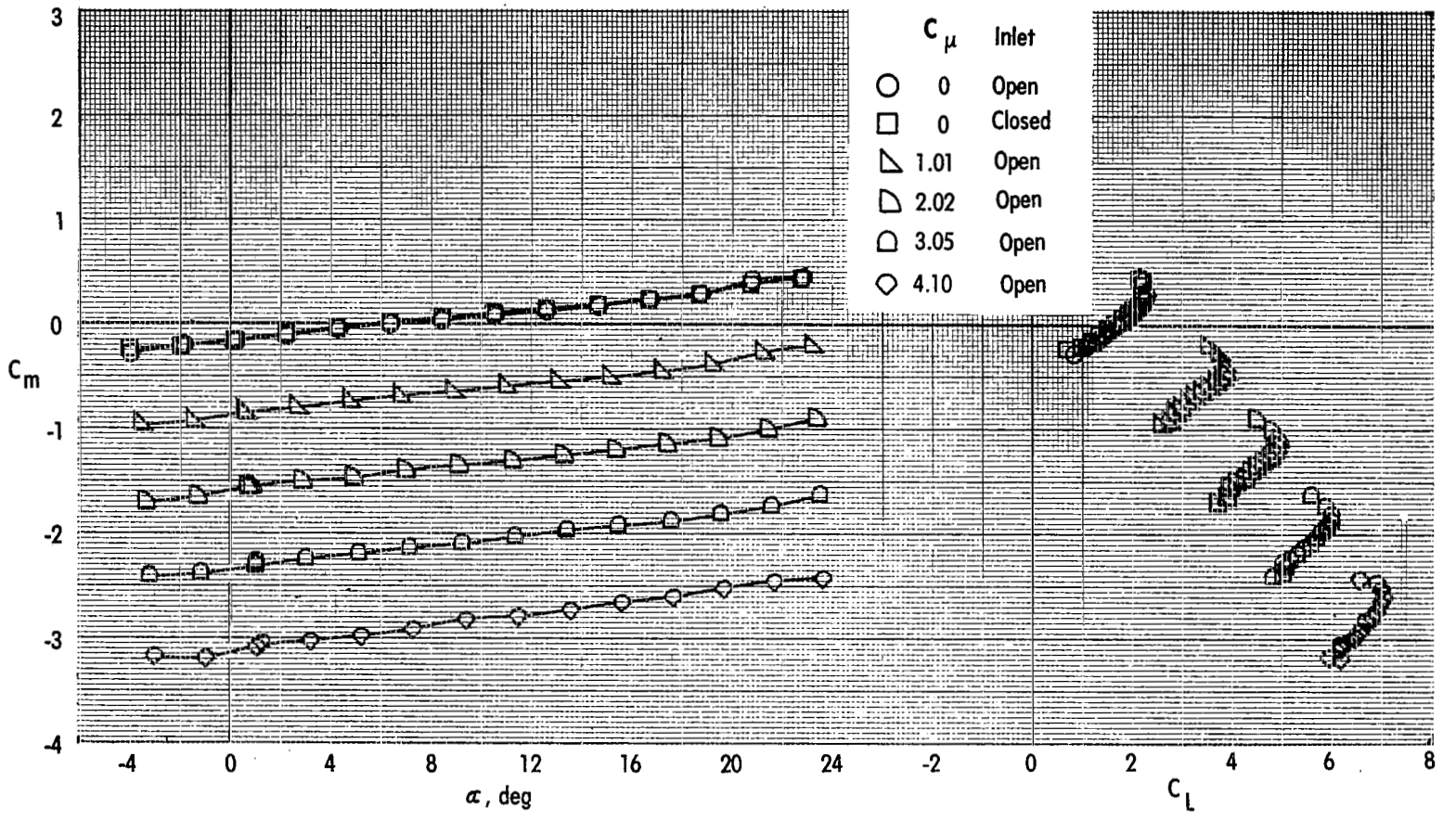

Figure 25.- Concluded.

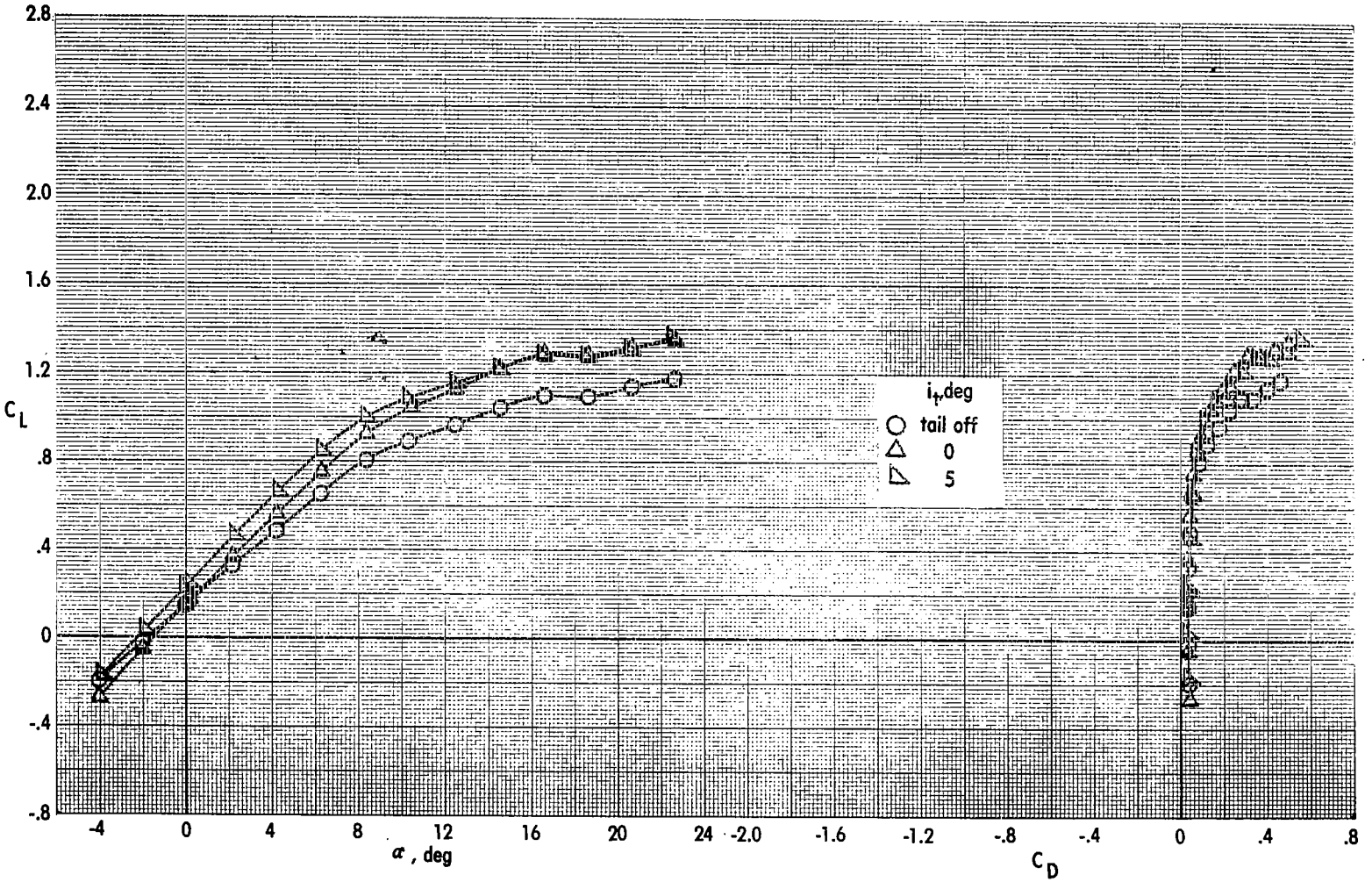

Figure 26.- Effect of tail incidence on longitudinal aerodynamic characteristics. Cruise configuration; basic engine; $C_\mu = 0$.

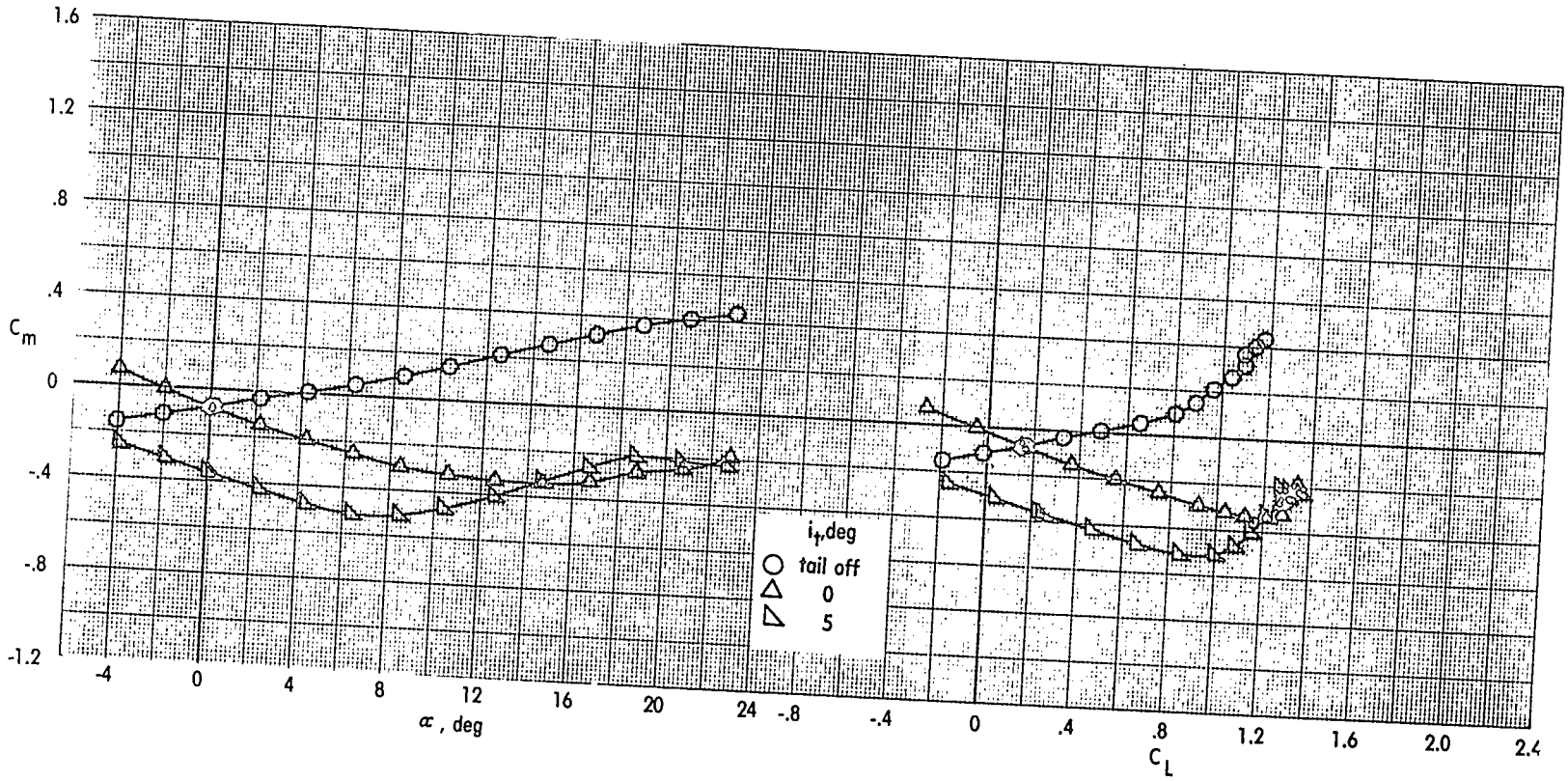

Figure 26.- Concluded.

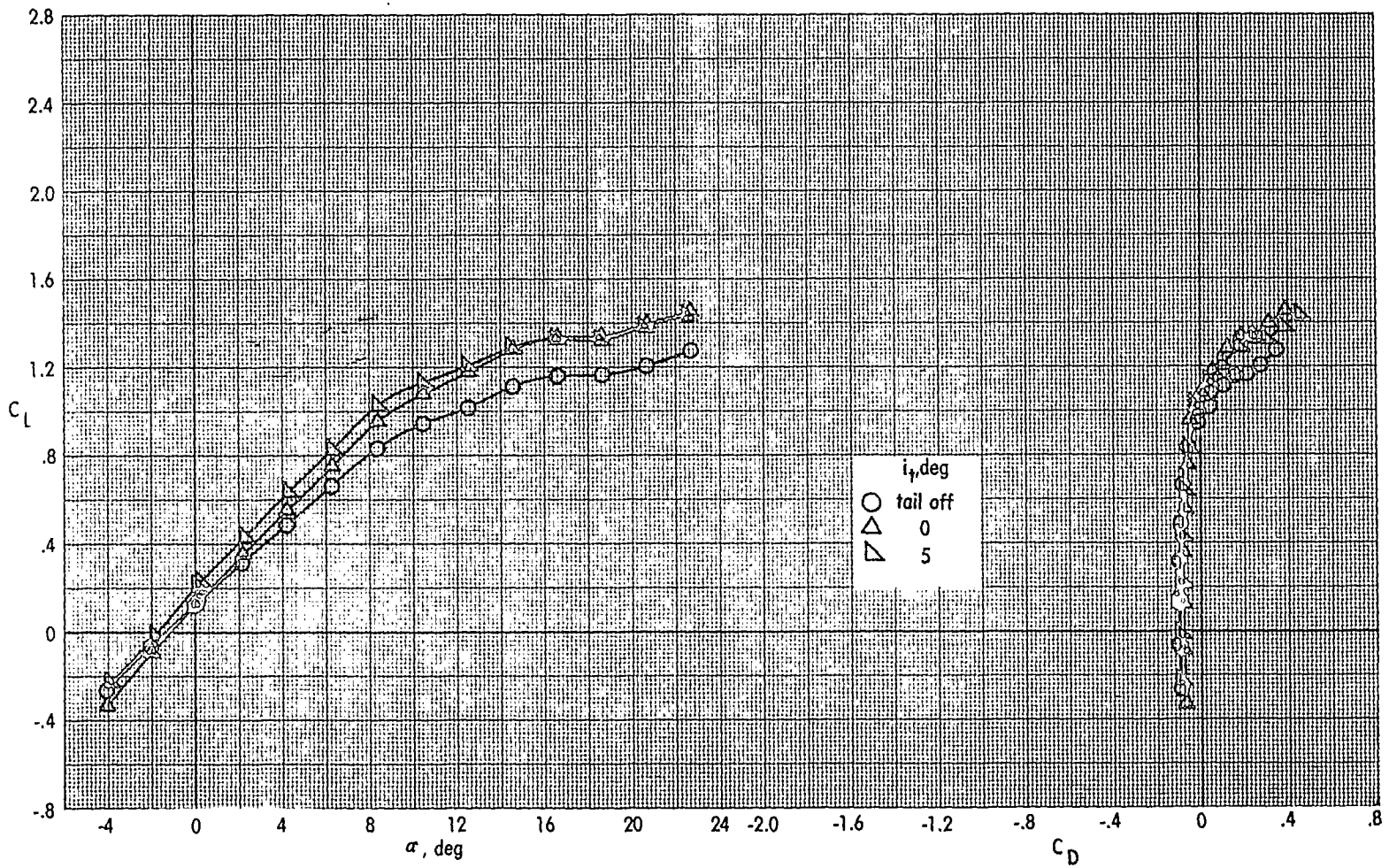

Figure 27.- Effect of tail incidence on longitudinal aerodynamic characteristics. Cruise configuration; basic engine; $C_\mu = 0.19$.

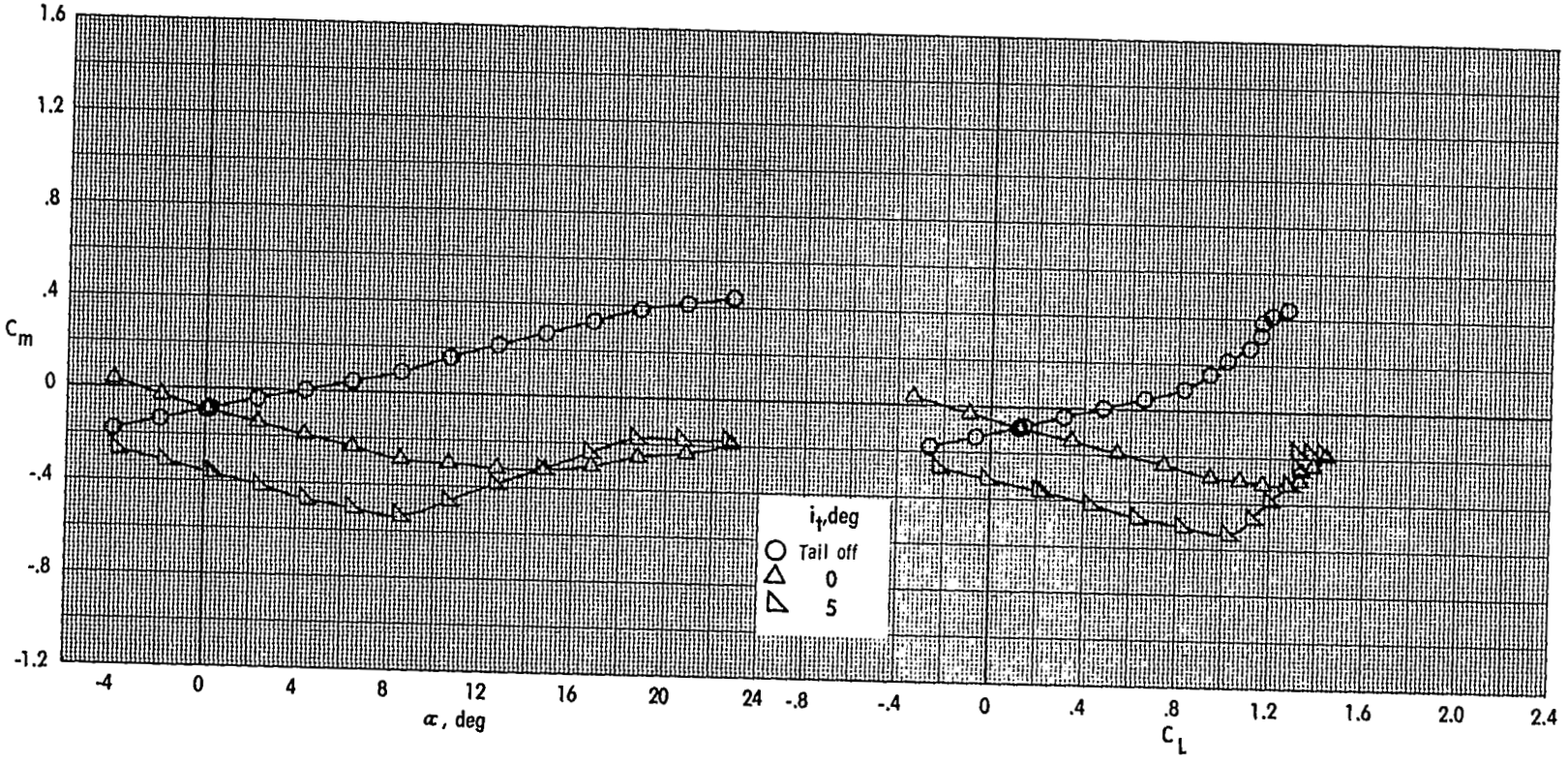

Figure 27.- Concluded.

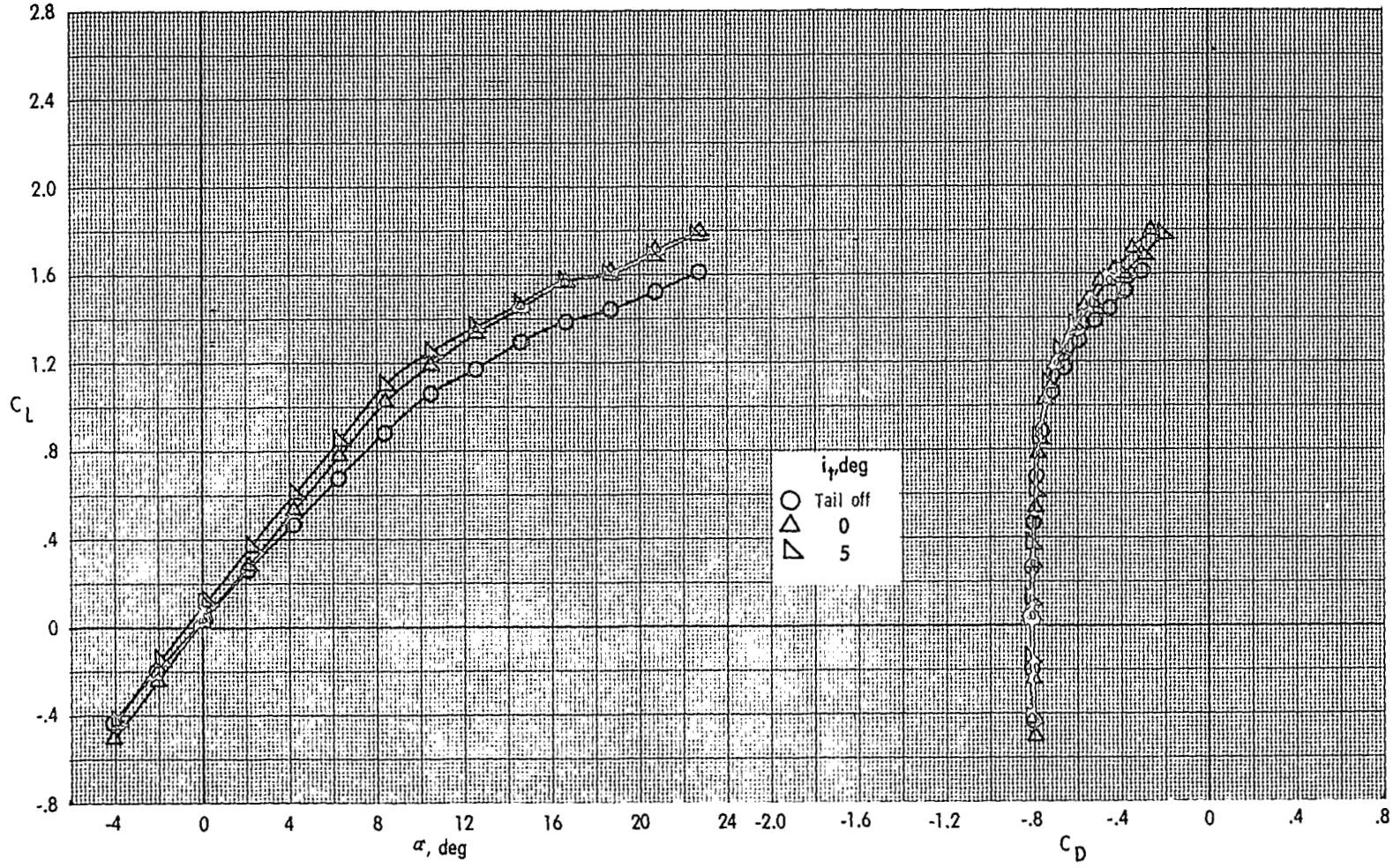

Figure 28.- Effect of tail incidence on longitudinal aerodynamic characteristics. Cruise configuration; basic engine; C_μ = 0.97.

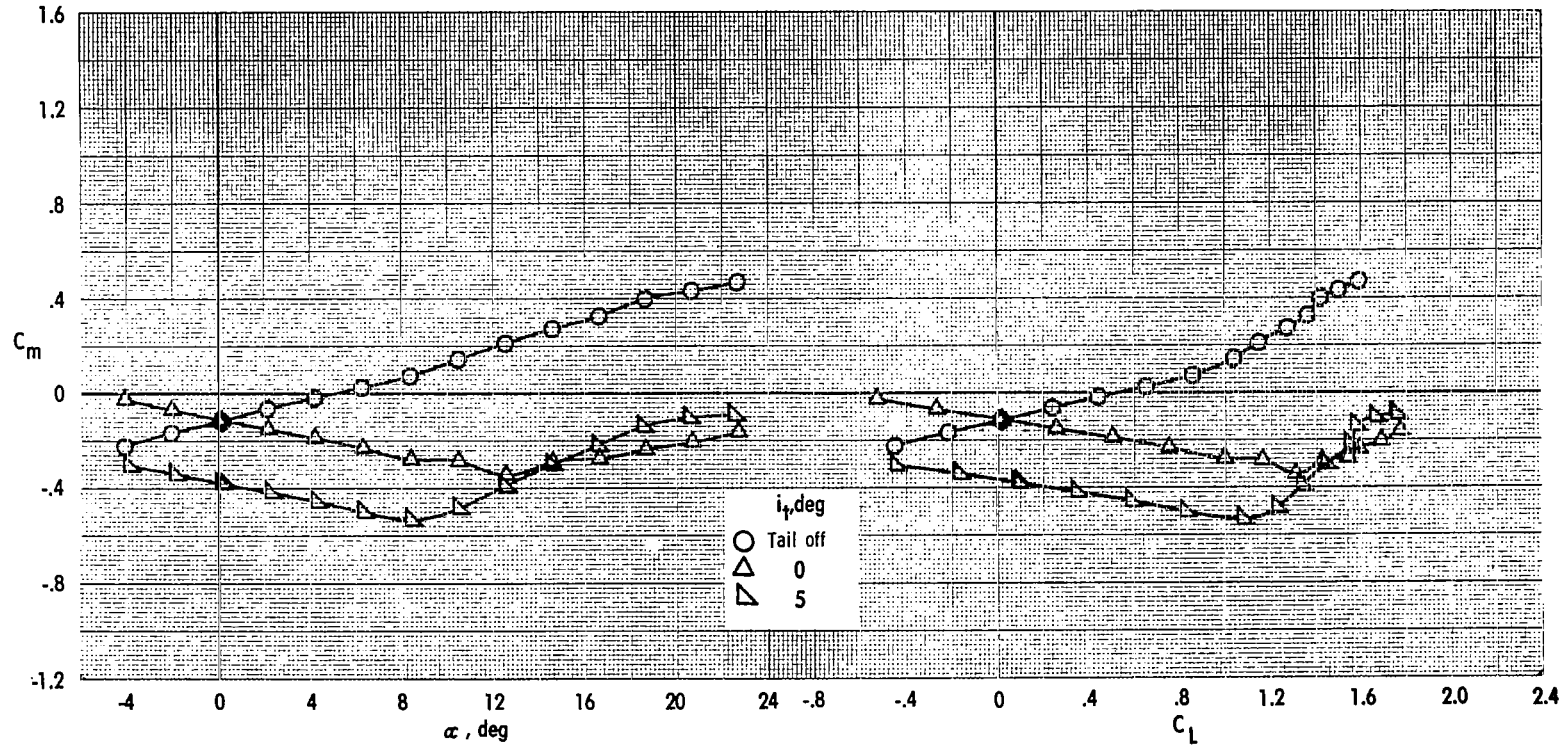

Figure 28.- Concluded.

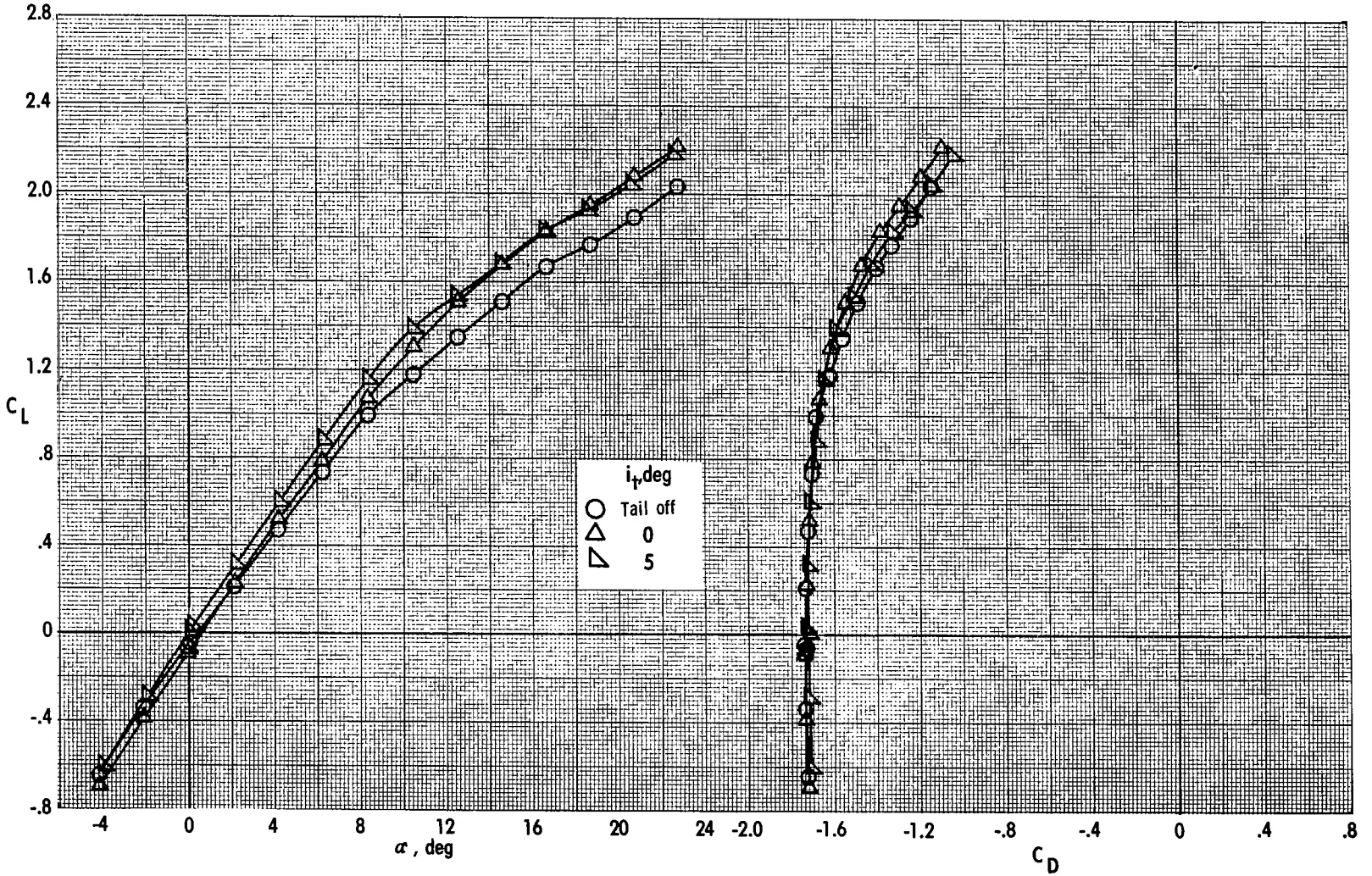

Figure 29.- Effect of tail incidence on longitudinal aerodynamic characteristics. Cruise configuration; basic engine; C_μ = 1.99.

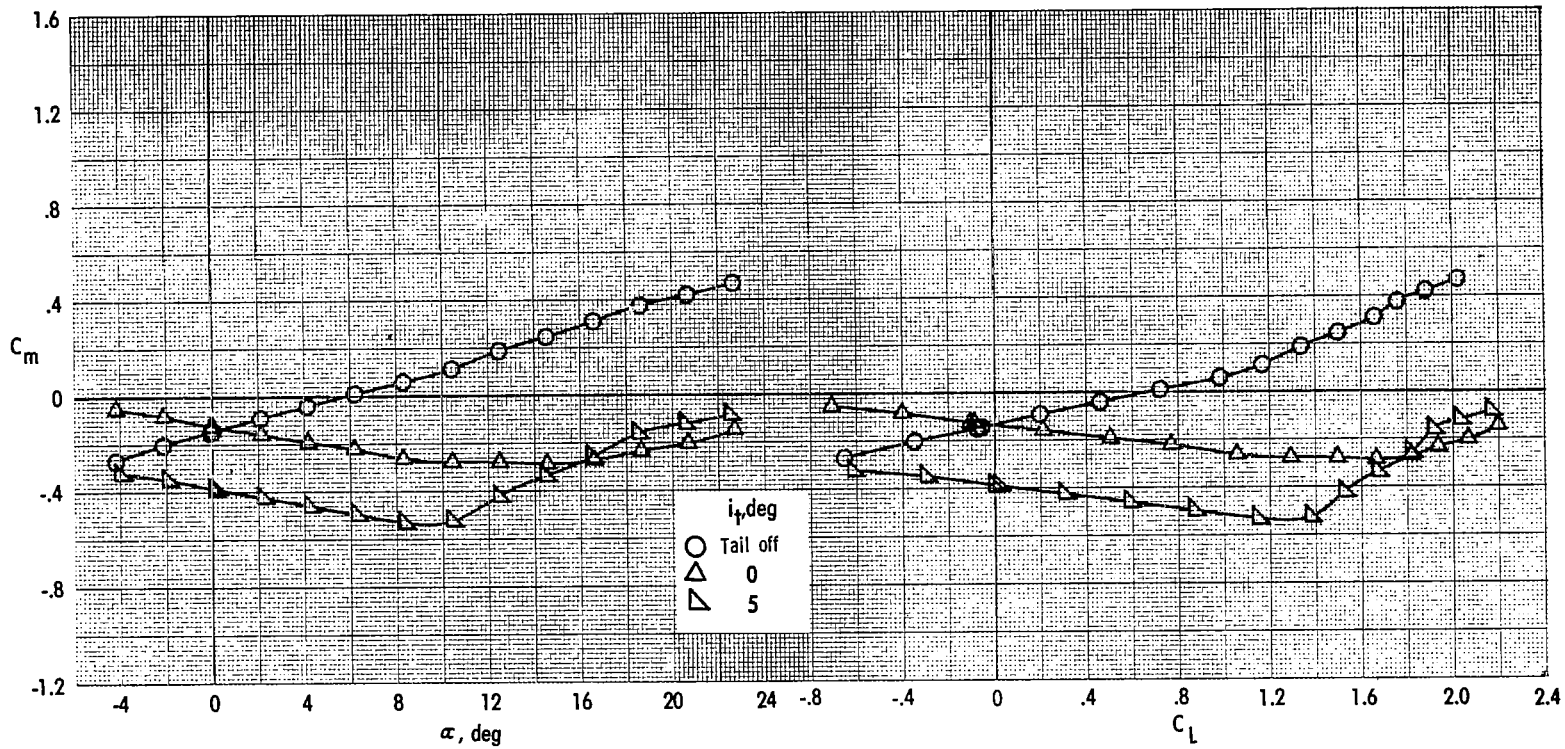

Figure 29.- Concluded.

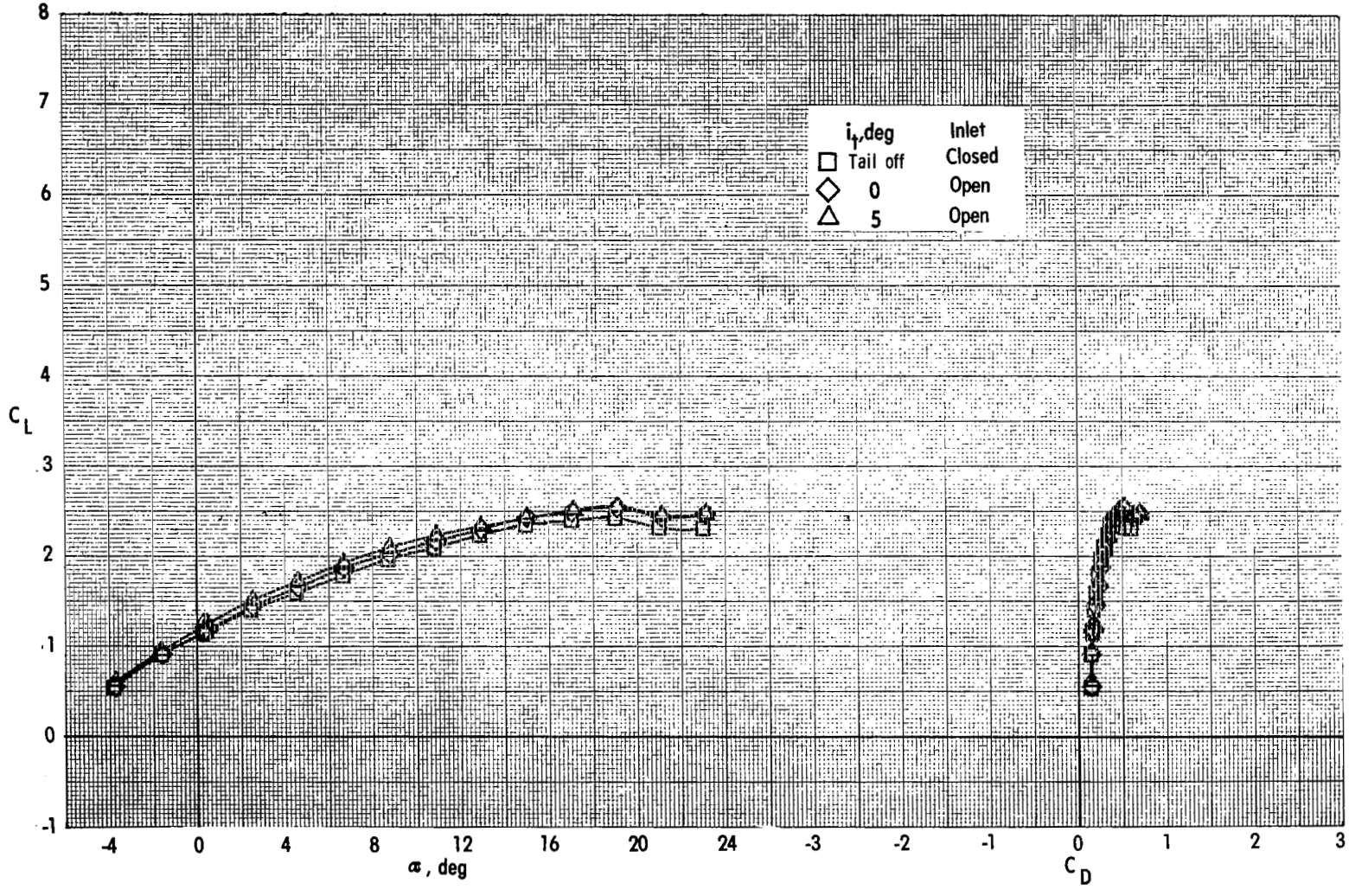

Figure 30.- Effect of tail incidence on longitudinal aerodynamic characteristics. Take-off configuration; basic engine; $C_\mu = 0$.

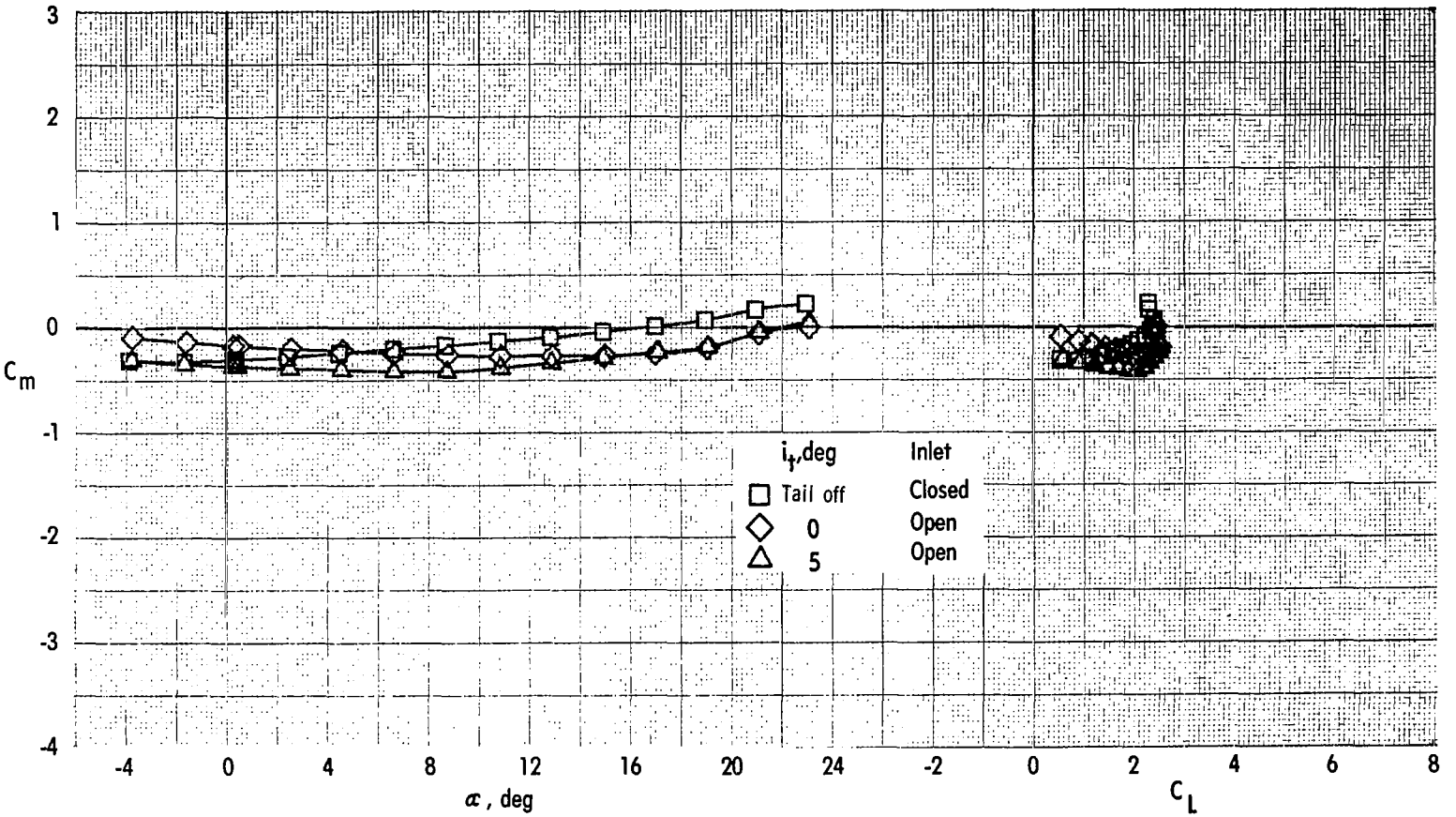

Figure 30.- Concluded.

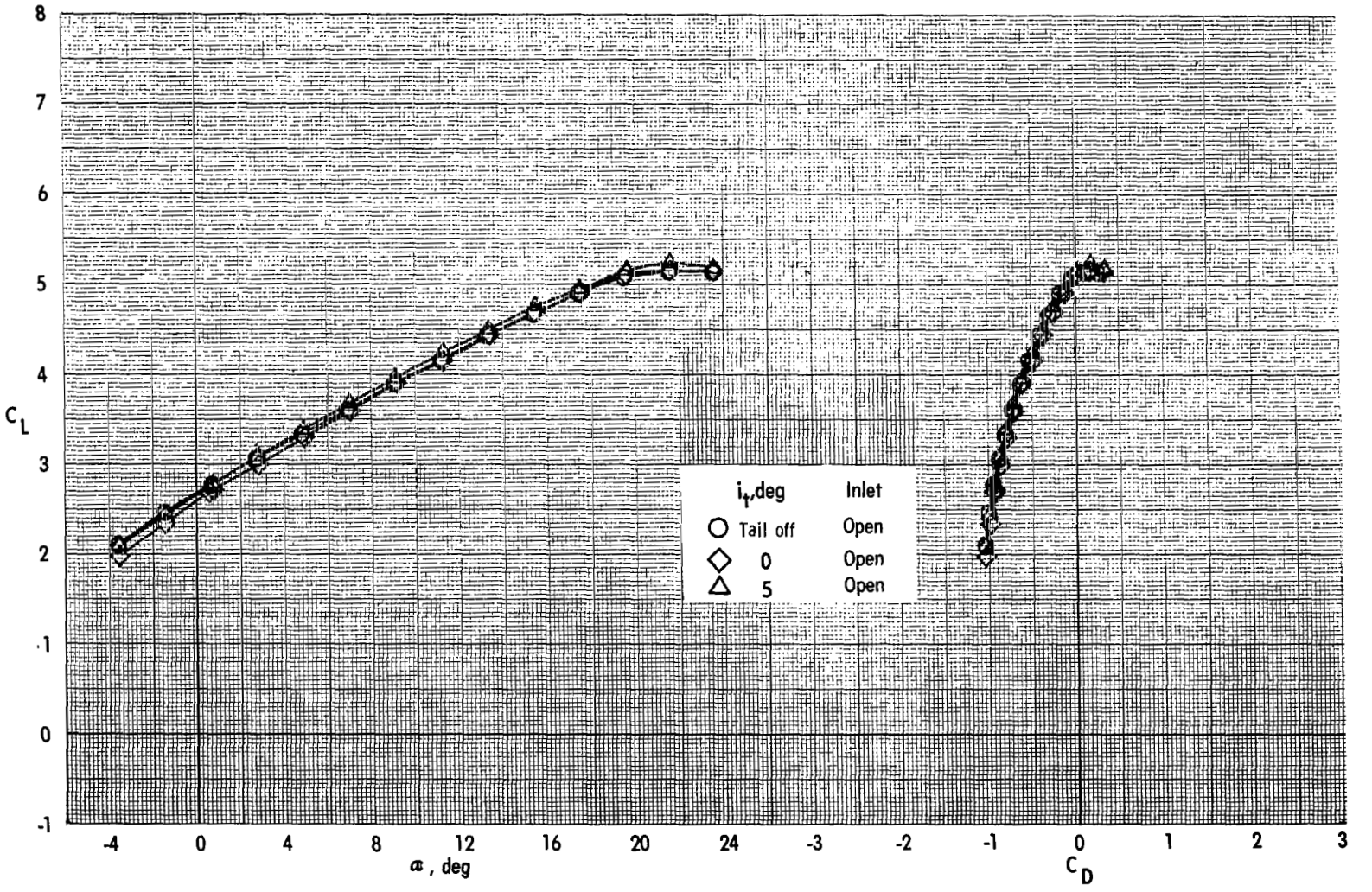

Figure 31.- Effect of tail incidence on longitudinal aerodynamic characteristics. Take-off configuration; basic engine; $C_\mu = 2.00$.

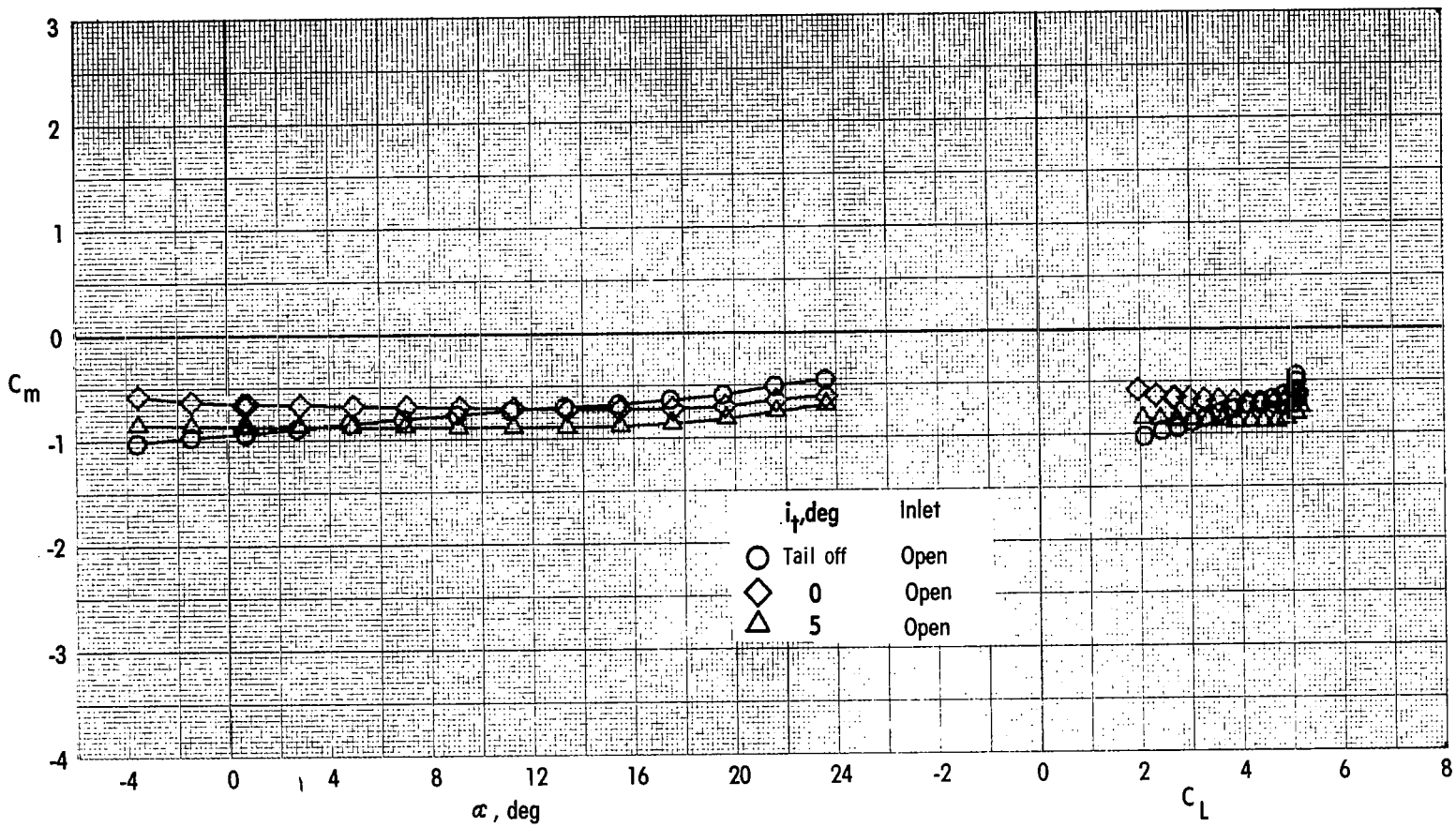

Figure 31.- Concluded.

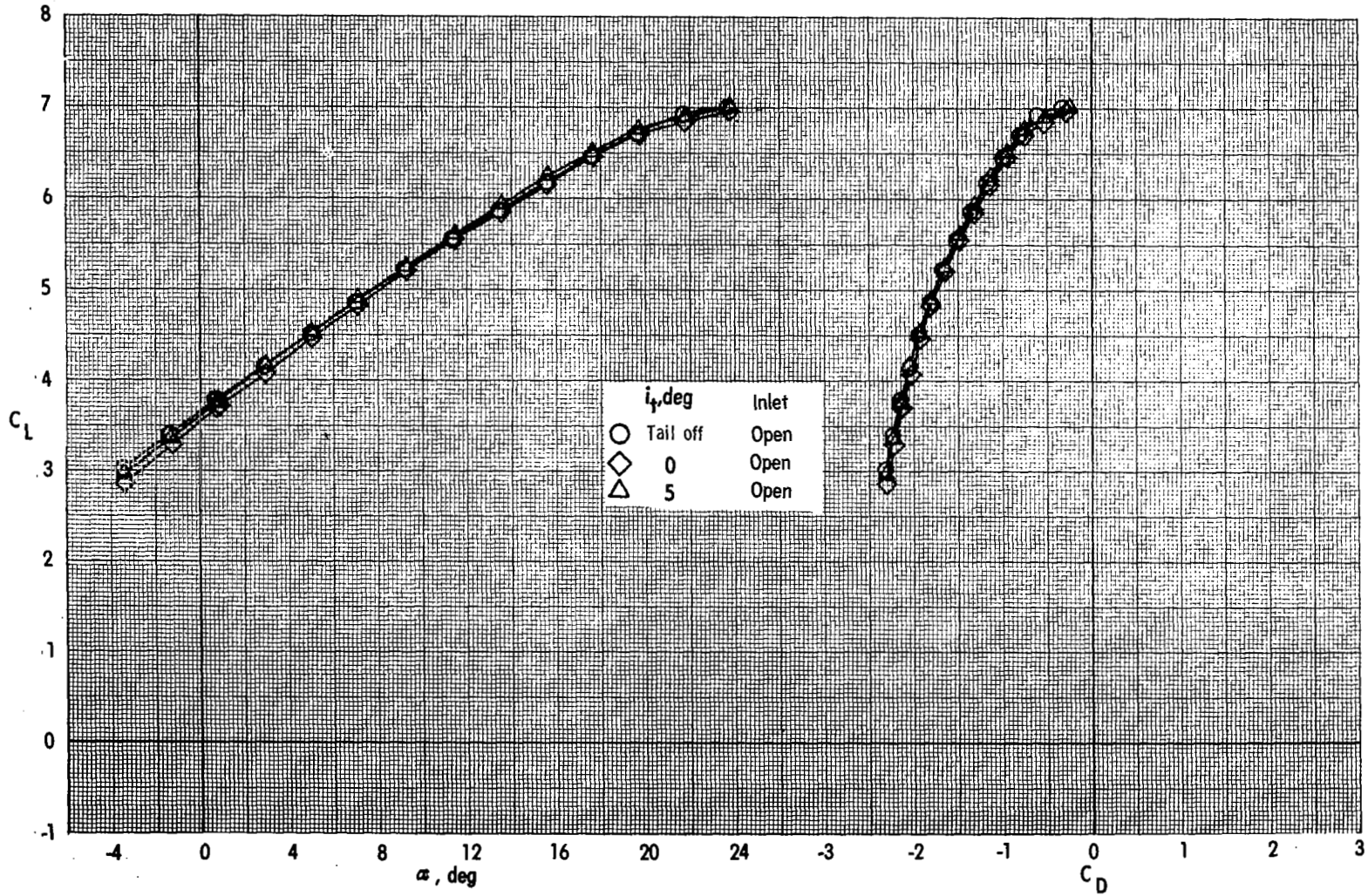

Figure 32.- Effect of tail incidence on longitudinal aerodynamic characteristics. Take-off configuration; basic engine; $C_\mu = 3.96$.

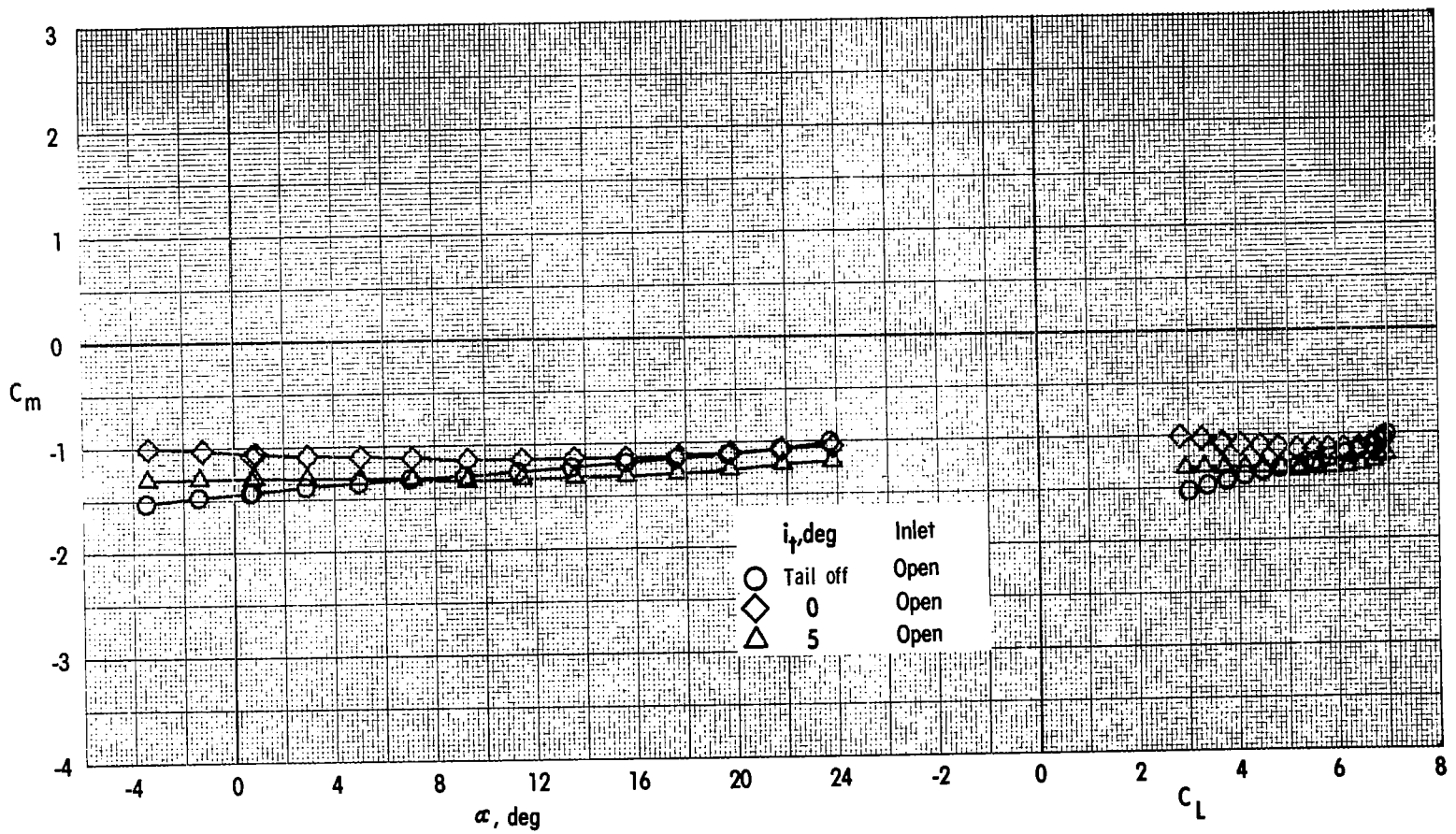

Figure 32.- Concluded.

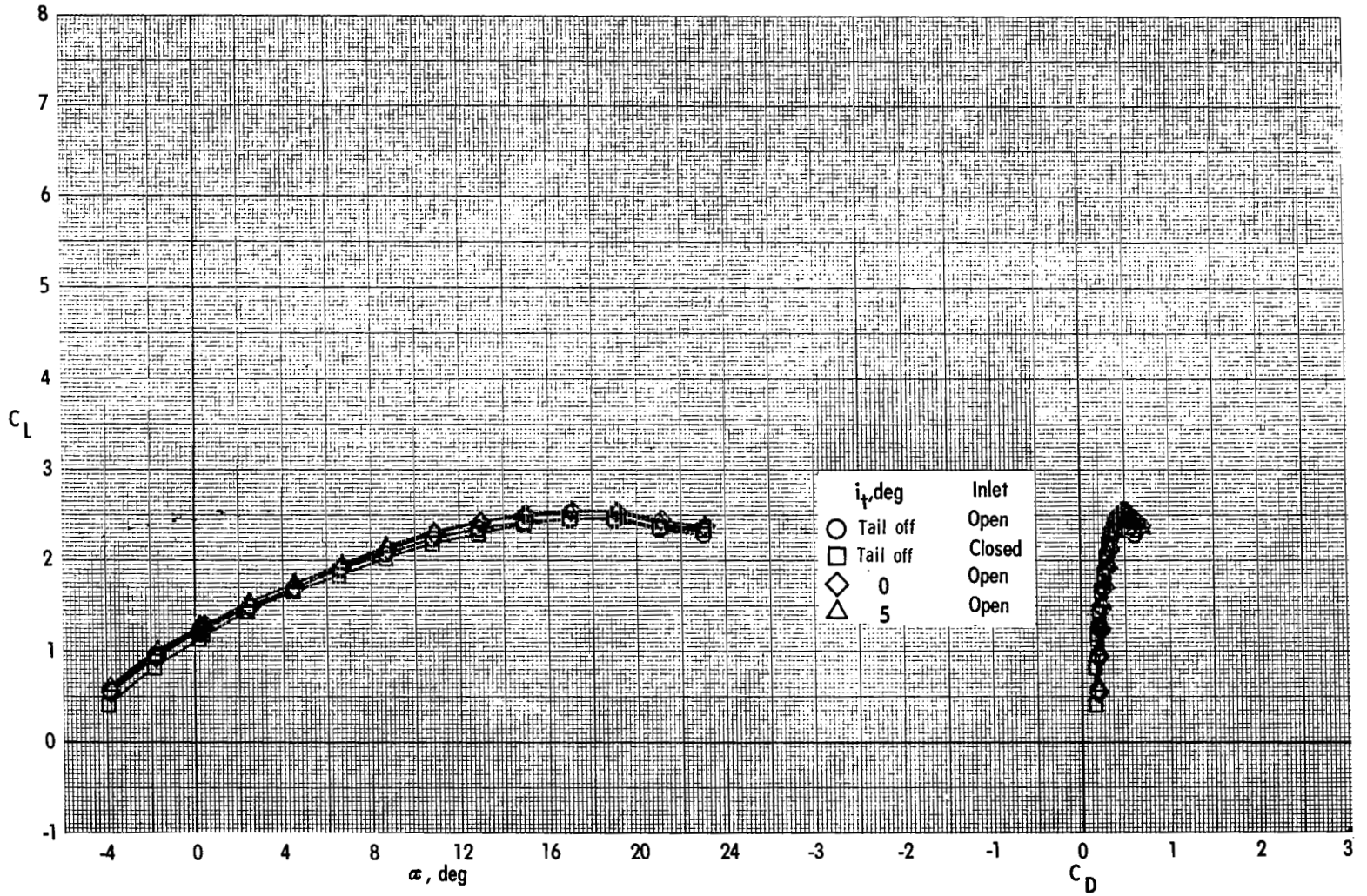

Figure 33.- Effect of tail incidence on longitudinal aerodynamic characteristics. Take-off configuration; engine 10-45; $C_\mu = 0$.

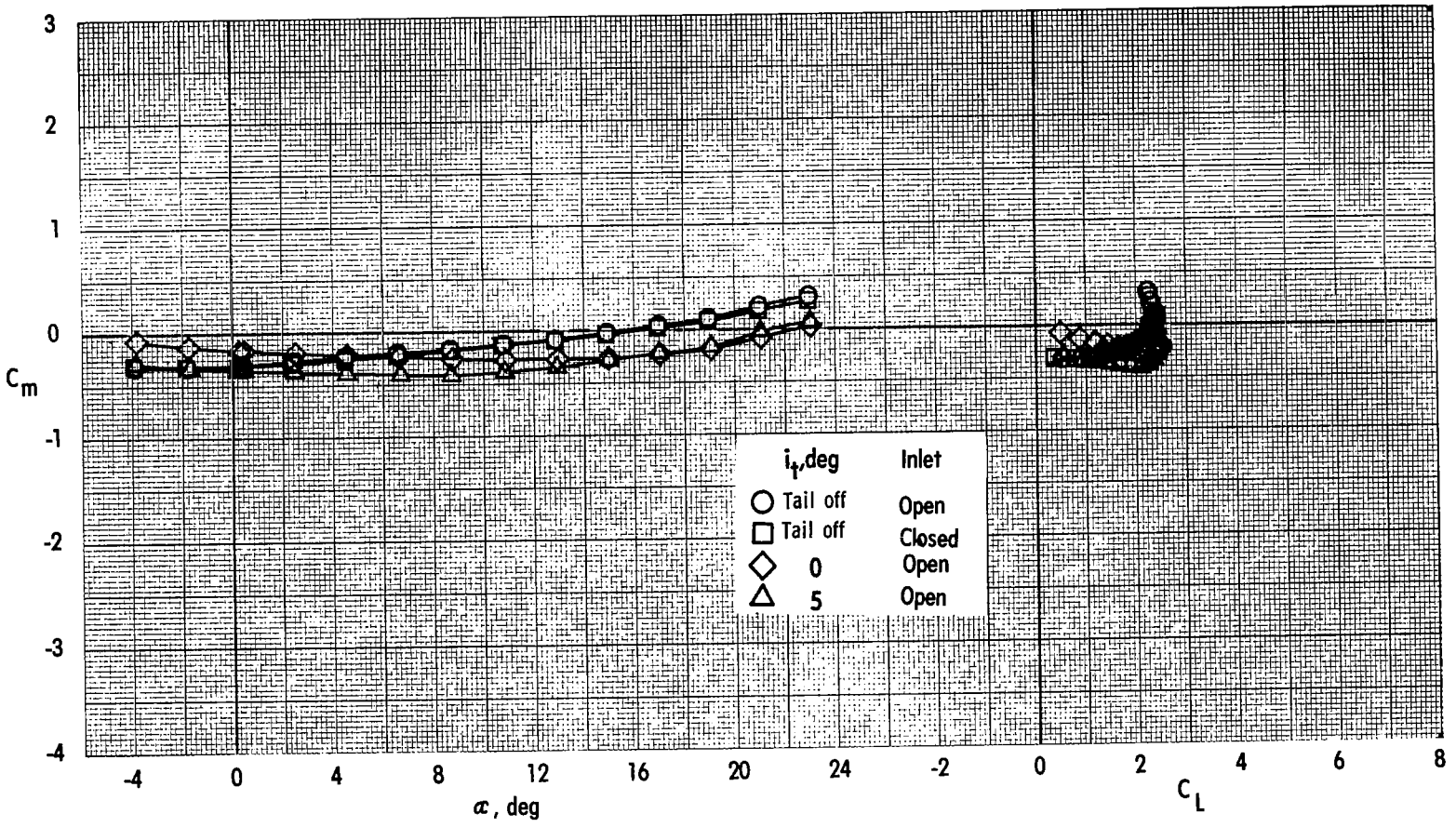

Figure 33.- Concluded.

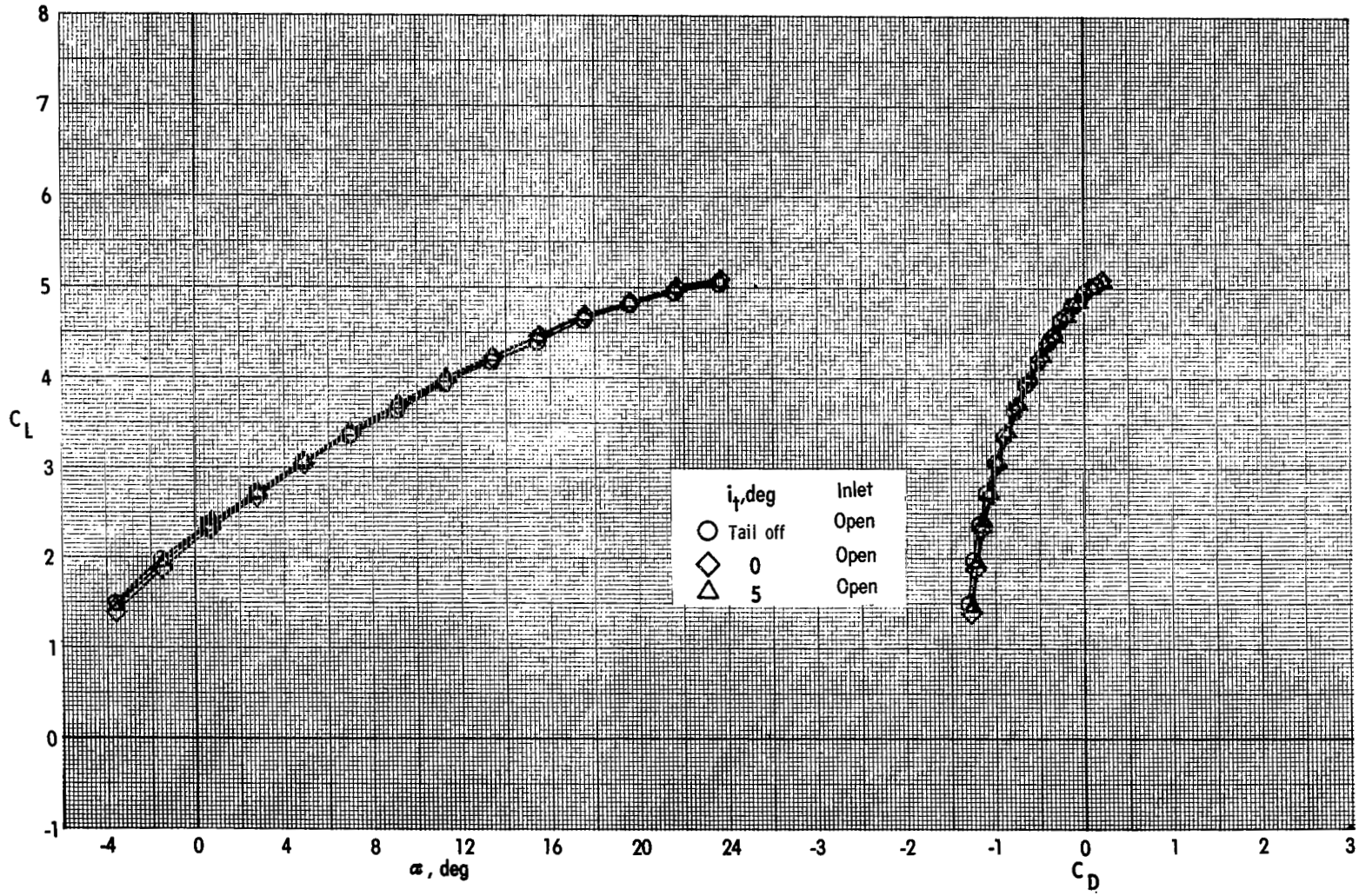

Figure 34.- Effect of tail incidence on longitudinal aerodynamic characteristics. Take-off configuration; engine 10-45; $C_\mu = 2.13$.

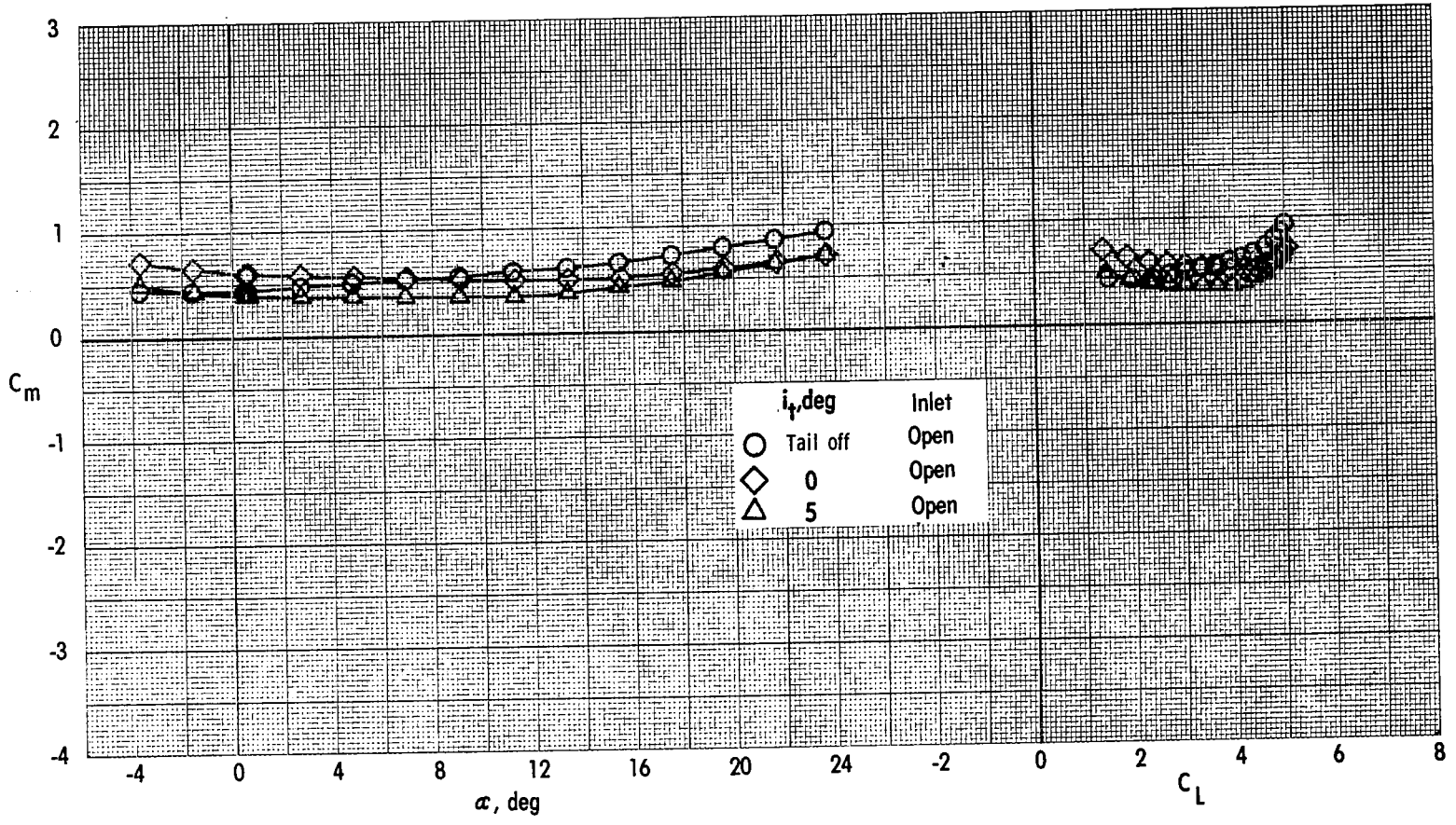

Figure 34.- Concluded.

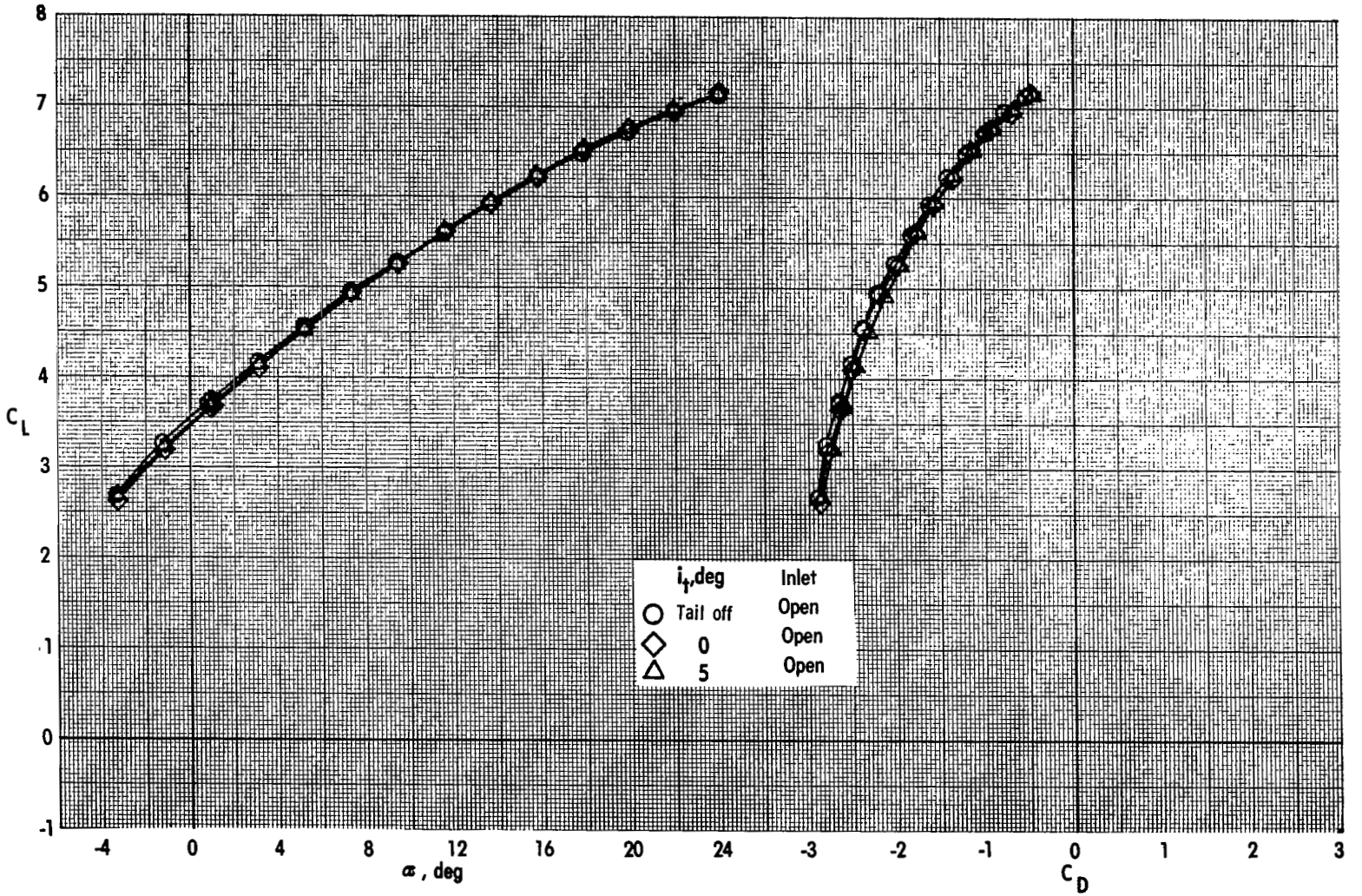

Figure 35.- Effect of tail incidence on longitudinal aerodynamic characteristics. Take-off configuration; engine 10-45; $C_\mu = 4.28$.

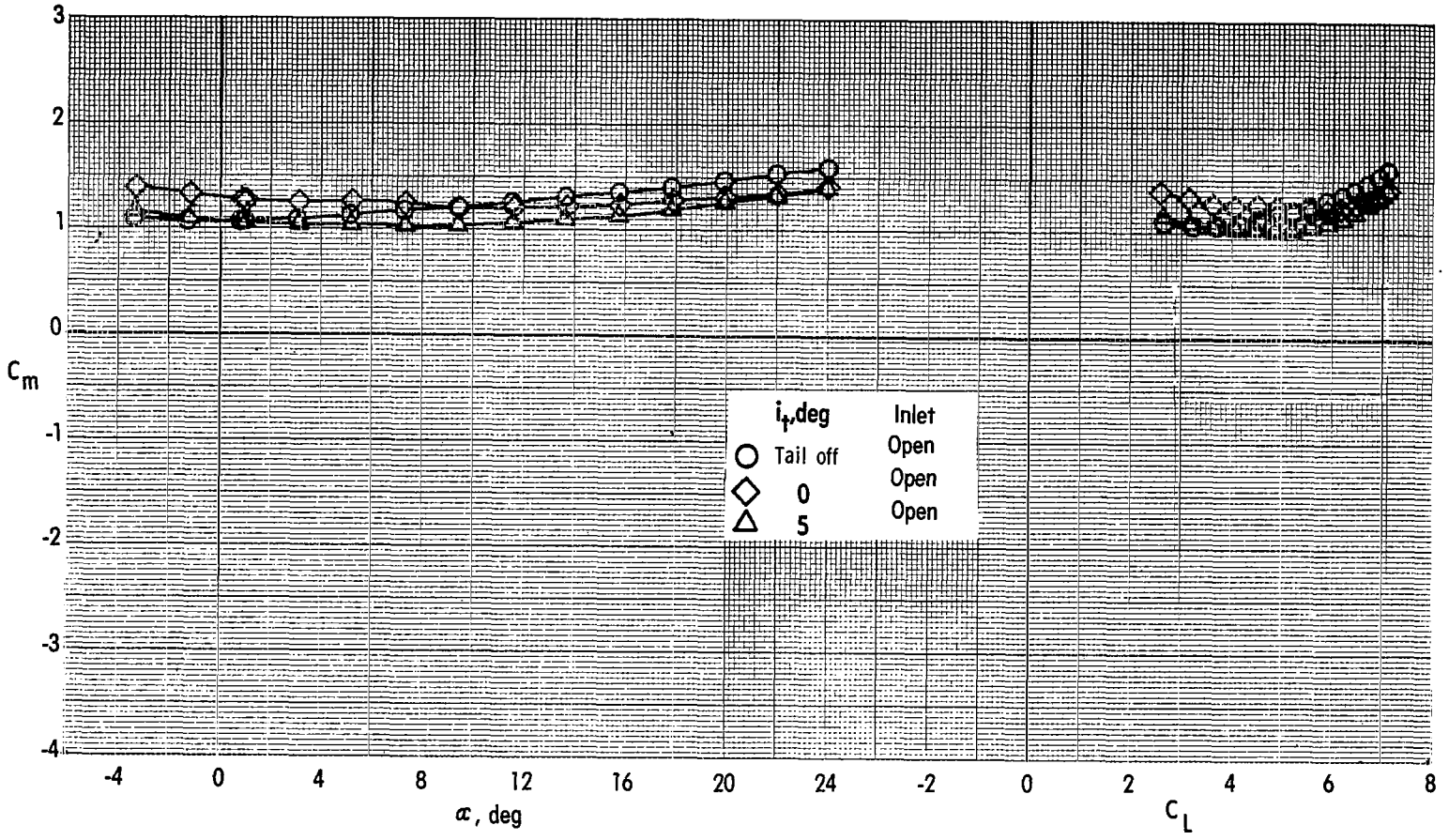

Figure 35.- Concluded.

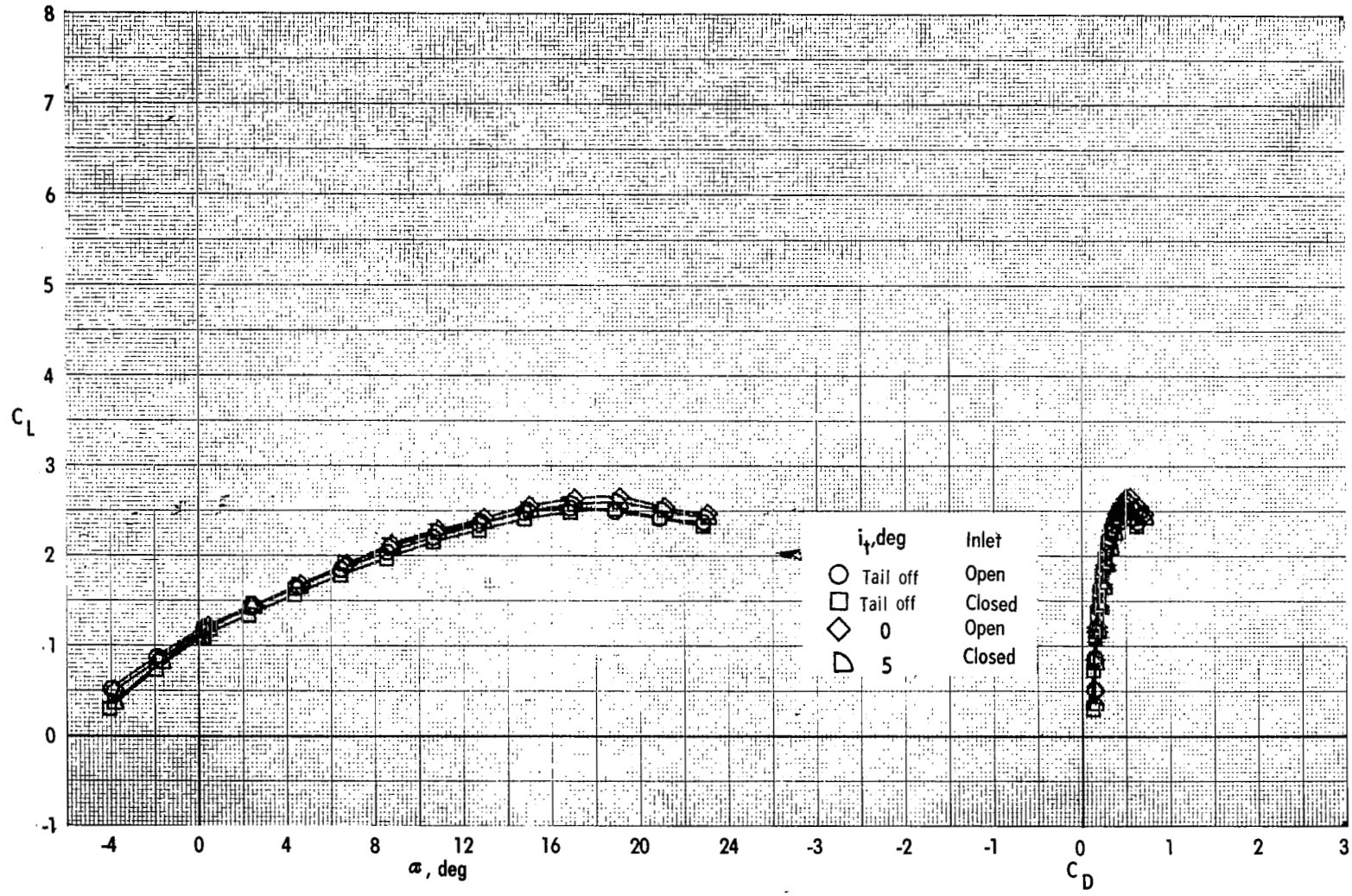

Figure 36.- Effect of tail incidence on longitudinal aerodynamic characteristics. Take-off configuration; engine 75-45; $C_\mu = 0$.

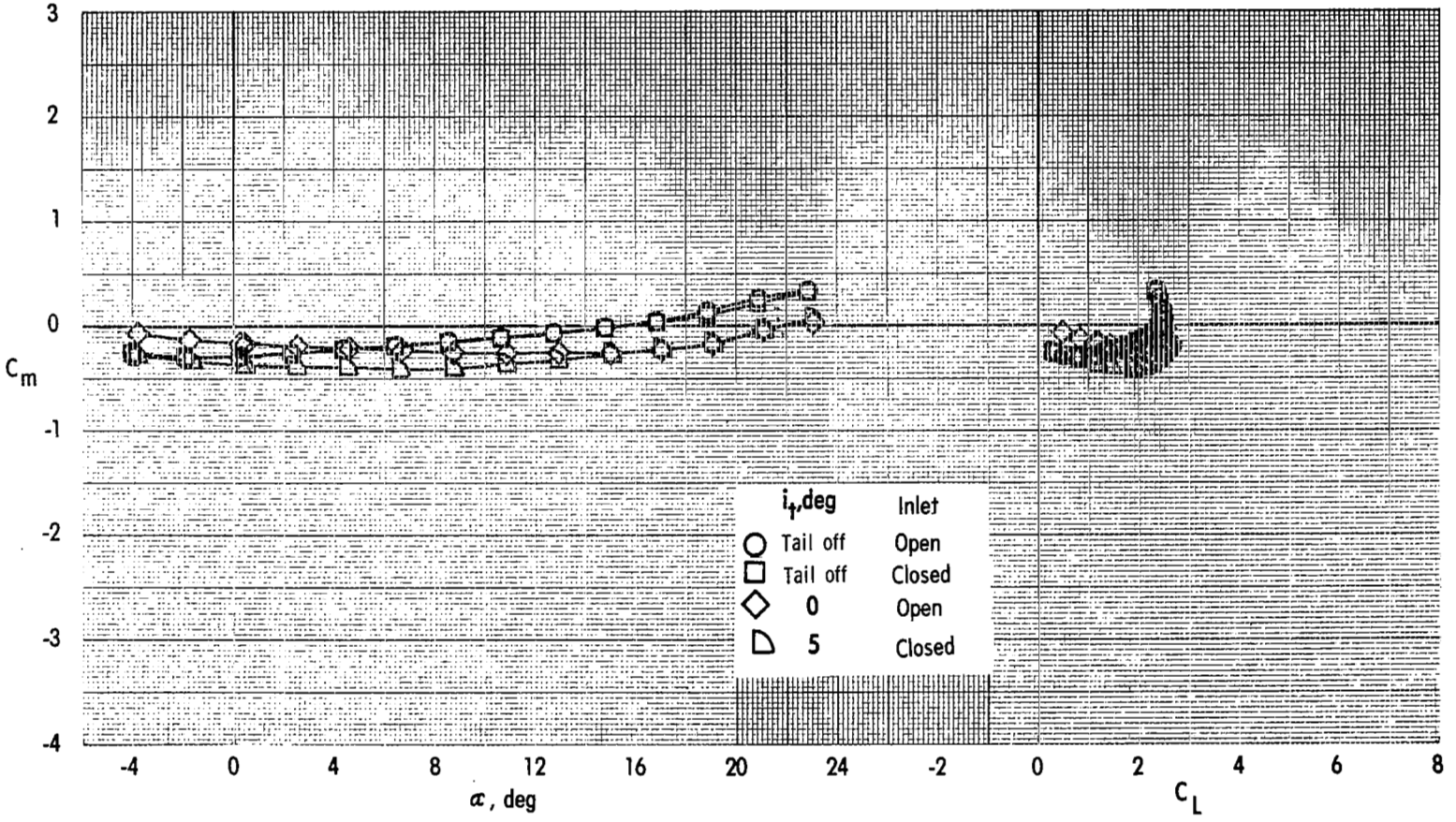

Figure 36.- Concluded.

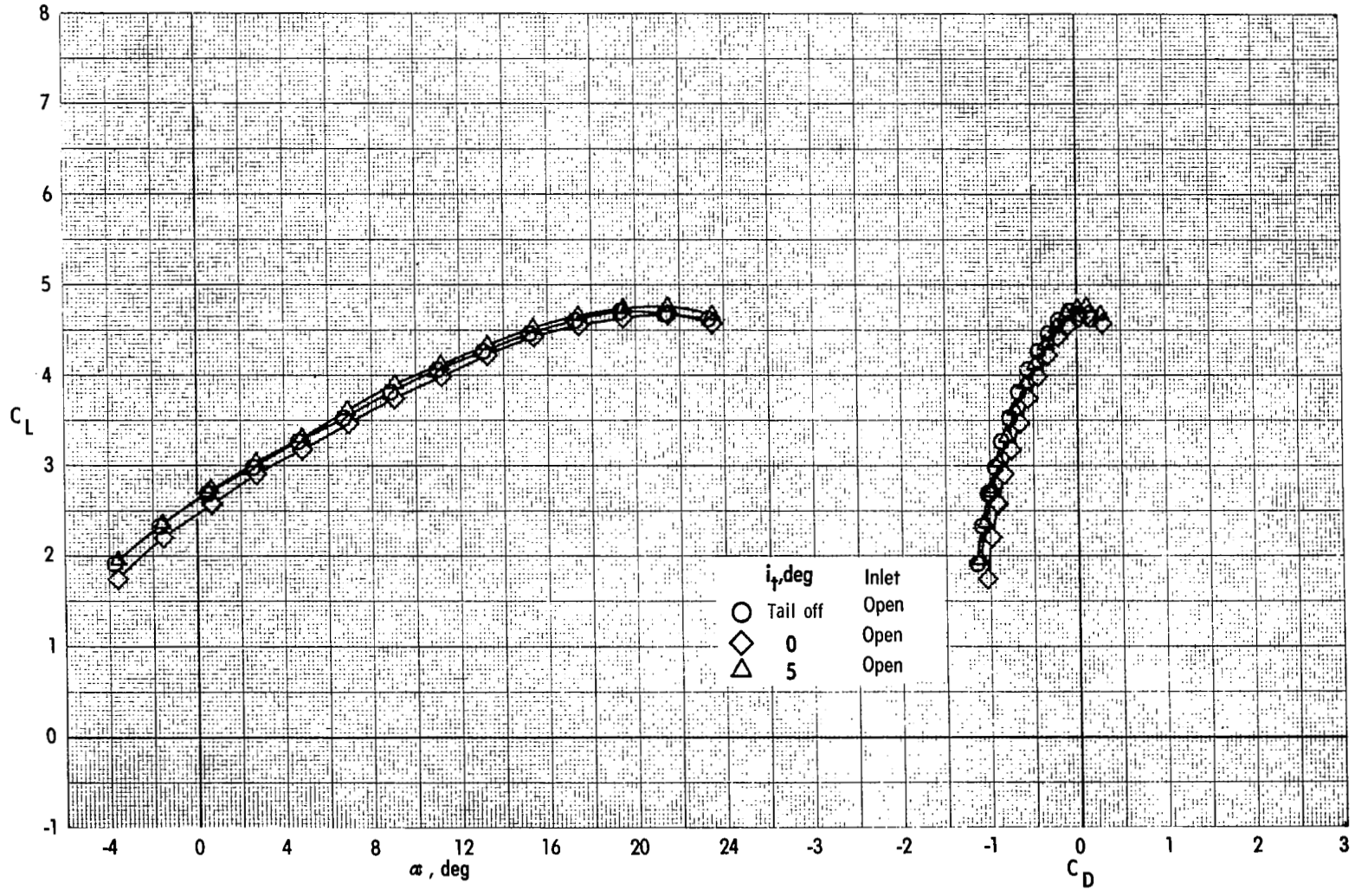

Figure 37.- Effect of tail incidence on longitudinal aerodynamic characteristics. Take-off configuration; engine 75-45; C_μ = 2.01.

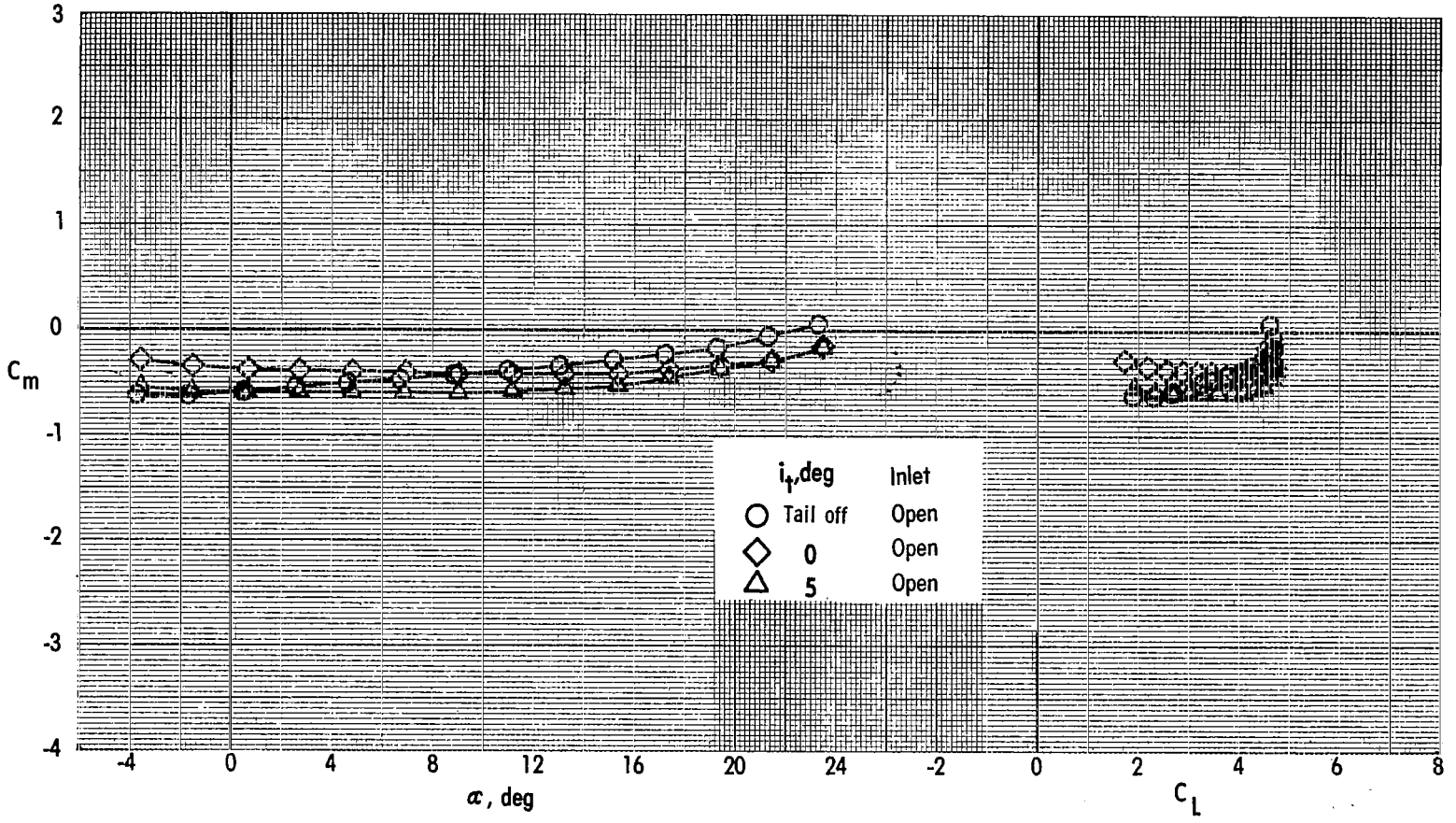

Figure 37.- Concluded.

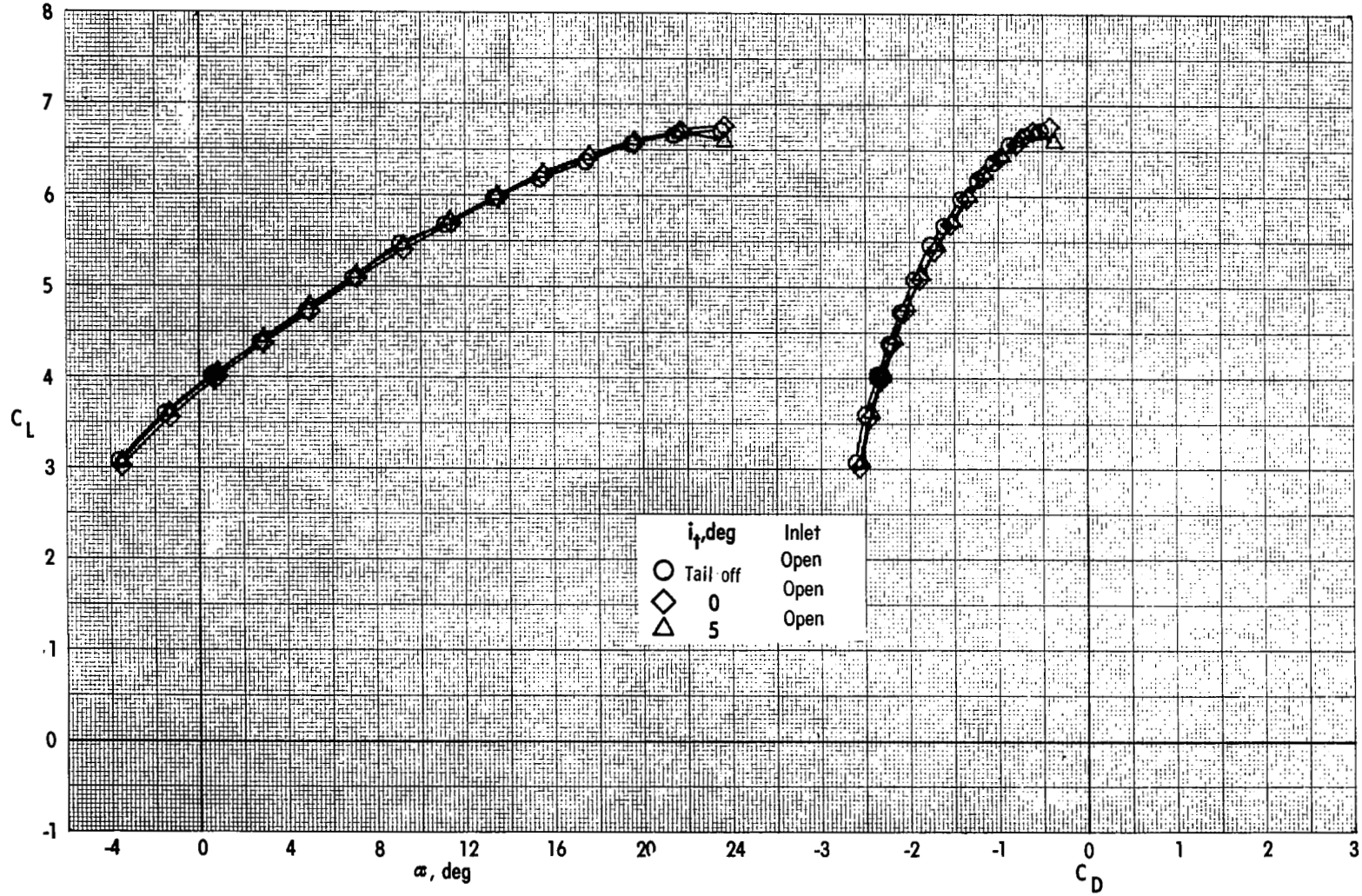

Figure 38.- Effect of tail incidence on longitudinal aerodynamic characteristics.
Take-off configuration; engine 75-45; C_μ = 4.03.

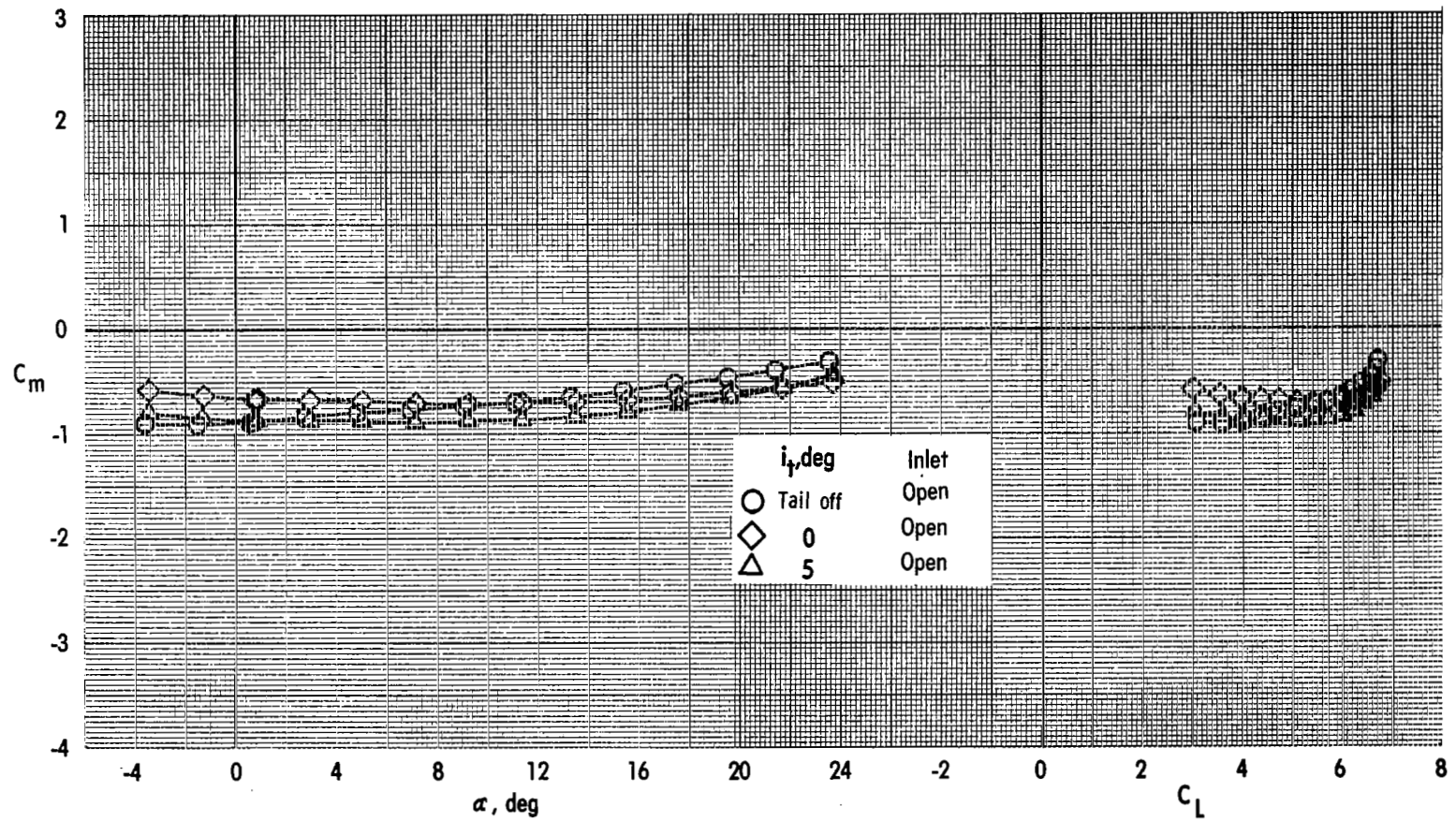

Figure 38.- Concluded.

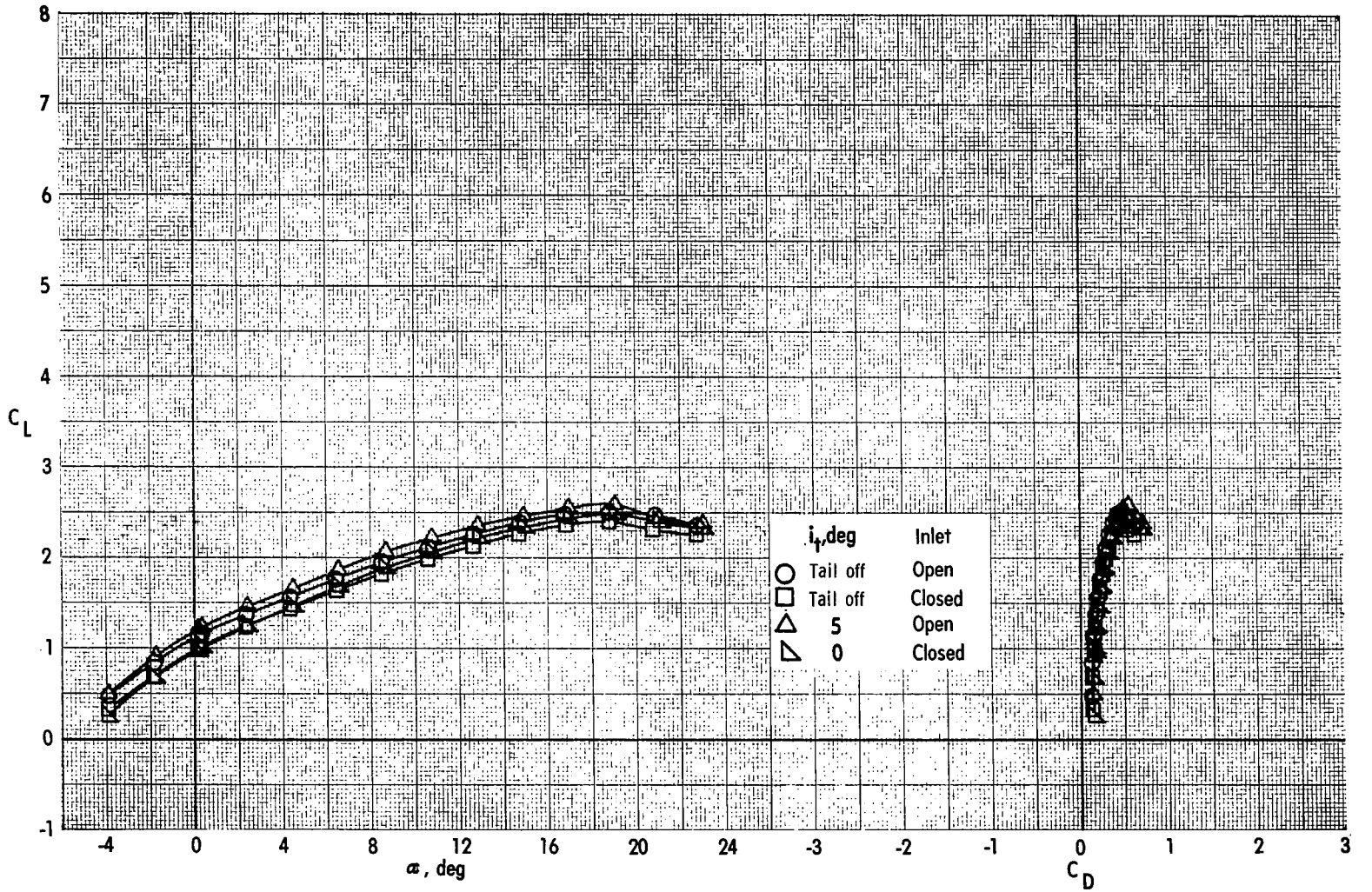

Figure 39.- Effect of tail incidence on longitudinal aerodynamic characteristics. Take-off configuration; engine 110-45; $C_\mu = 0$.

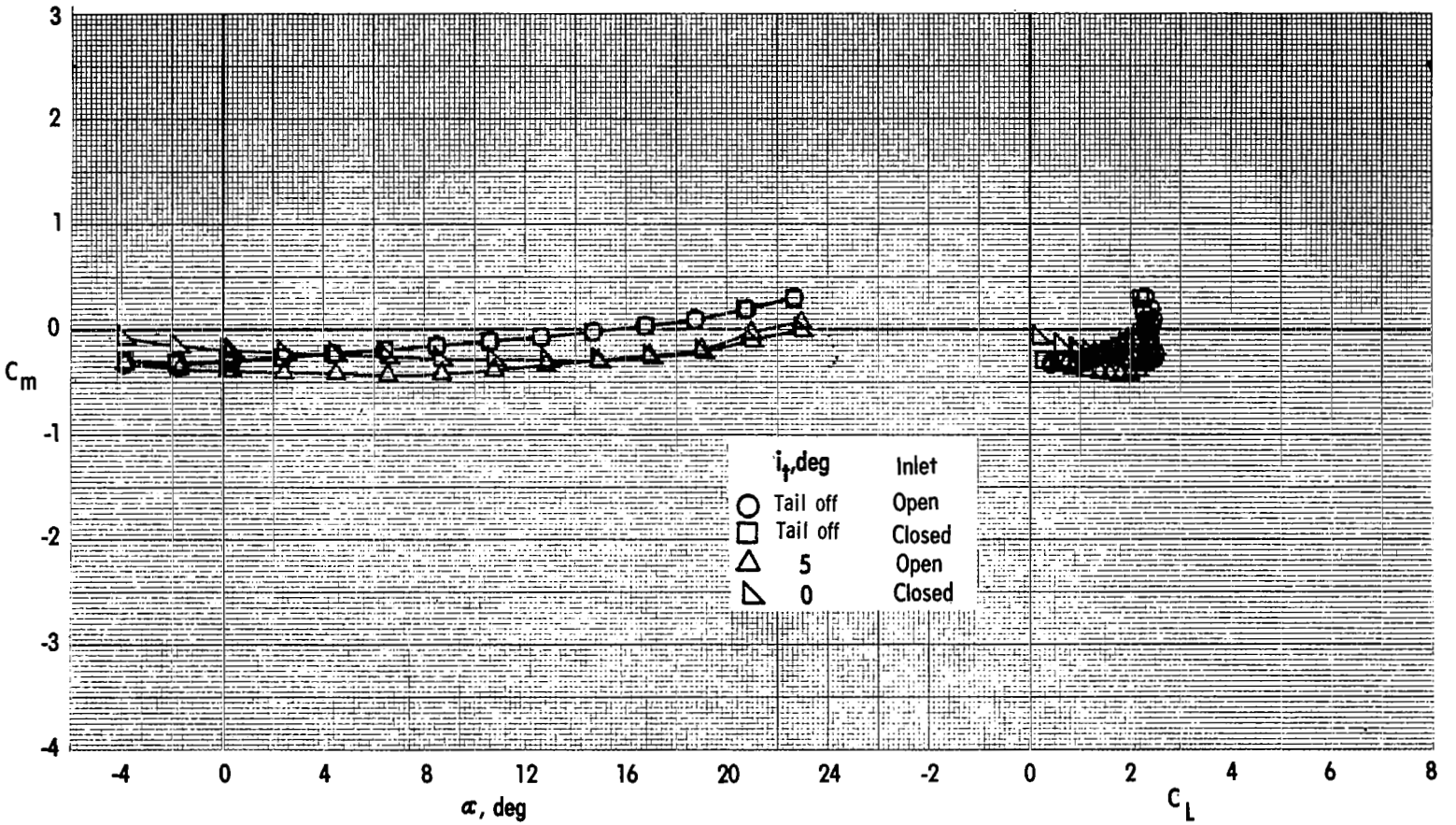

Figure 39.- Concluded.

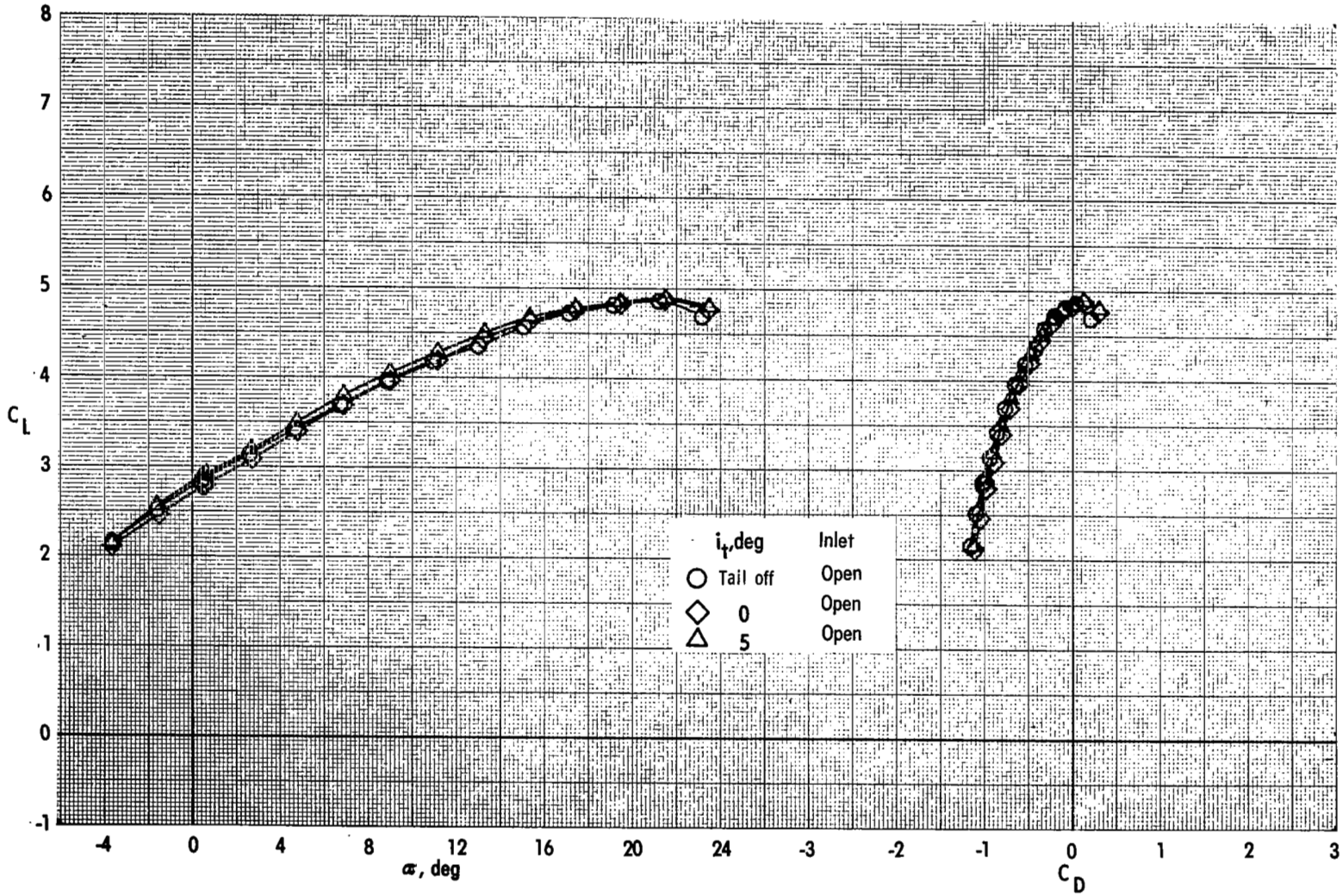

Figure 40.- Effect of tail incidence on longitudinal aerodynamic characteristics. Take-off configuration; engine 110-45; C_μ = 2.02.

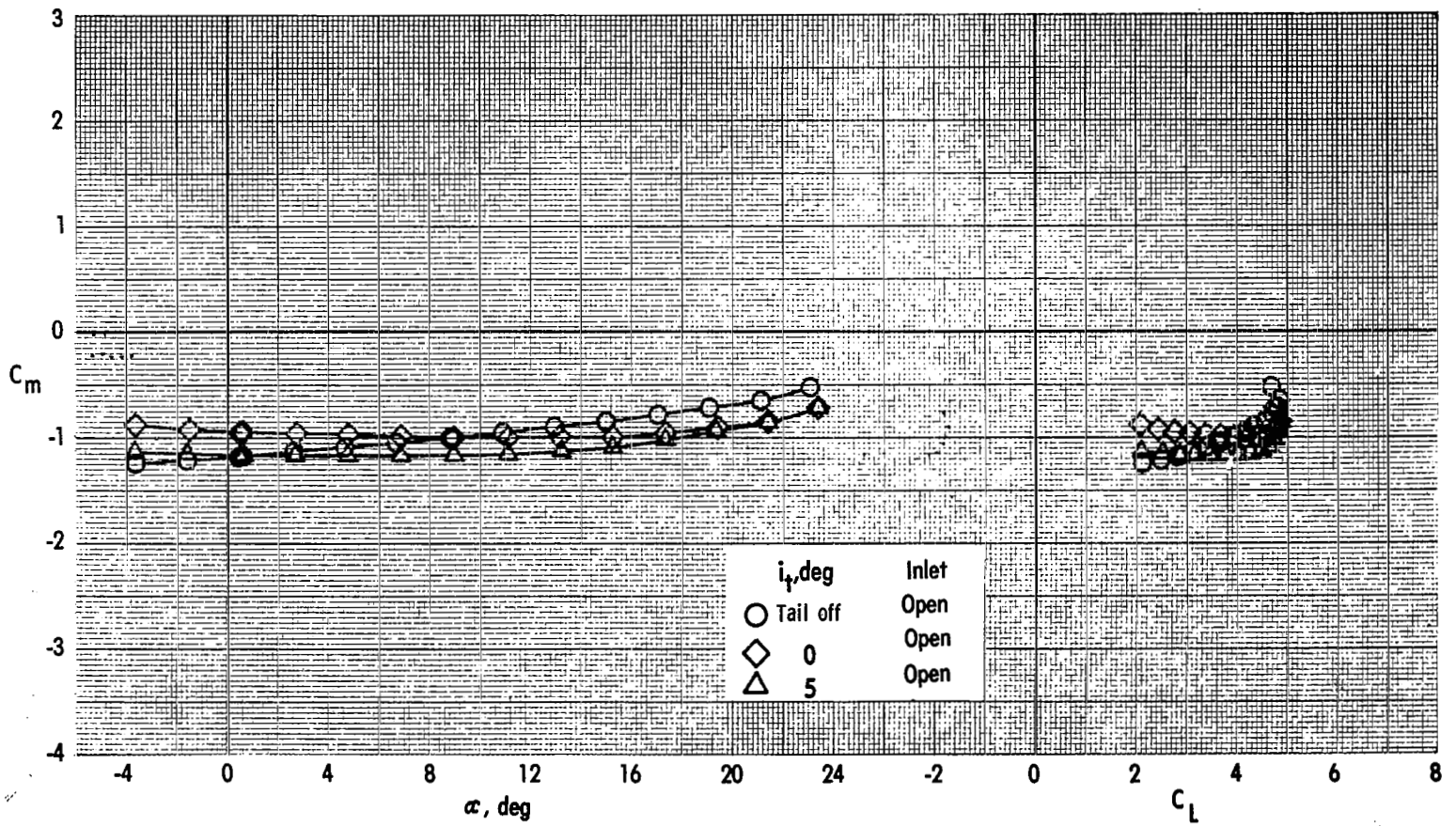

Figure 40.- Concluded.

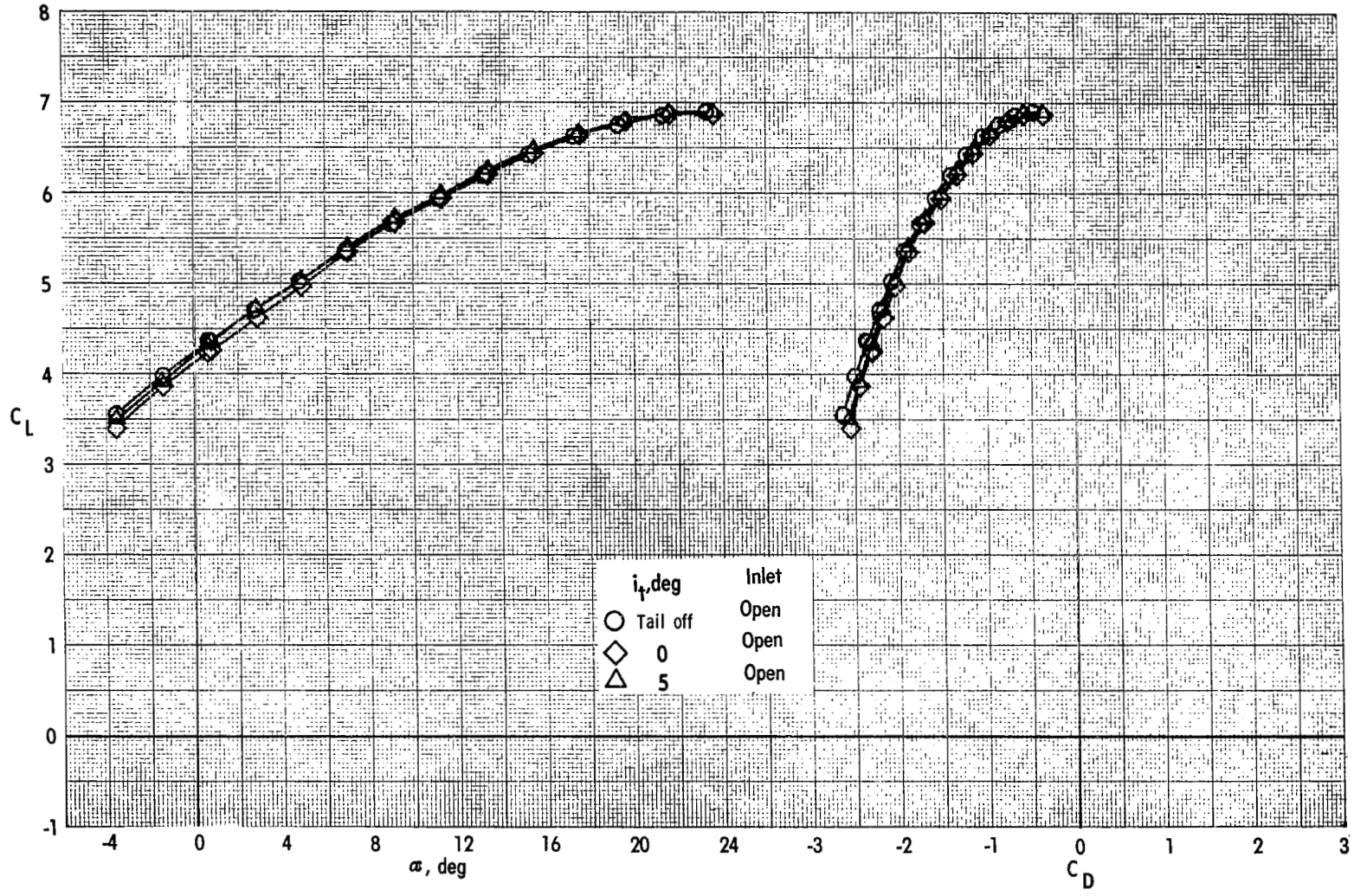

Figure 41.- Effect of tail incidence on longitudinal aerodynamic characteristics. Take-off configuration; engine 110-45; $C_\mu = 4.02$.

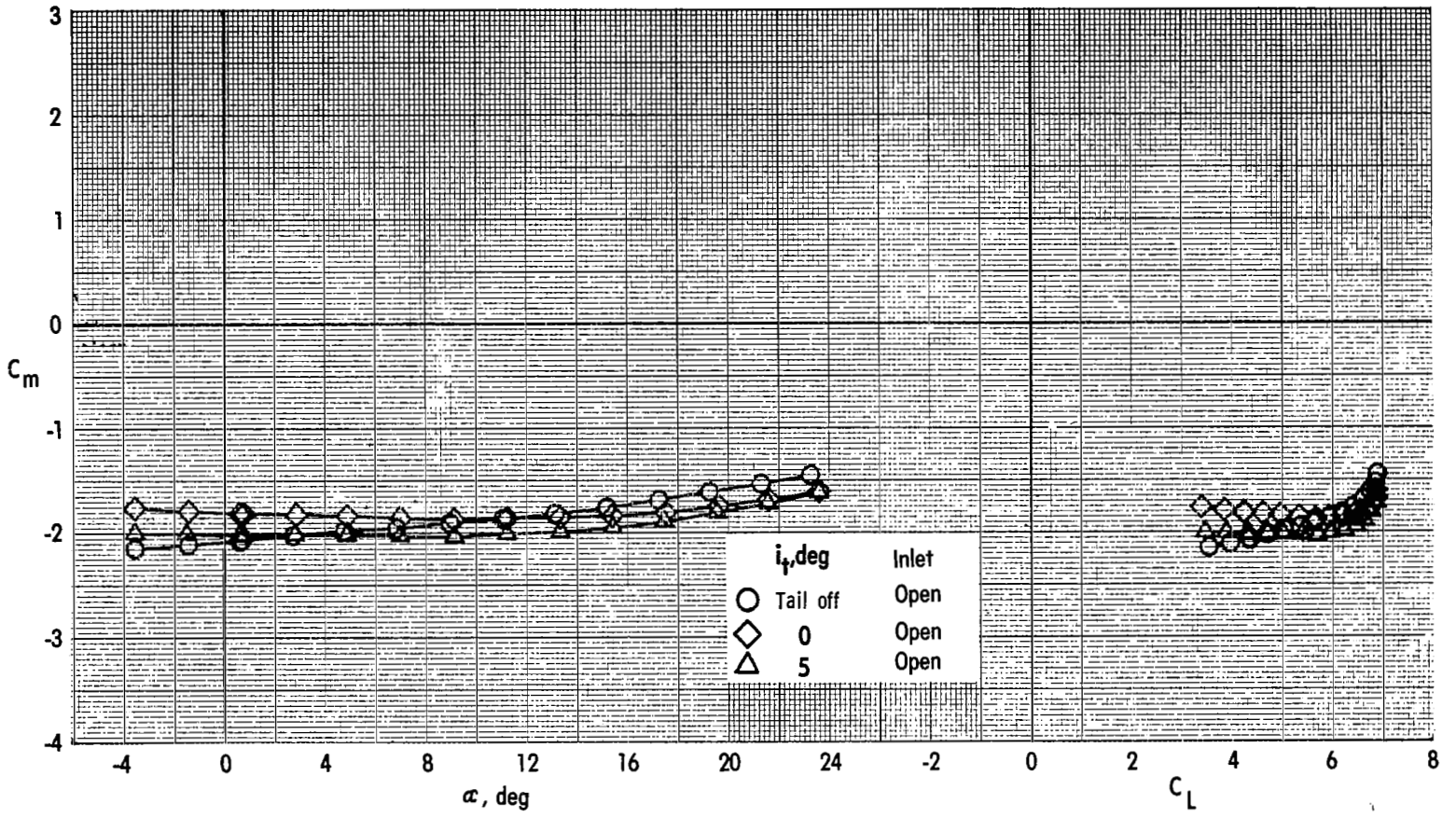

Figure 41.- Concluded.

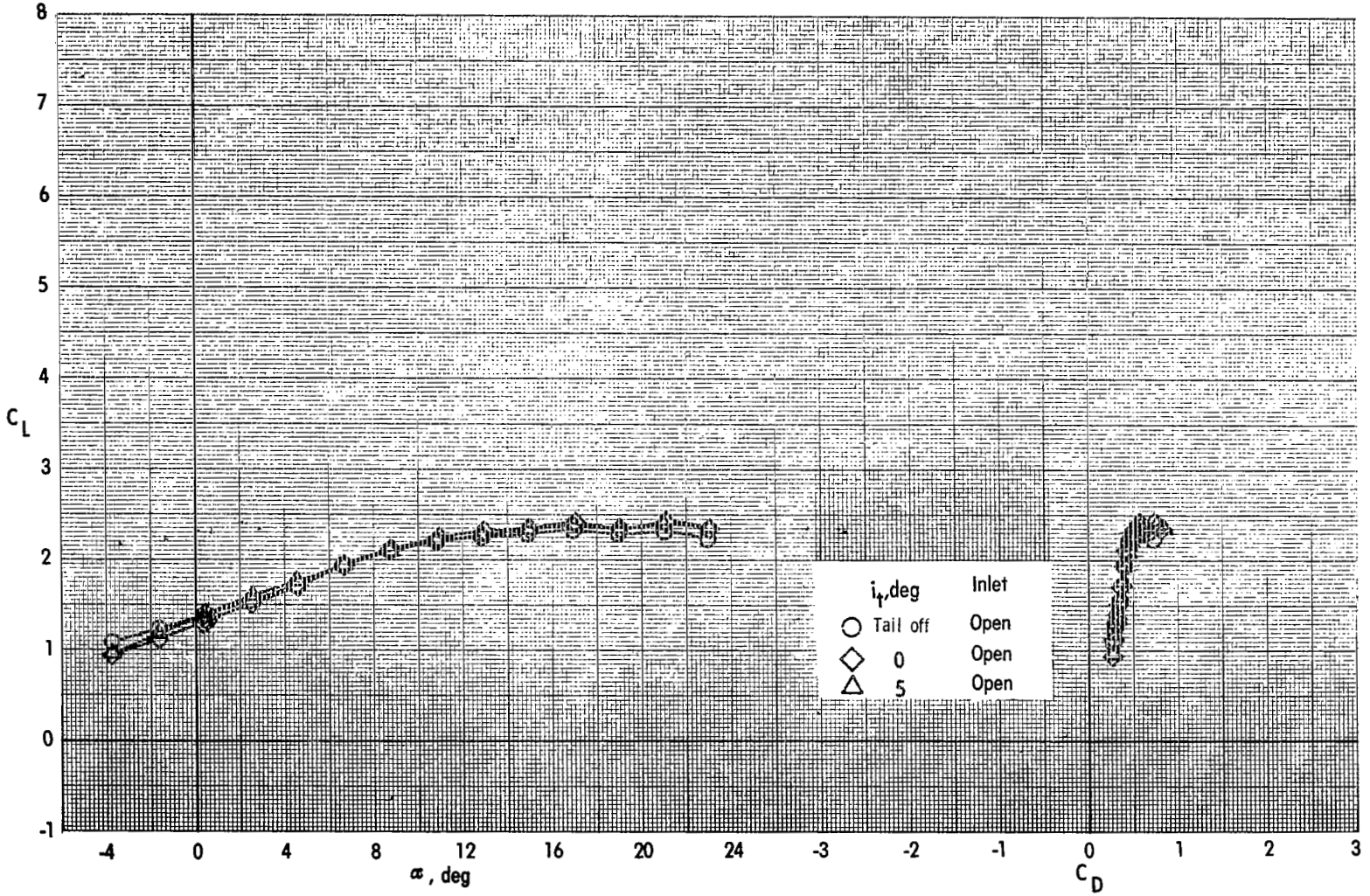

Figure 42.- Effect of tail incidence on longitudinal aerodynamic characteristics. Landing configuration; basic engine; $C_\mu = 0$.

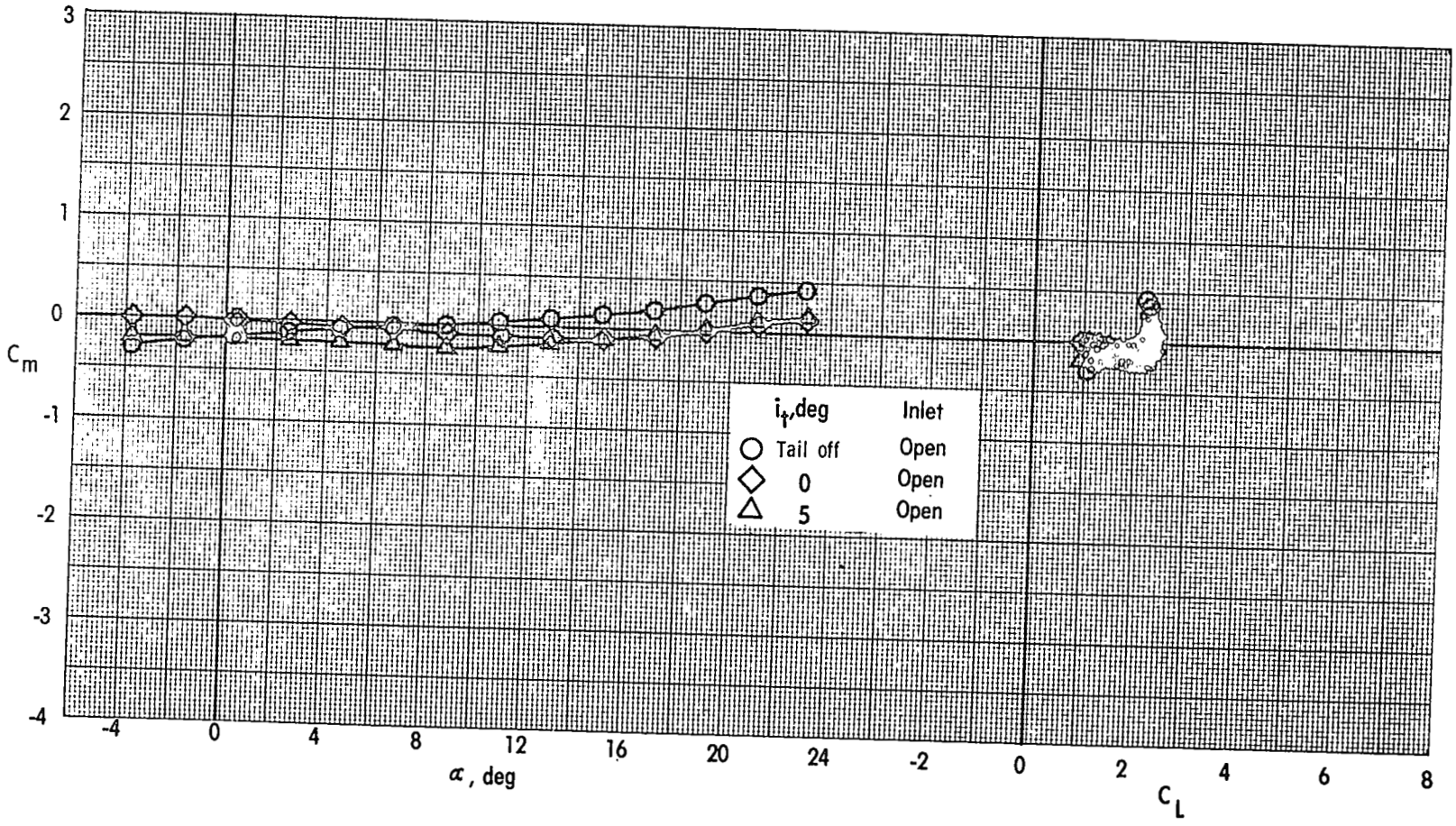

Figure 42.- Concluded.

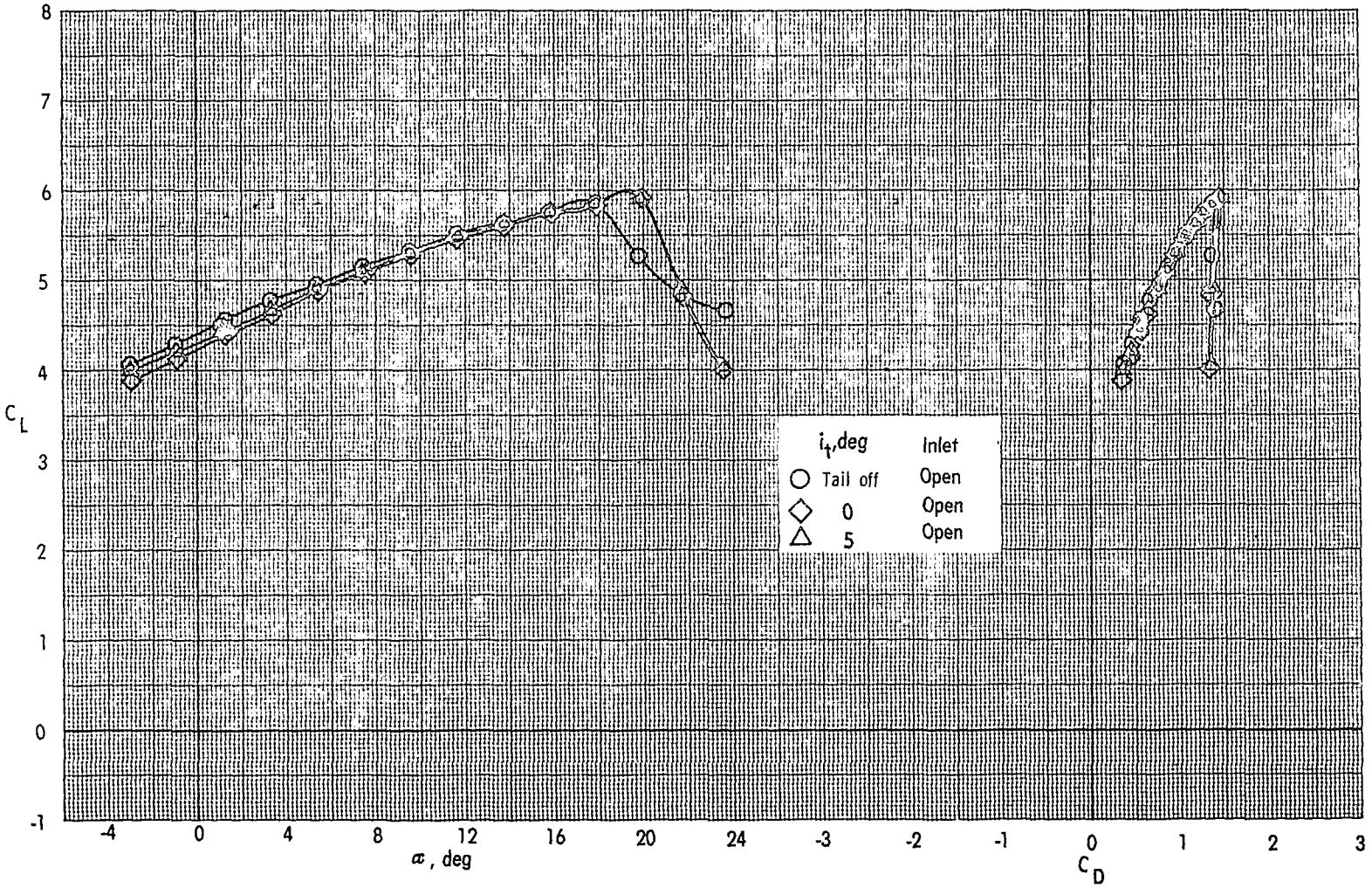

Figure 43.- Effect of tail incidence on longitudinal aerodynamic characteristics. Landing configuration; basic engine; C_μ = 2.00.

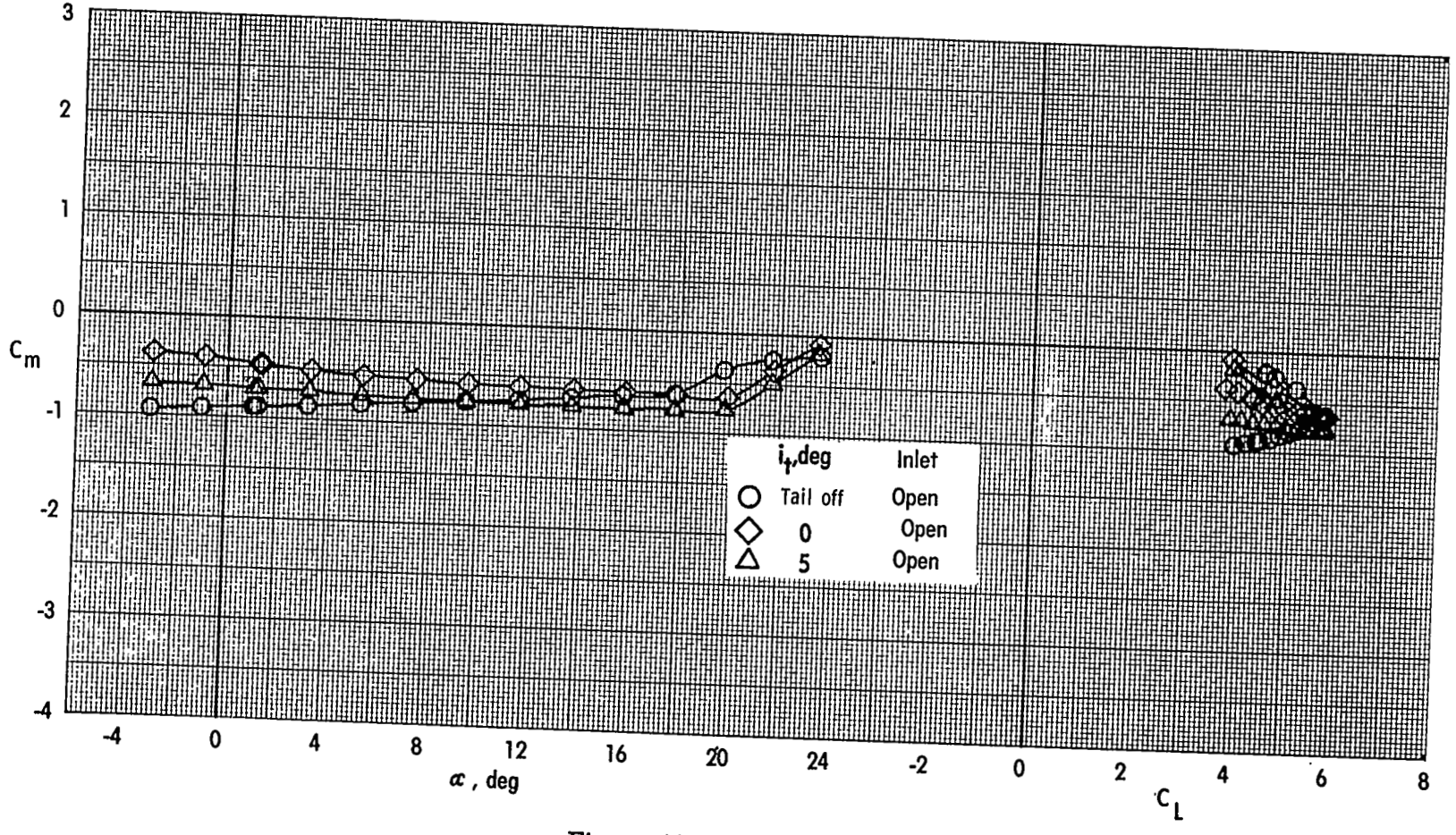

Figure 43.- Concluded.

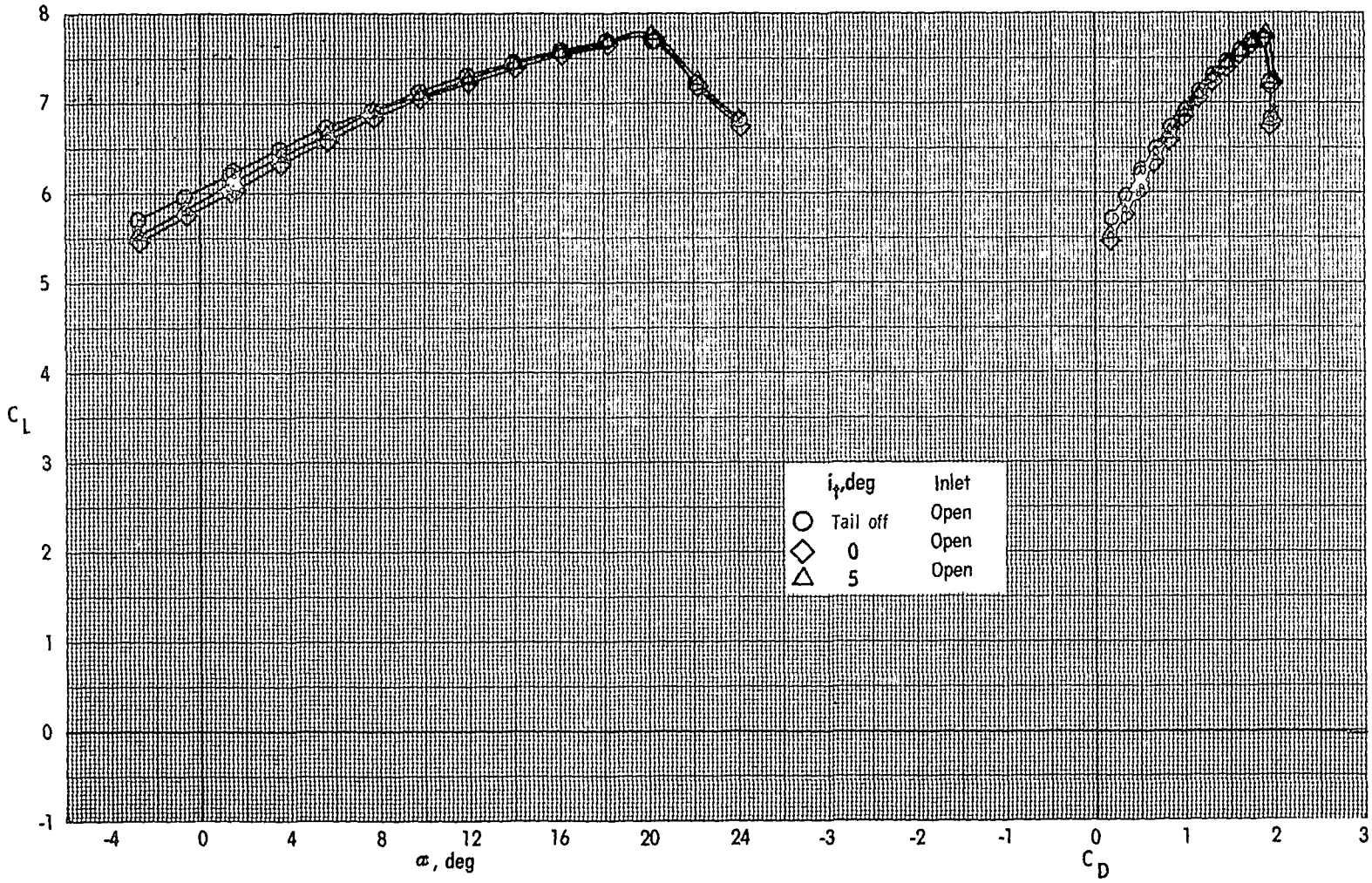

Figure 44.- Effect of tail incidence on longitudinal aerodynamic characteristics. Landing configuration; basic engine; $C_\mu = 3.96$.

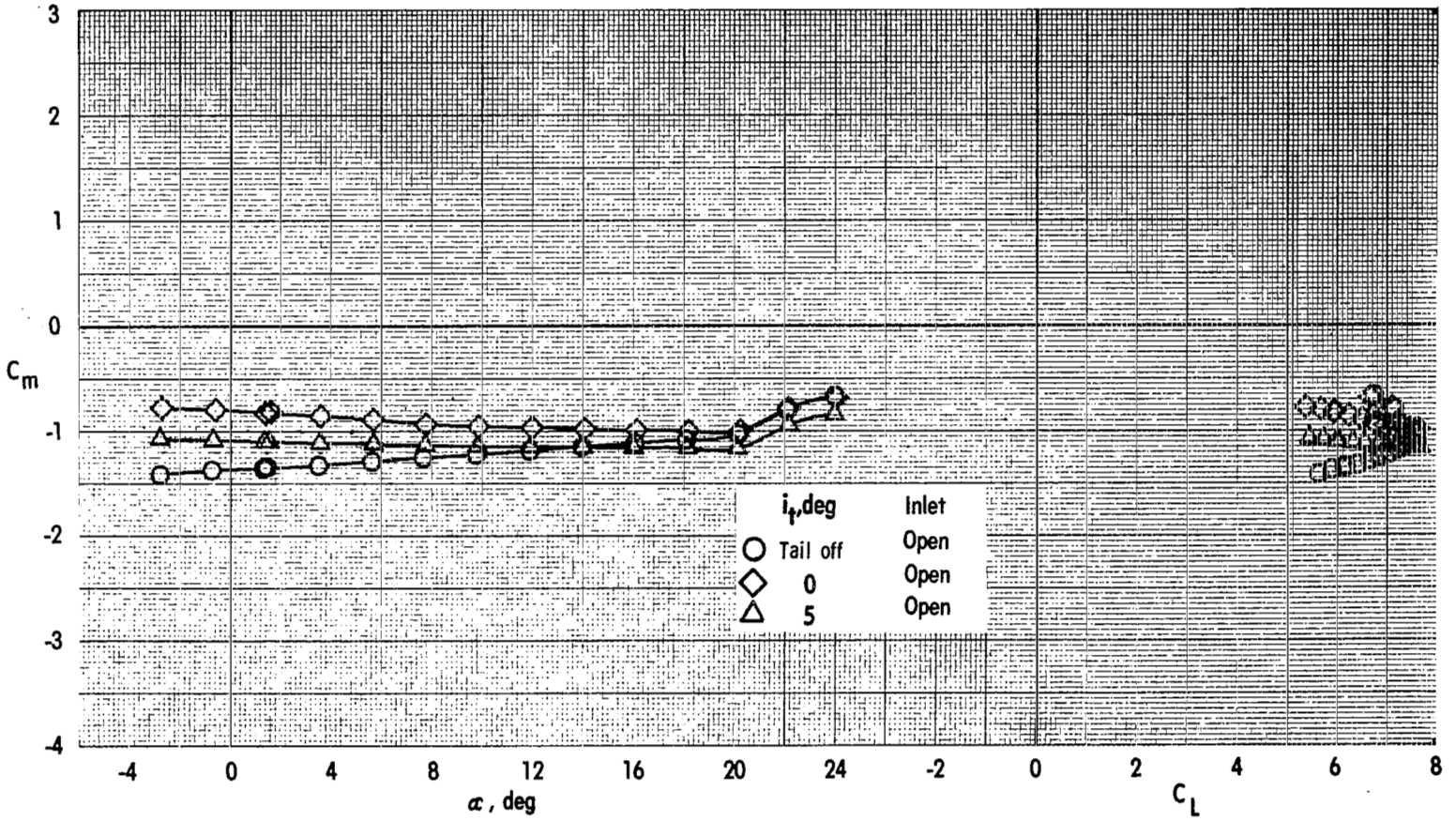

Figure 44.- Concluded.

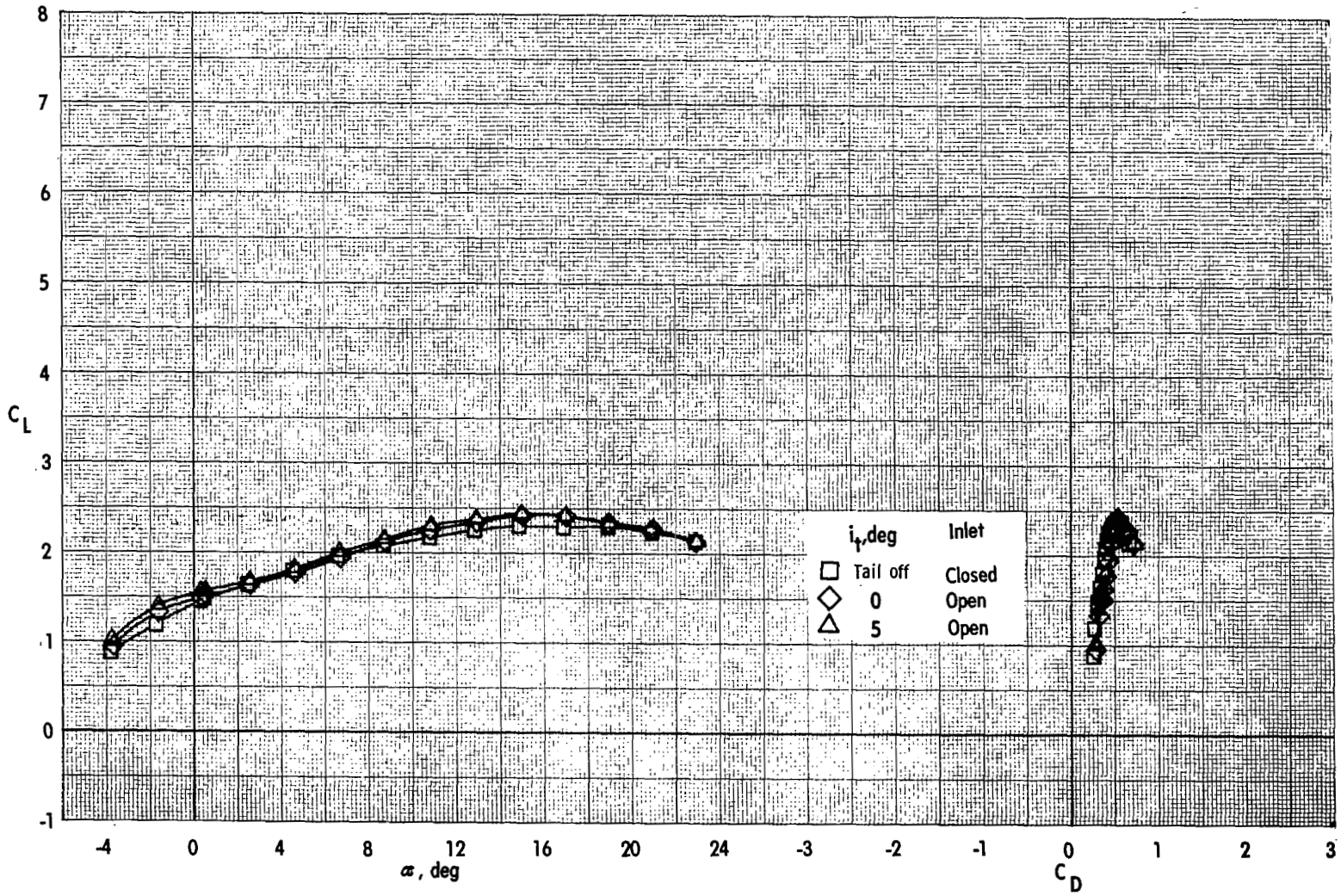

Figure 45.- Effect of tail incidence on longitudinal aerodynamic characteristics. Landing configuration; engine 10-45; $C_\mu = 0$.

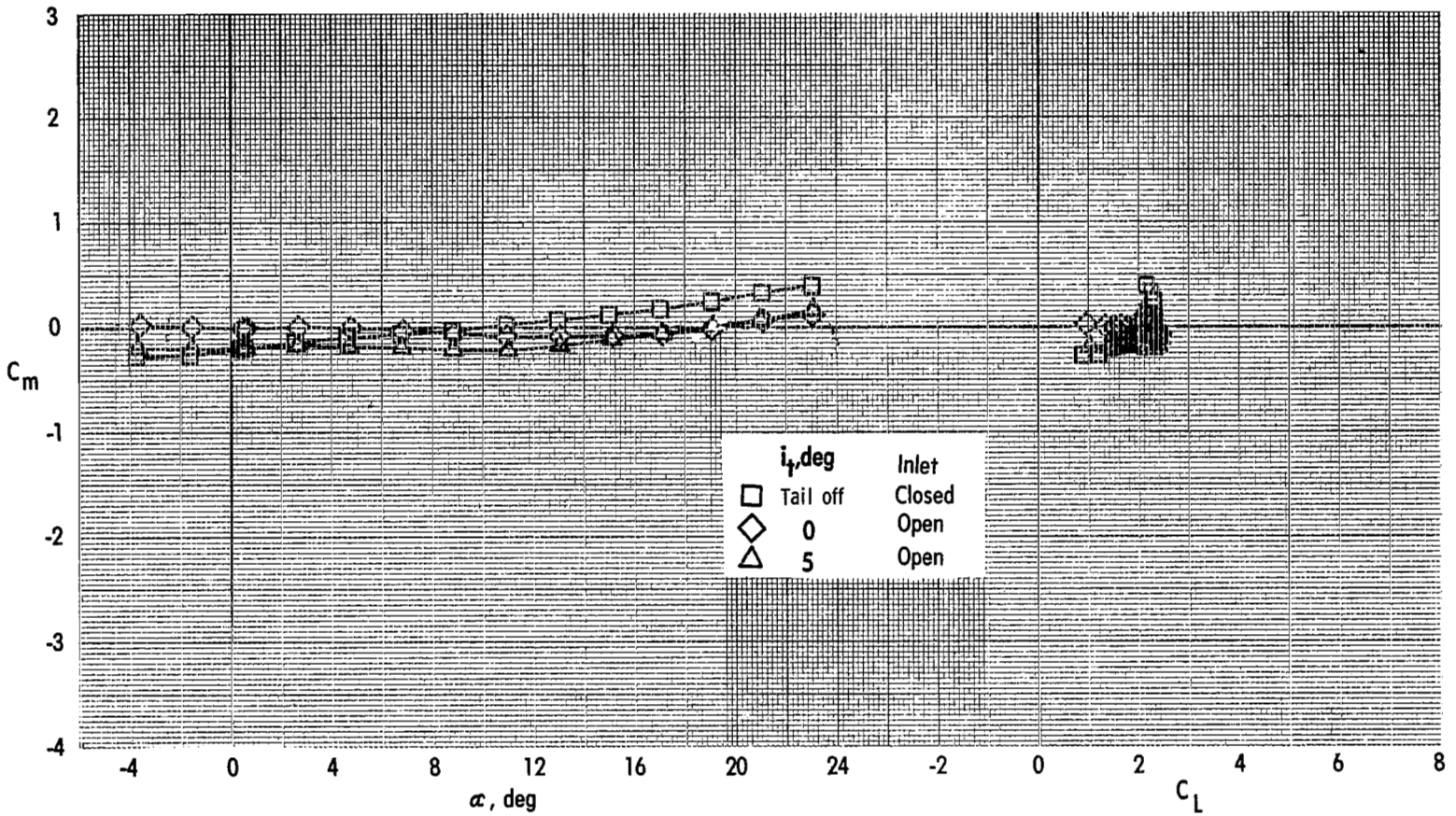

Figure 45.- Concluded.

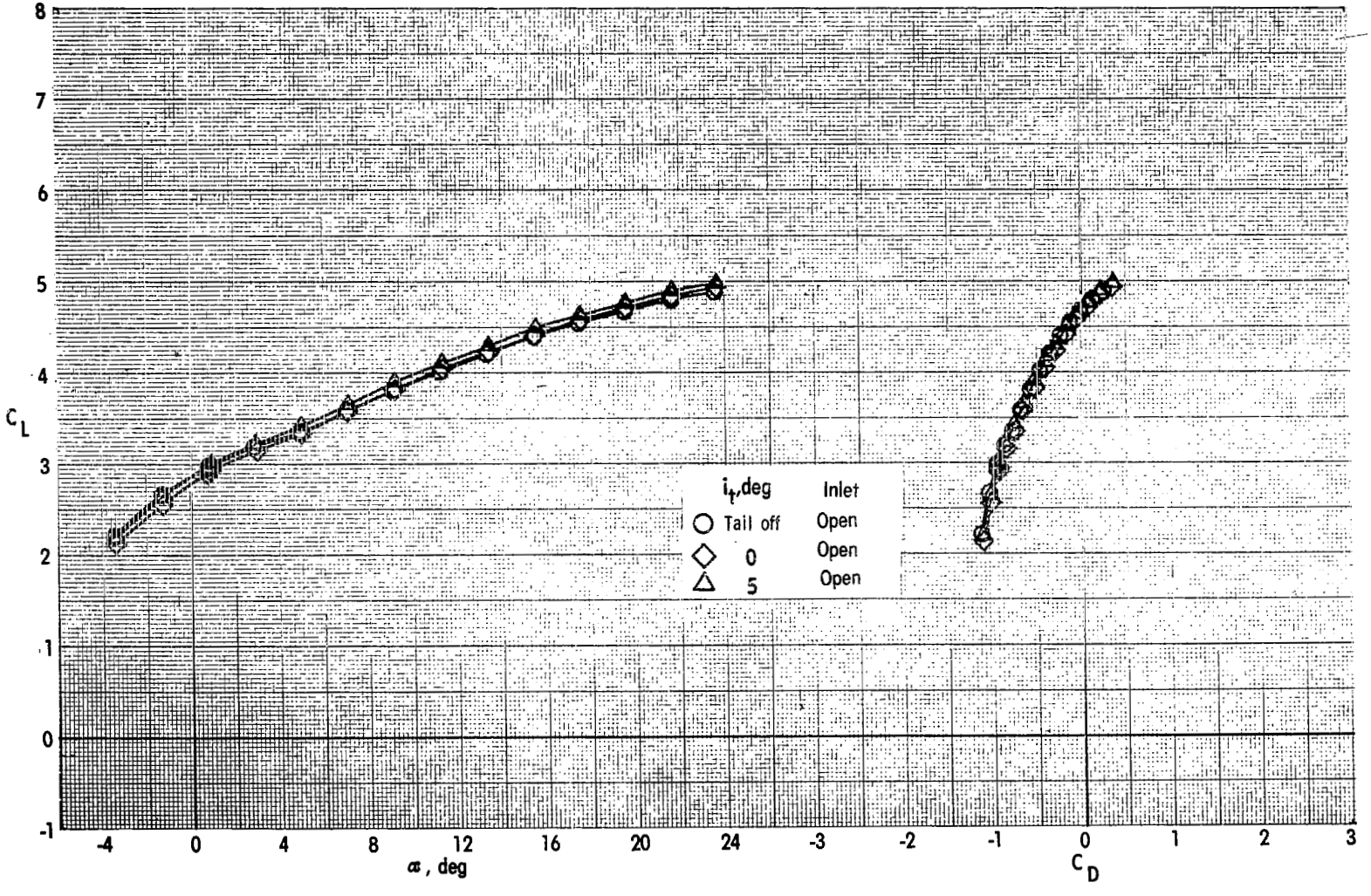

Figure 46.- Effect of tail incidence on longitudinal aerodynamic characteristics. Landing configuration; engine 10-45; C_μ = 2.13.

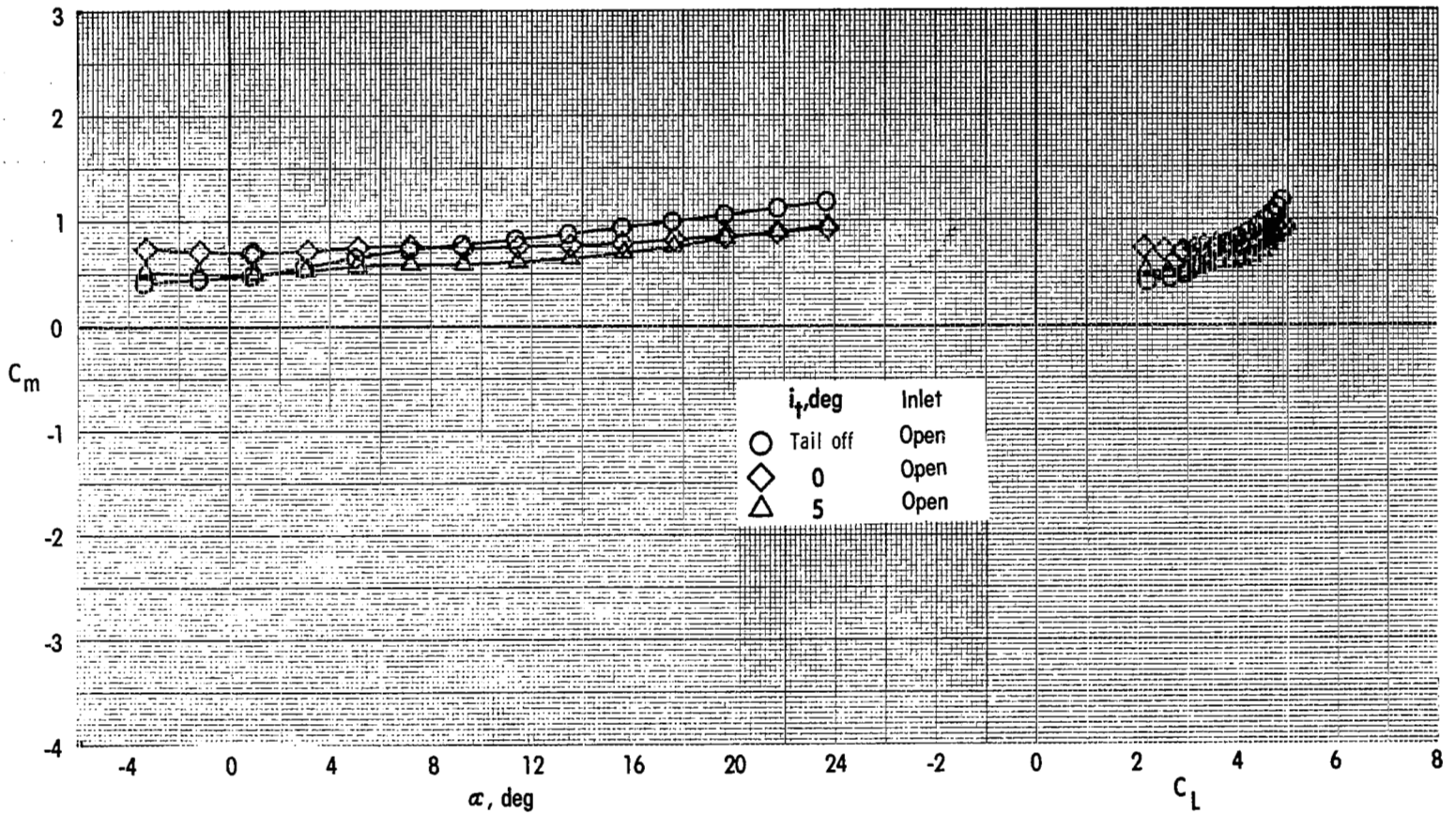

Figure 46.- Concluded.

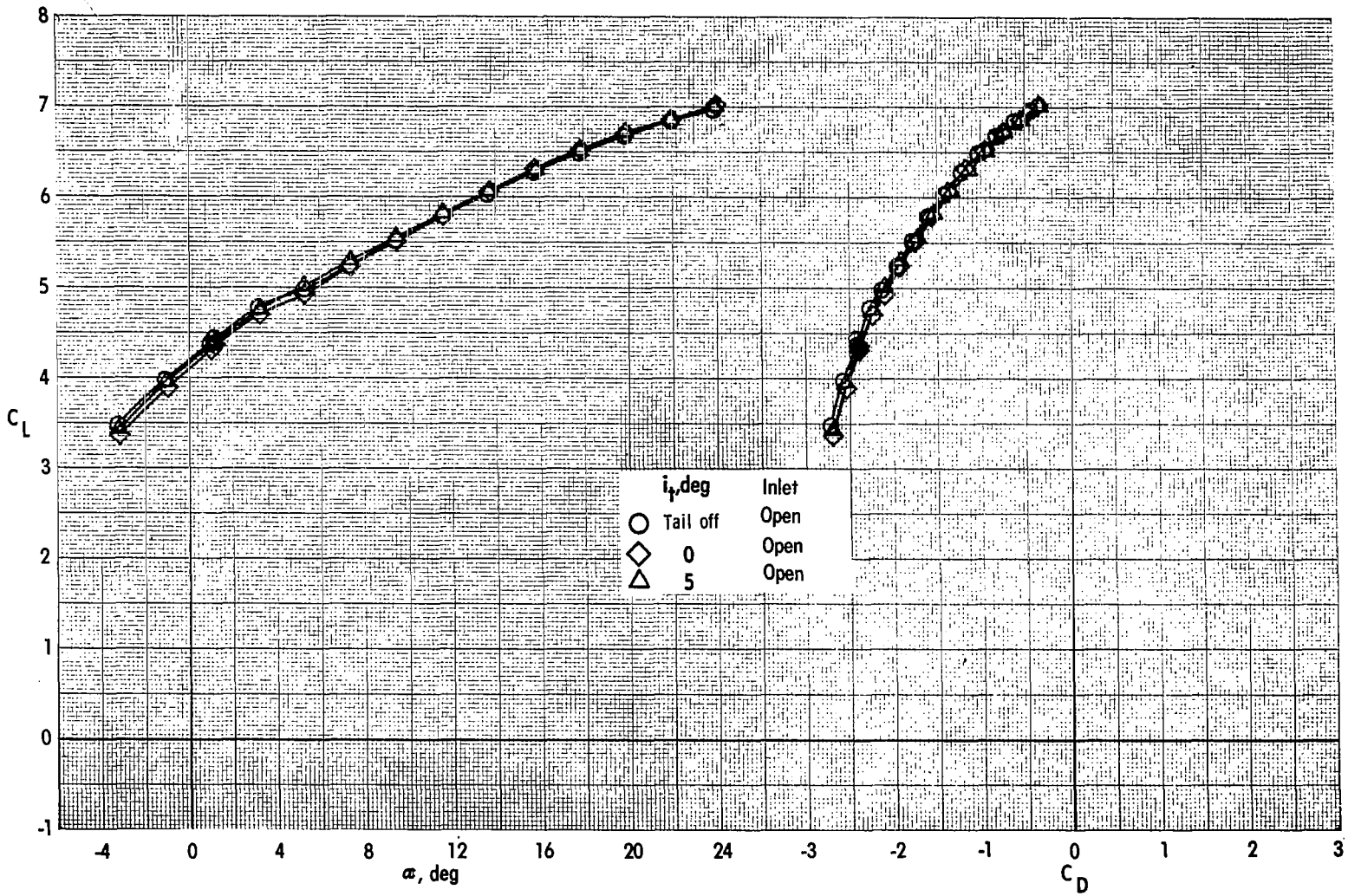

Figure 47.- Effect of tail incidence on longitudinal aerodynamic characteristics. Landing configuration; engine 10-45; $C_\mu = 4.26$.

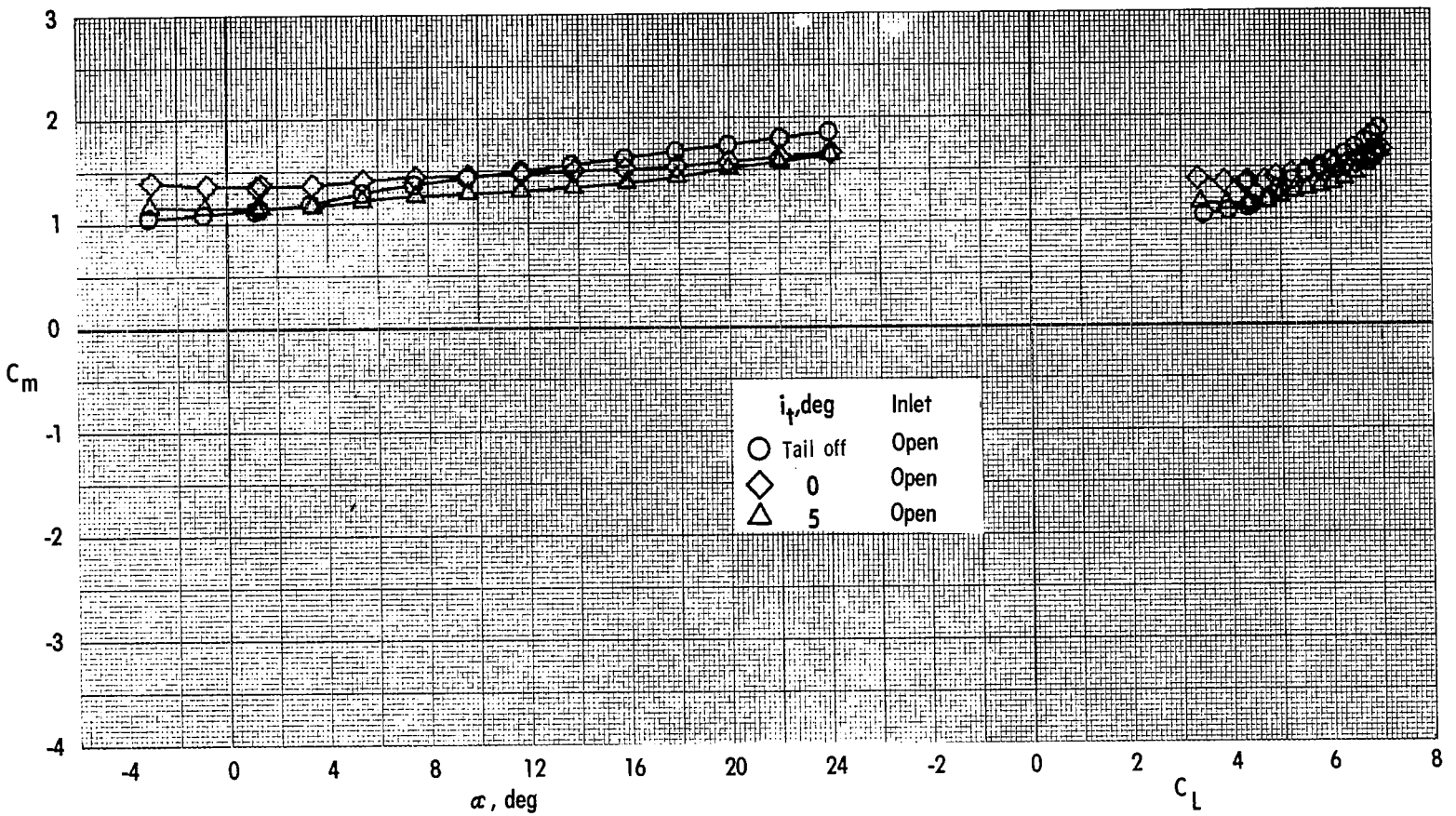

Figure 47.- Concluded.

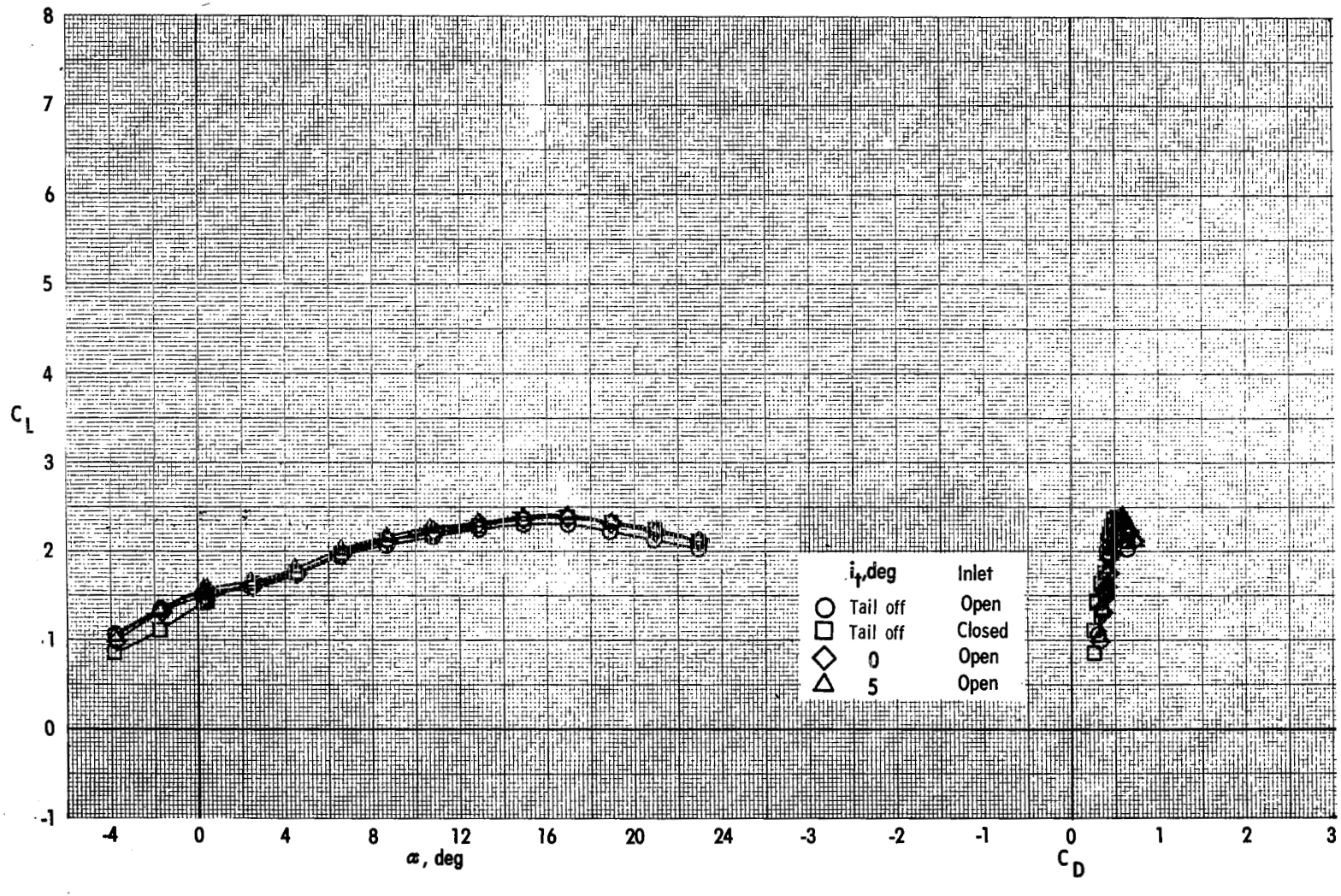

Figure 48.- Effect of tail incidence on longitudinal aerodynamic characteristics. Landing configuration; engine 10-90; $C_\mu = 0$.

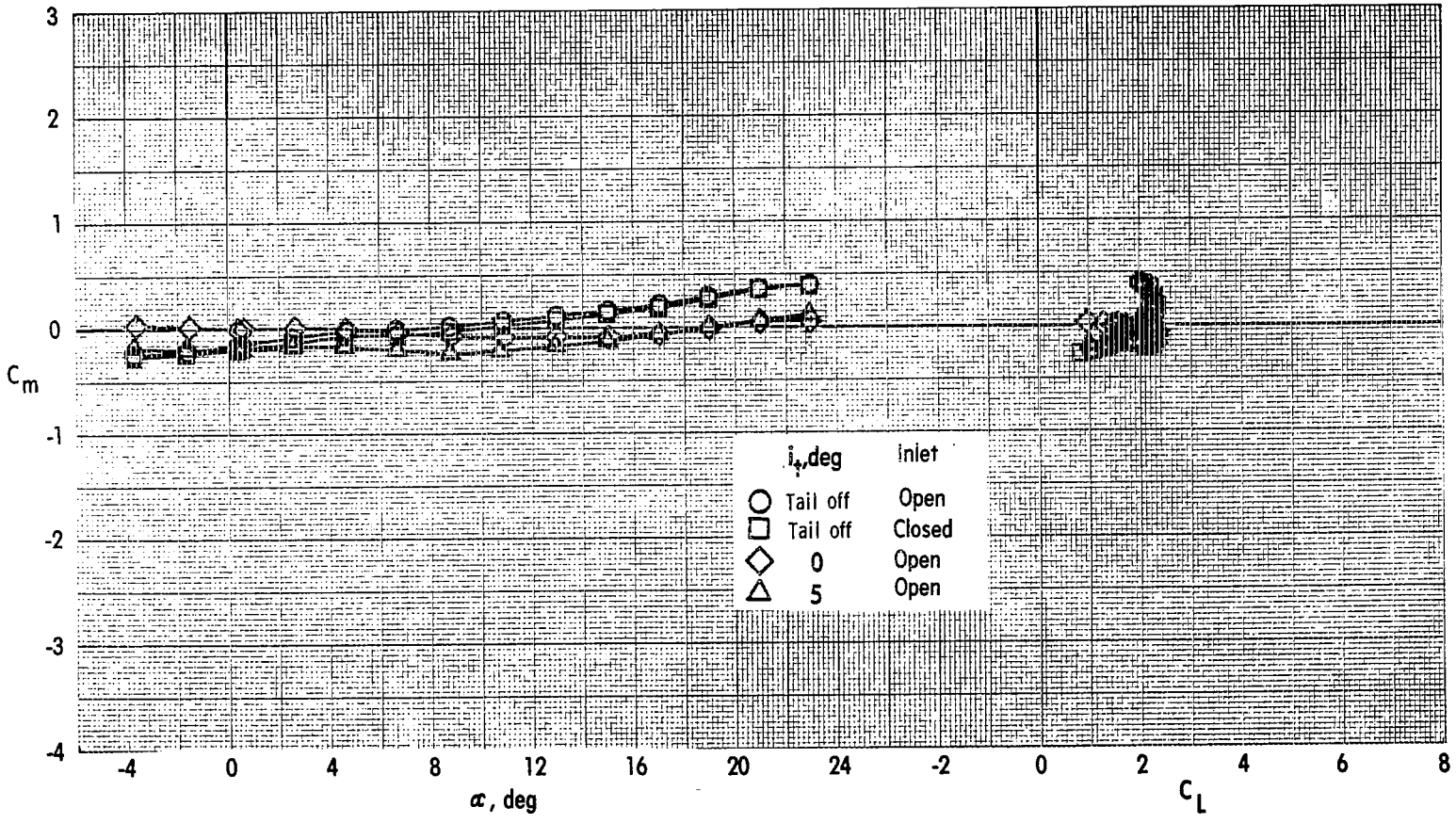

Figure 48.– Concluded.

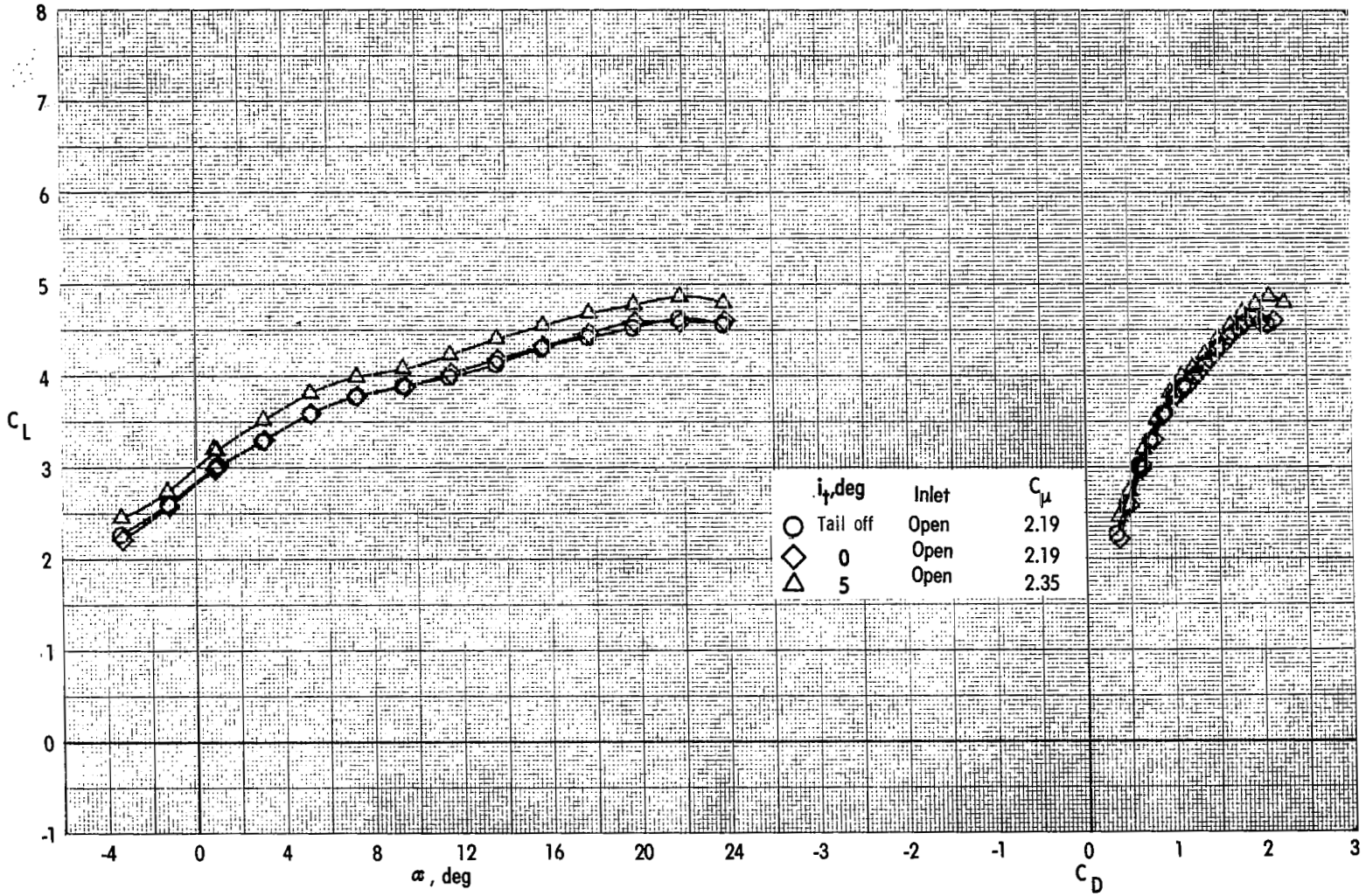

Figure 49.- Effect of tail incidence on longitudinal aerodynamic characteristics. Landing configuration; engine 10-90.

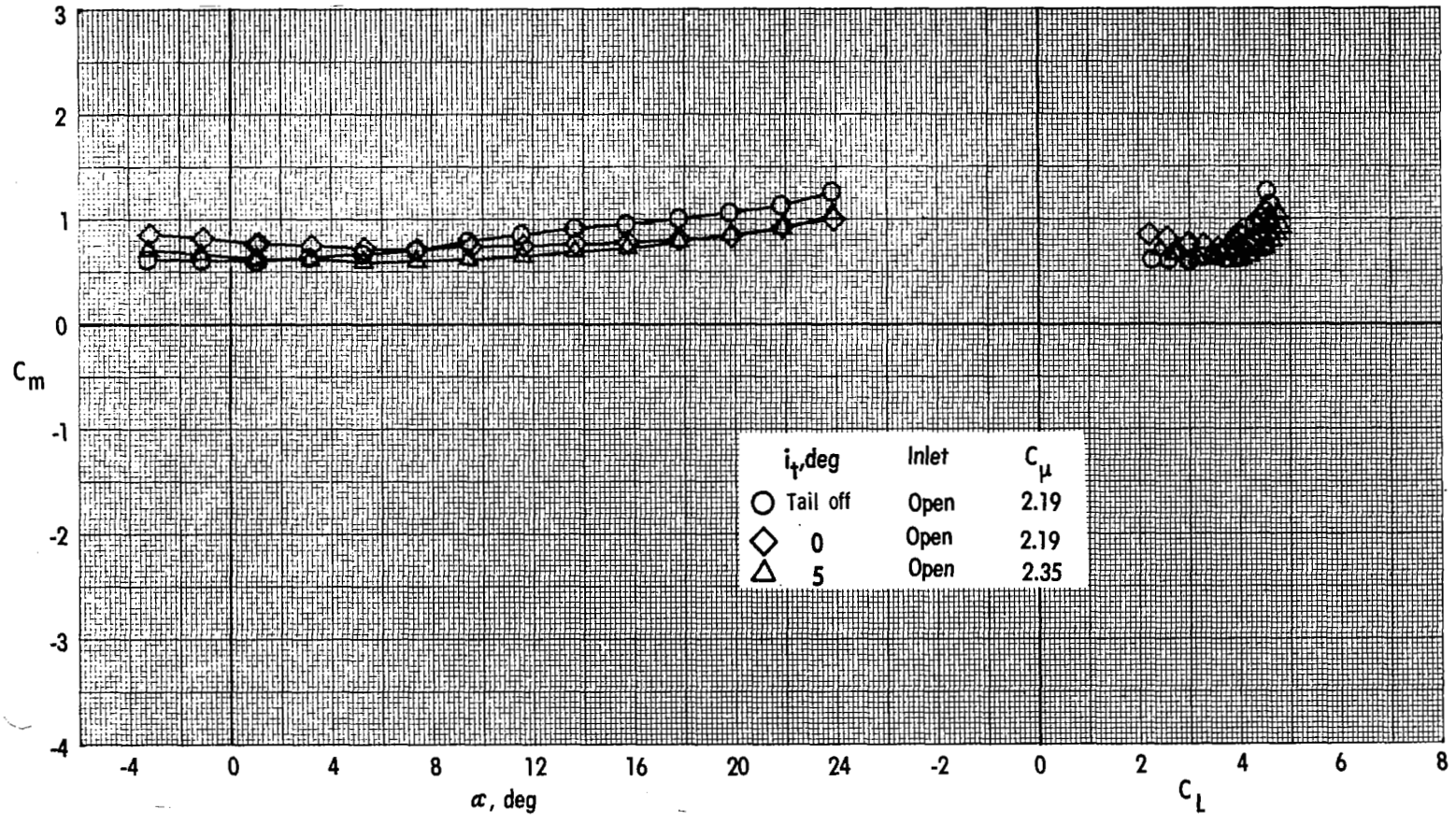

Figure 49.- Concluded.

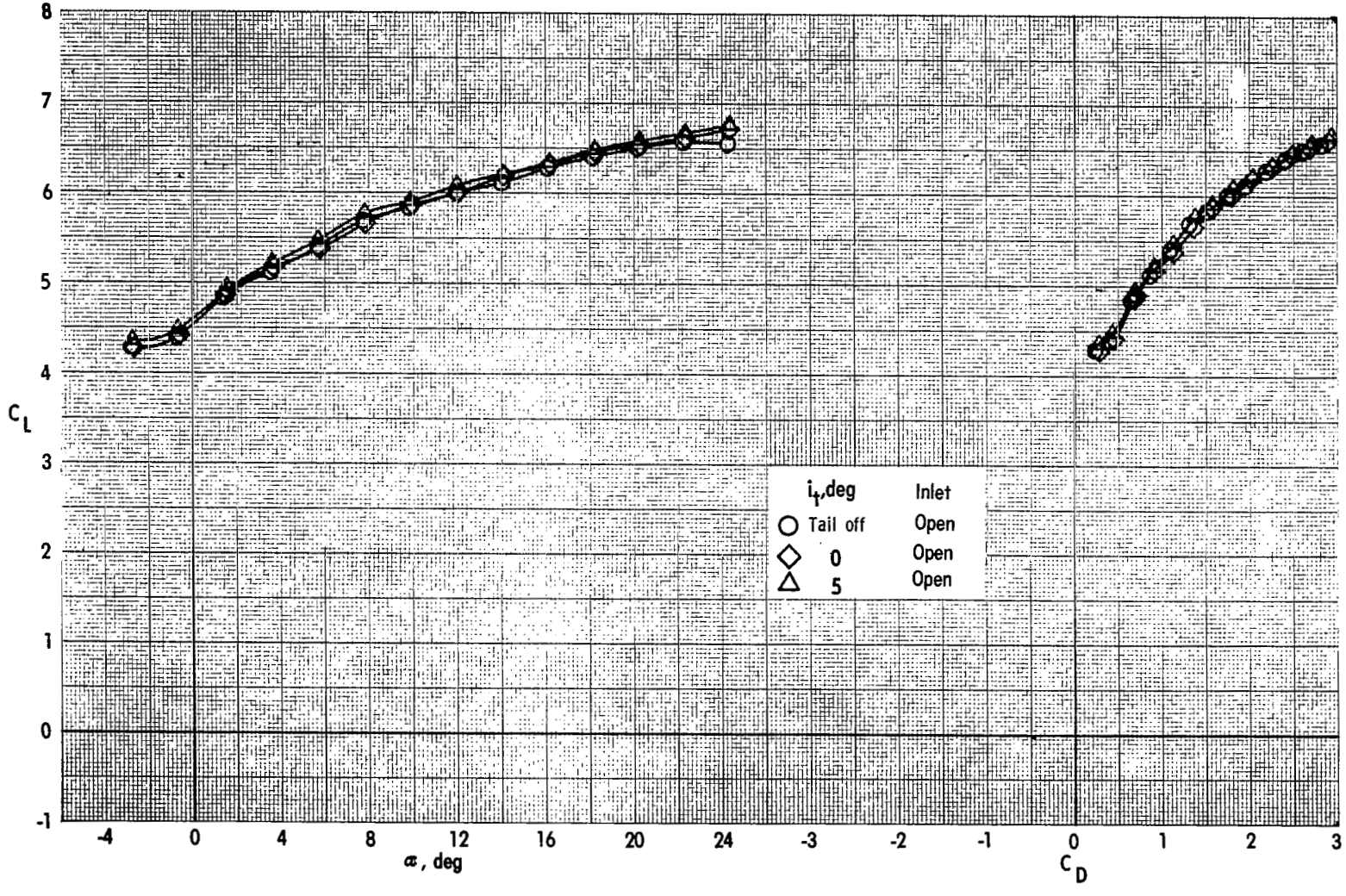

Figure 50.- Effect of tail incidence on longitudinal aerodynamic characteristics. Landing configuration; engine 10-90; C_μ = 4.40.

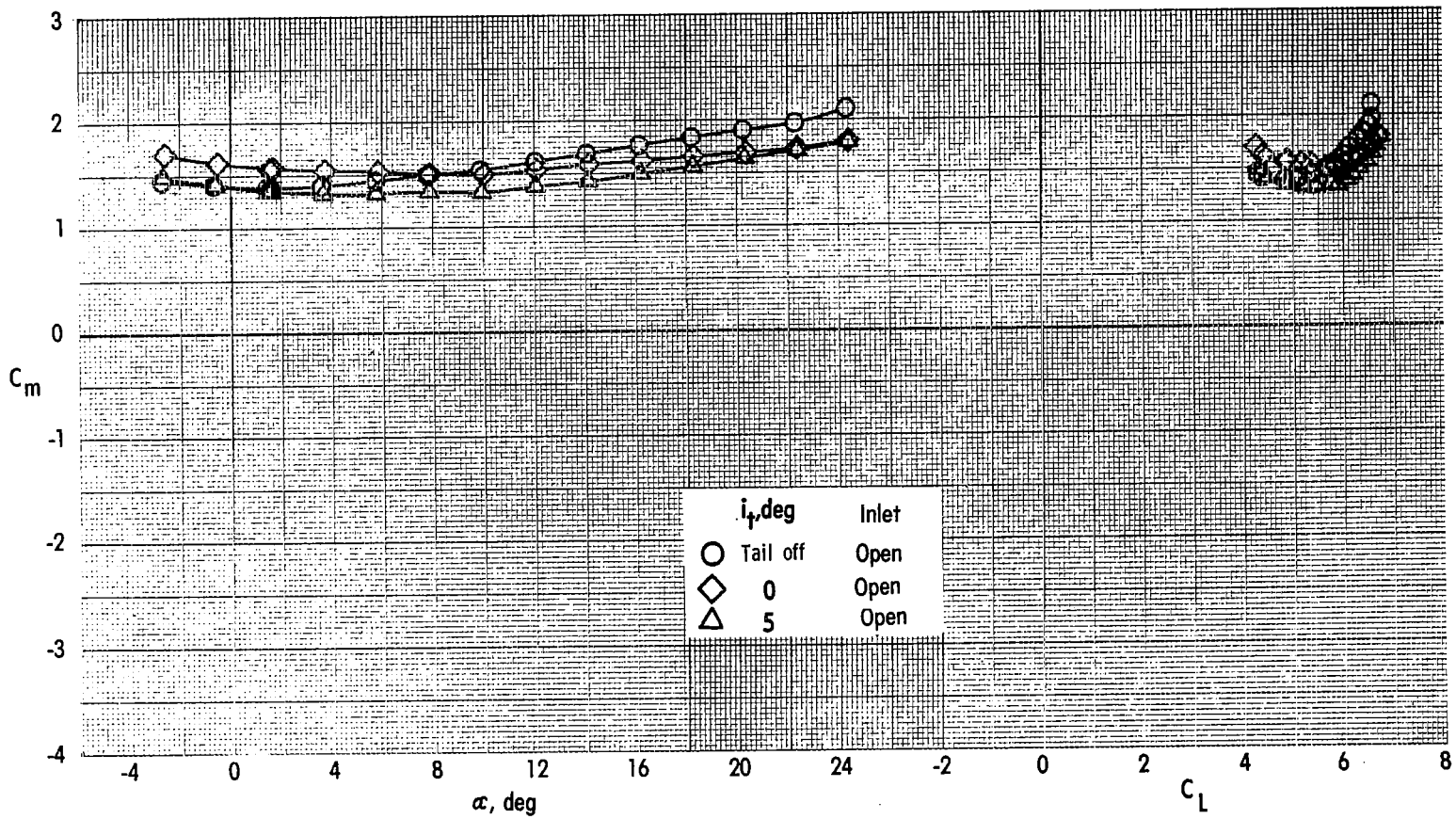

Figure 50.- Concluded.

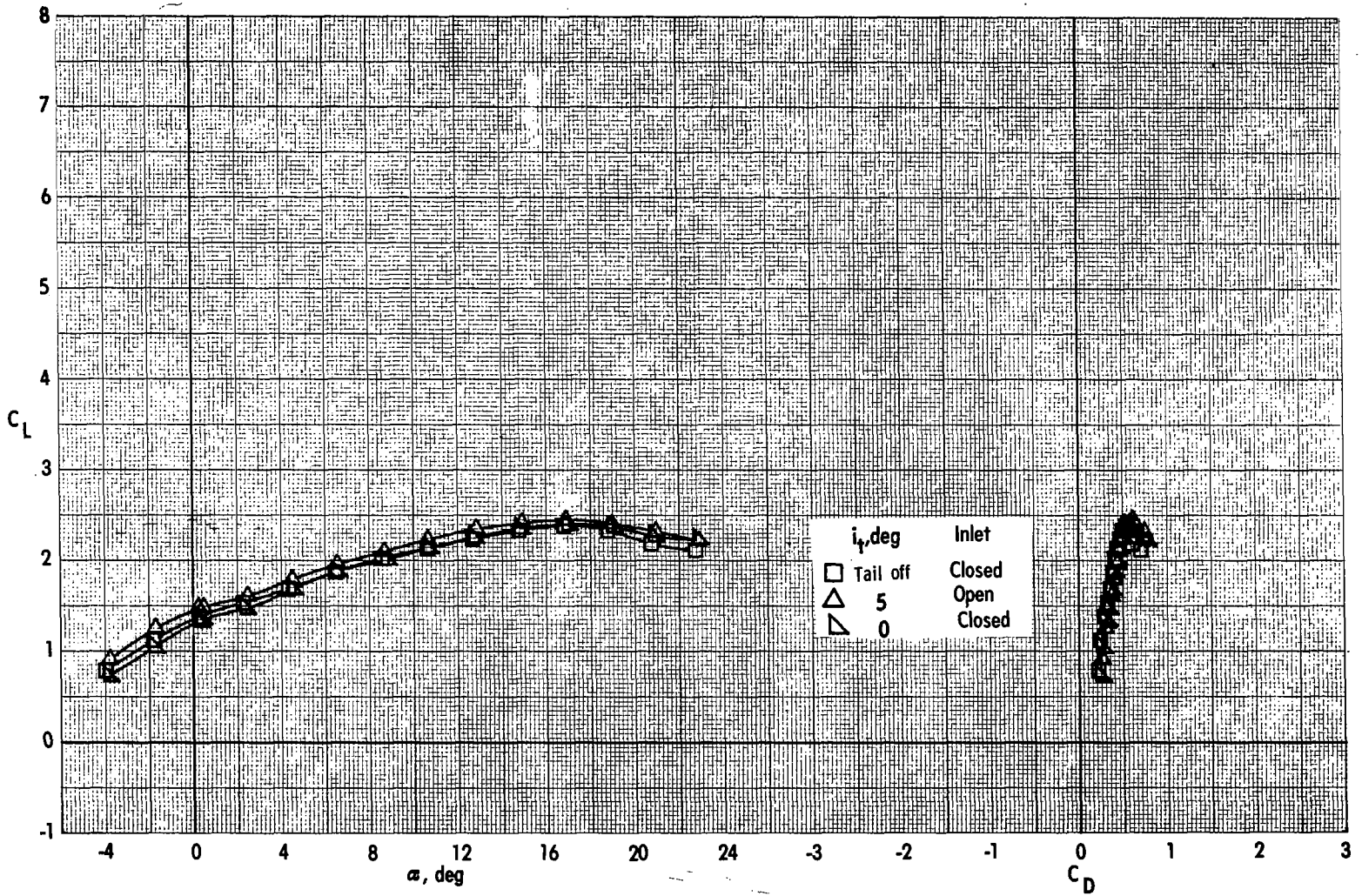

Figure 51.- Effect of tail incidence on longitudinal aerodynamic characteristics. Landing configuration; engine 75-65; $C_\mu = 0$.

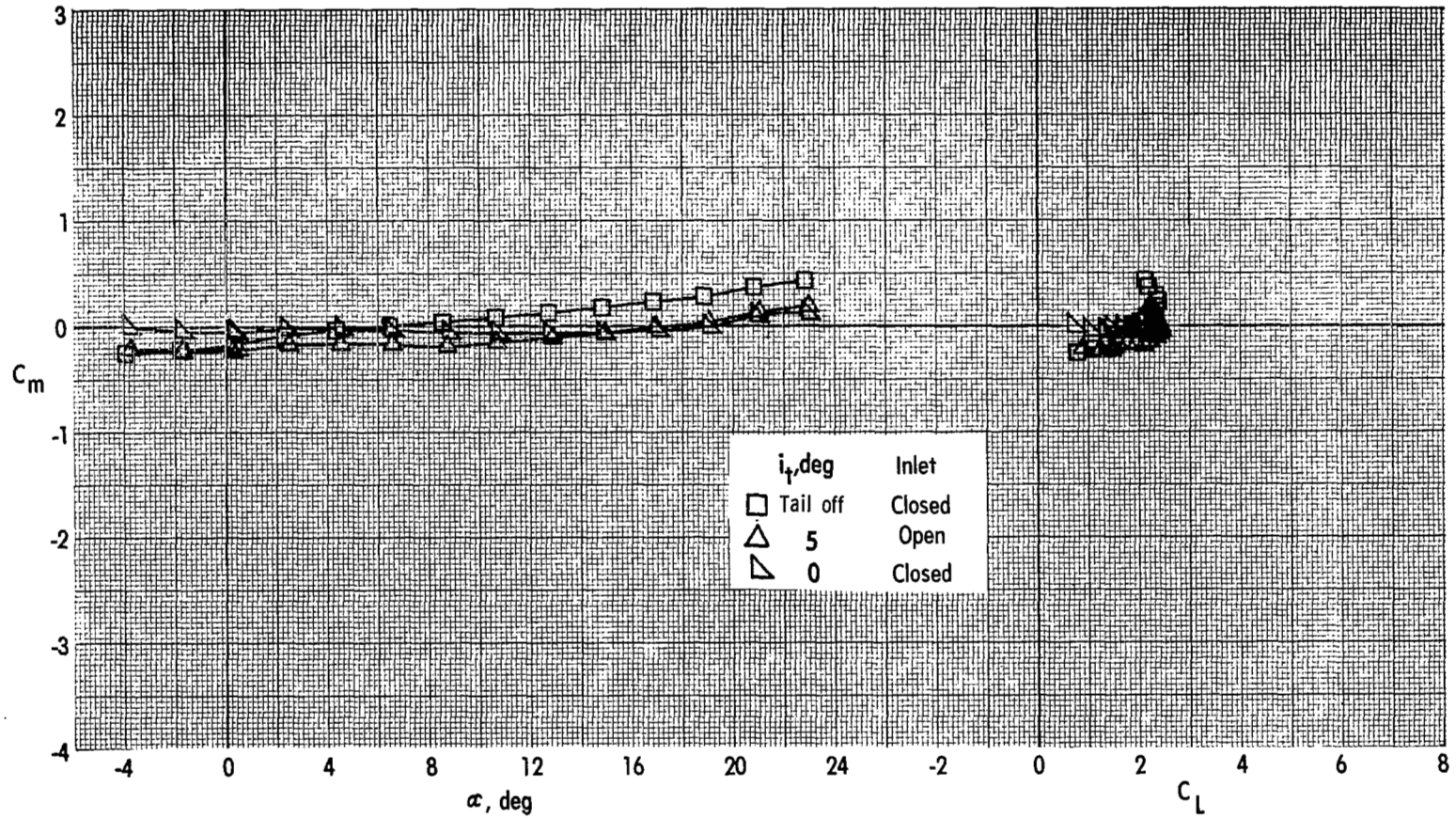

Figure 51.- Concluded.

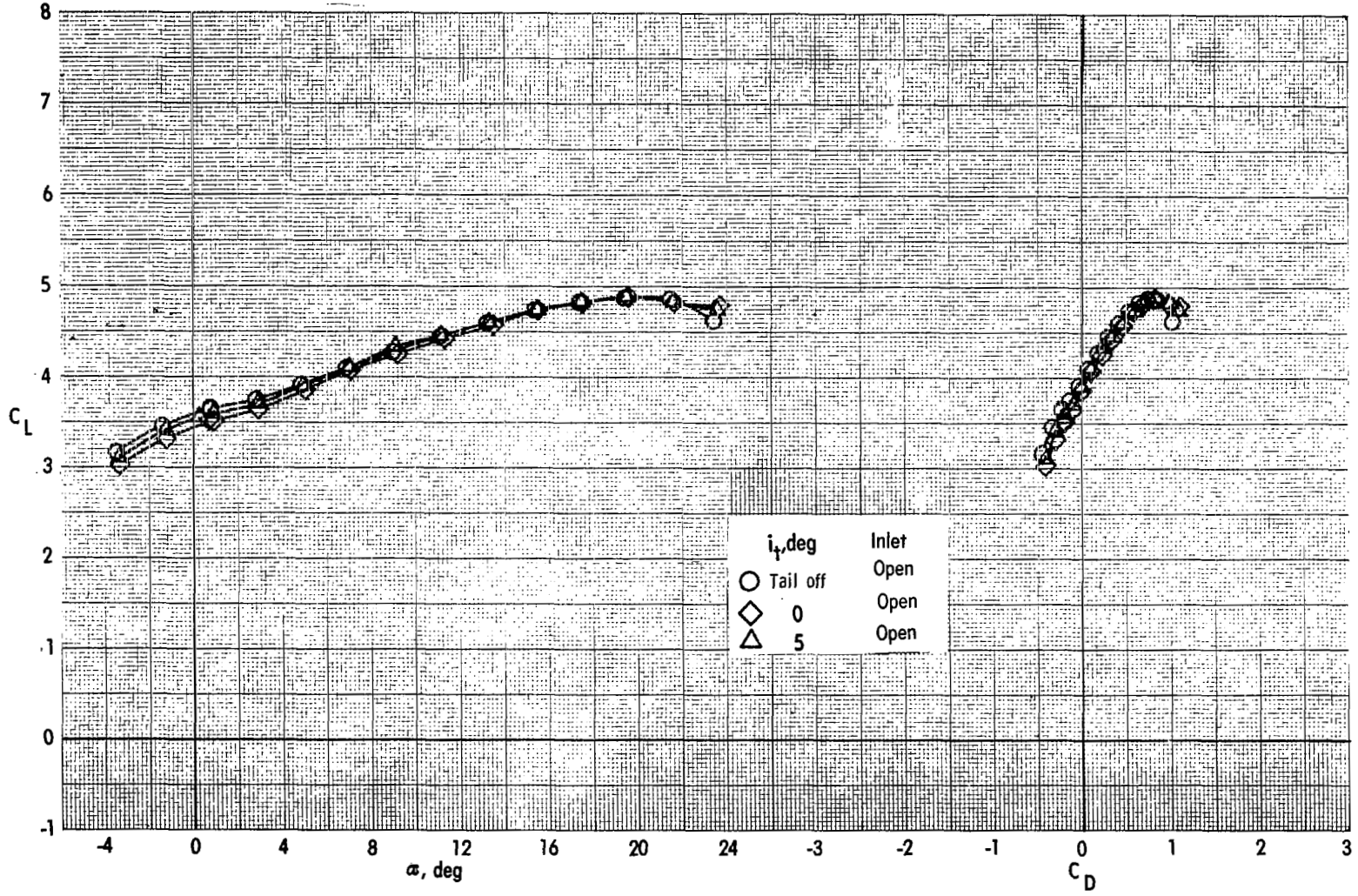

Figure 52.- Effect of tail incidence on longitudinal aerodynamic characteristics. Landing configuration; engine 75-65; C_μ = 2.01.

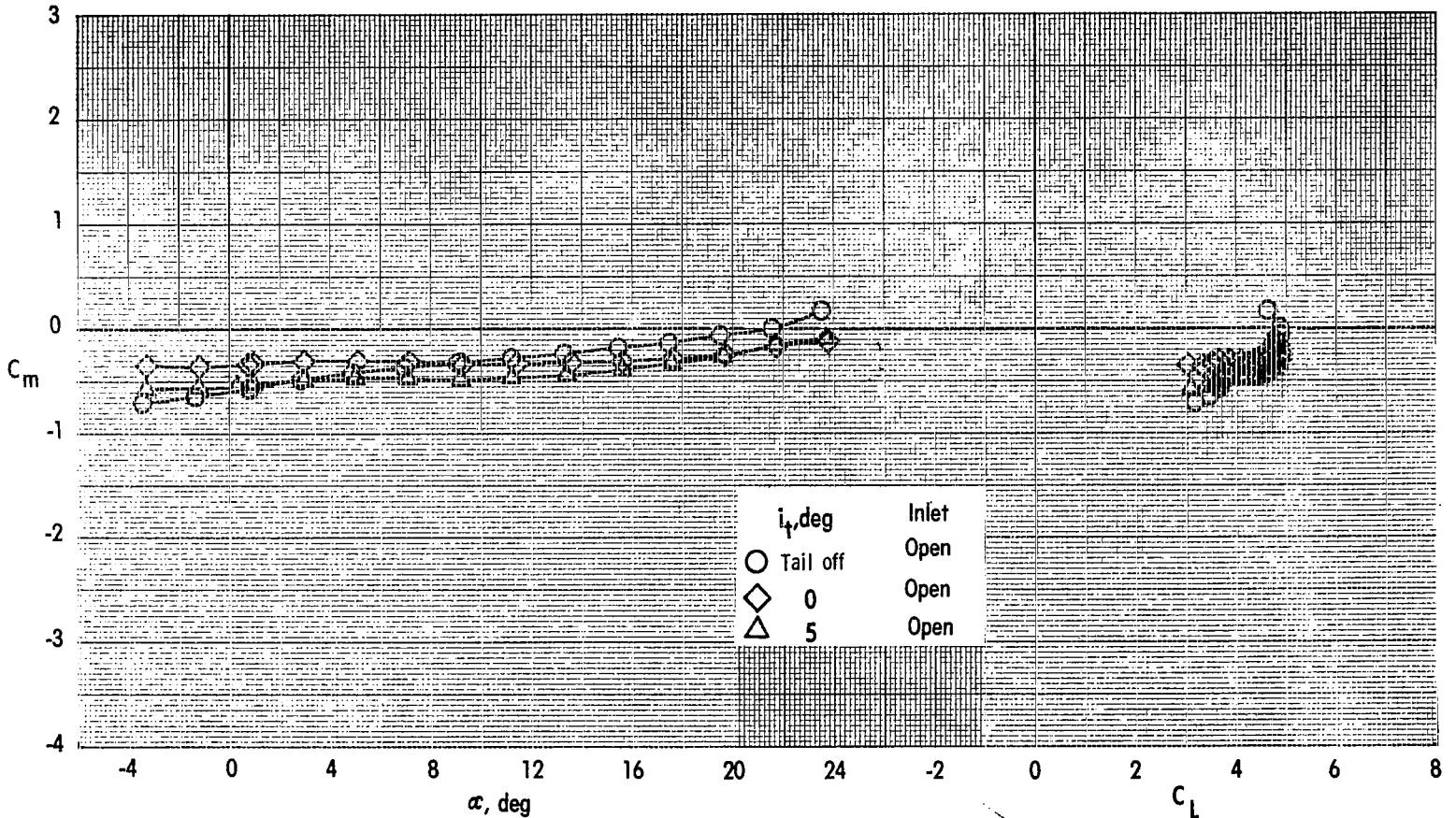

Figure 52.- Concluded.

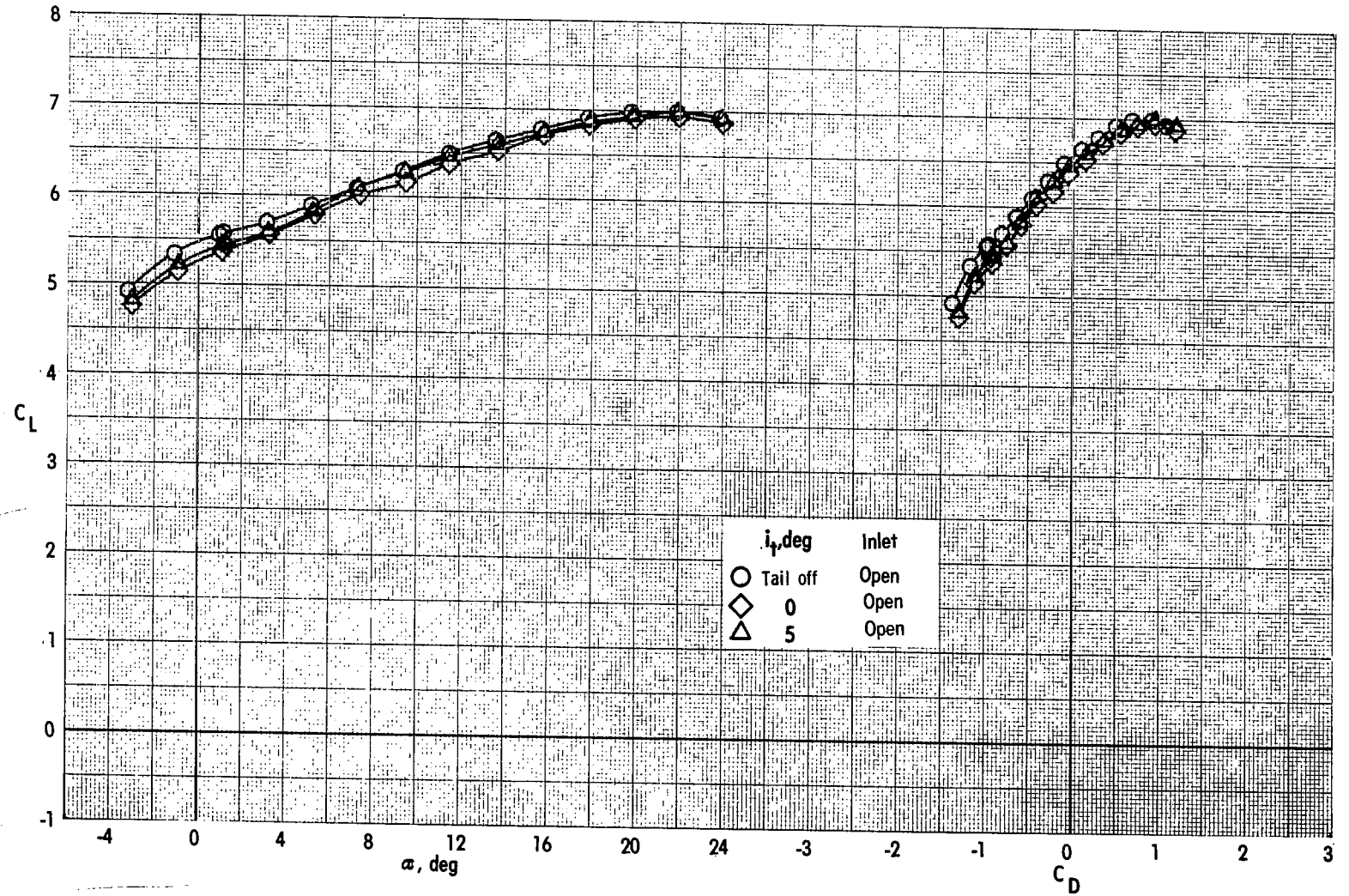

Figure 53.- Effect of tail incidence on longitudinal aerodynamic characteristics. Landing configuration; engine 75-65; $C_\mu = 4.06$.

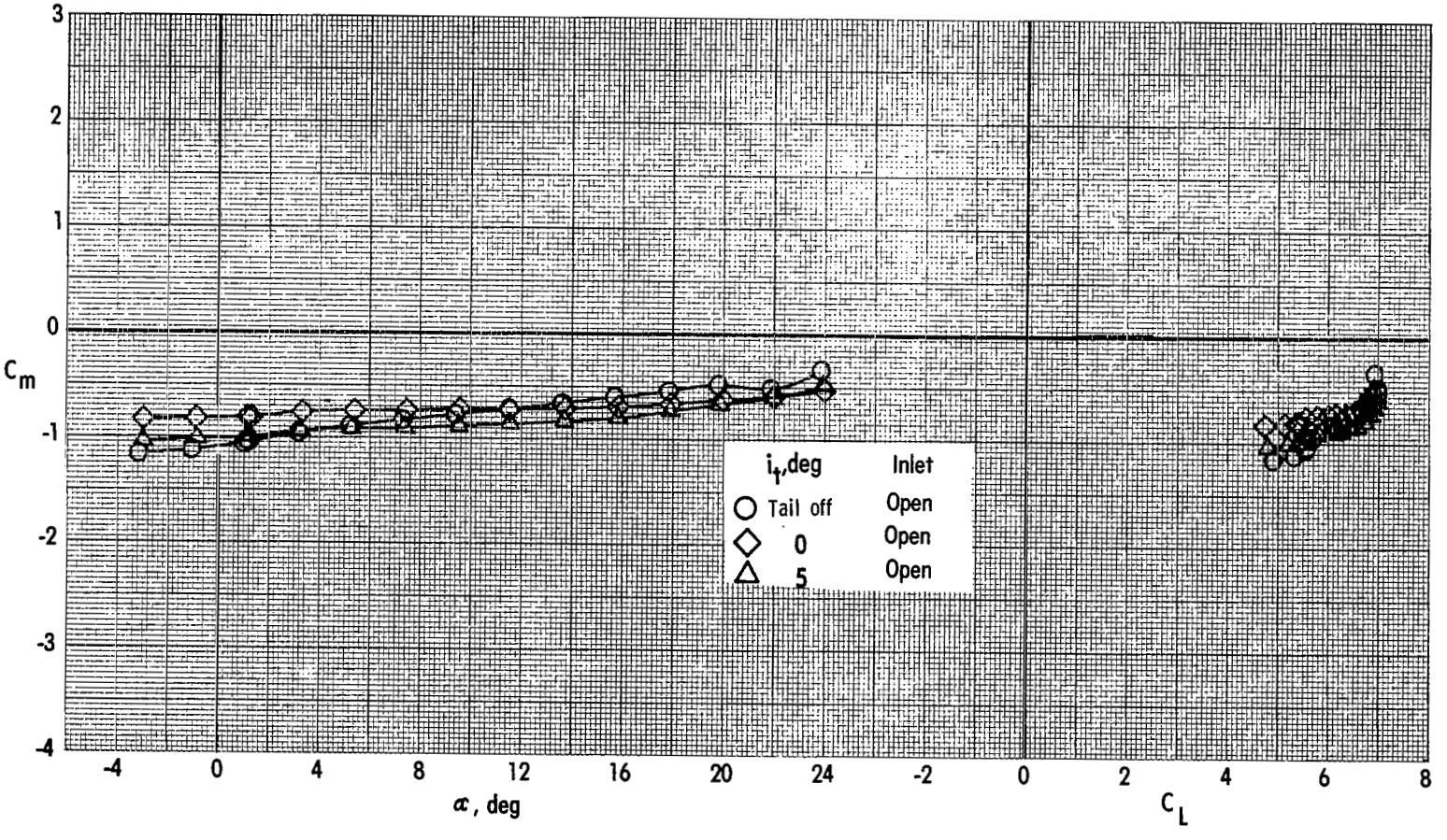

Figure 53.- Concluded.

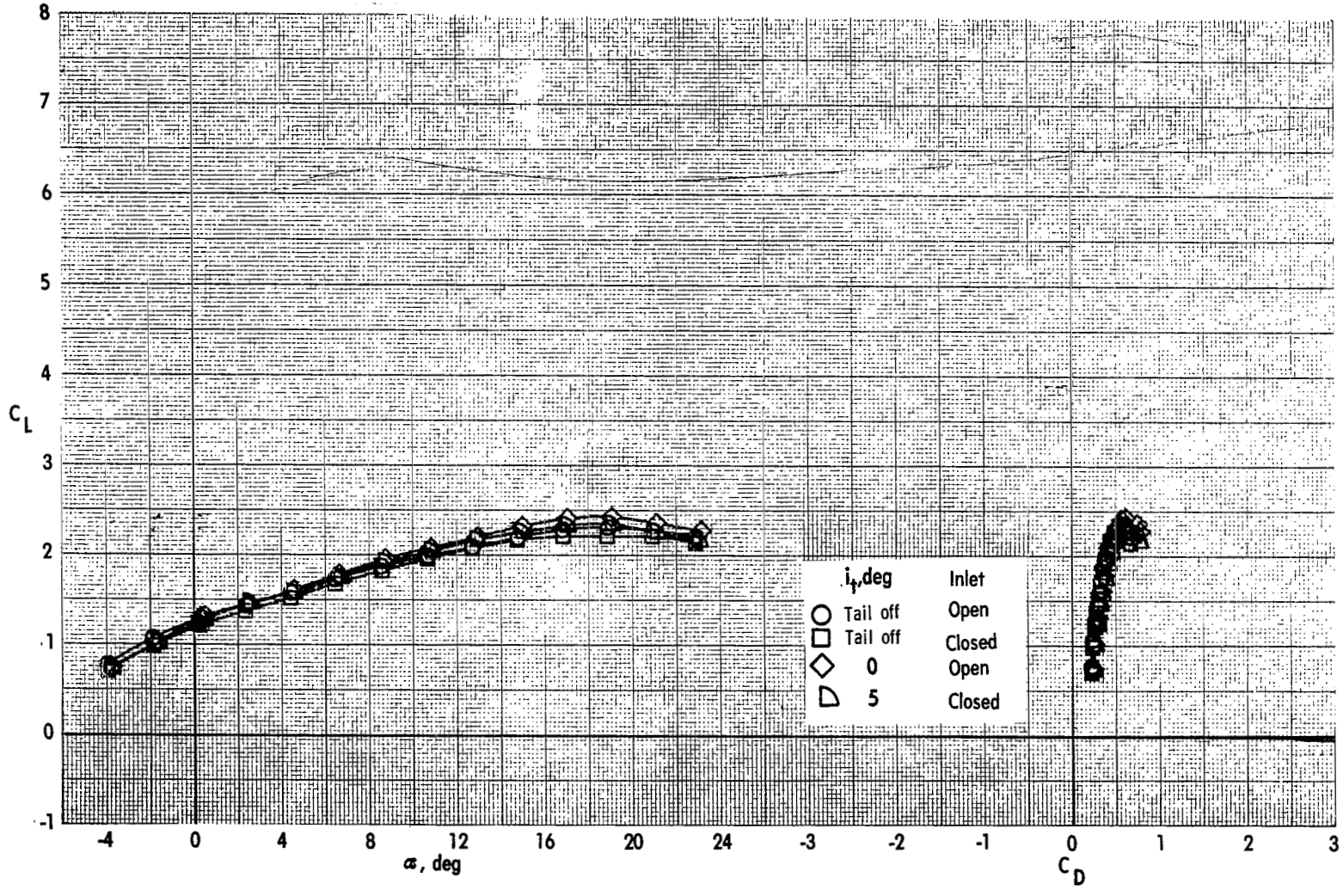

Figure 54.- Effect of tail incidence on longitudinal aerodynamic characteristics. Landing configuration; engine 110-65; $C_\mu = 0$.

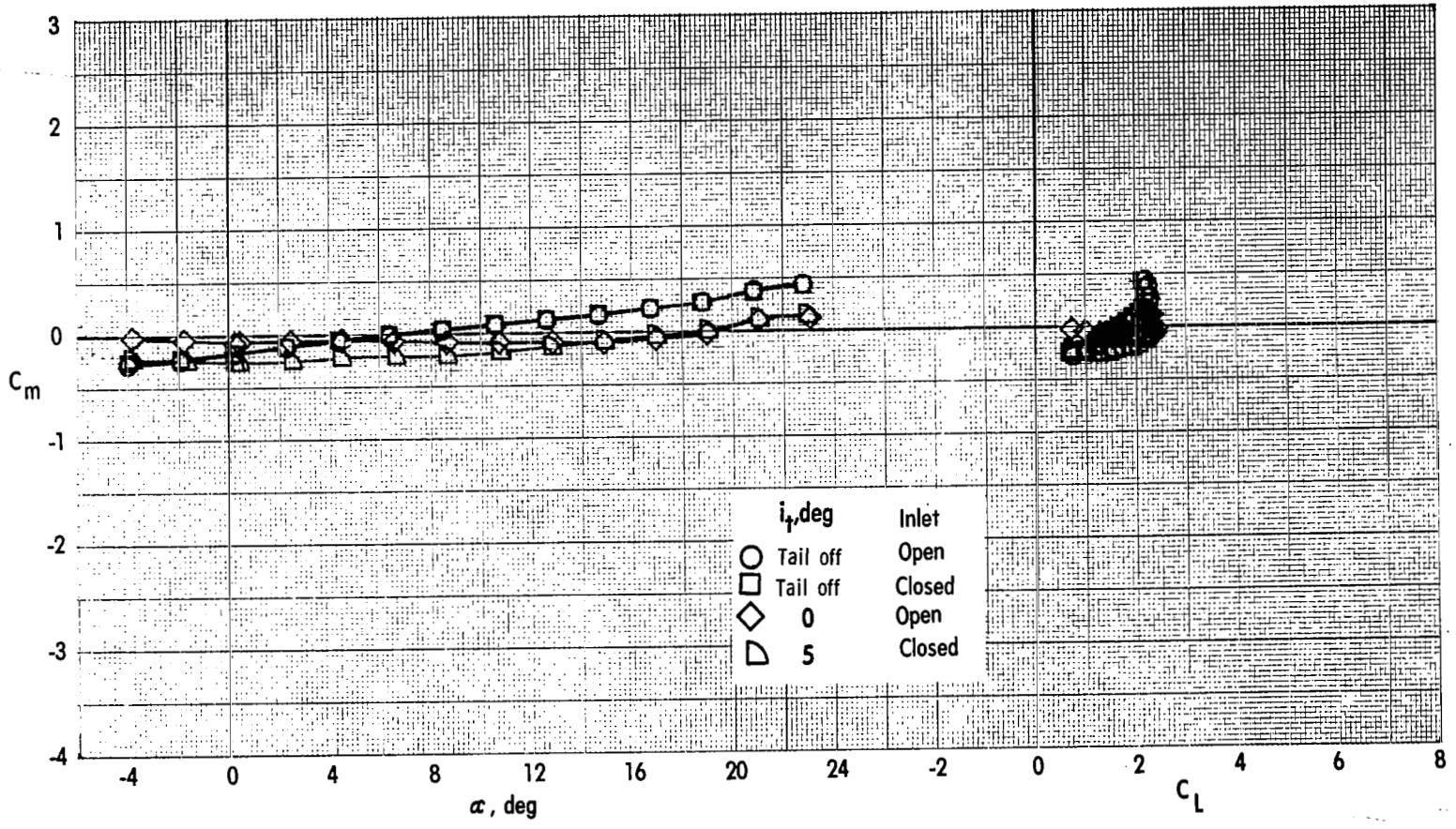

Figure 54.- Concluded.

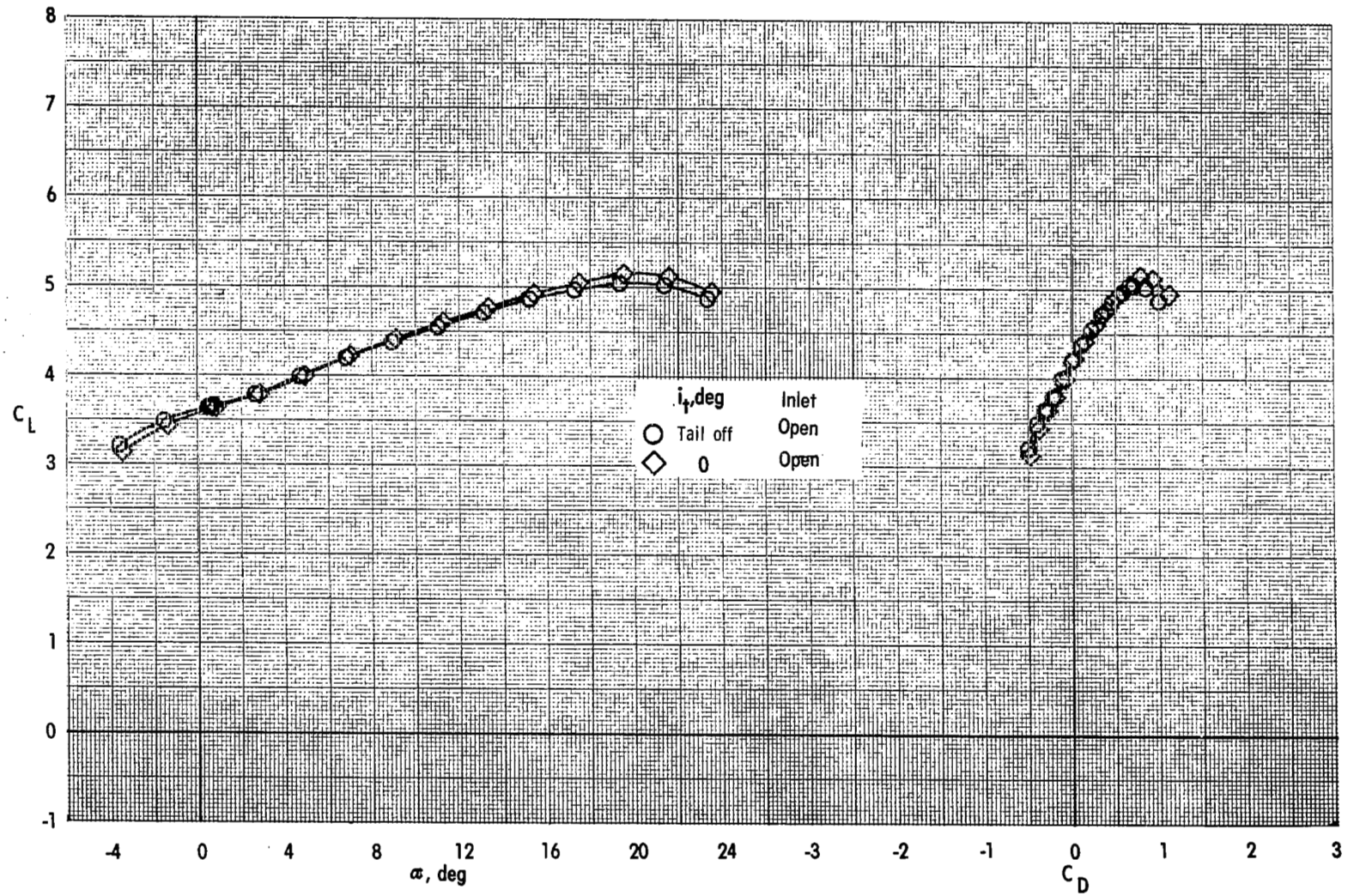

Figure 55.- Effect of tail incidence on longitudinal aerodynamic characteristics. Landing configuration; engine 110-65; C_μ = 2.05.

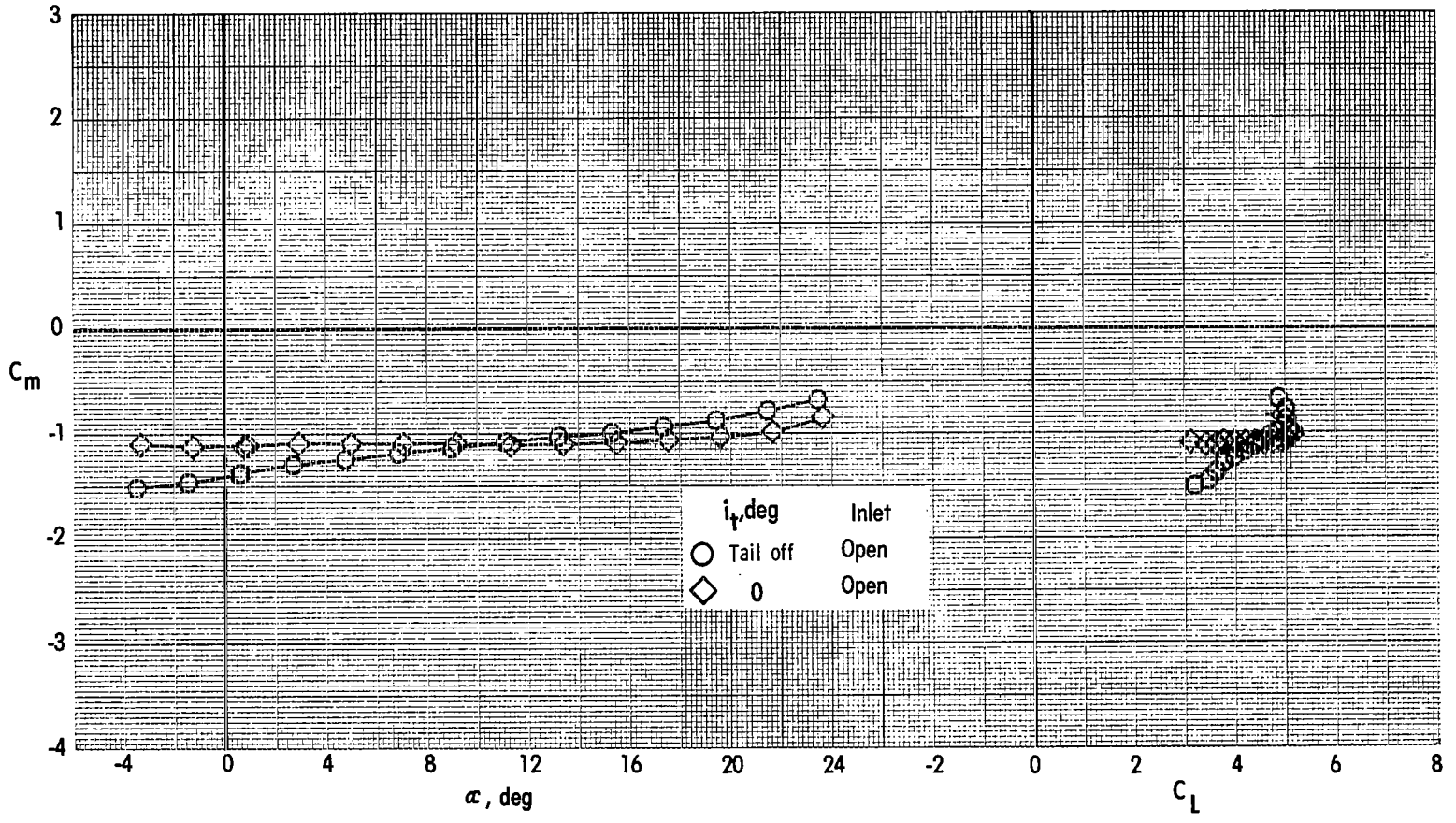

Figure 55.- Concluded.

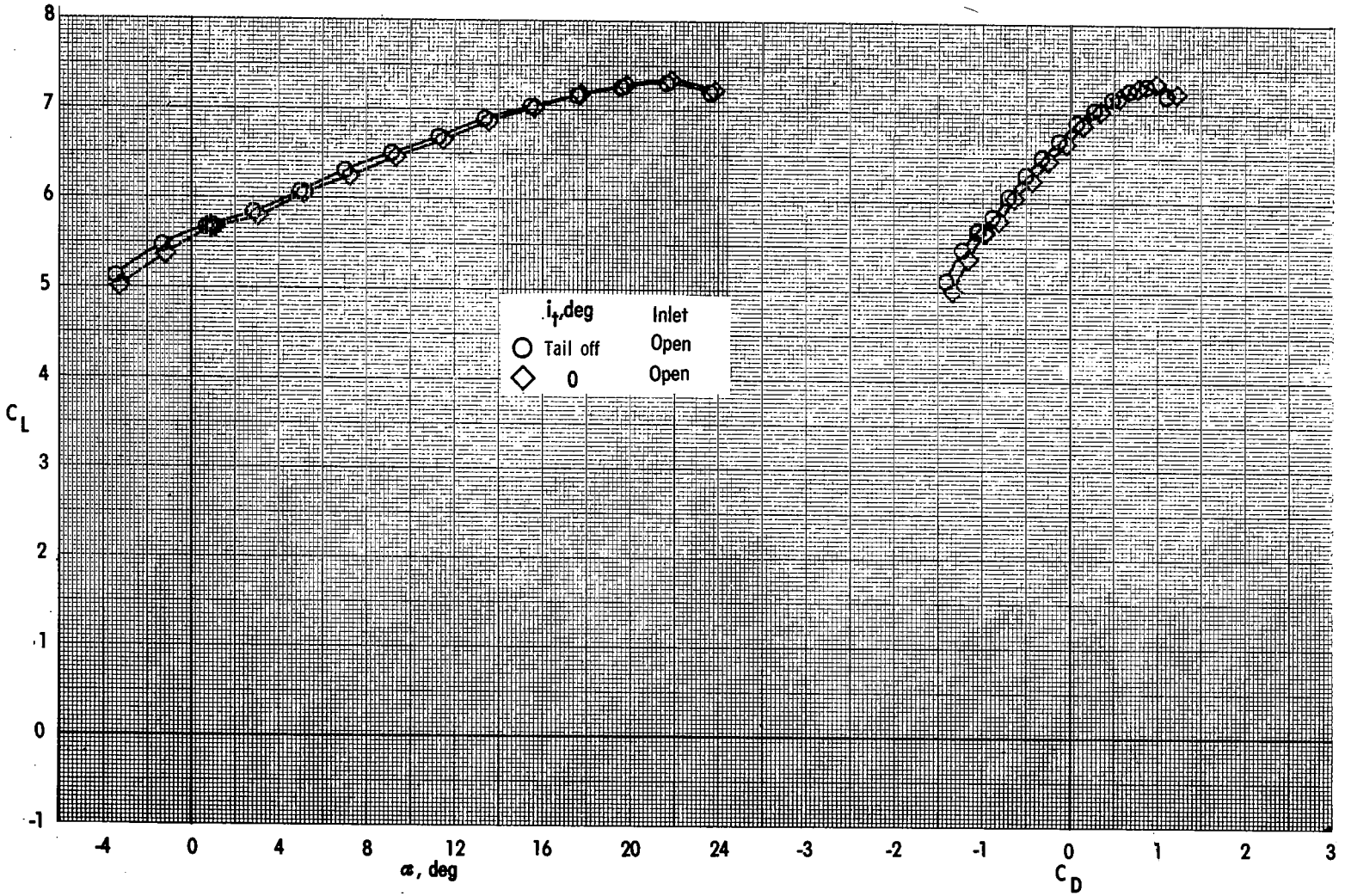

Figure 56.- Effect of tail incidence on longitudinal aerodynamic characteristics. Landing configuration; engine 110-65; C_μ = 4.08.

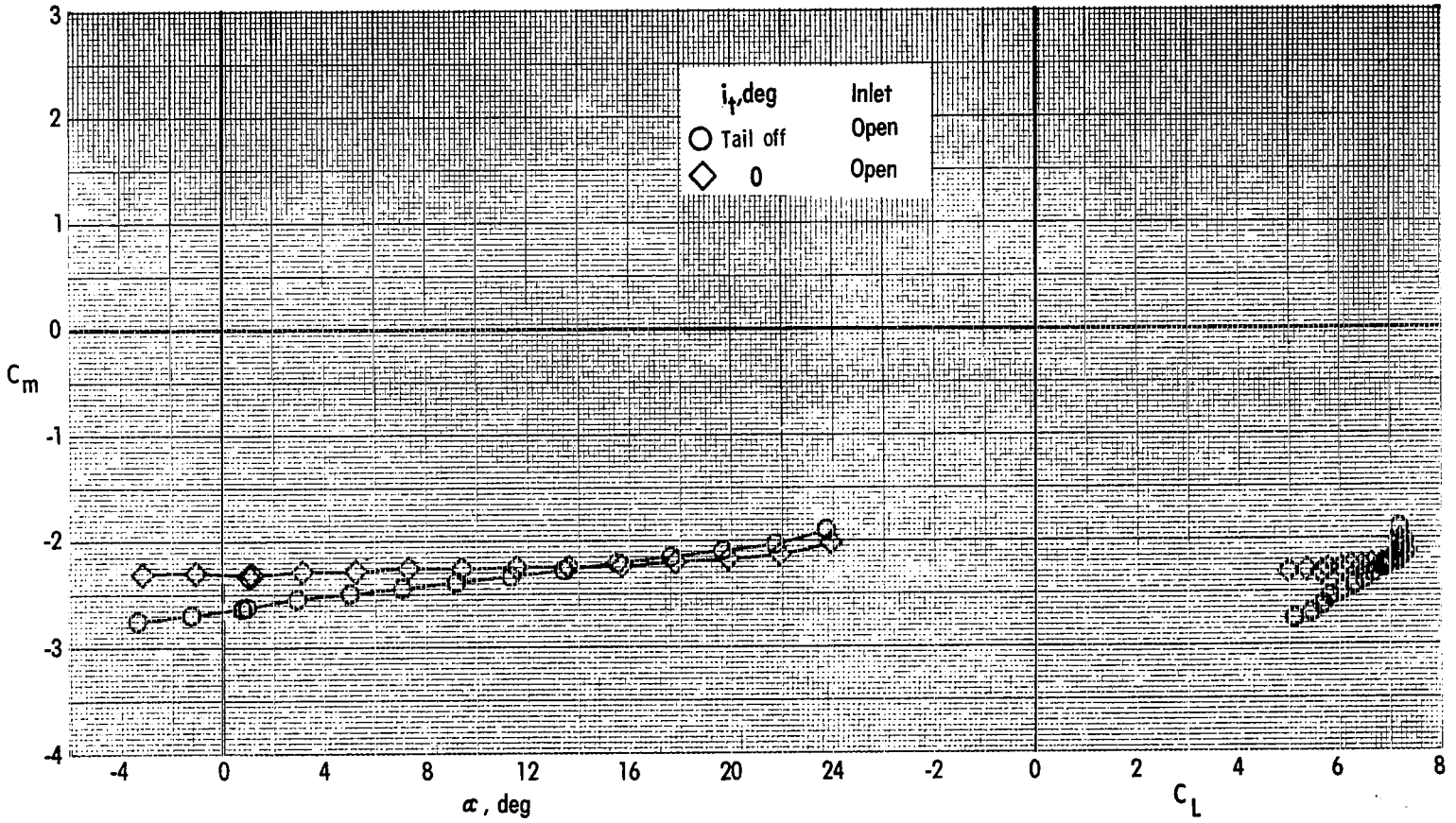

Figure 56.- Concluded.

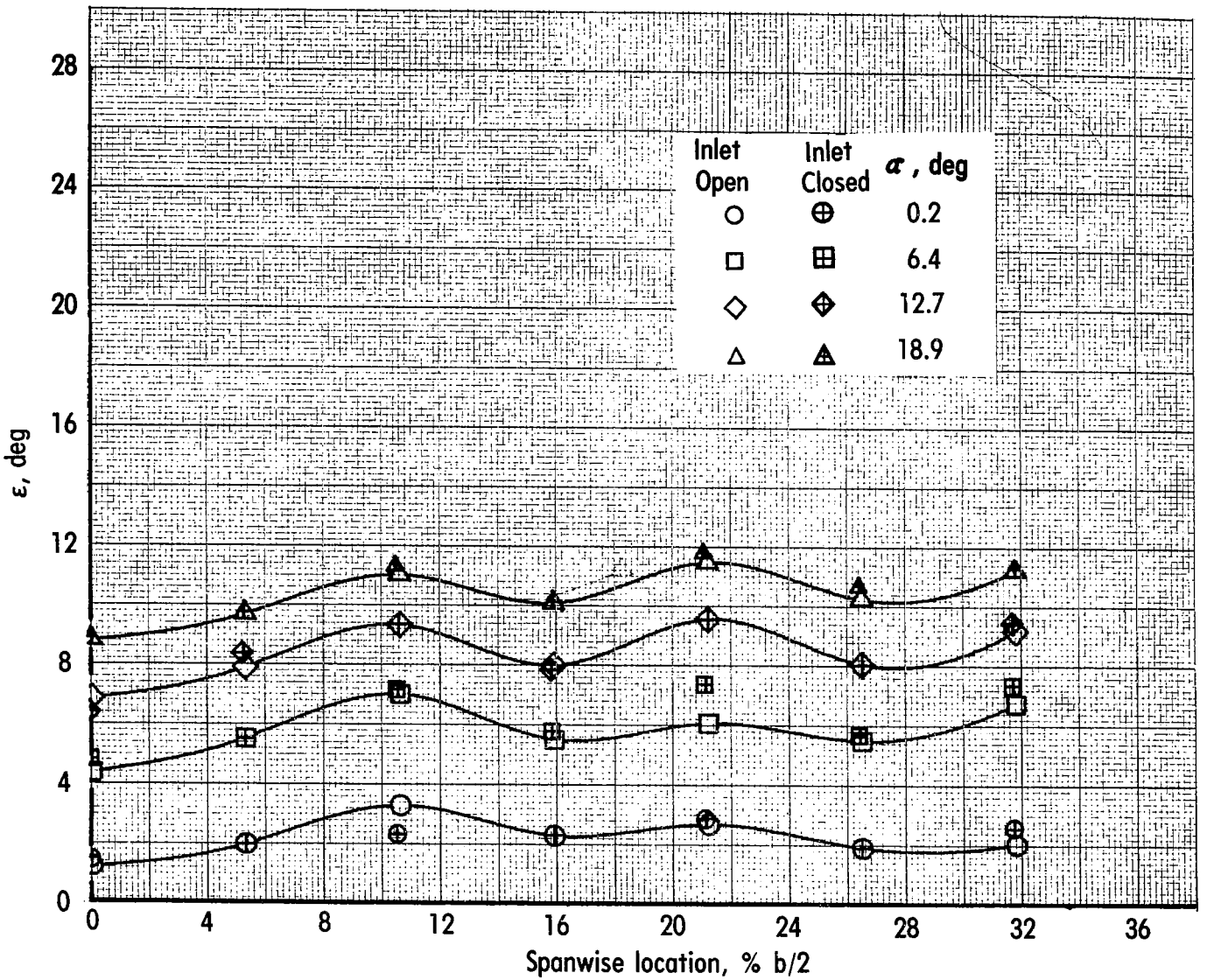

(a) $C_\mu = 0$.

Figure 57.- Effect of angle of attack on downwash angle at horizontal-tail location. Take-off configuration; engine 75-0; vertical tail and horizontal tail off.

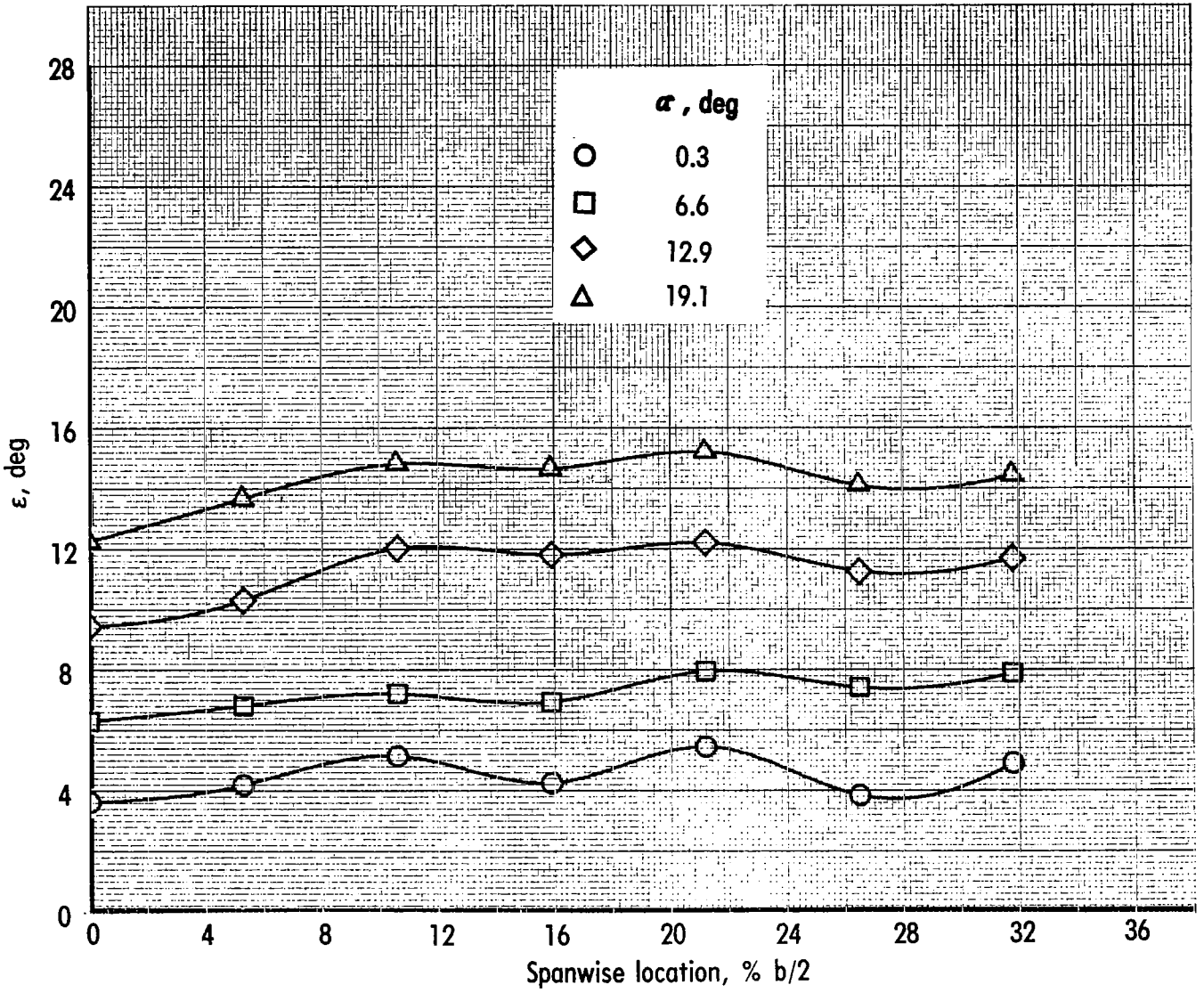

(b) C_μ = 0.99; inlets open.

Figure 57.- Continued.

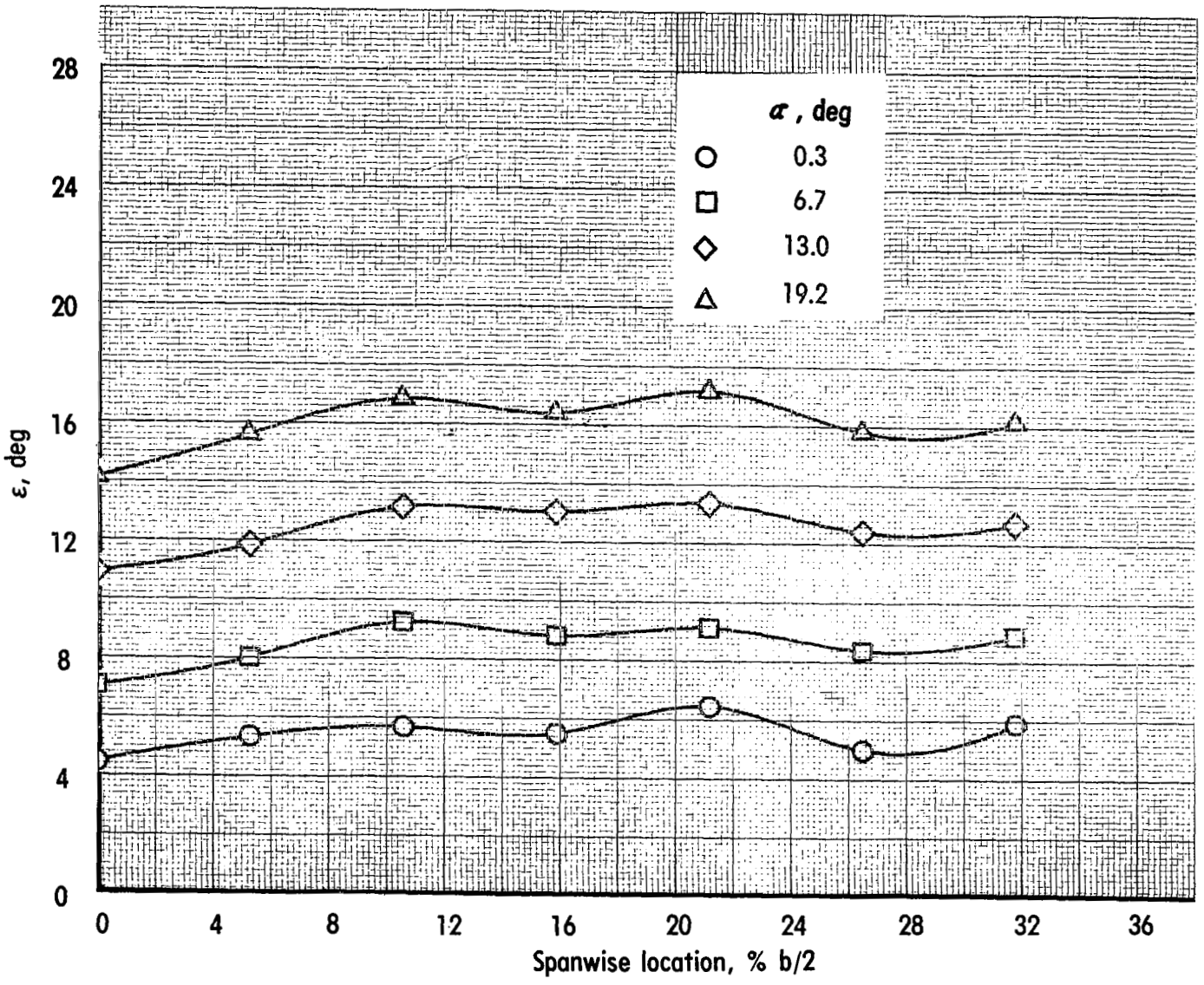

(c) C_μ = 2.00; inlets open.

Figure 57.- Continued.

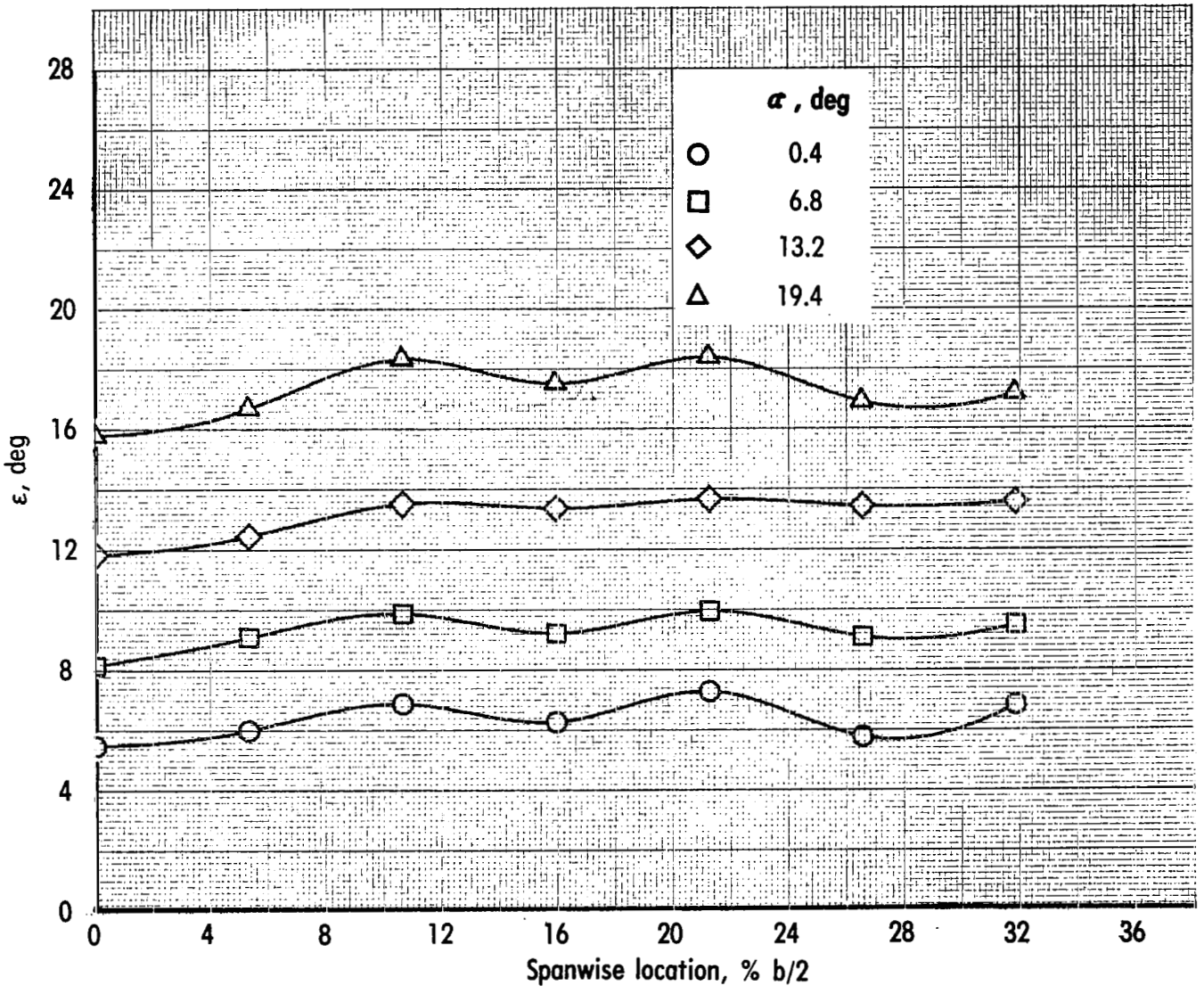

(d) C_μ = 2.97; inlets open.

Figure 57.- Continued.

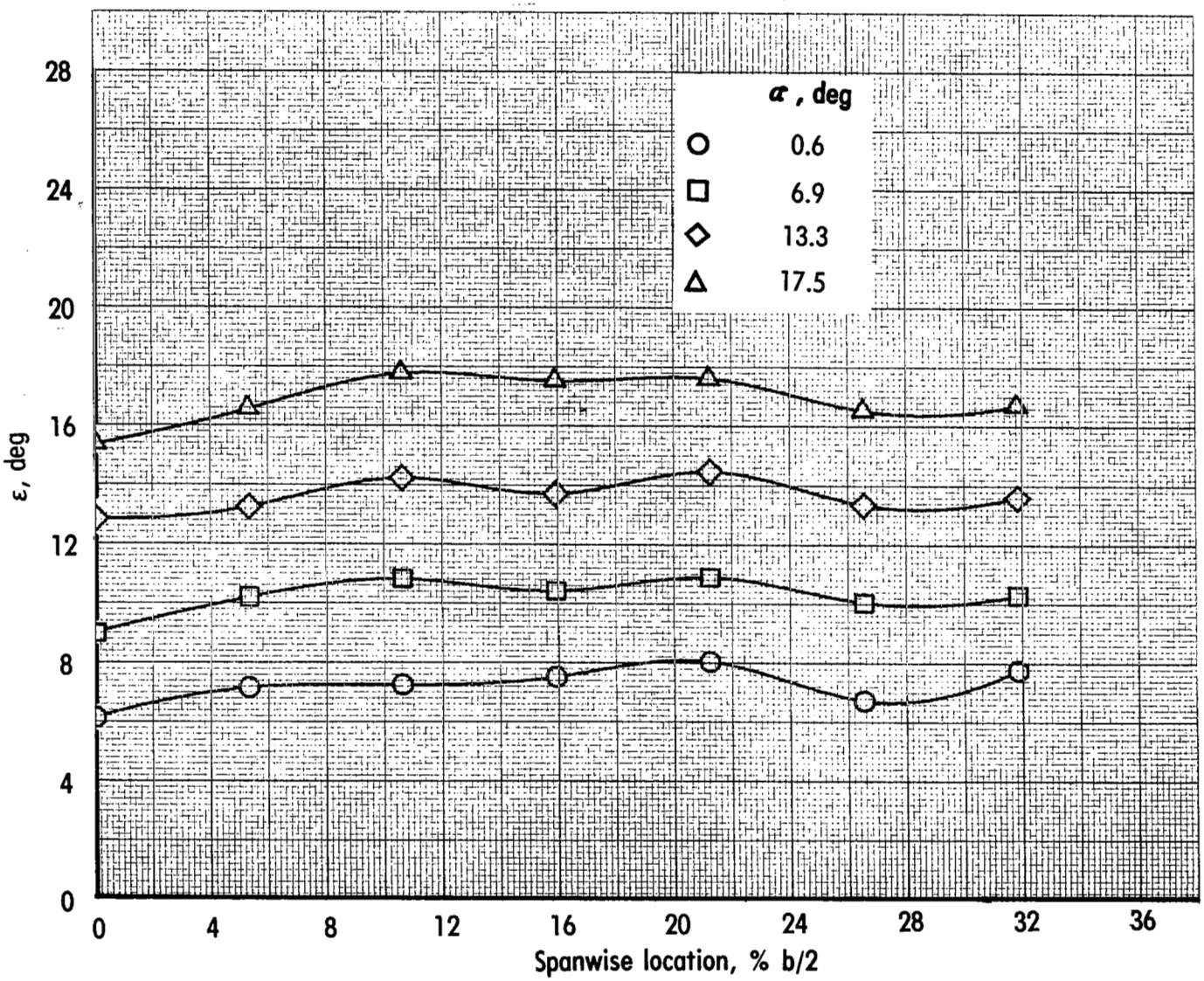

(e) C_μ = 3.94; inlets open.

Figure 57.- Concluded.

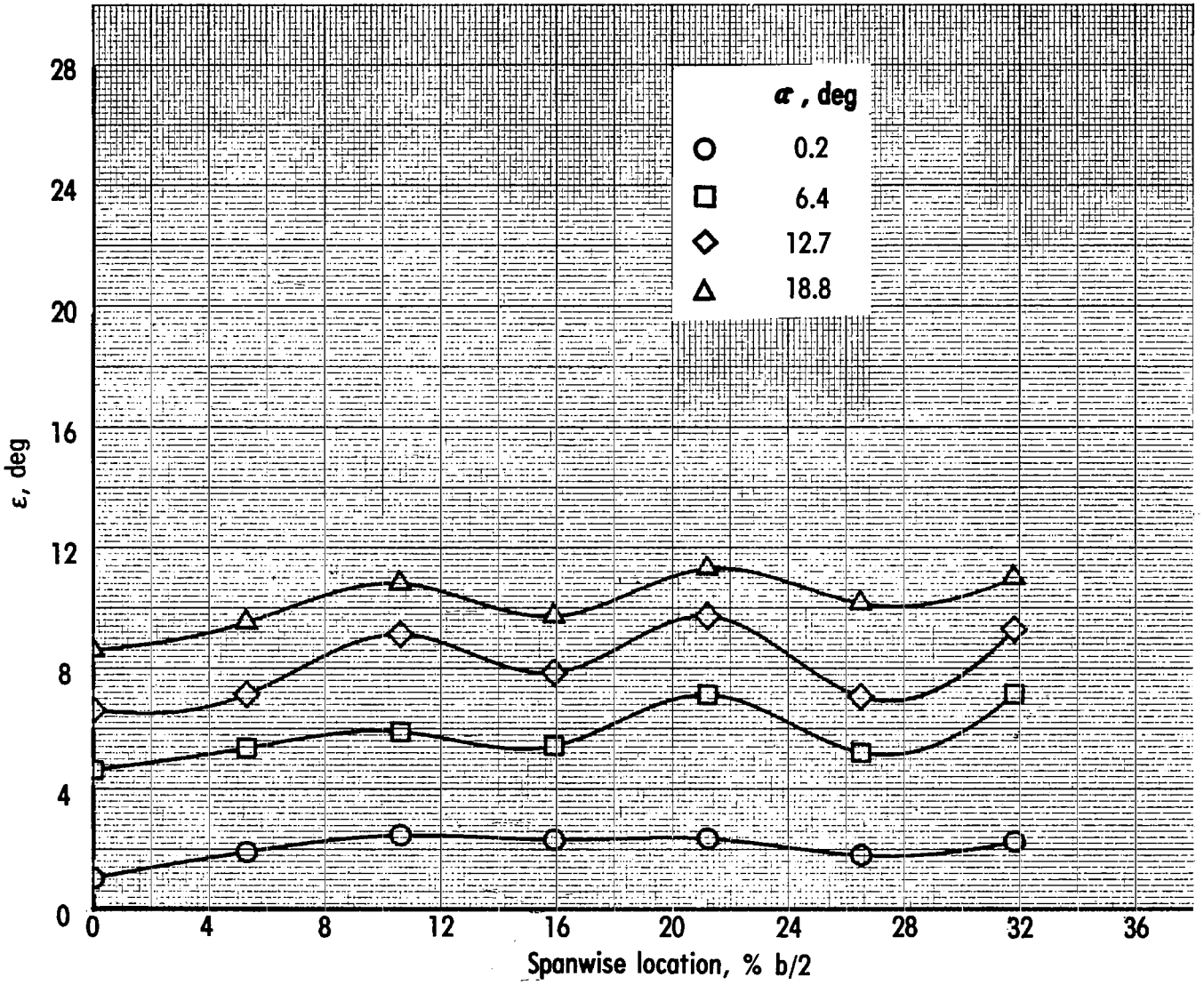

(a) C_μ = 0; inlets closed.

Figure 58.- Effect of angle of attack on downwash angle at horizontal-tail location. Take-off configuration; engine 75-25; vertical tail and horizontal tail off.

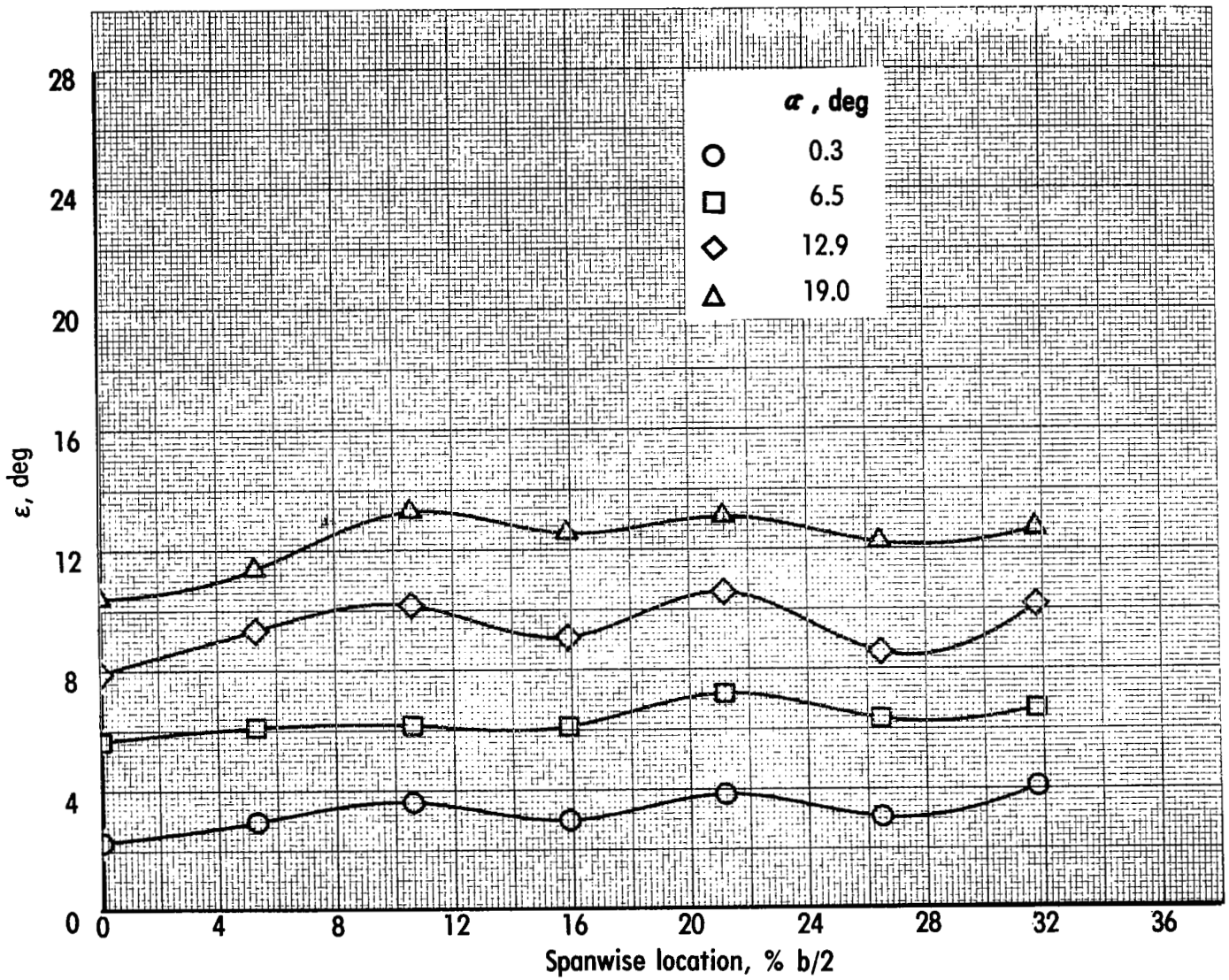

(b) C_μ = 1.00; inlets open.

Figure 58.- Continued.

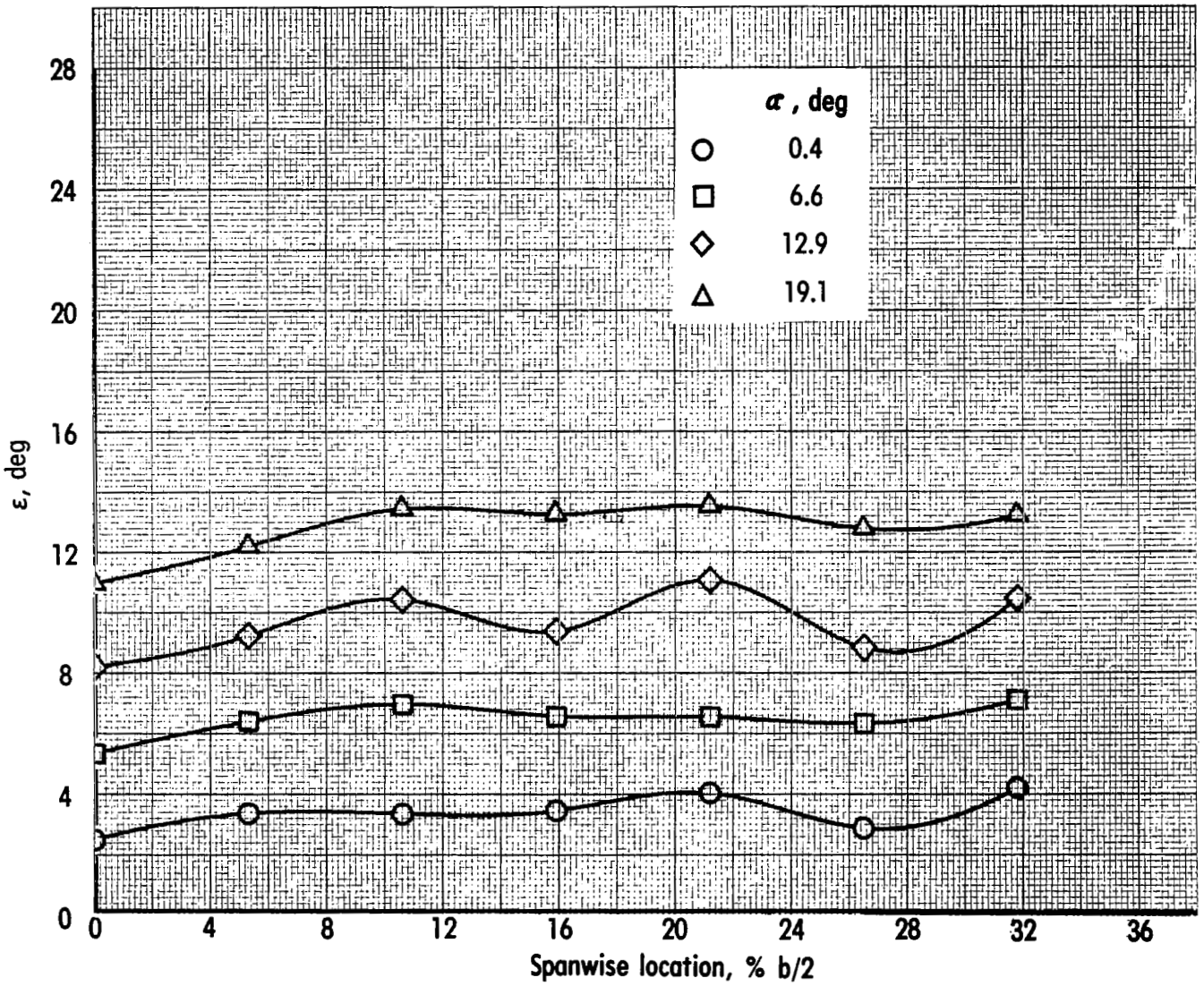

(c) C_μ = 1.99; inlets open.

Figure 58.- Continued.

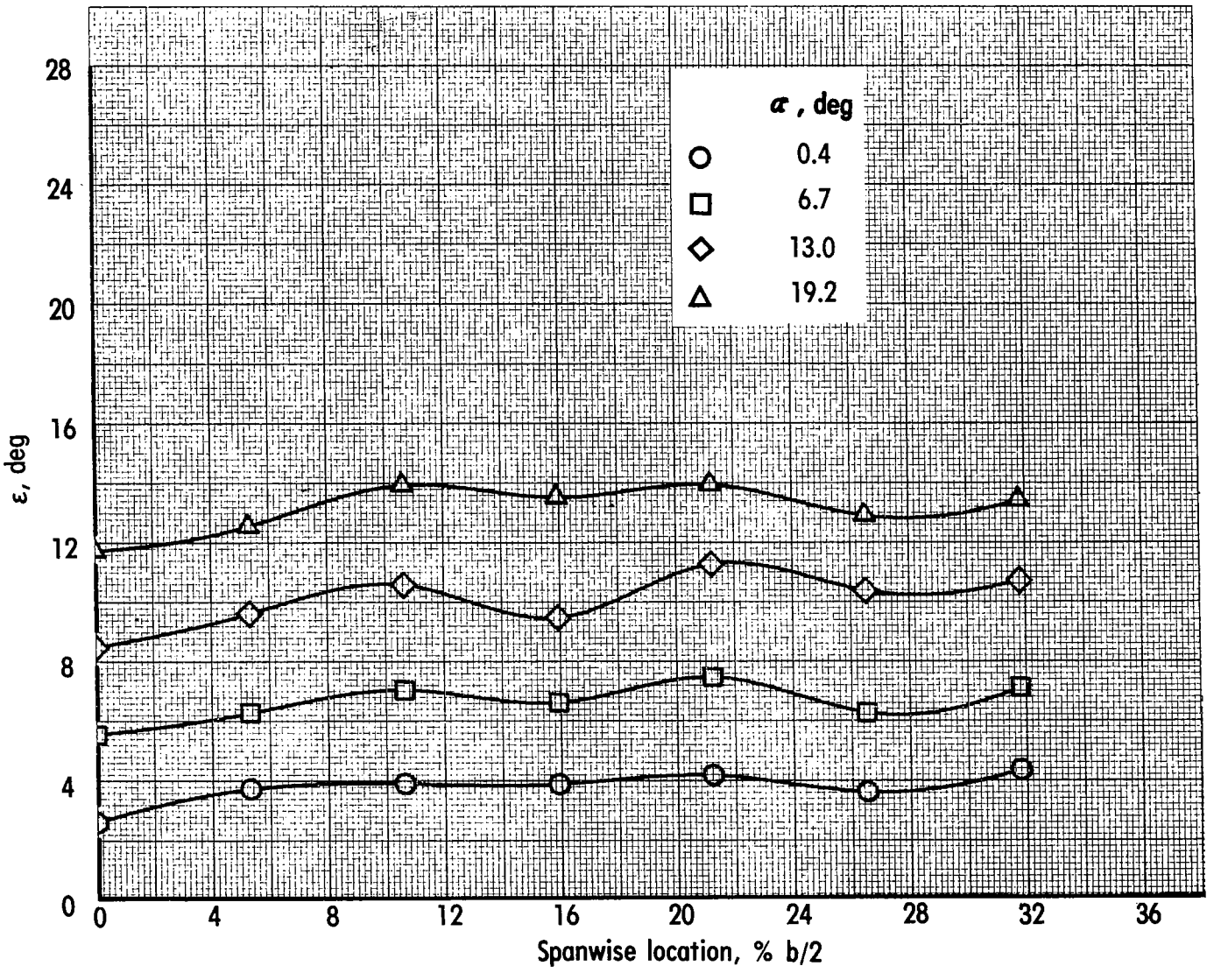

(d) C_μ = 3.01; inlets open.

Figure 58.- Continued.

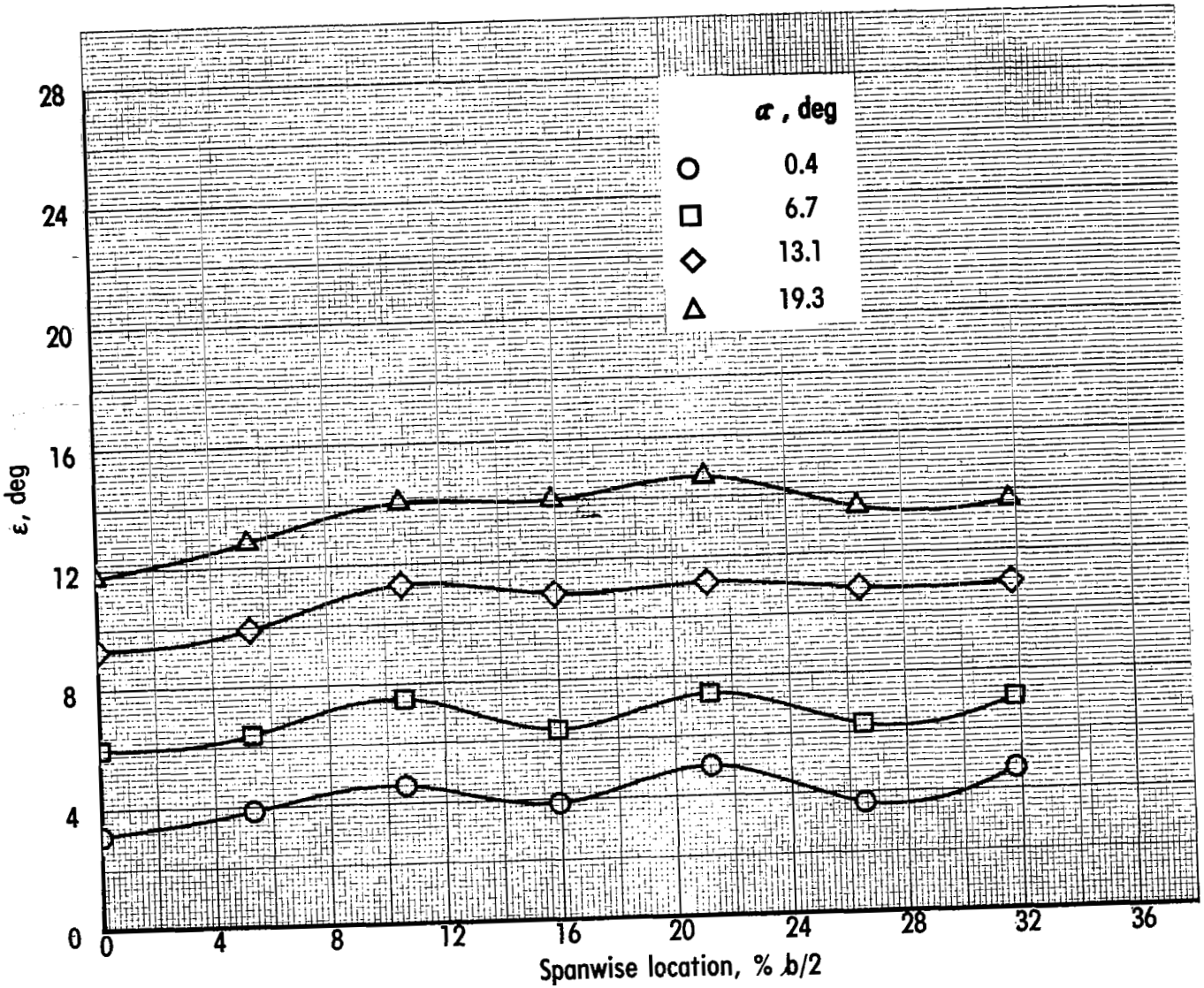

(e) C_μ = 4.00; inlets open.

Figure 58.- Concluded.

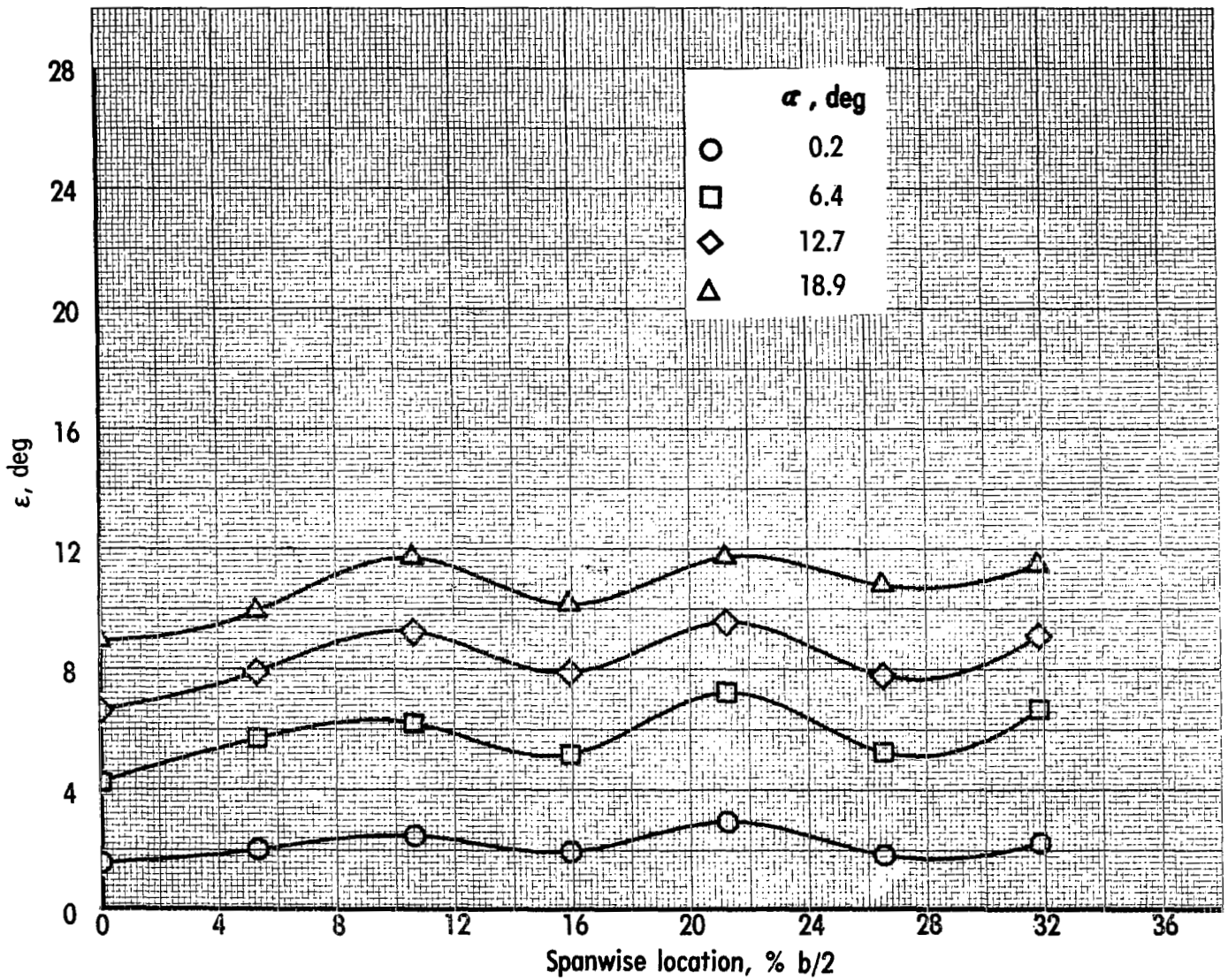

(a) $C_\mu = 0$; inlets closed.

Figure 59.- Effect of angle of attack on downwash angle at horizontal-tail location. Take-off configuration; engine 75-45; vertical tail and horizontal tail off.

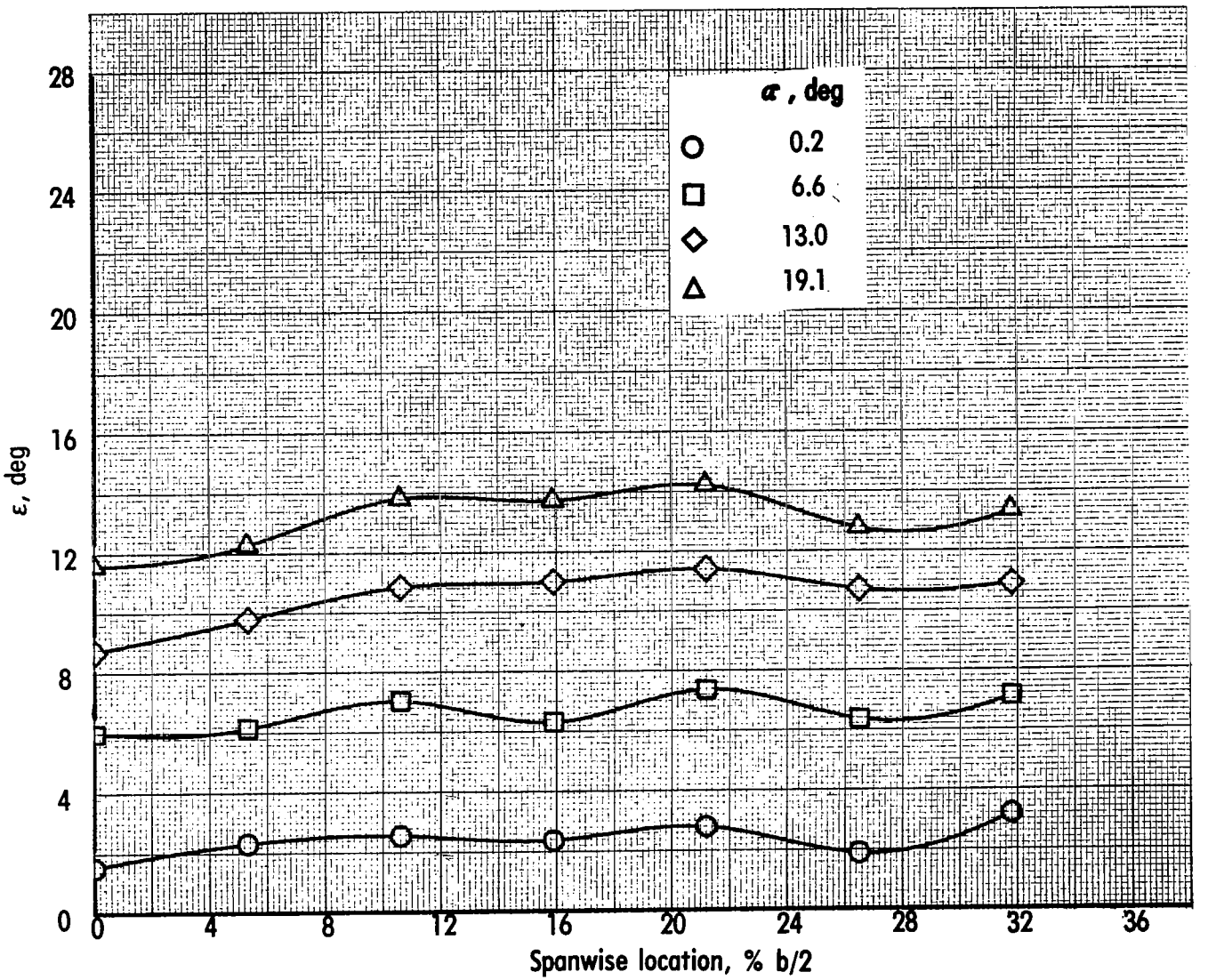

(b) C_μ = 0.96; inlets open.

Figure 59.- Continued.

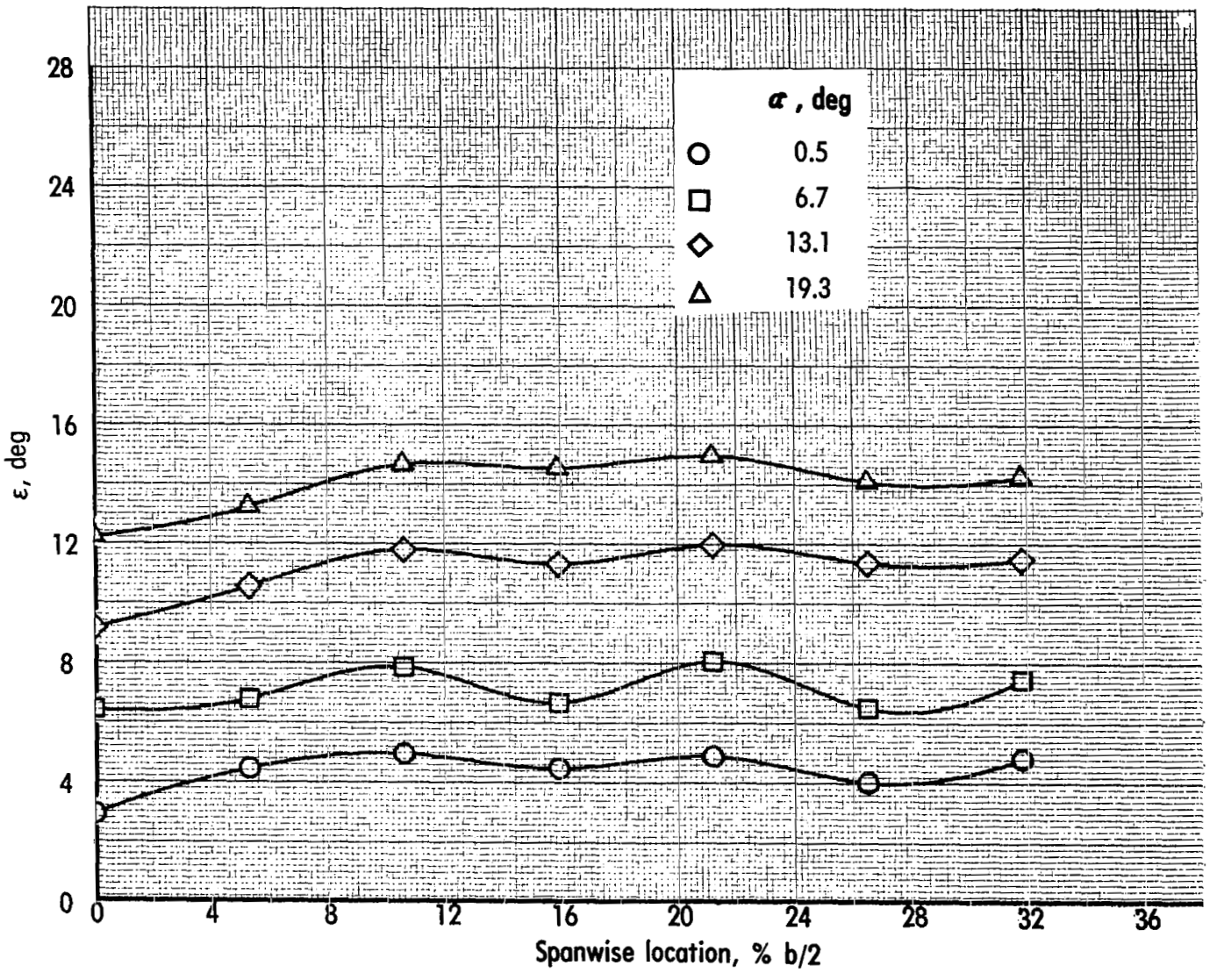

(c) C_μ = 2.01; inlets open.

Figure 59.- Continued.

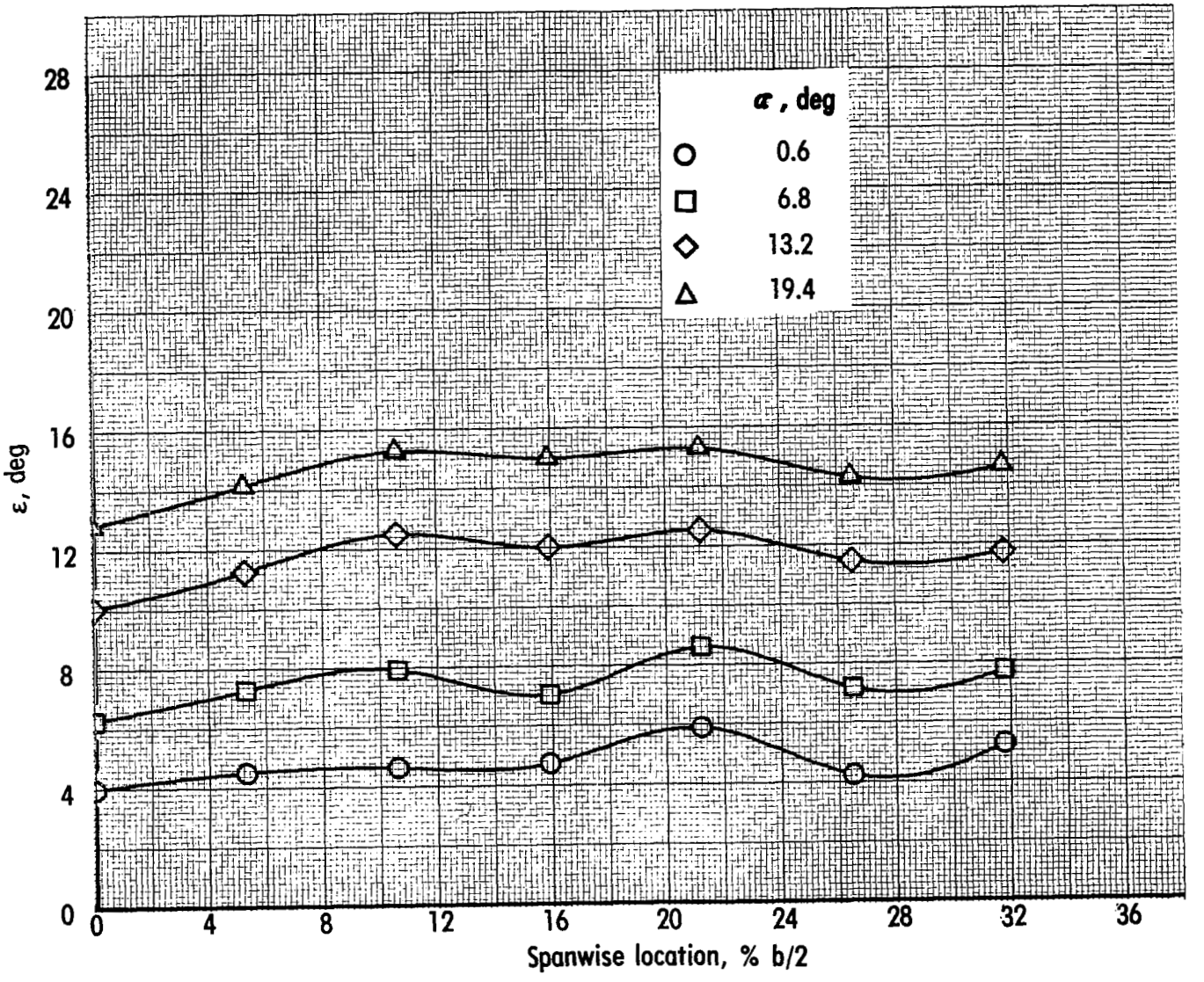

(d) C_μ = 3.01; inlets open.

Figure 59.- Continued.

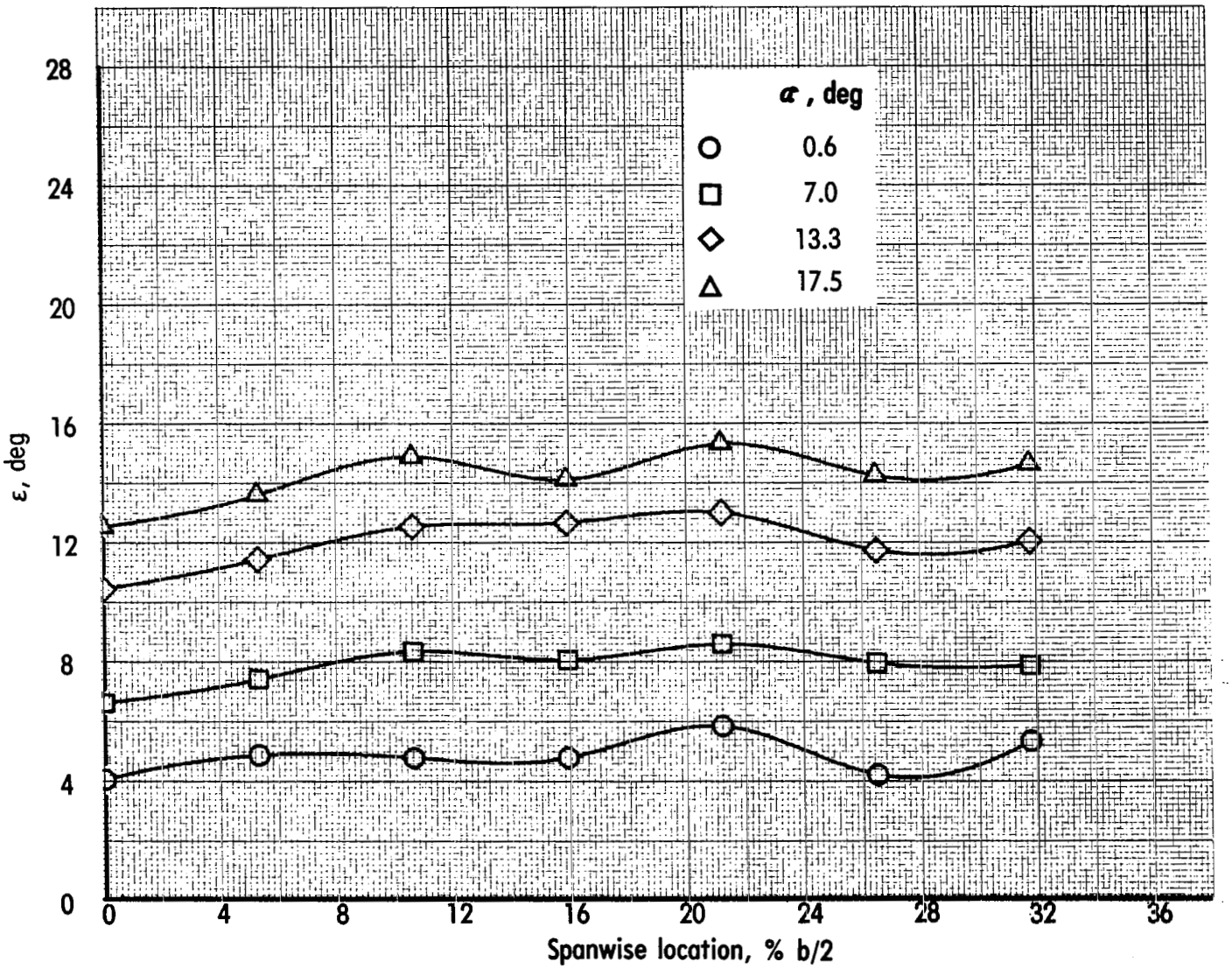

(e) C_μ = 3.99; inlets open.

Figure 59.- Concluded.

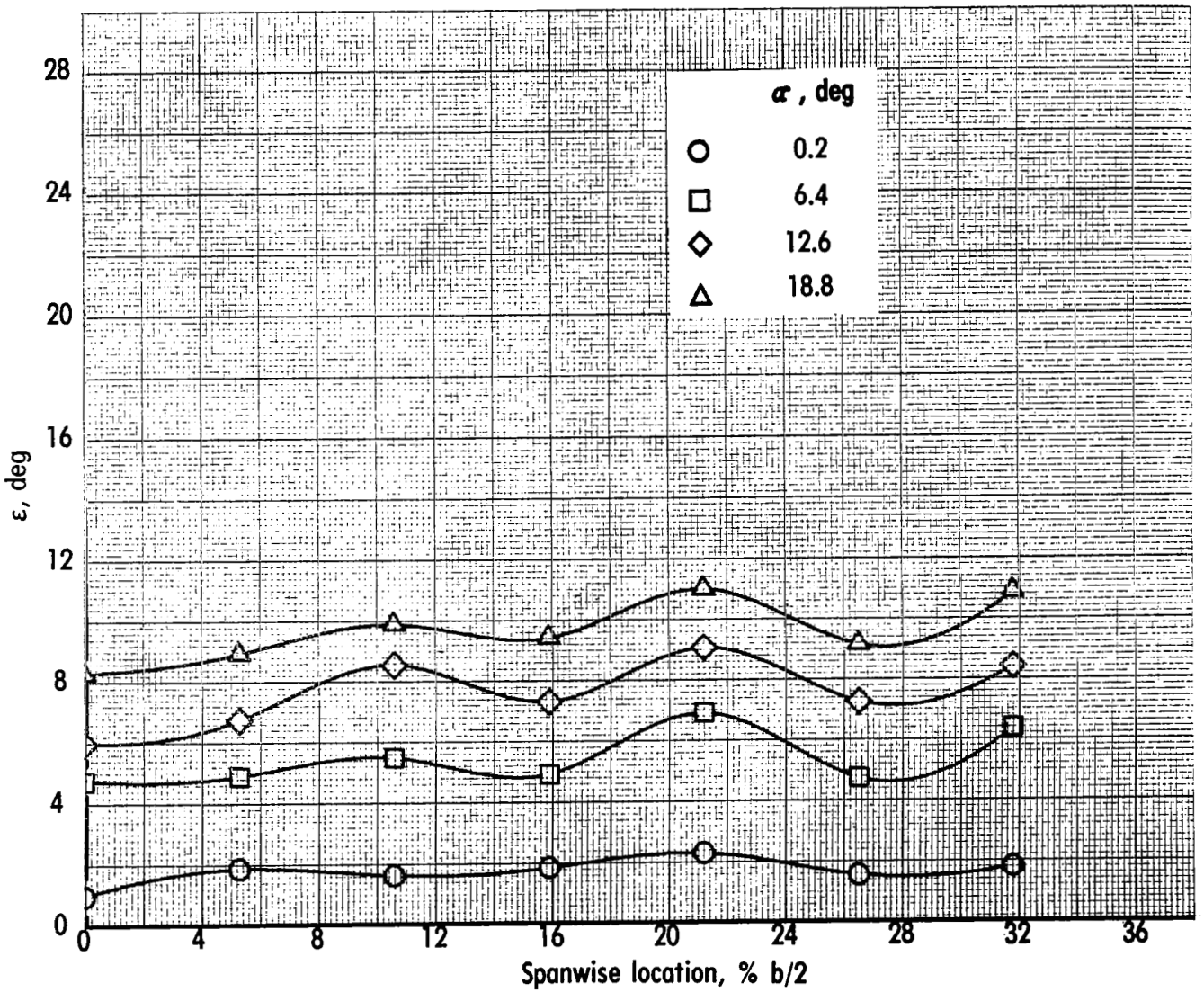

(a) $C_\mu = 0$; inlets closed.

Figure 60.- Effect of angle of attack on downwash angle at horizontal-tail location. Take-off configuration; engine 110-25; vertical tail and horizontal tail off.

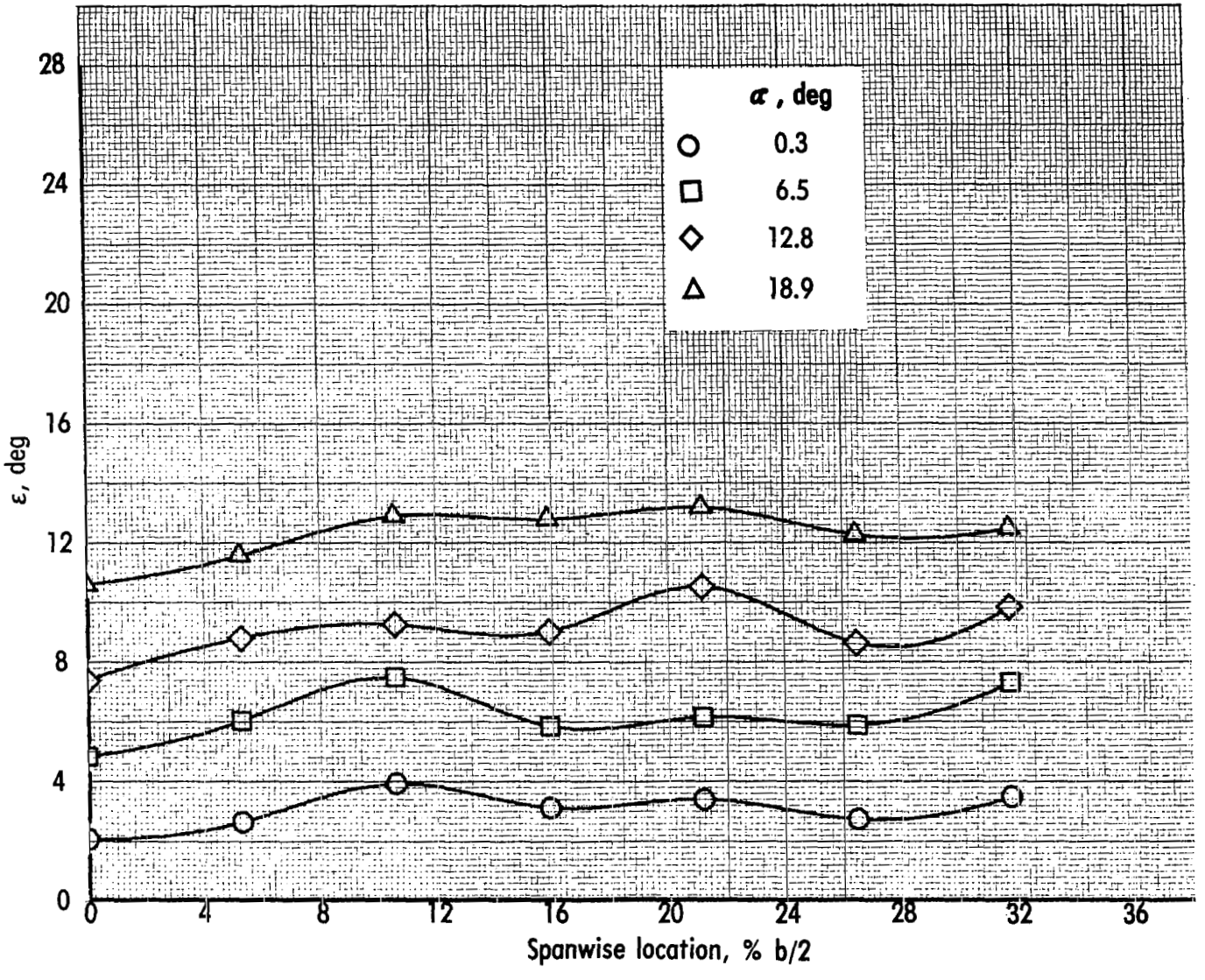

(b) C_μ = 0.97; inlets open.

Figure 60.- Continued.

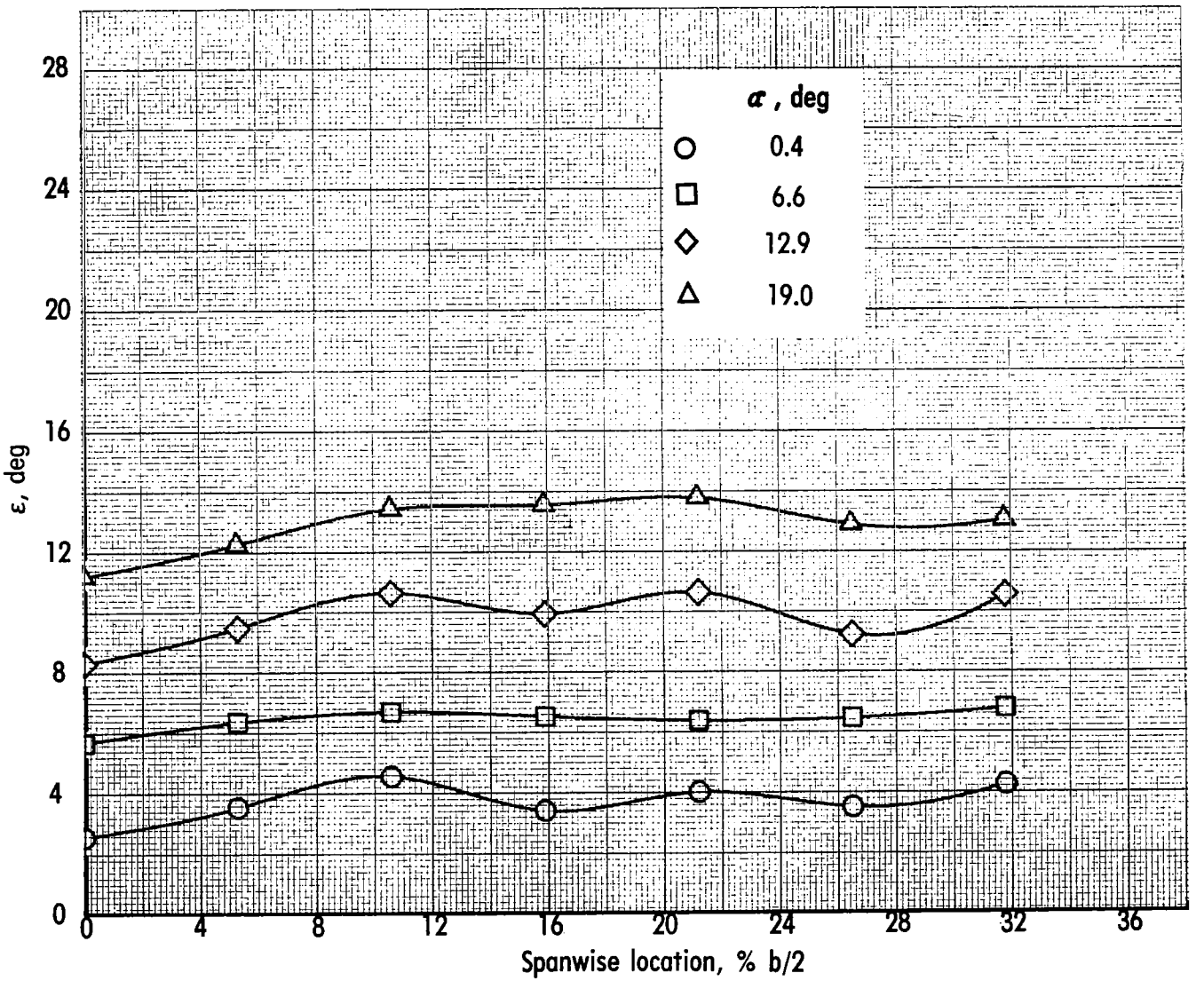

(c) C_μ = 2.01; inlets open.

Figure 60.- Continued.

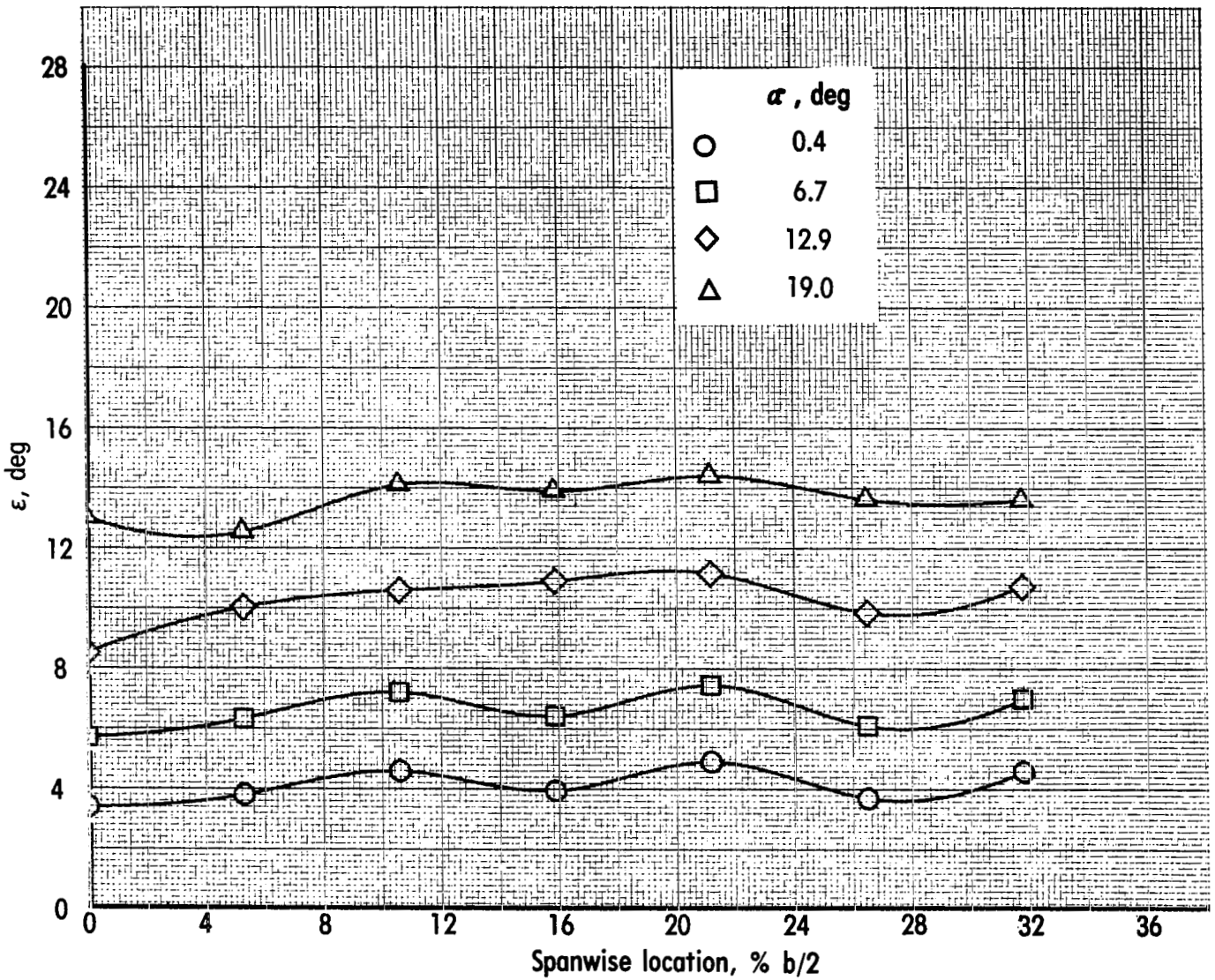

(d) C_μ = 3.02; inlets open.

Figure 60.- Continued.

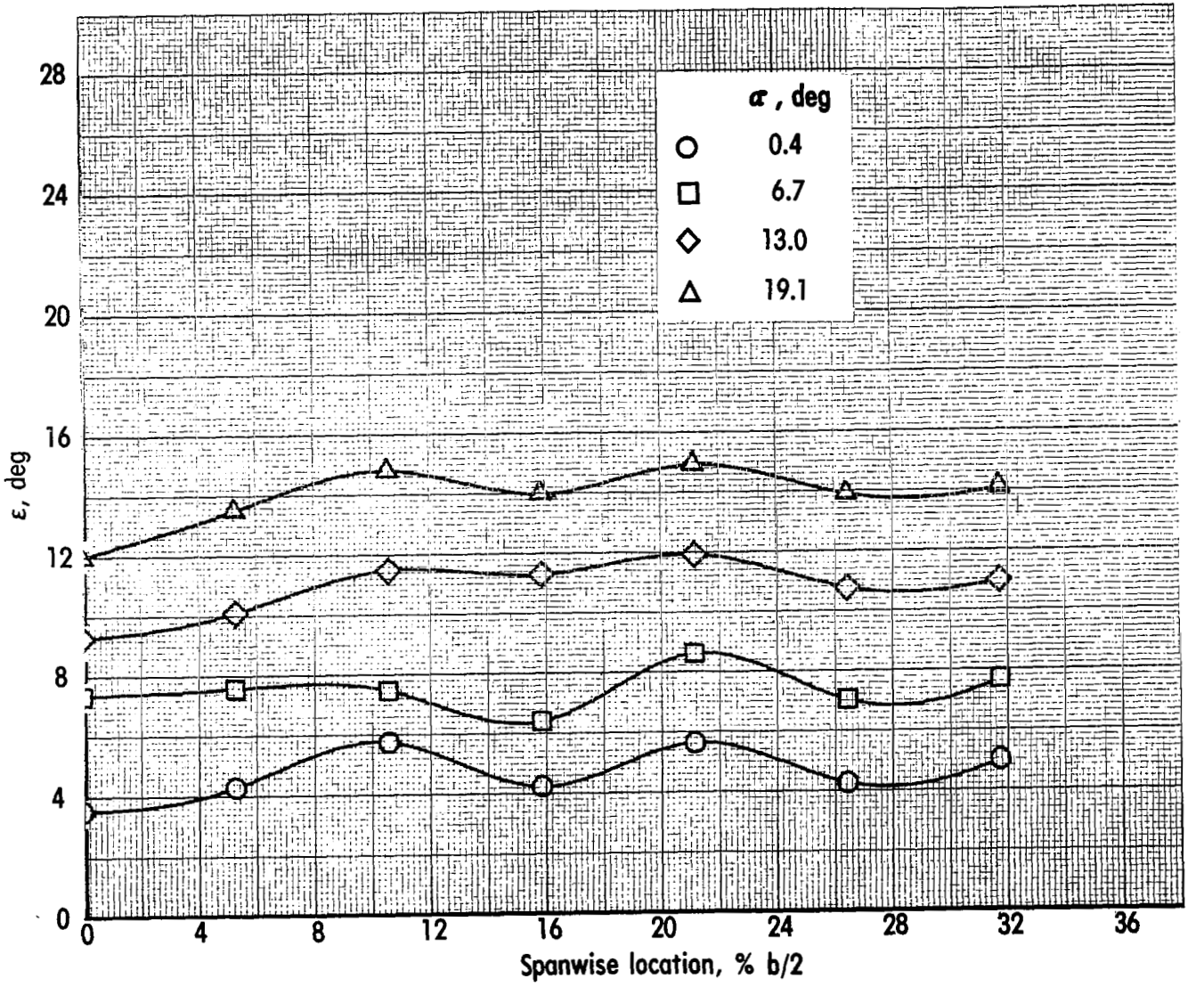

(e) C_μ = 4.05; inlets open.

Figure 60.- Concluded.

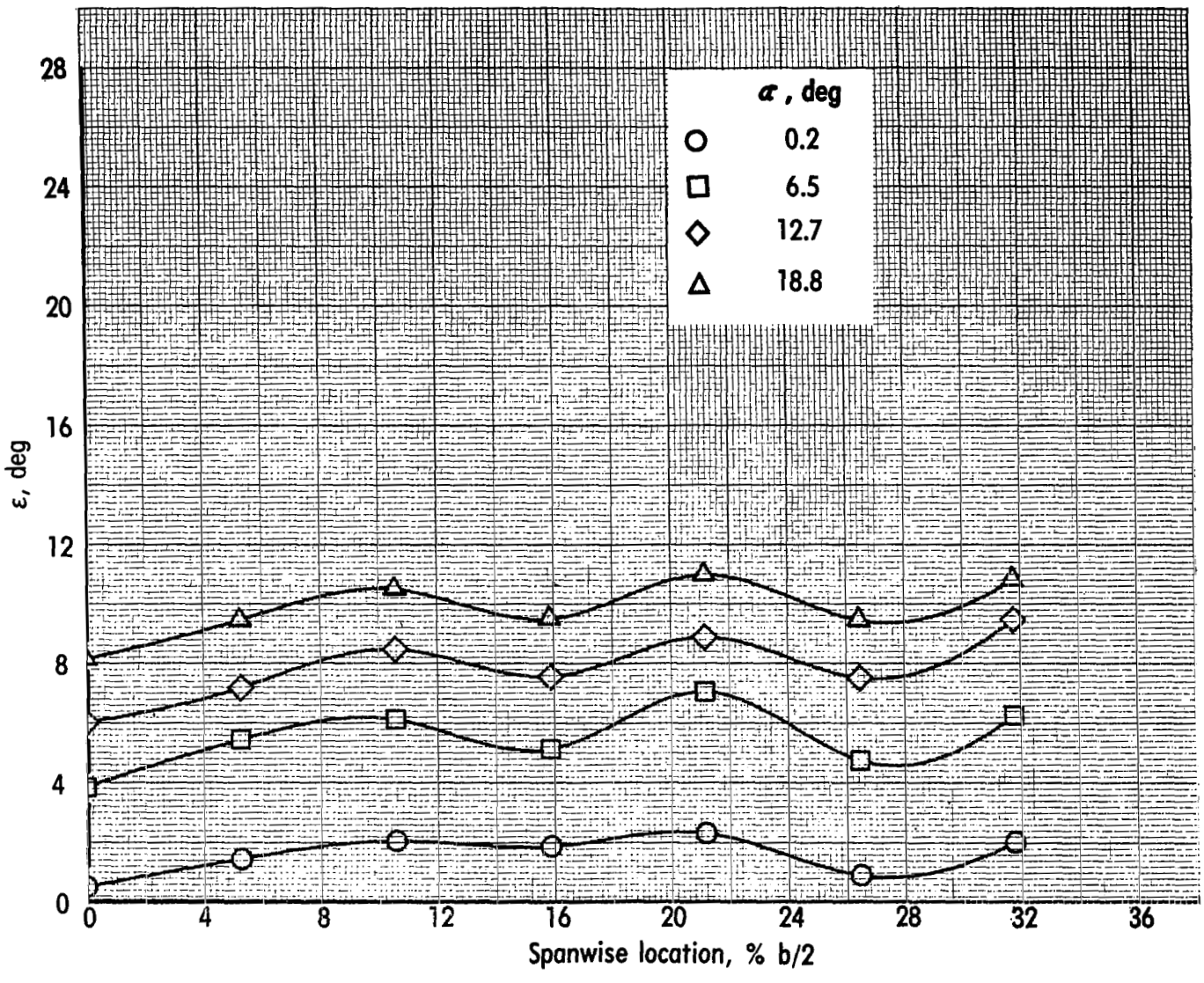

(a) $C_\mu = 0$; inlets closed.

Figure 61.- Effect of angle of attack on downwash angle at horizontal-tail location. Take-off configuration; engine 110-45; vertical tail and horizontal tail off.

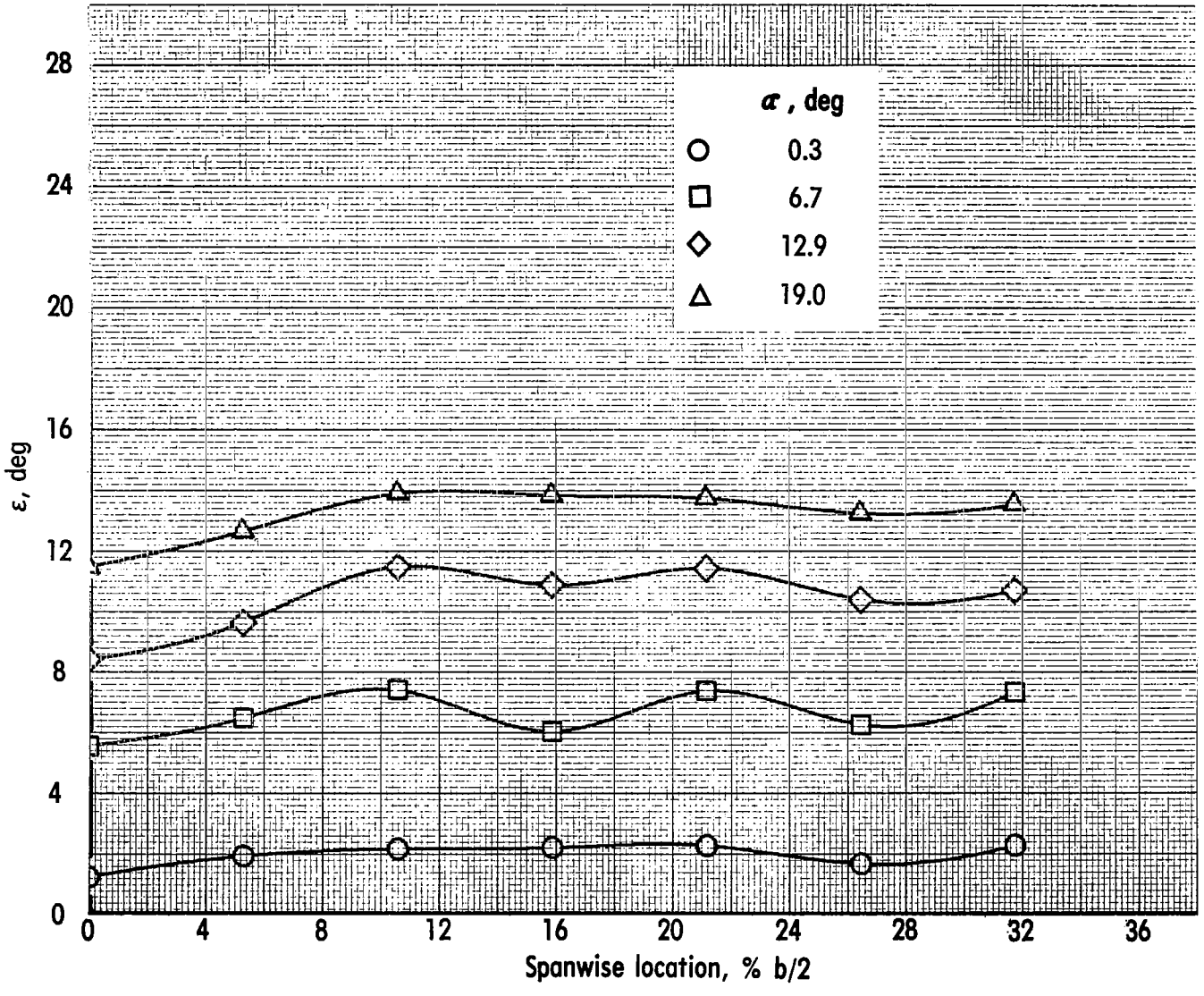

(b) C_μ = 0.97; inlets open.

Figure 61.- Continued.

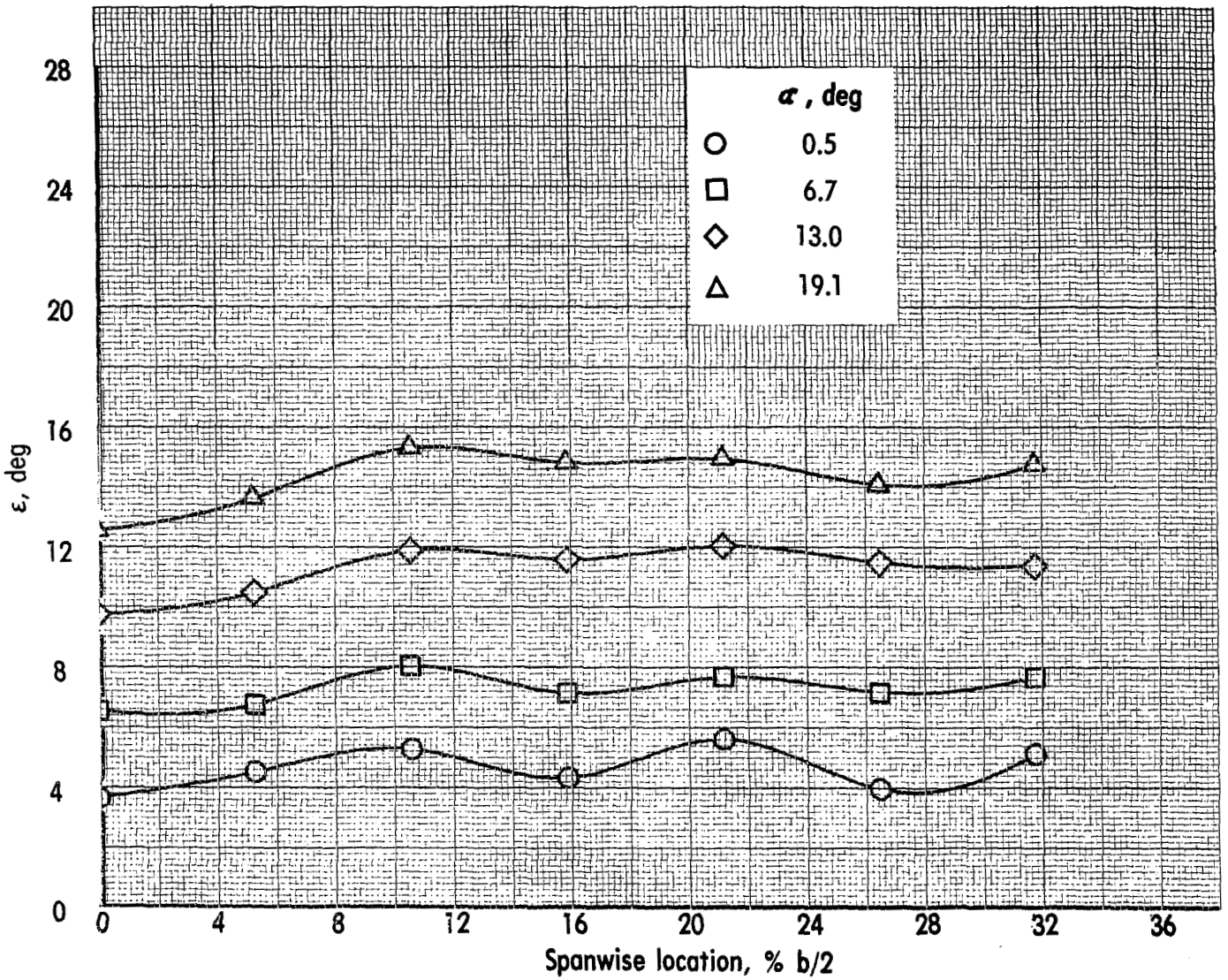

(c) C_μ = 2.02; inlets open.

Figure 61.- Continued.

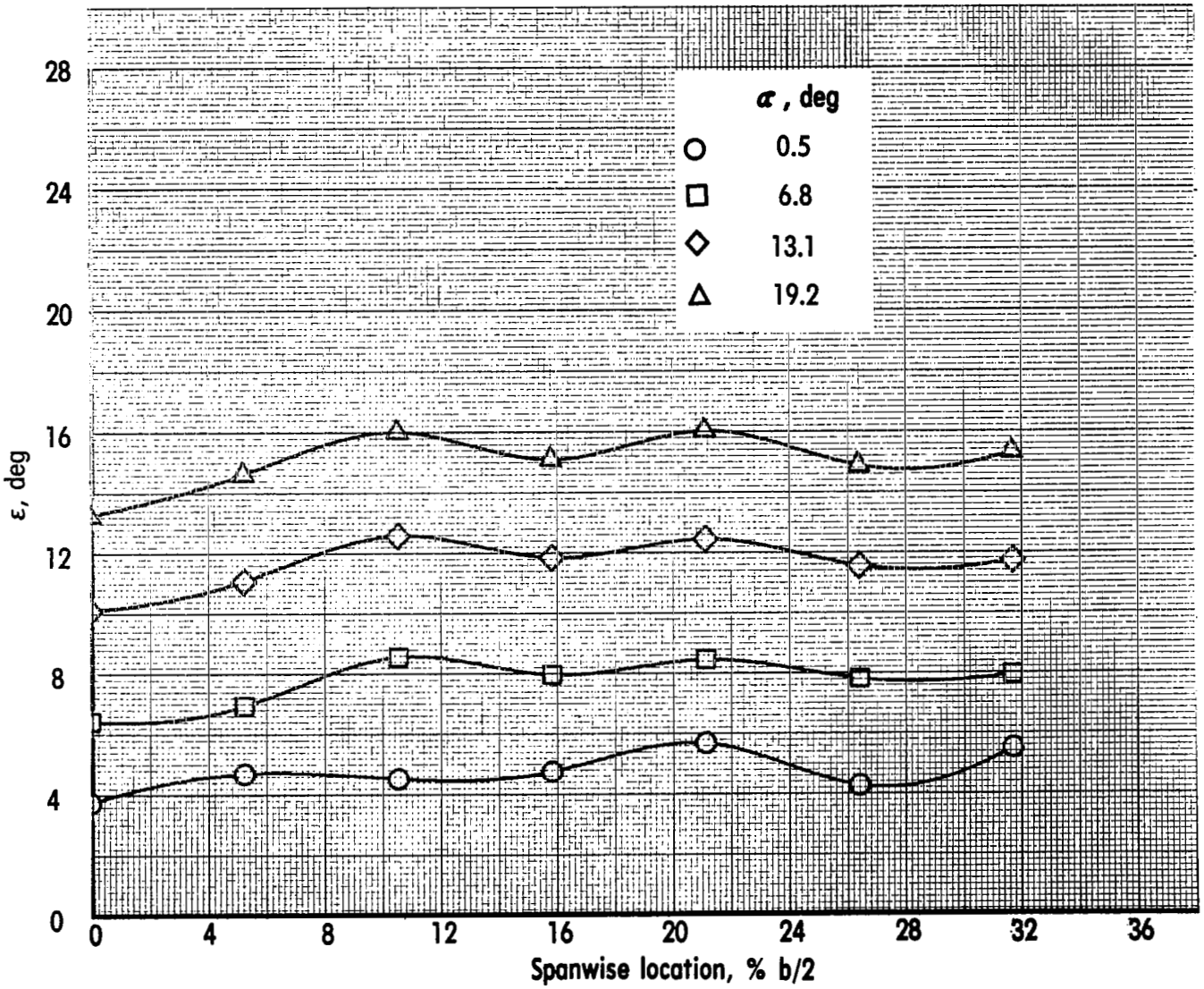

(d) C_μ = 3.03; inlets open.

Figure 61.- Continued.

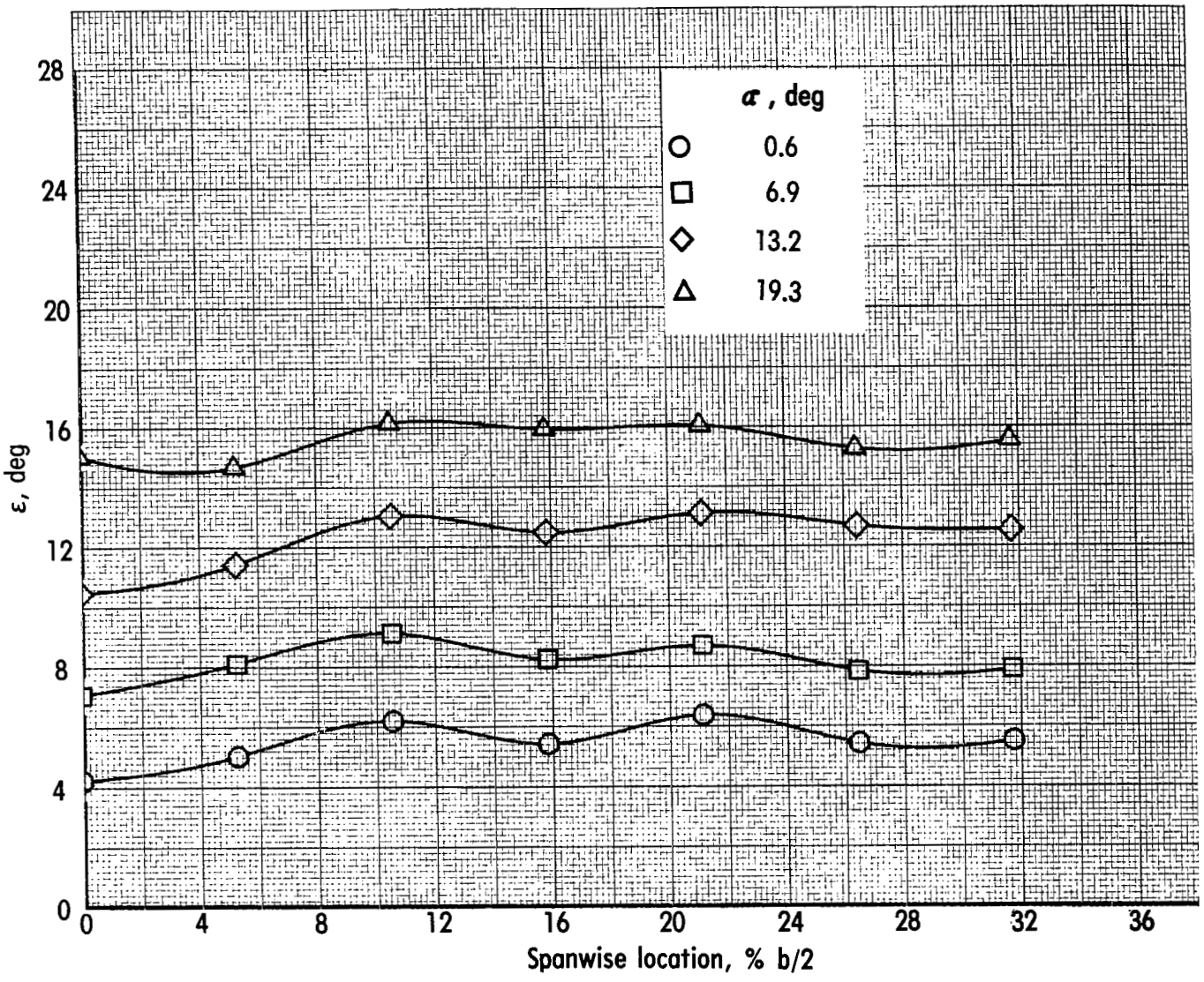

(e) C_μ = 4.04; inlets open.

Figure 61.- Concluded.

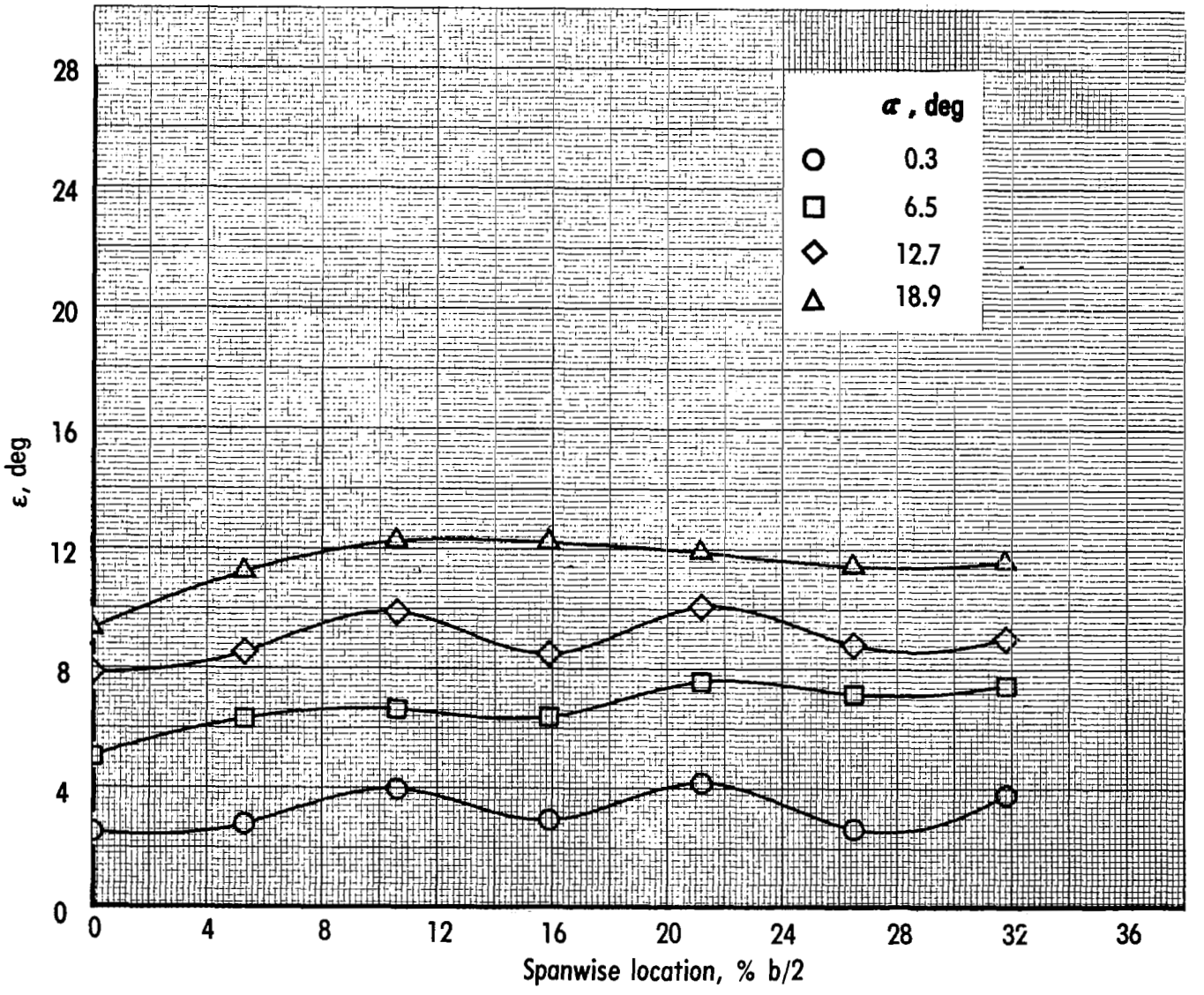

(a) $C_\mu = 0$; inlets closed.

Figure 62.- Effect of angle of attack on downwash angle at horizontal-tail location. Landing configuration; engine 75-0; vertical tail and horizontal tail off.

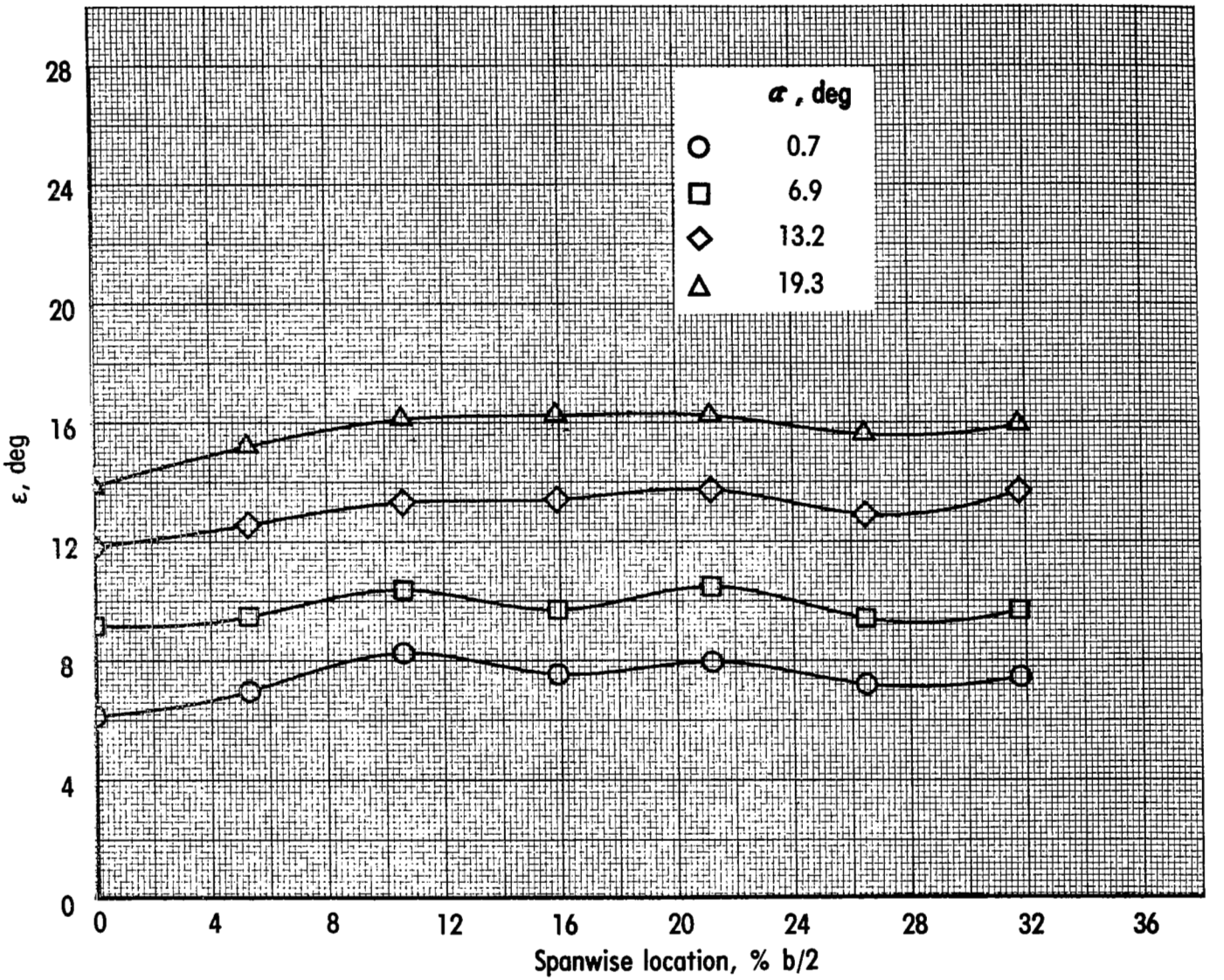

(b) C_μ = 0.97; inlets open.

Figure 62.- Continued.

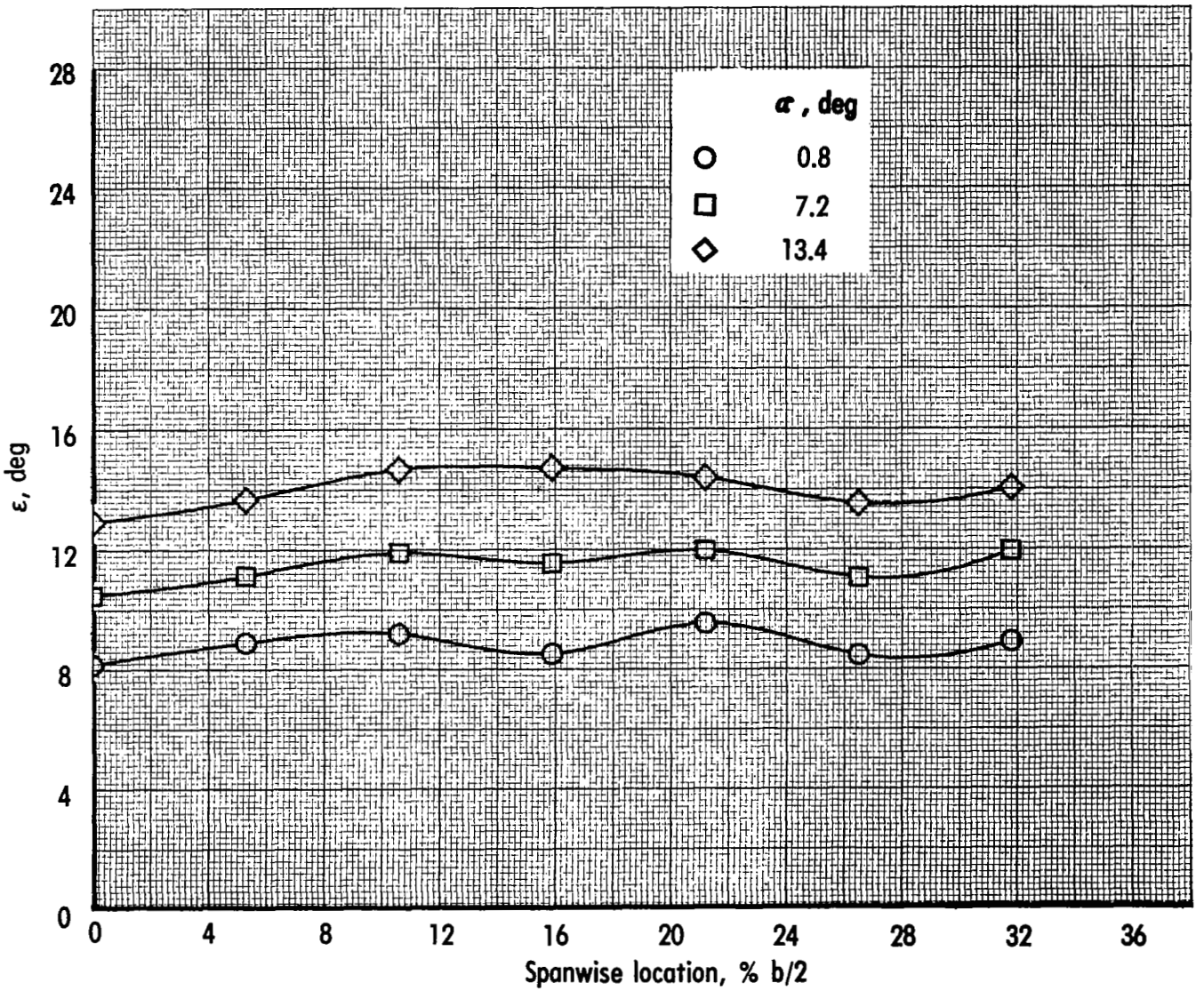

(c) C_μ = 1.99; inlets open.

Figure 62.- Continued.

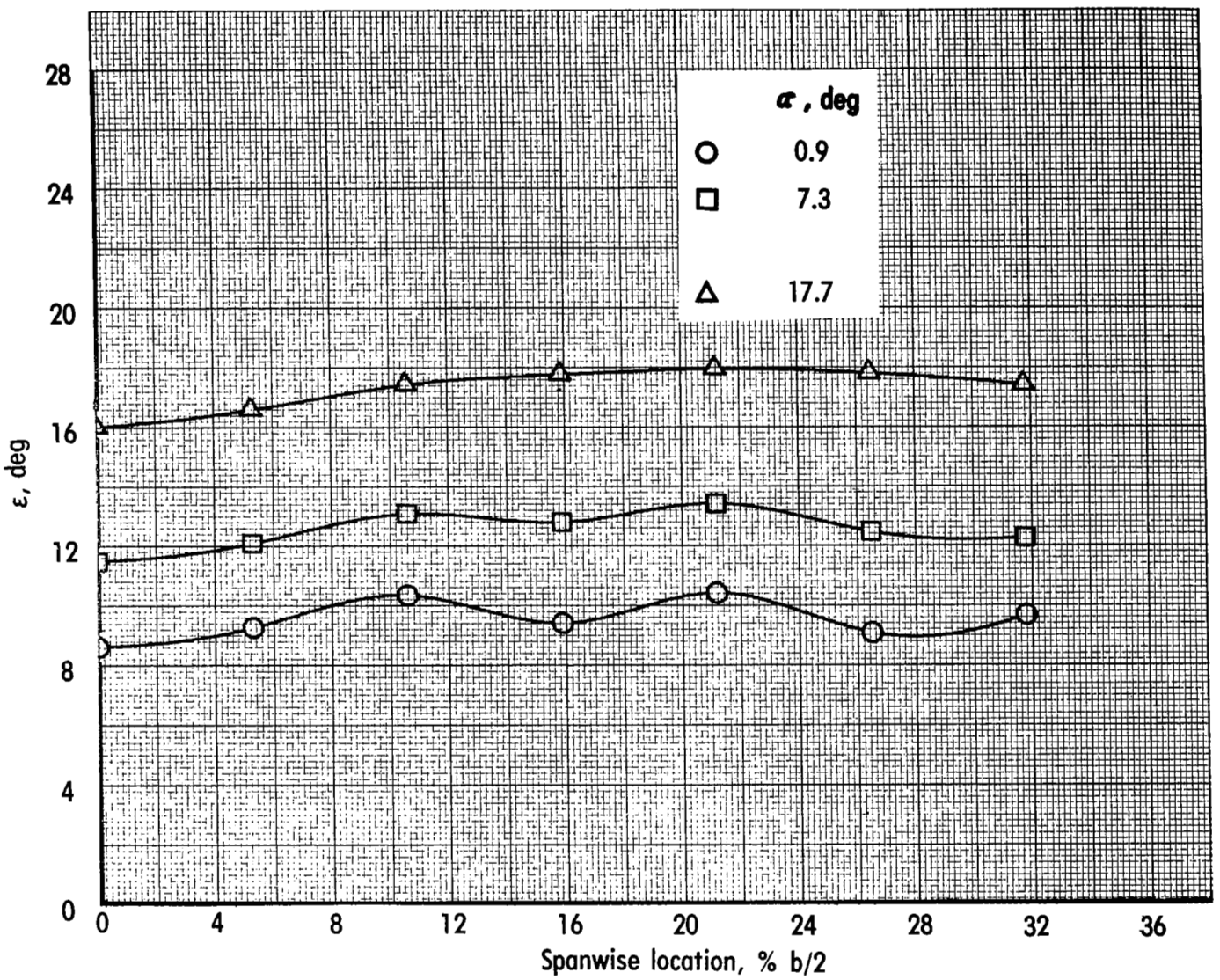

(d) C_μ = 2.98; inlets open.

Figure 62.- Continued.

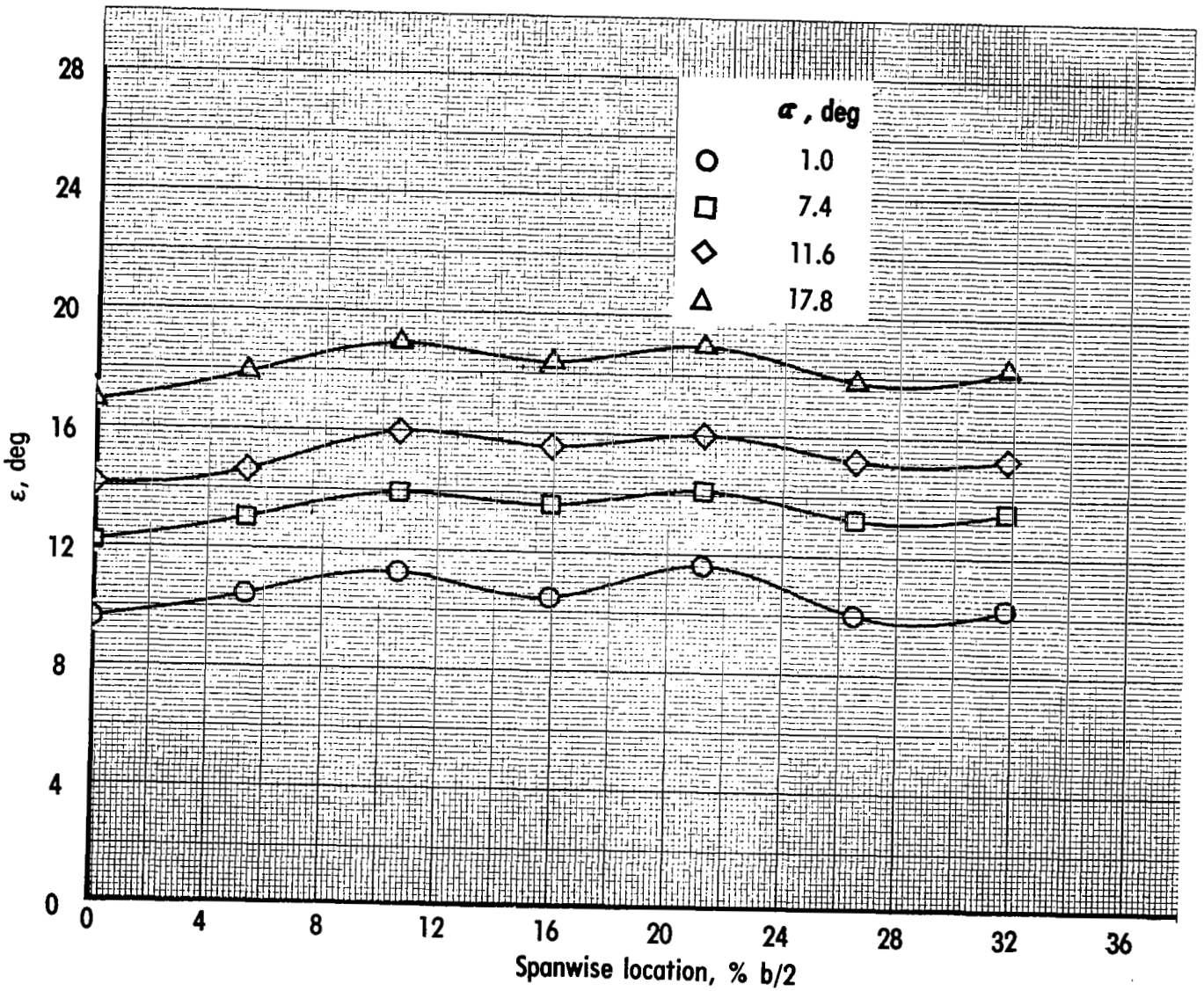

(e) C_μ = 3.96; inlets open.

Figure 62.- Concluded.

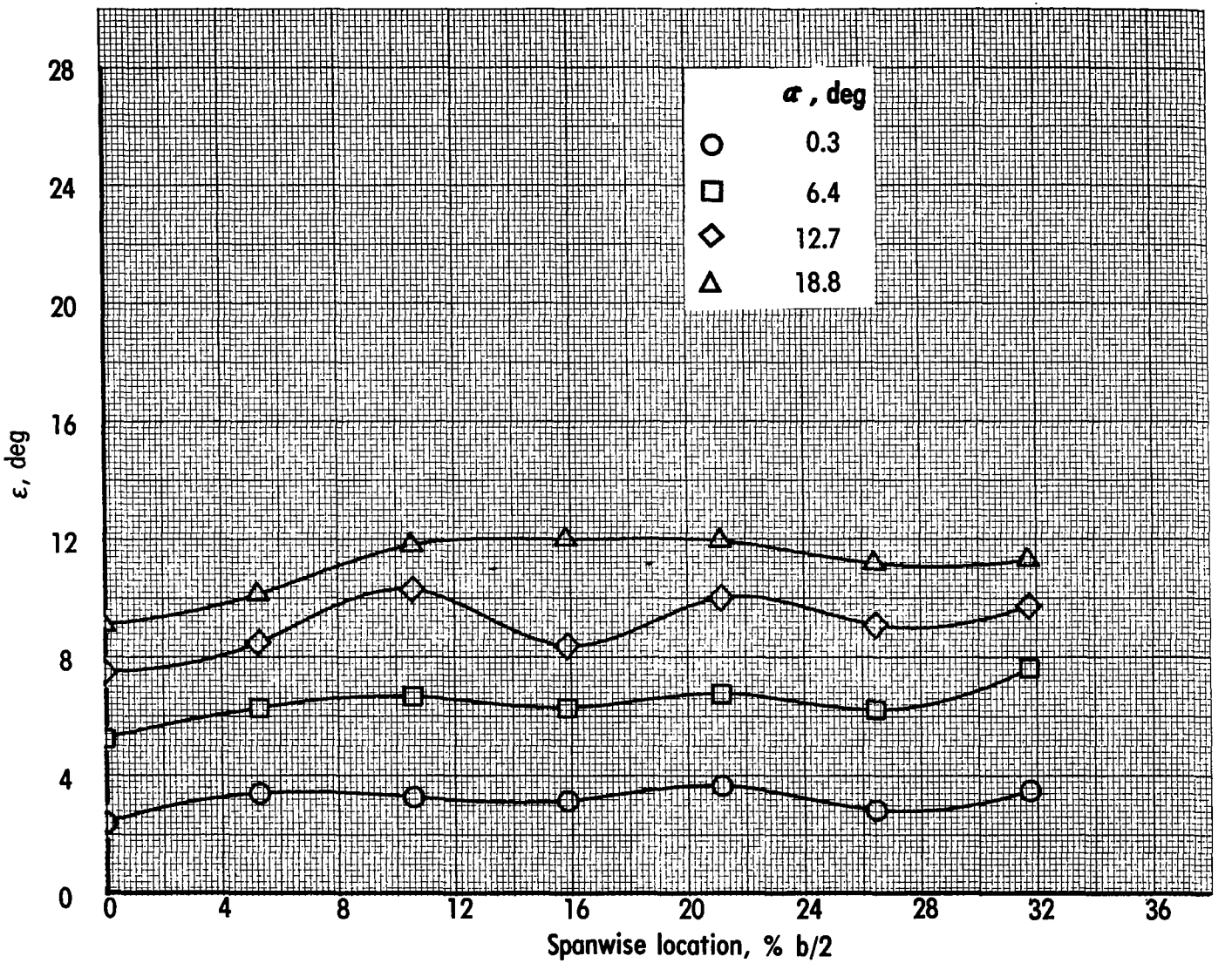

(a) $C_\mu = 0$; inlets closed.

Figure 63.- Effect of angle of attack on downwash angle at horizontal-tail location. Landing configuration; engine 75-45; vertical tail and horizontal tail off.

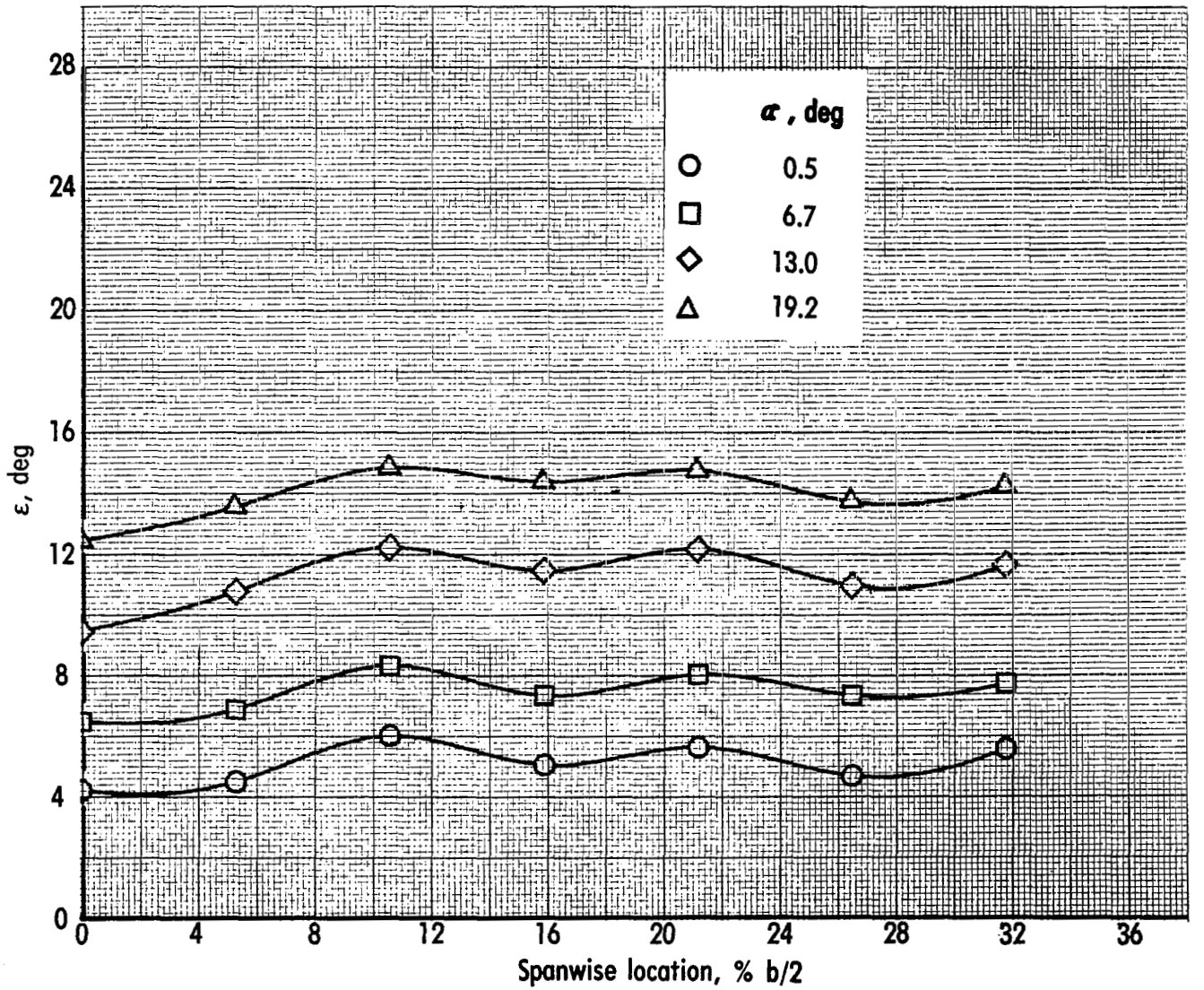

(b) C_μ = 0.96; inlets open.

Figure 63.- Continued.

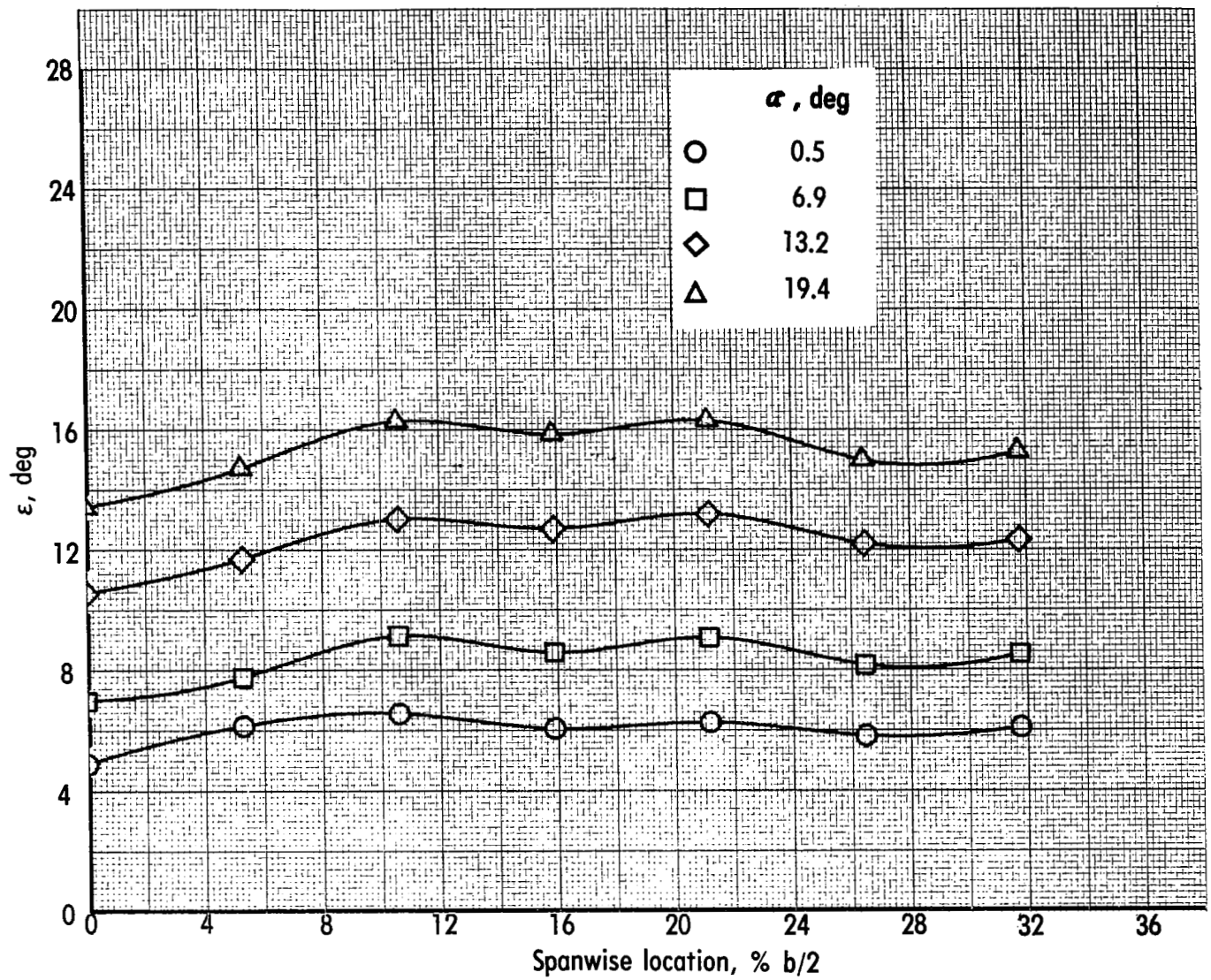

(c) C_μ = 2.00; inlets open.

Figure 63.- Continued.

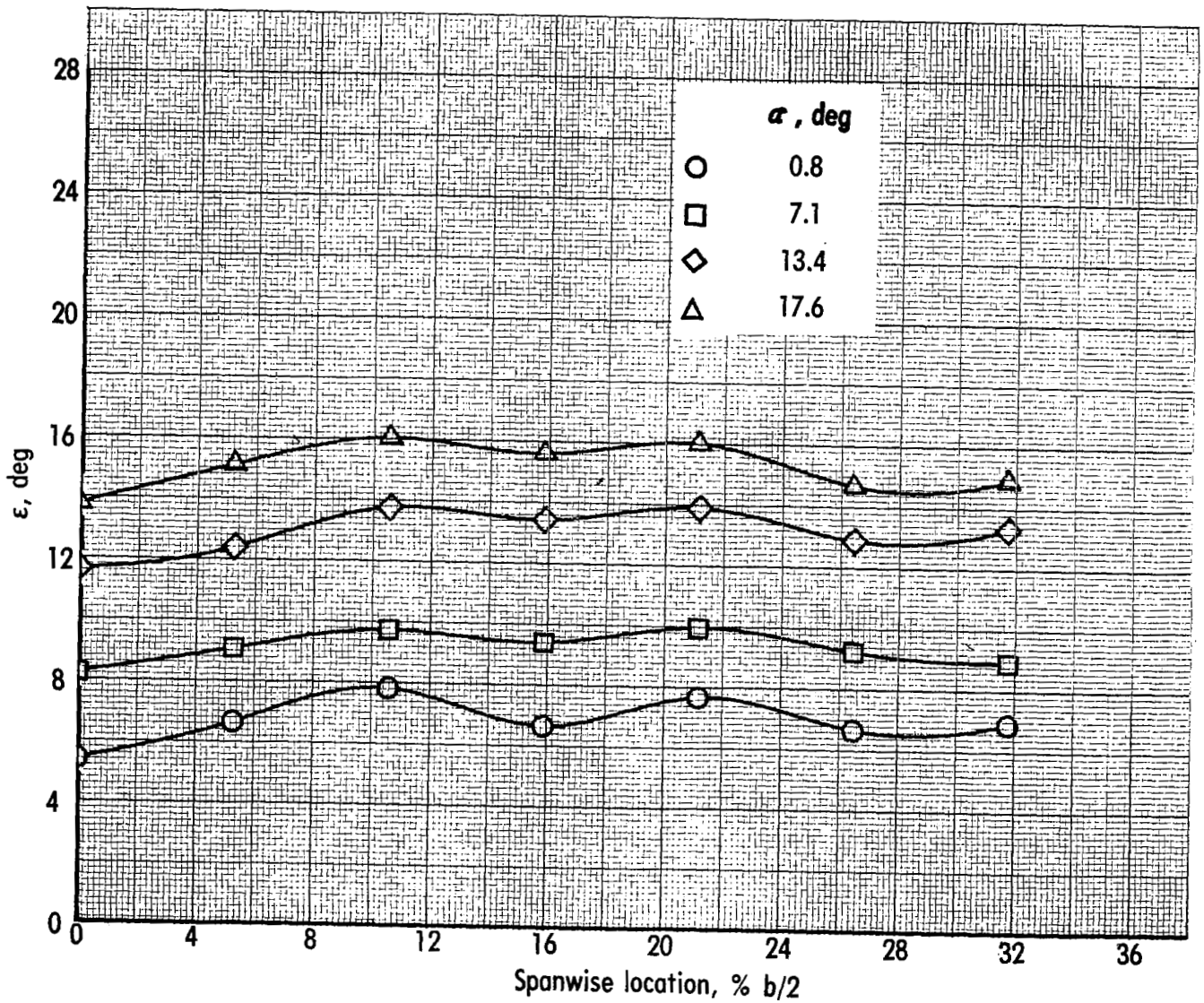

(d) C_μ = 3.02; inlets open.

Figure 63.- Continued.

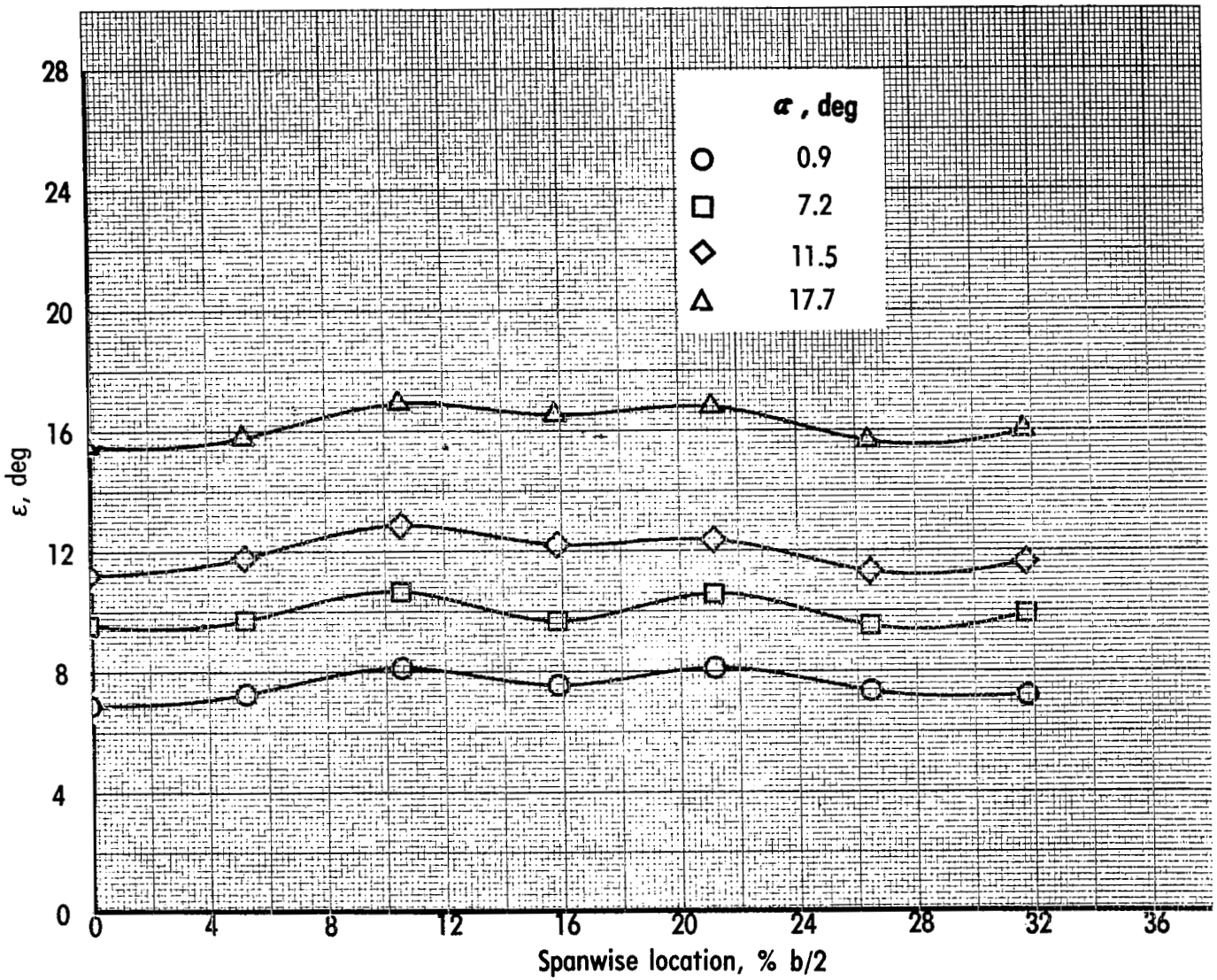

(e) C_μ = 4.03; inlets open.

Figure 63.- Concluded.

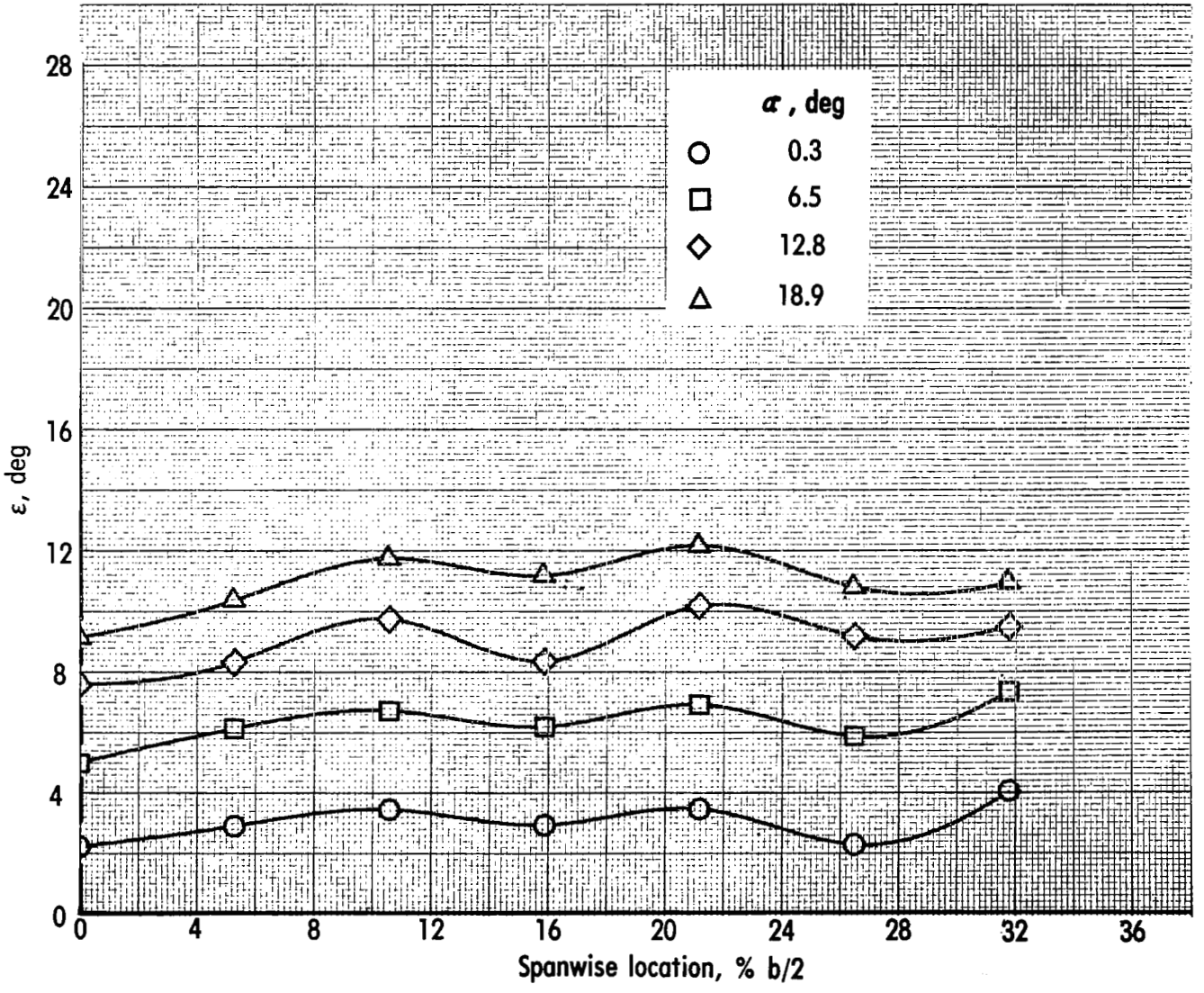

(a) $C_\mu = 0$; inlets closed.

Figure 64.- Effect of angle of attack on downwash angle at horizontal-tail location. Landing configuration; engine 75-65; vertical tail and horizontal tail off.

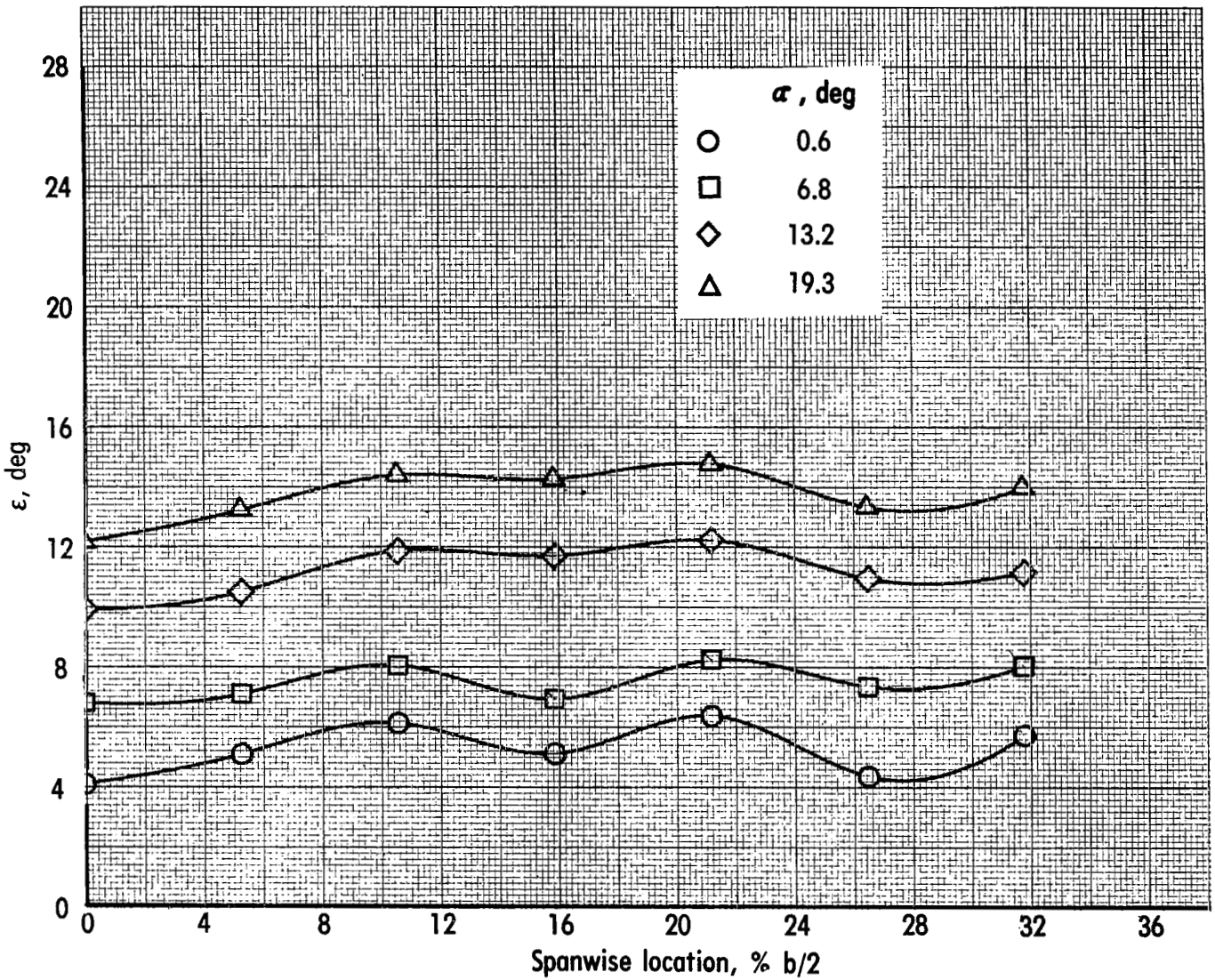

(b) C_μ = 1.01; inlets open.

Figure 64.- Continued.

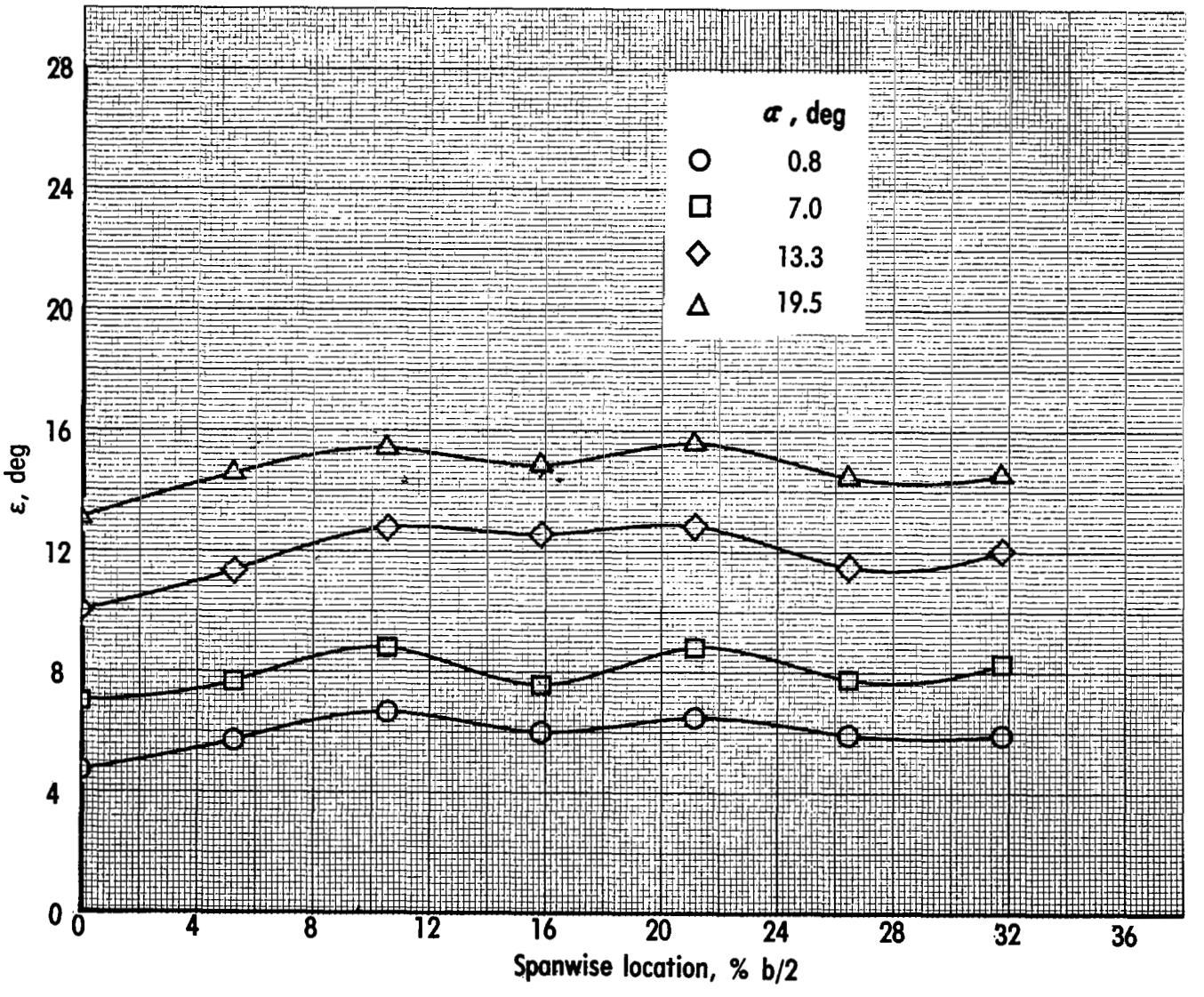

(c) C_μ = 2.02; inlets open.

Figure 64.- Continued.

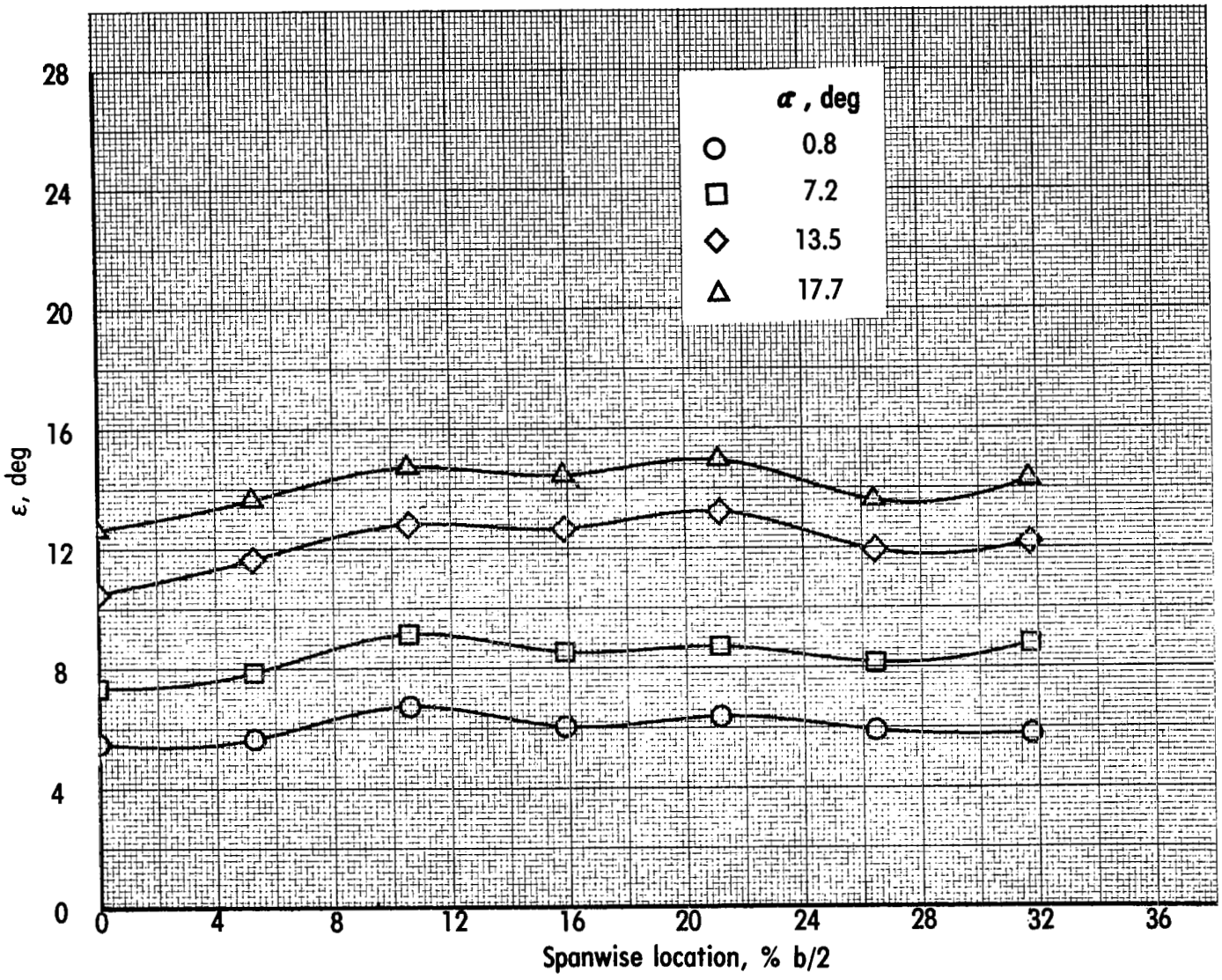

(d) C_μ = 3.05; inlets open.

Figure 64.- Continued.

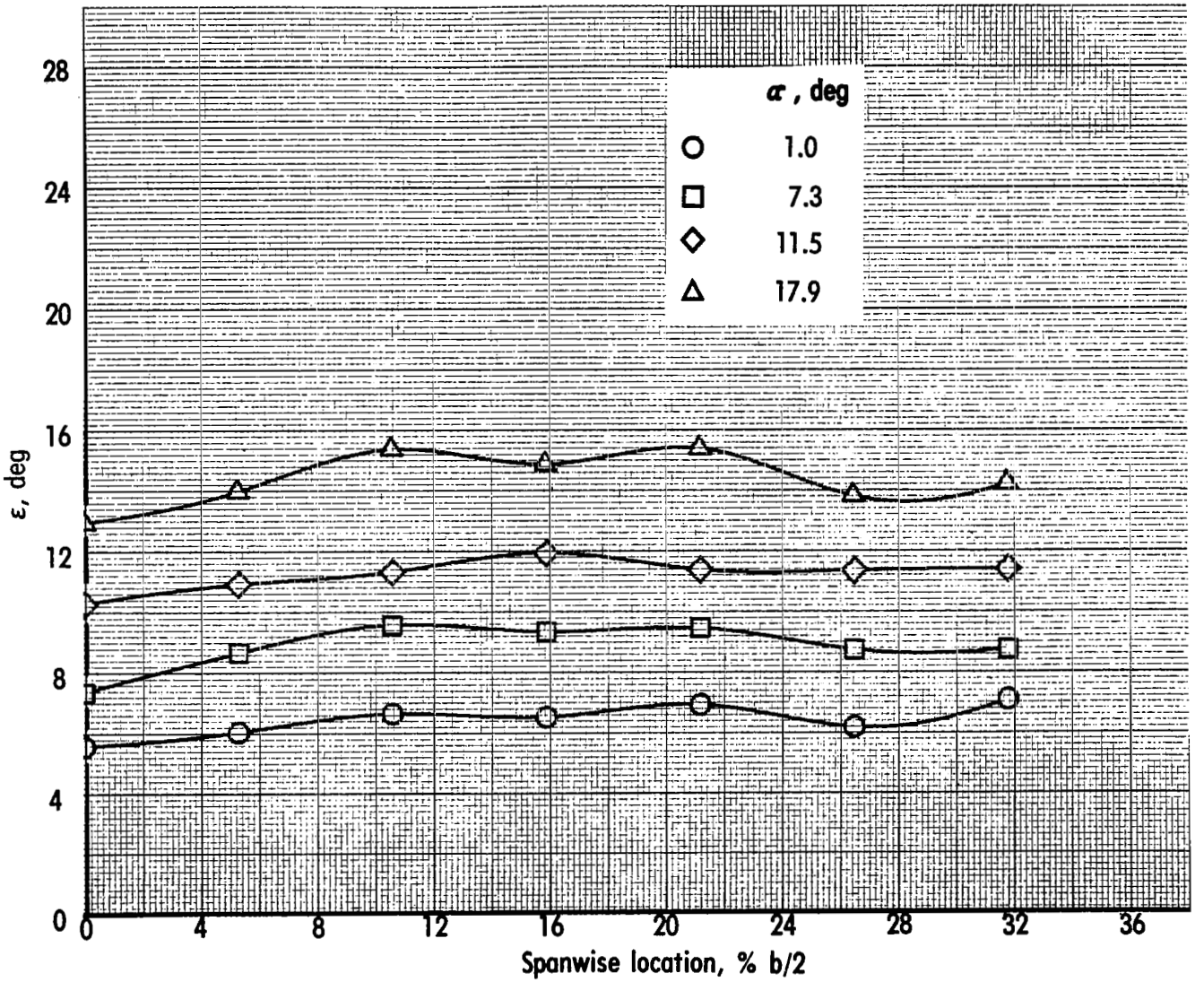

(e) C_μ = 4.07; inlets open.

Figure 64.- Concluded.

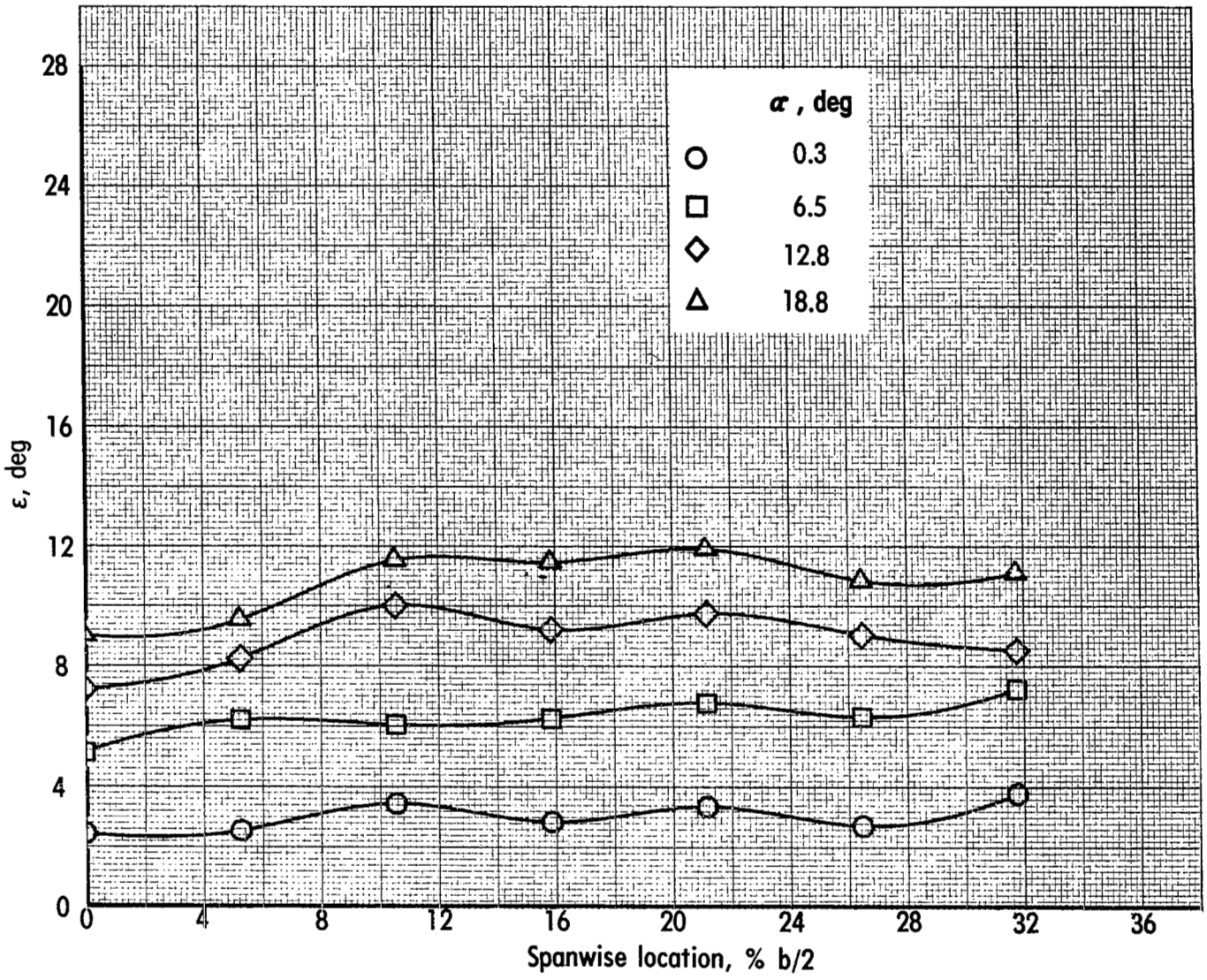

(a) $C_\mu = 0$; inlets closed.

Figure 65.- Effect of angle of attack on downwash angle at horizontal-tail location. Landing configuration; engine 75-90; vertical tail and horizontal tail off.

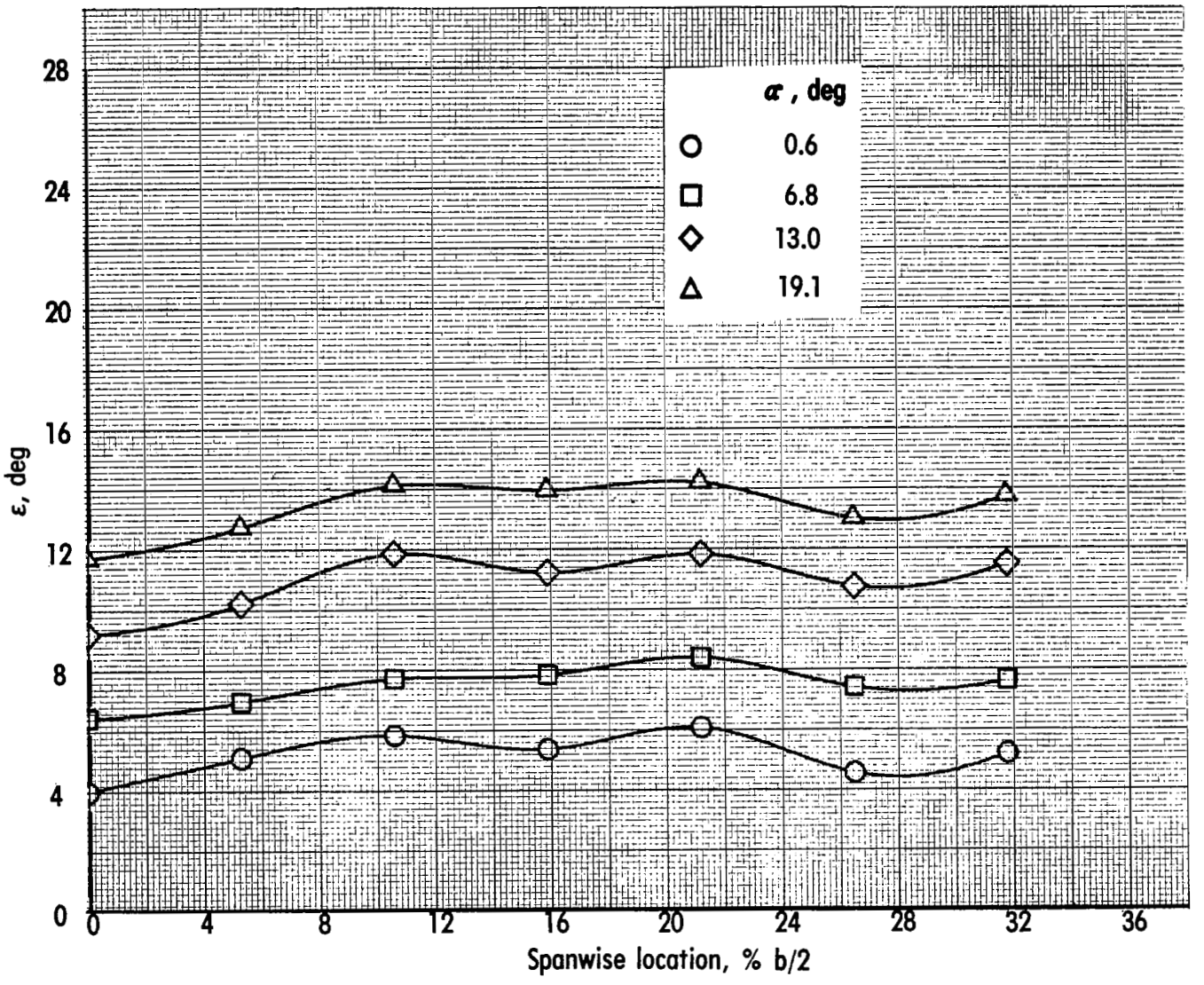

(b) C_μ = 1.00; inlets open.

Figure 65.- Continued.

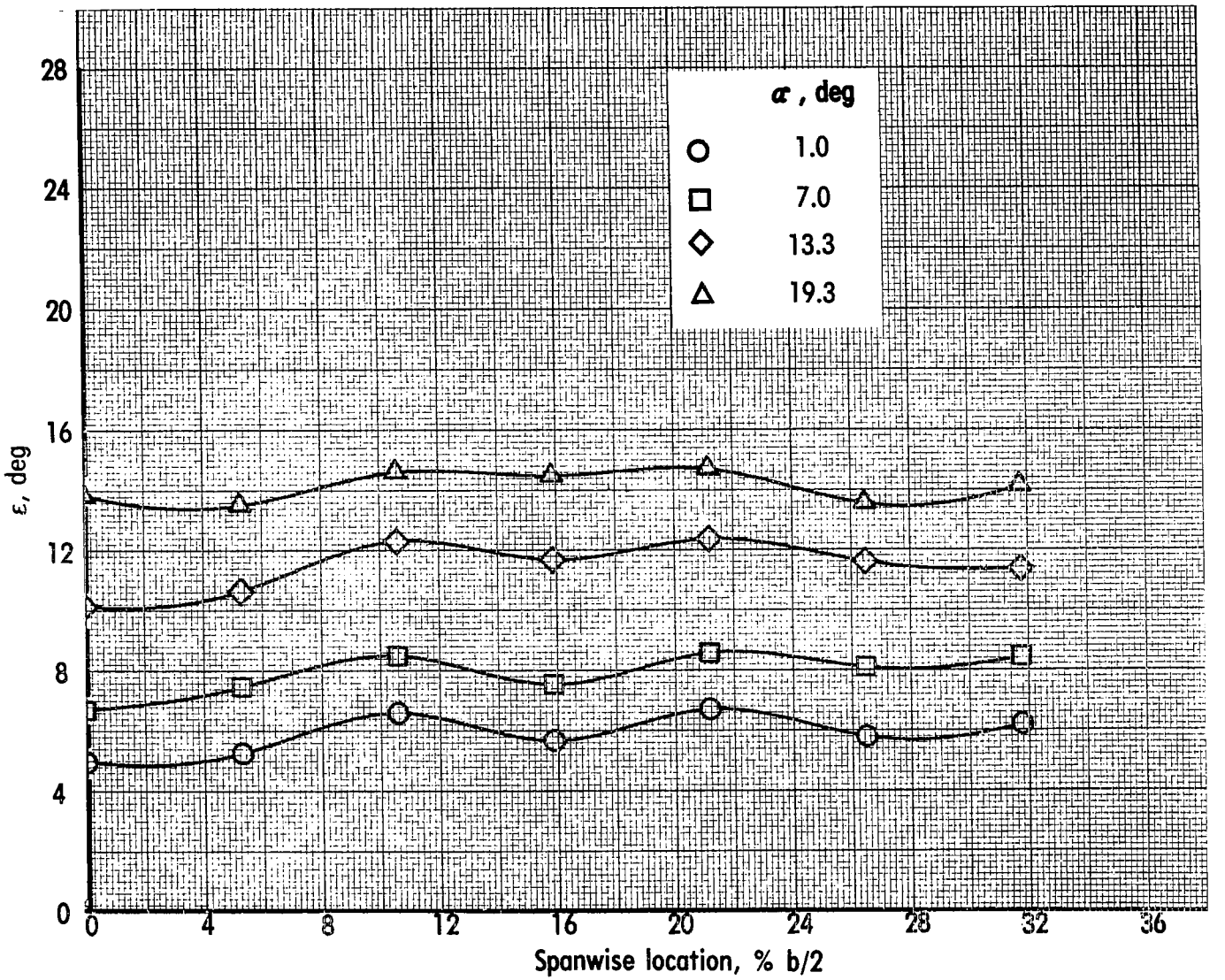

(c) C_μ = 2.03; inlets open.

Figure 65.- Continued.

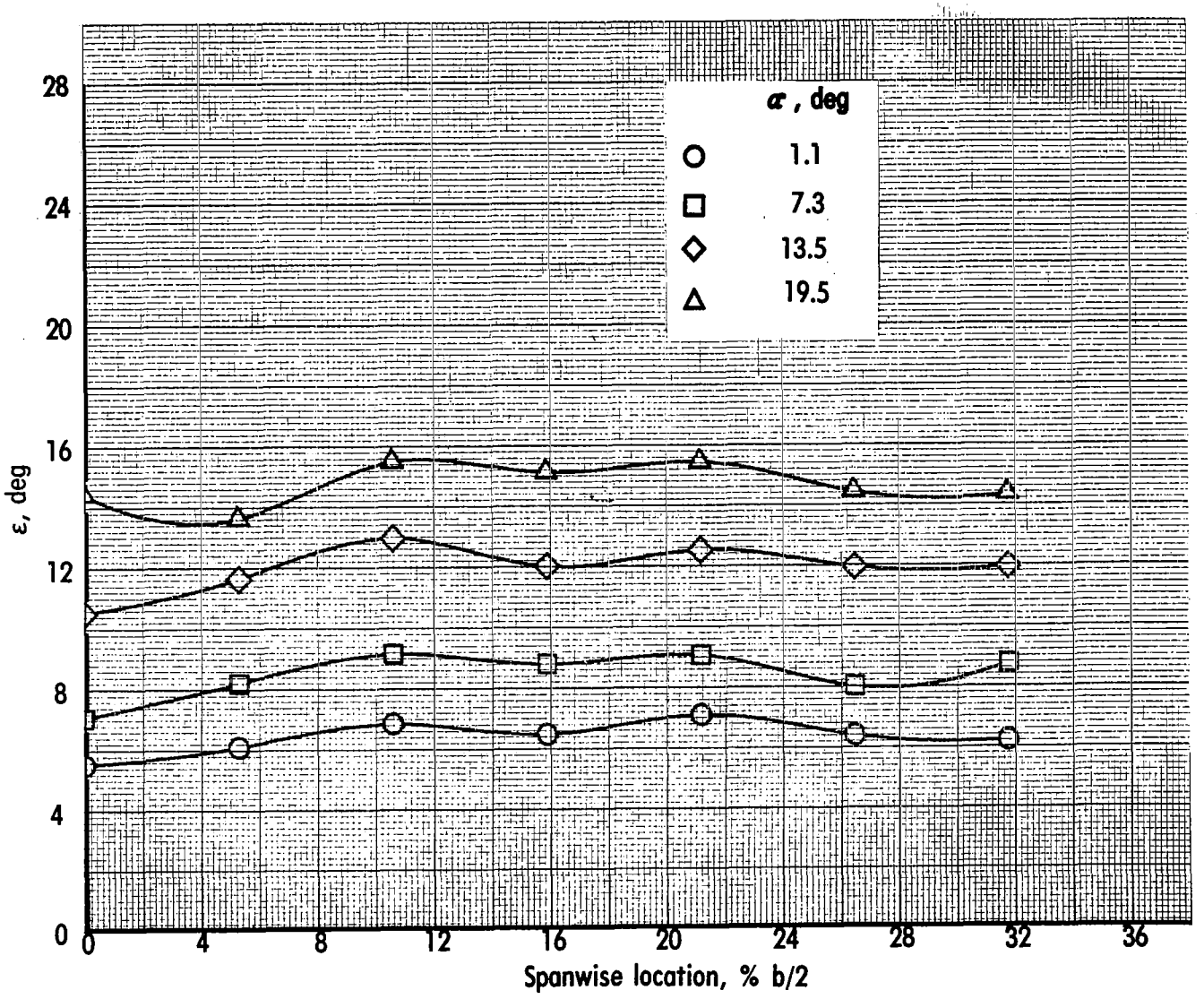

(d) C_μ = 3.25; inlets open.

Figure 65.- Continued.

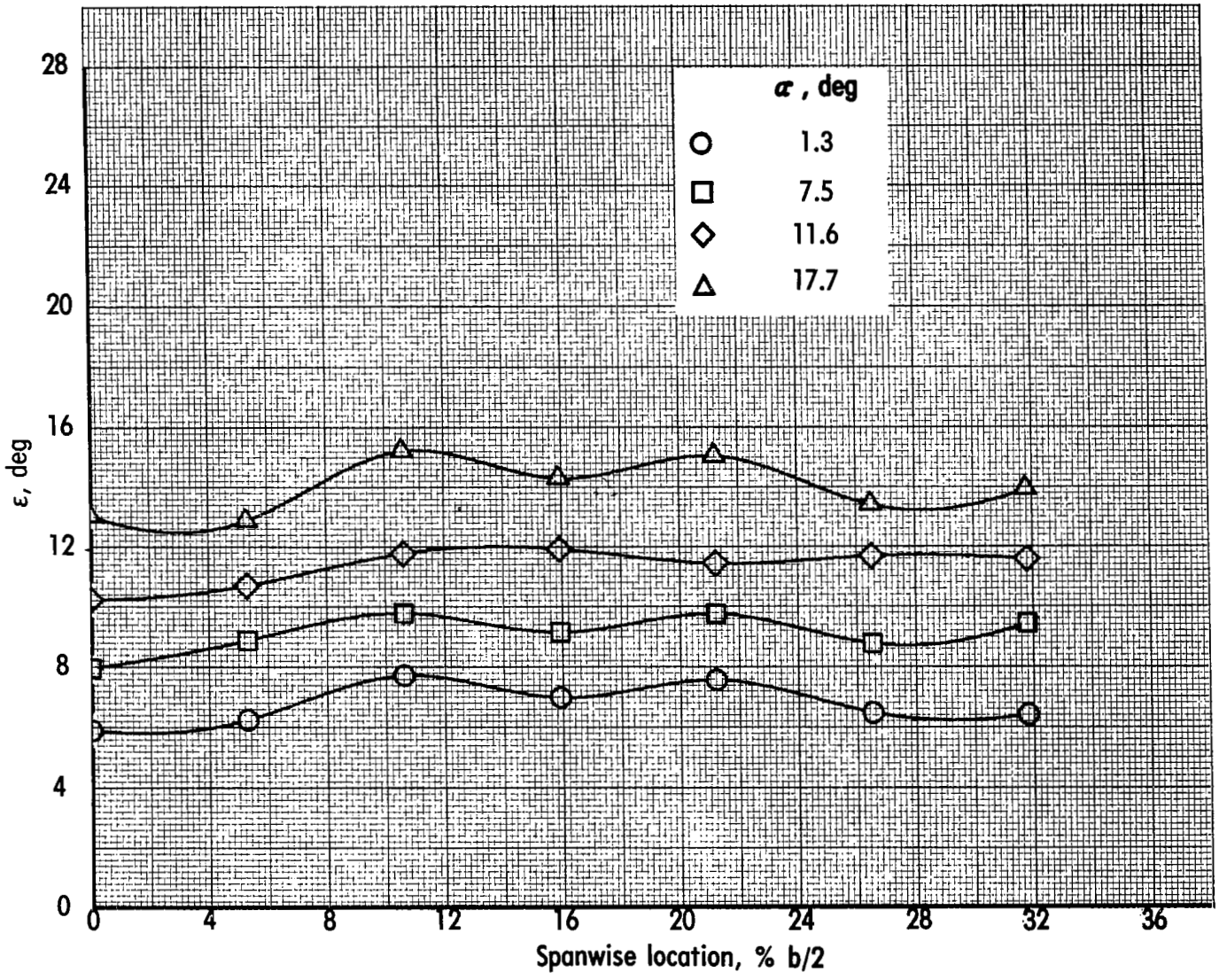

(e) C_μ = 4.30; inlets open.

Figure 65.- Concluded.

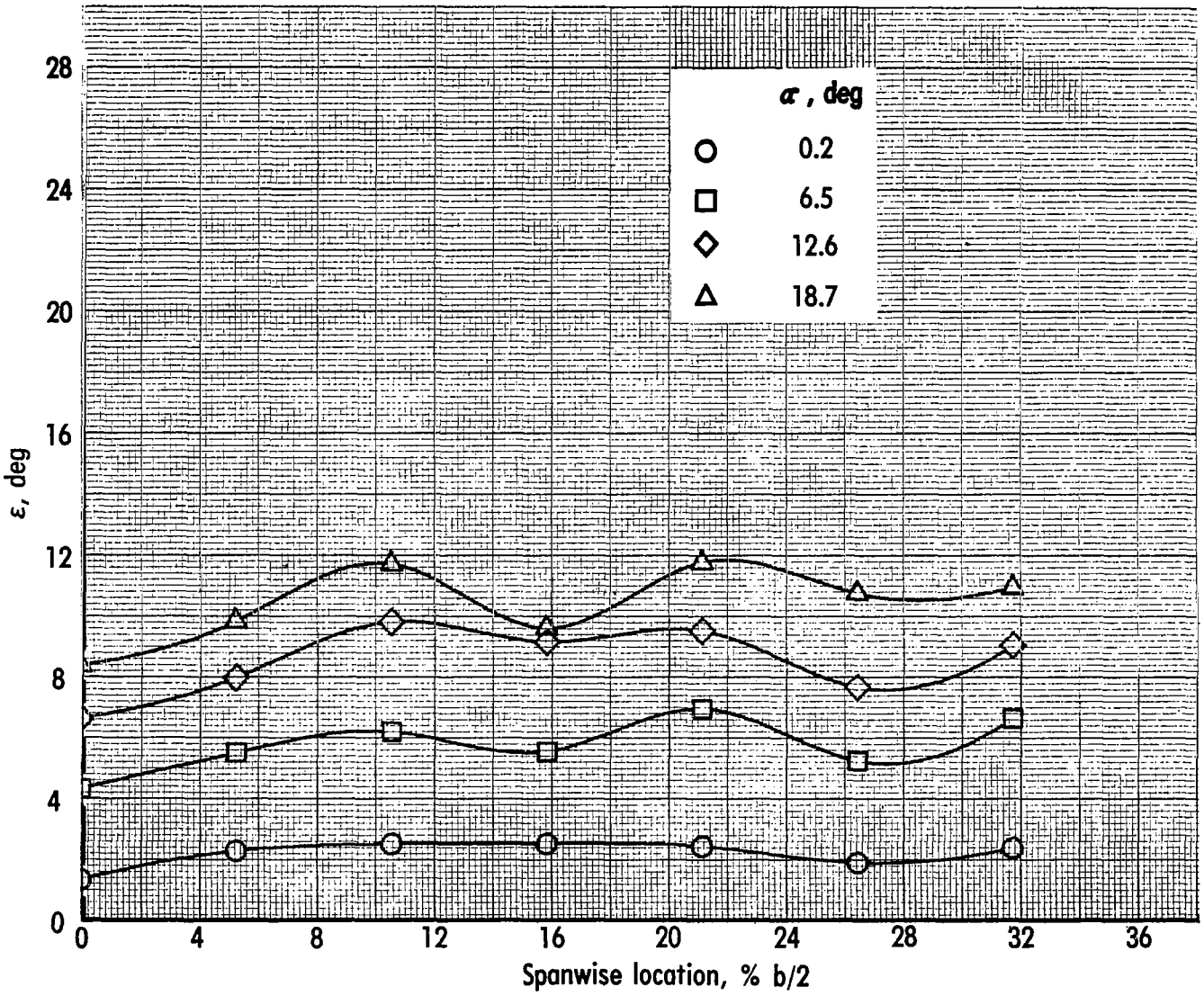

(a) $C_\mu = 0$; inlets closed.

Figure 66.- Effect of angle of attack on downwash angle at horizontal-tail location. Landing configuration; engine 110-45; vertical tail and horizontal tail off.

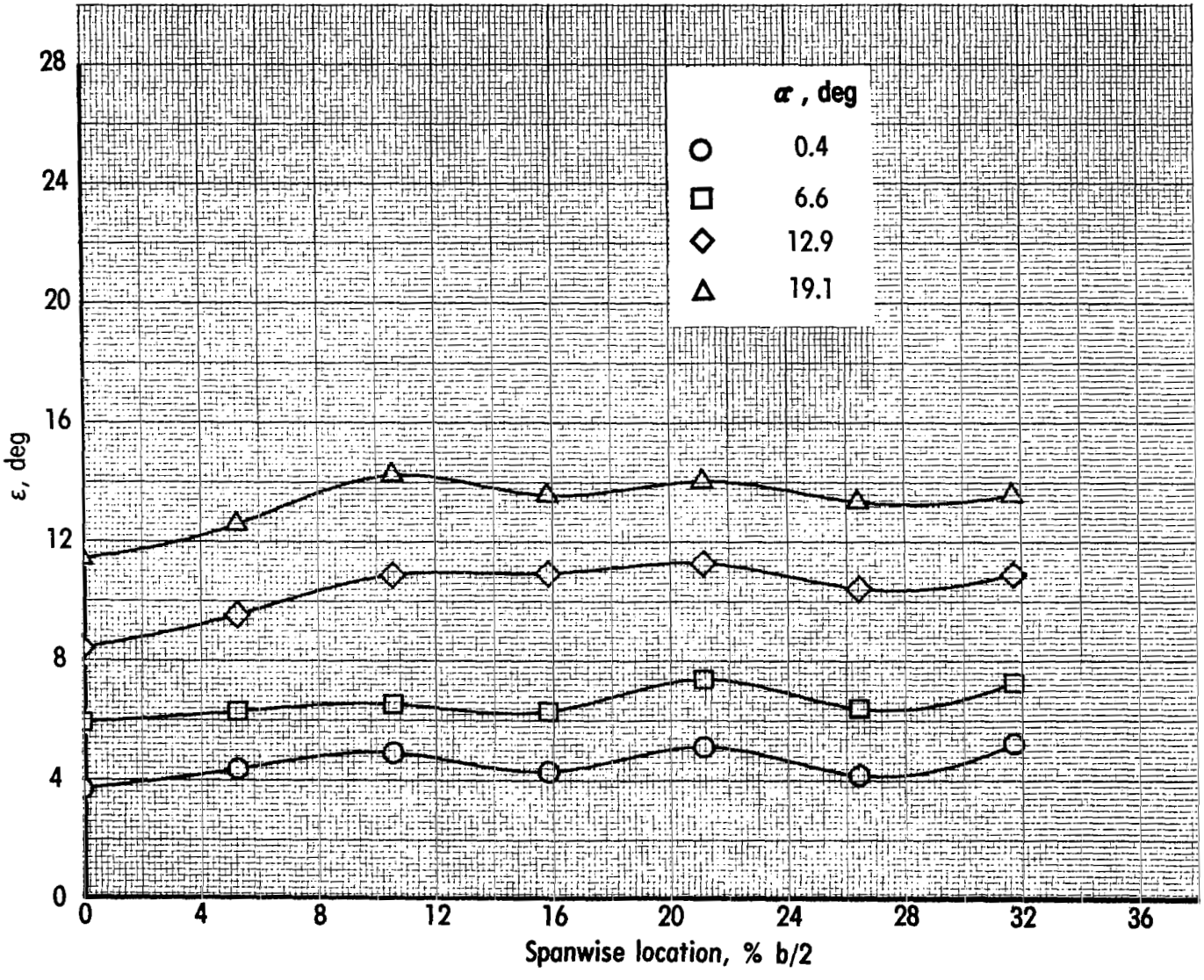

(b) C_μ = 0.99; inlets open.

Figure 66.- Continued.

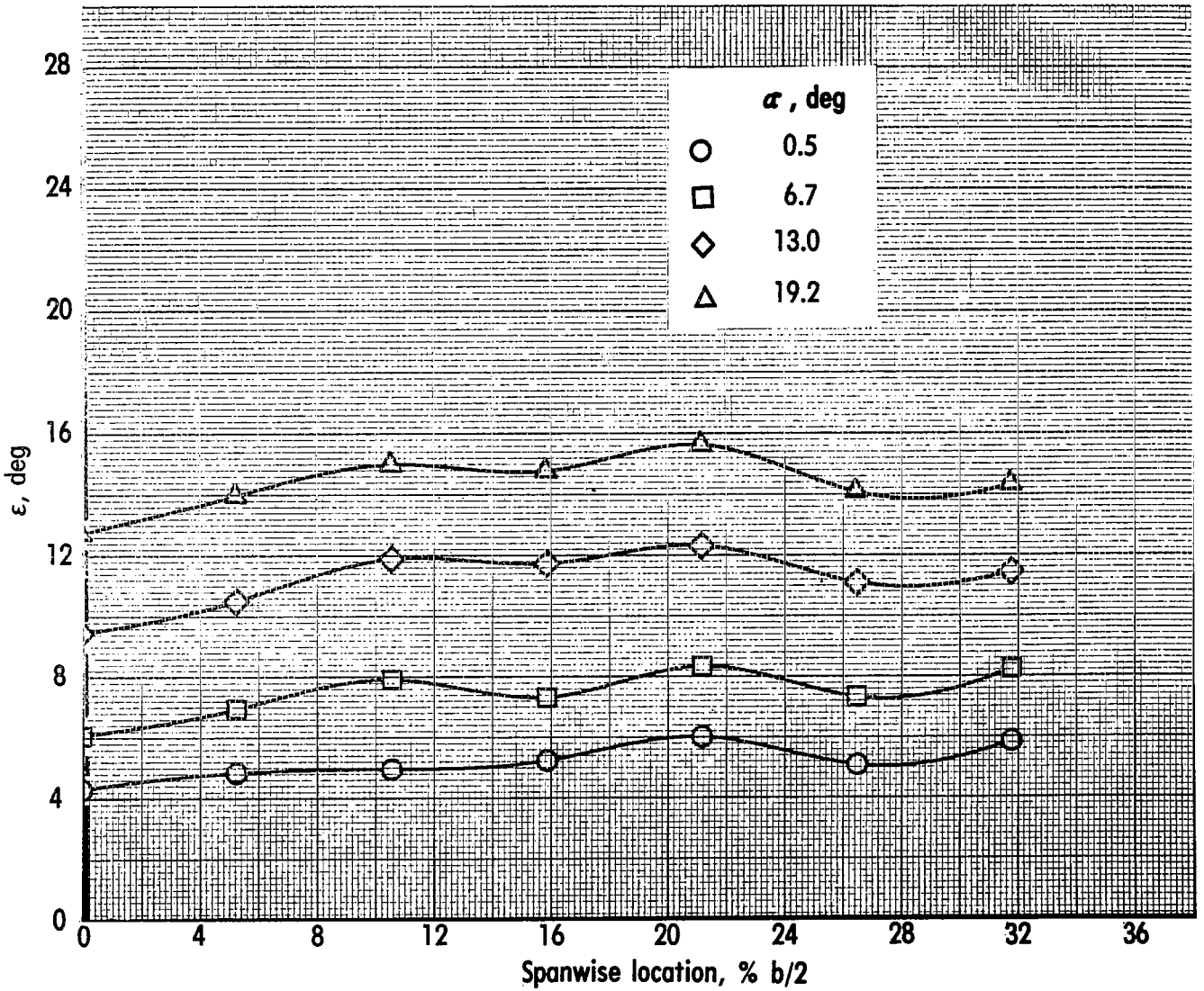

(c) C_μ = 2.01; inlets open.

Figure 66.- Continued.

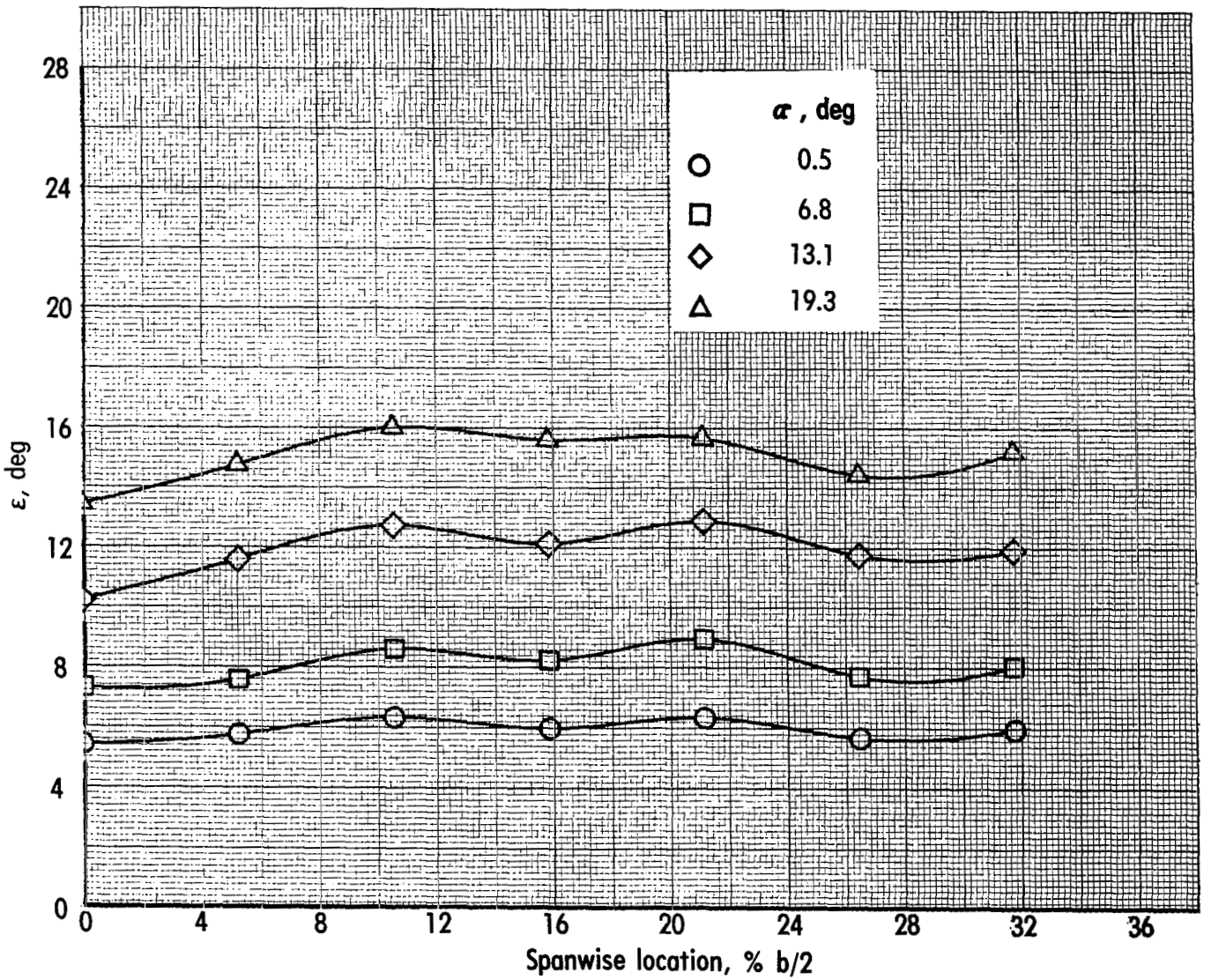

(d) C_μ = 3.03; inlets open.

Figure 66.- Continued.

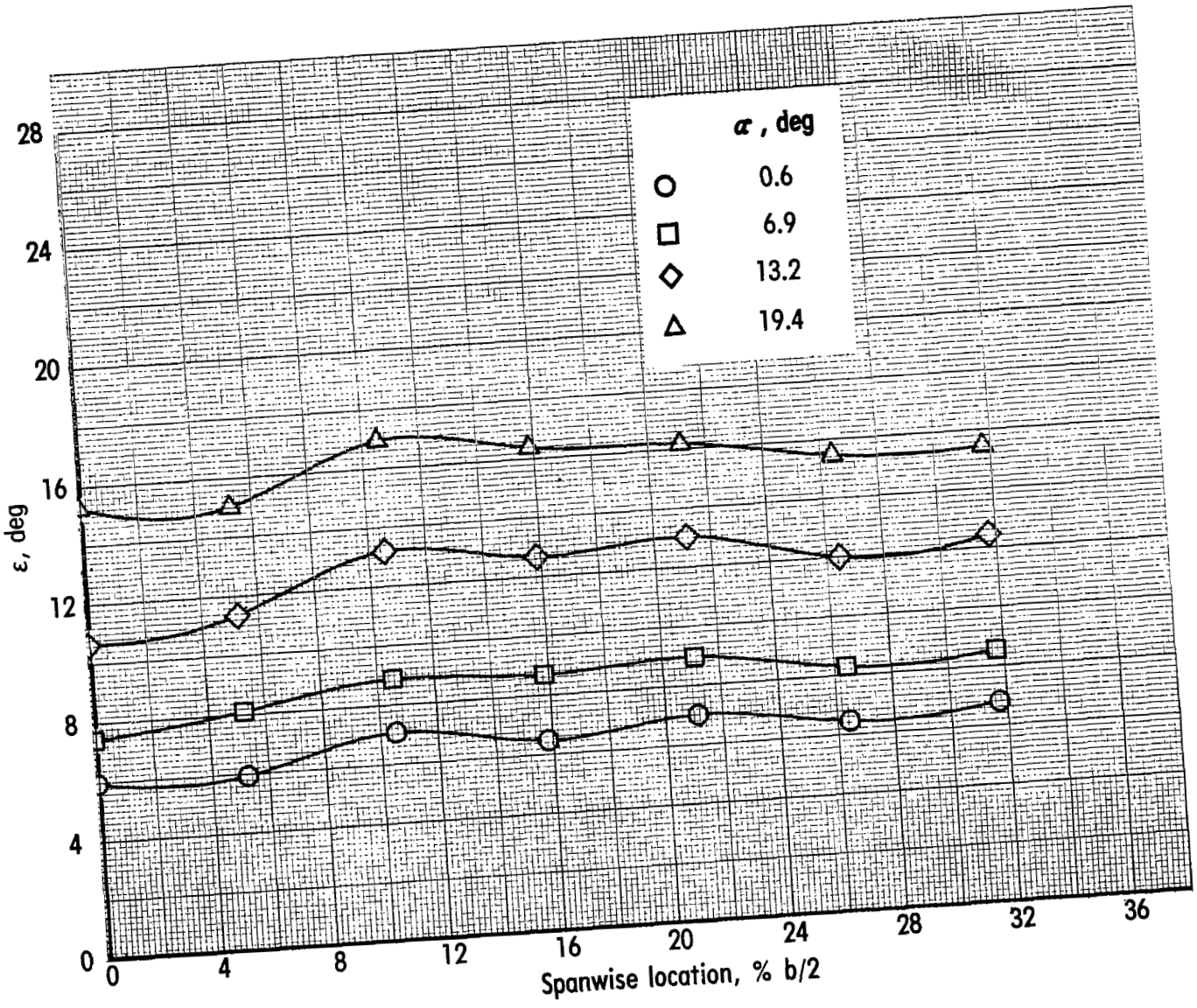

(e) C_μ = 4.03; inlets open.

Figure 66.- Concluded.

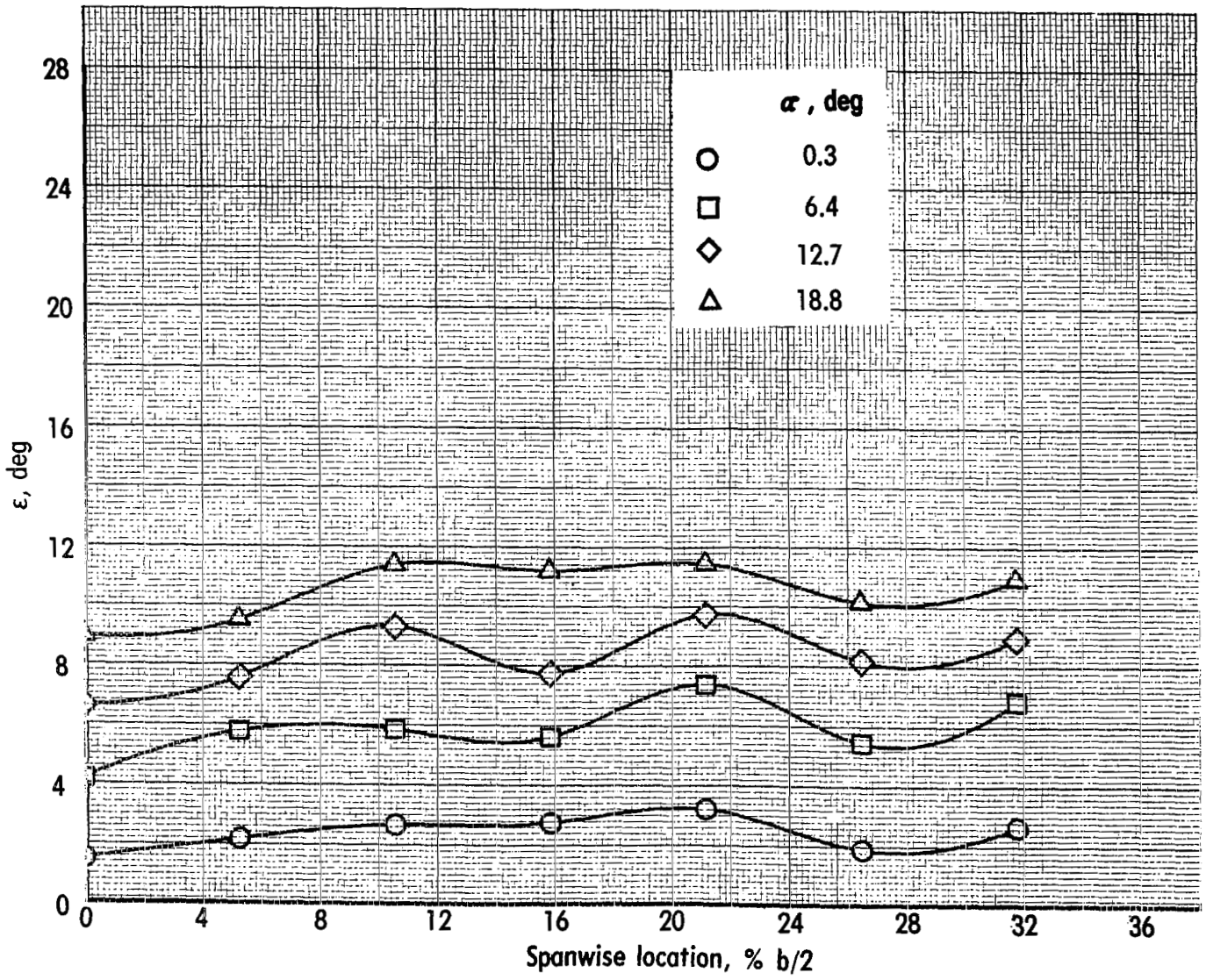

(a) $C_\mu = 0$; inlets closed.

Figure 67.- Effect of angle of attack on downwash angle at horizontal-tail location. Landing configuration; engine 110-65; vertical tail and horizontal tail off.

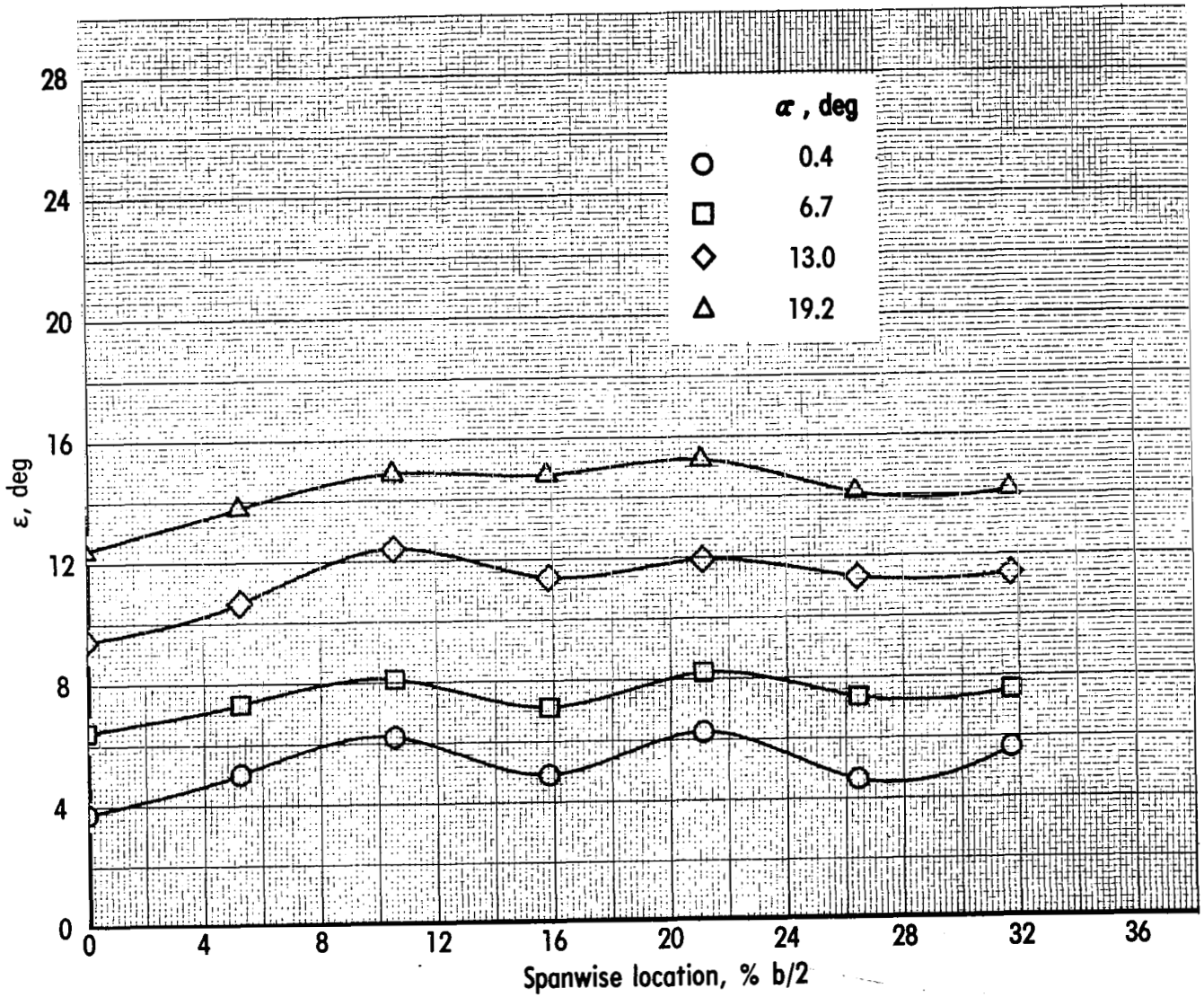

(b) C_μ = 1.01; inlets open.

Figure 67.- Continued.

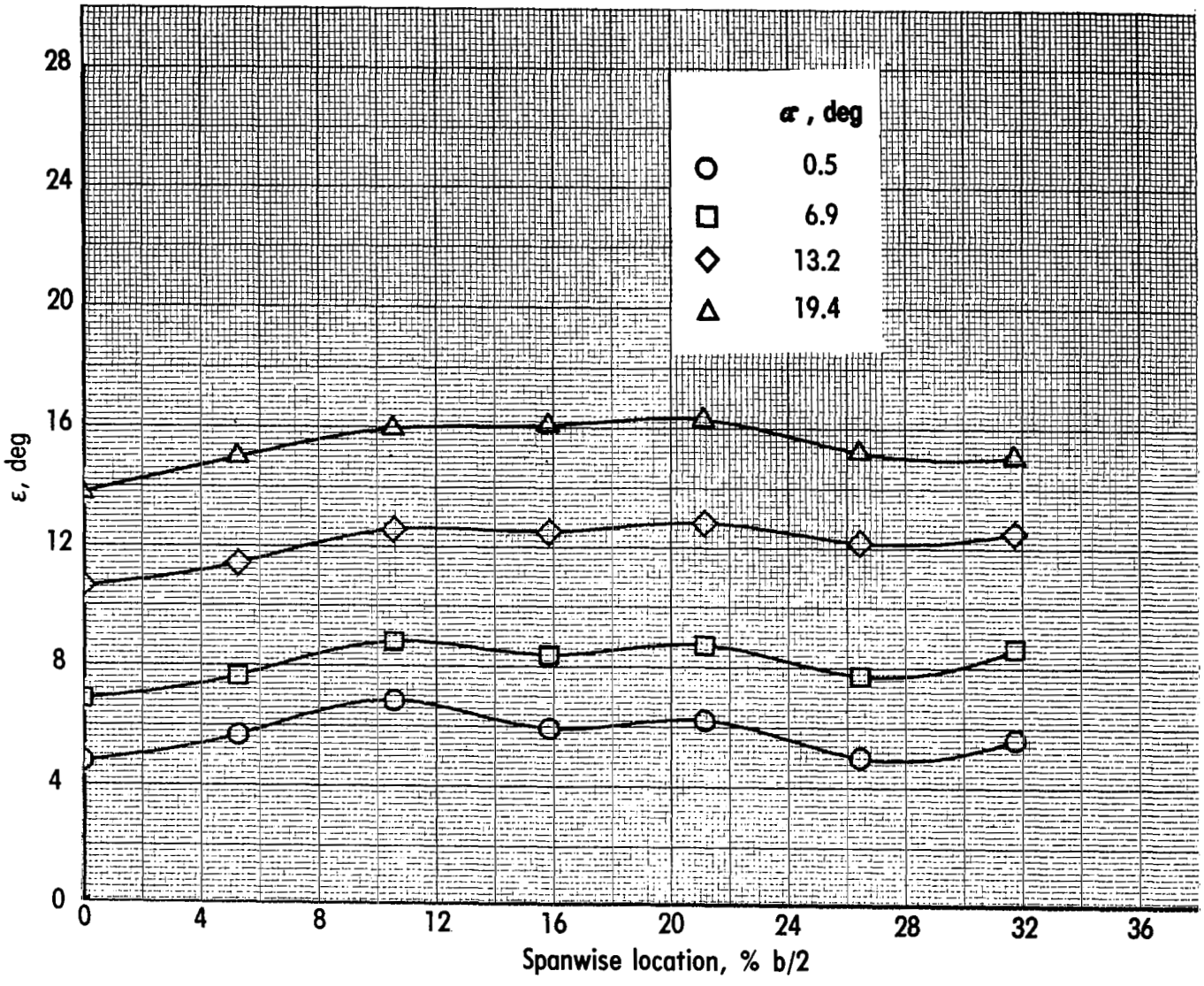

(c) C_μ = 2.05; inlets open.

Figure 67.- Continued.

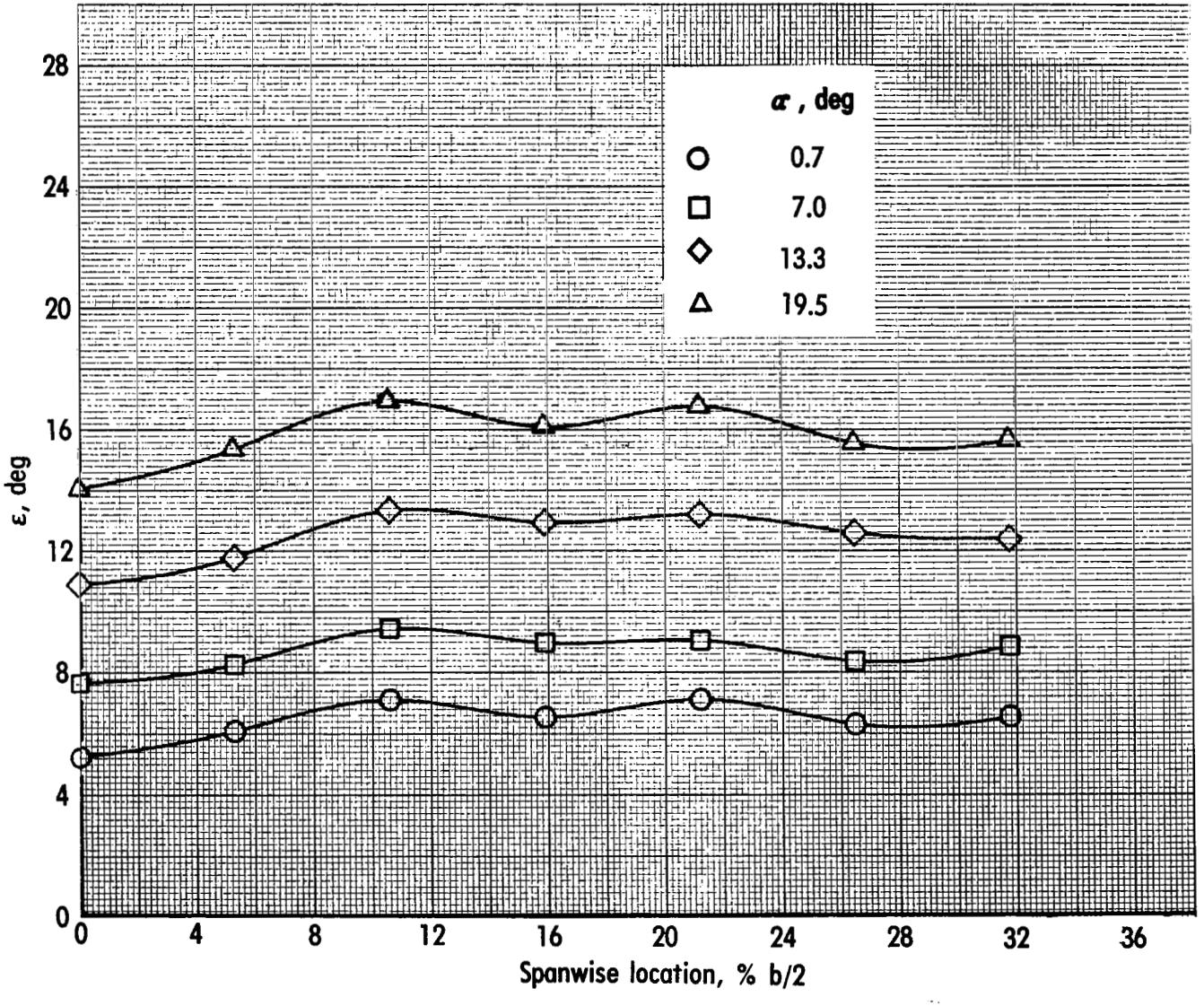

(d) C_μ = 3.05; inlets open.

Figure 67.- Continued.

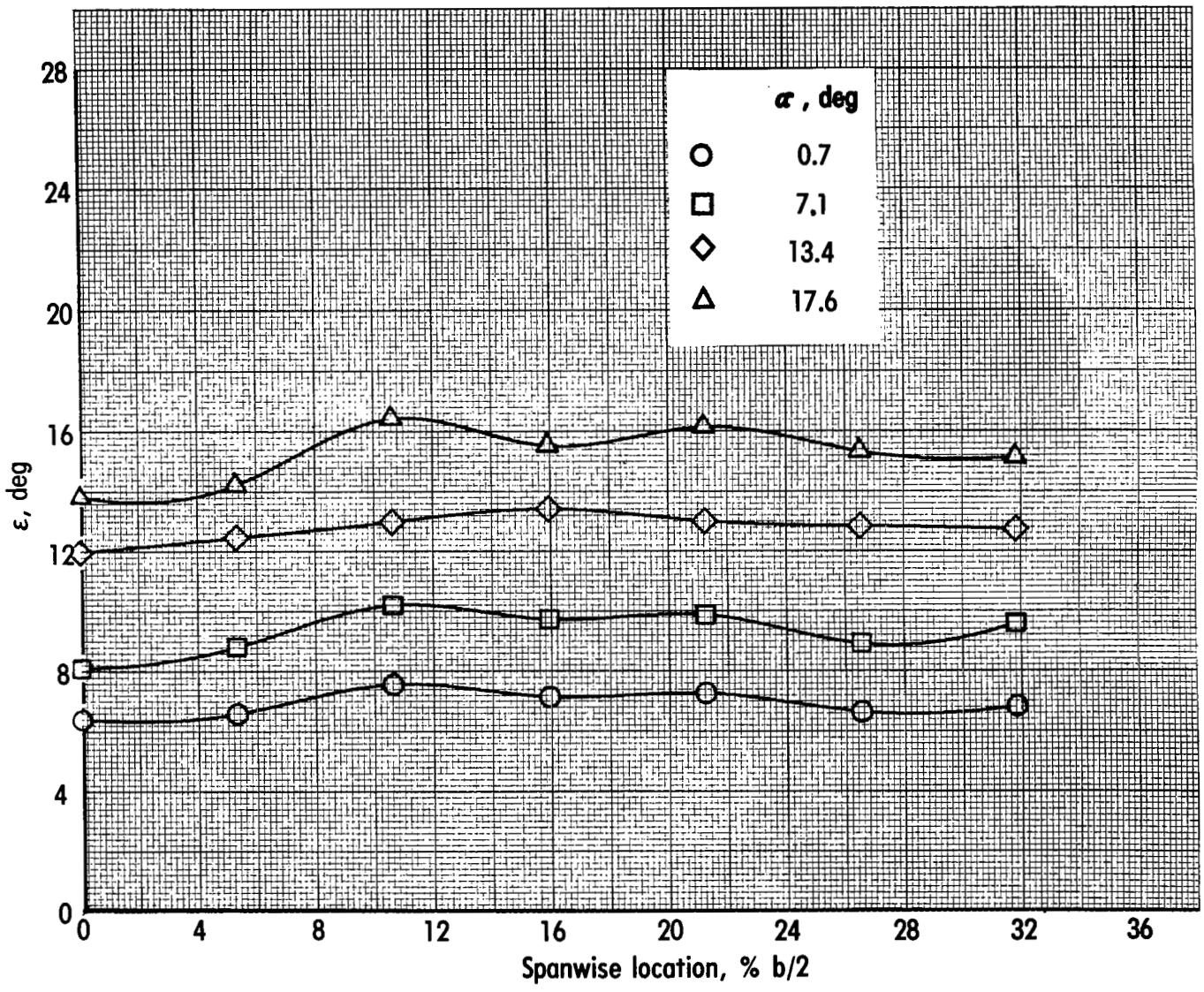

(e) C_μ = 4.08; inlets open.

Figure 67.- Concluded.

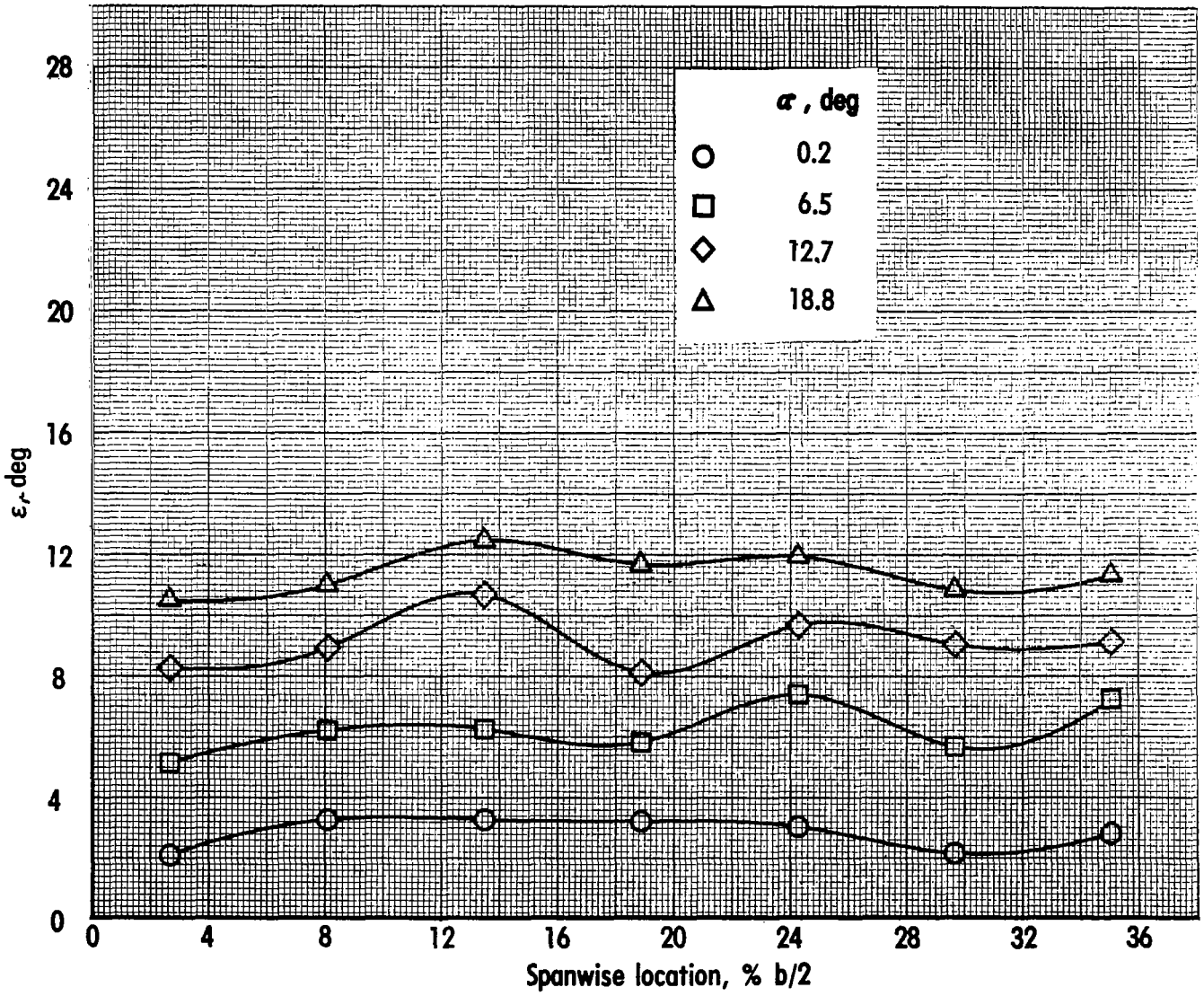

(a) $C_\mu = 0$; inlets closed.

Figure 68.- Effect of angle of attack on downwash angle at horizontal-tail location. Landing configuration; engine 110-65; vertical tail on; horizontal tail off.

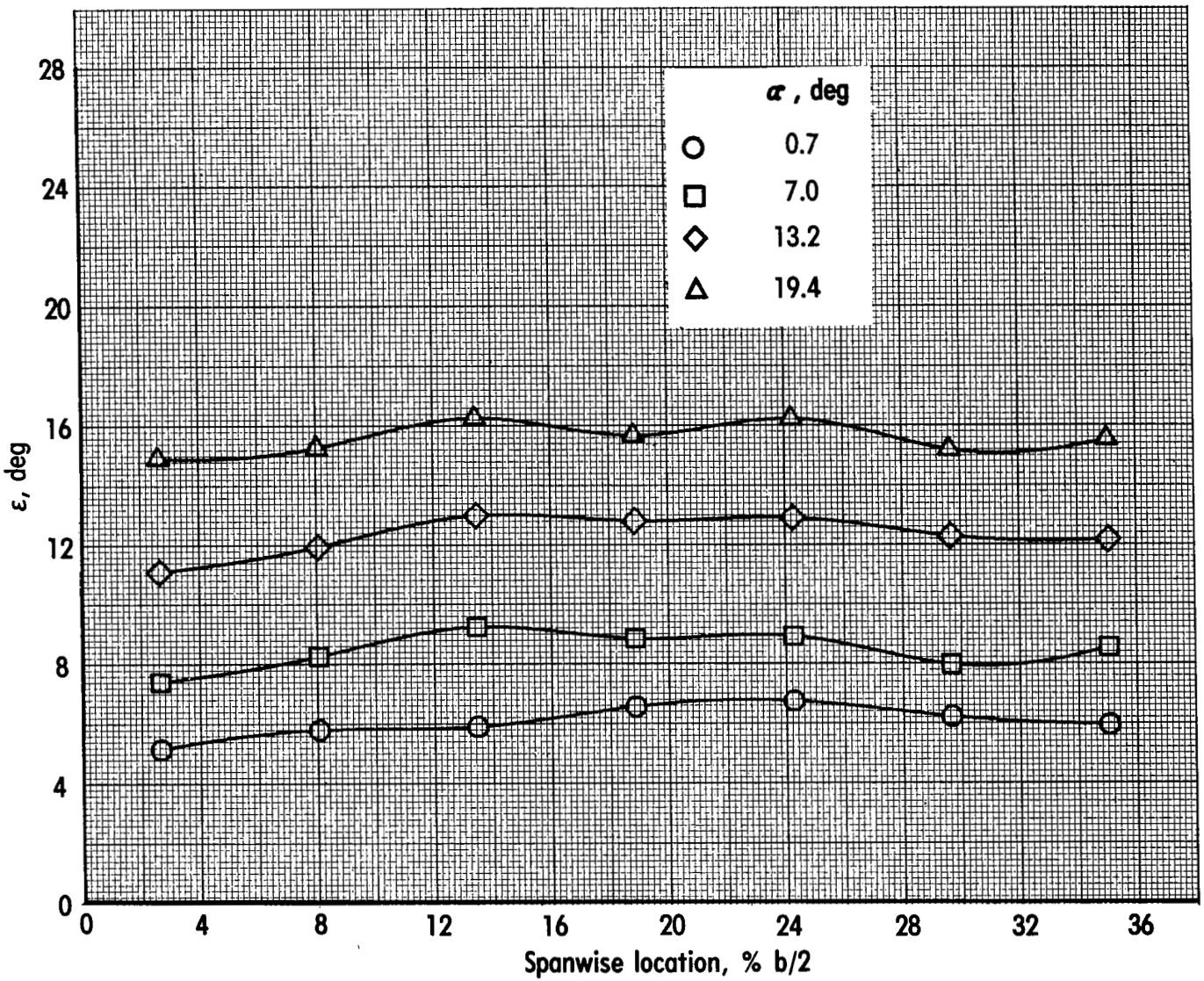

(b) C_μ = 2.04; inlets open.

Figure 68.- Continued.

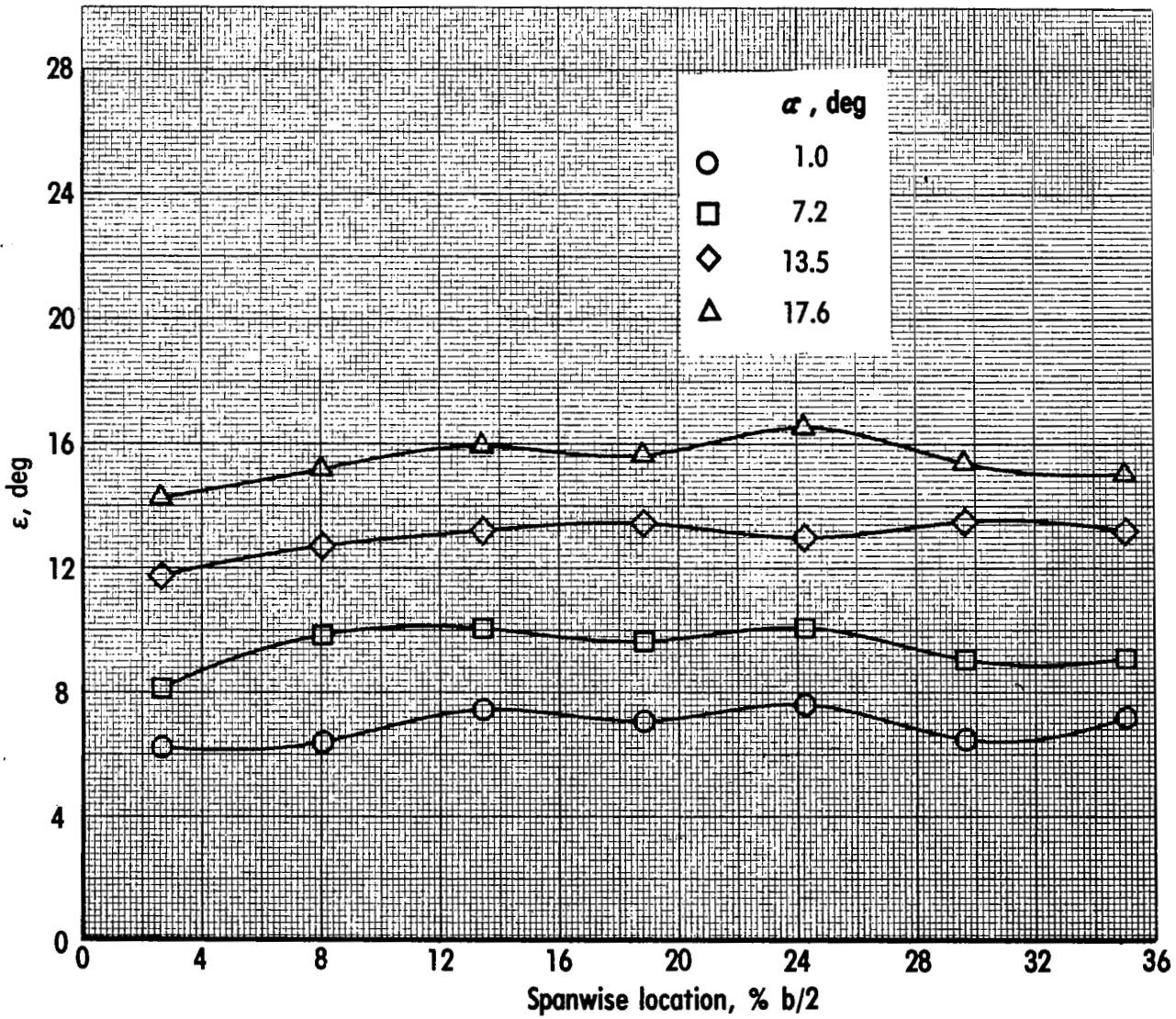

(c) C_μ = 4.08; inlets open.

Figure 68.- Concluded.

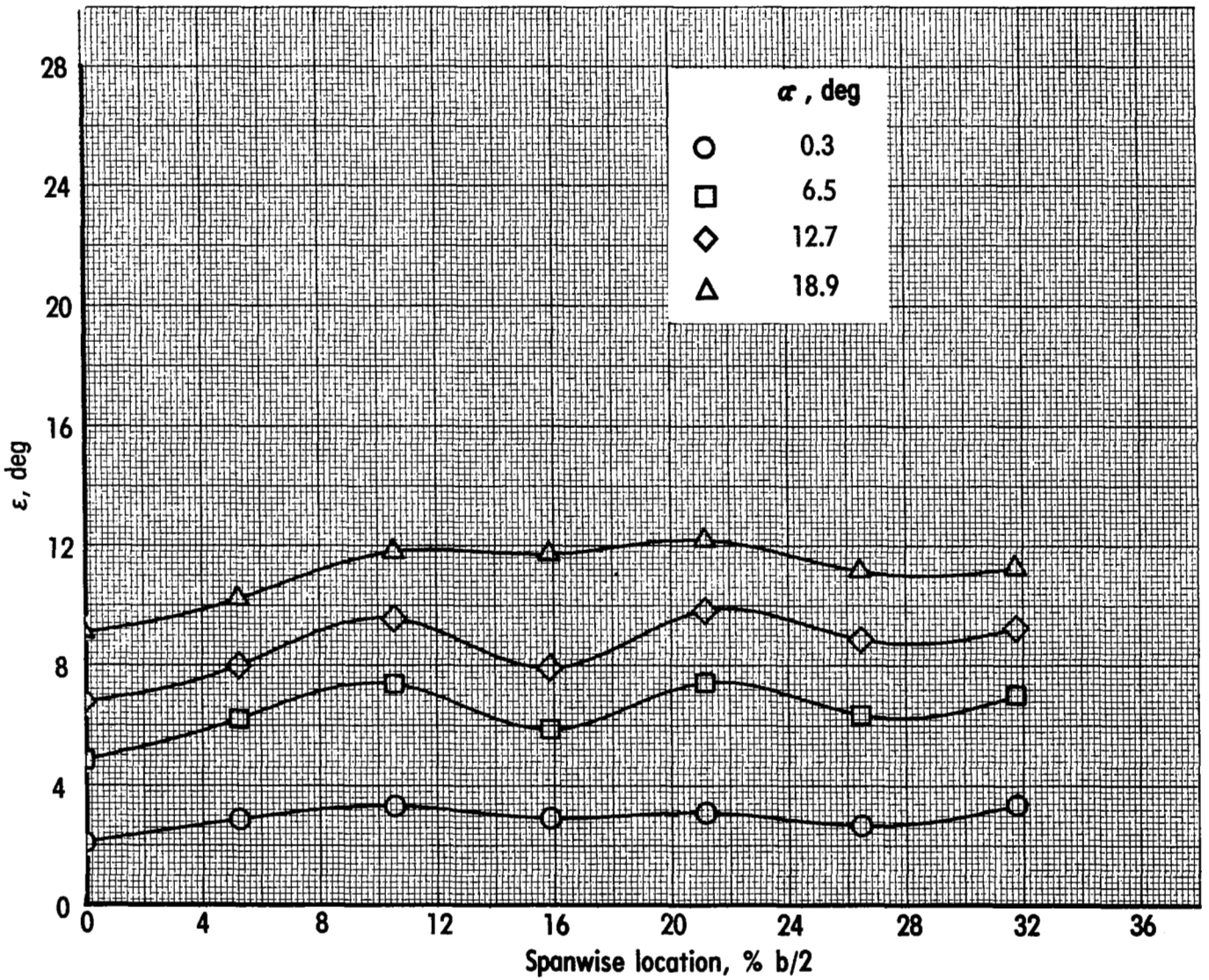

(a) $C_\mu = 0$; inlets closed.

Figure 69.- Effect of angle of attack on downwash angle at horizontal-tail location. Landing configuration; engine 110-90; vertical tail and horizontal tail off.

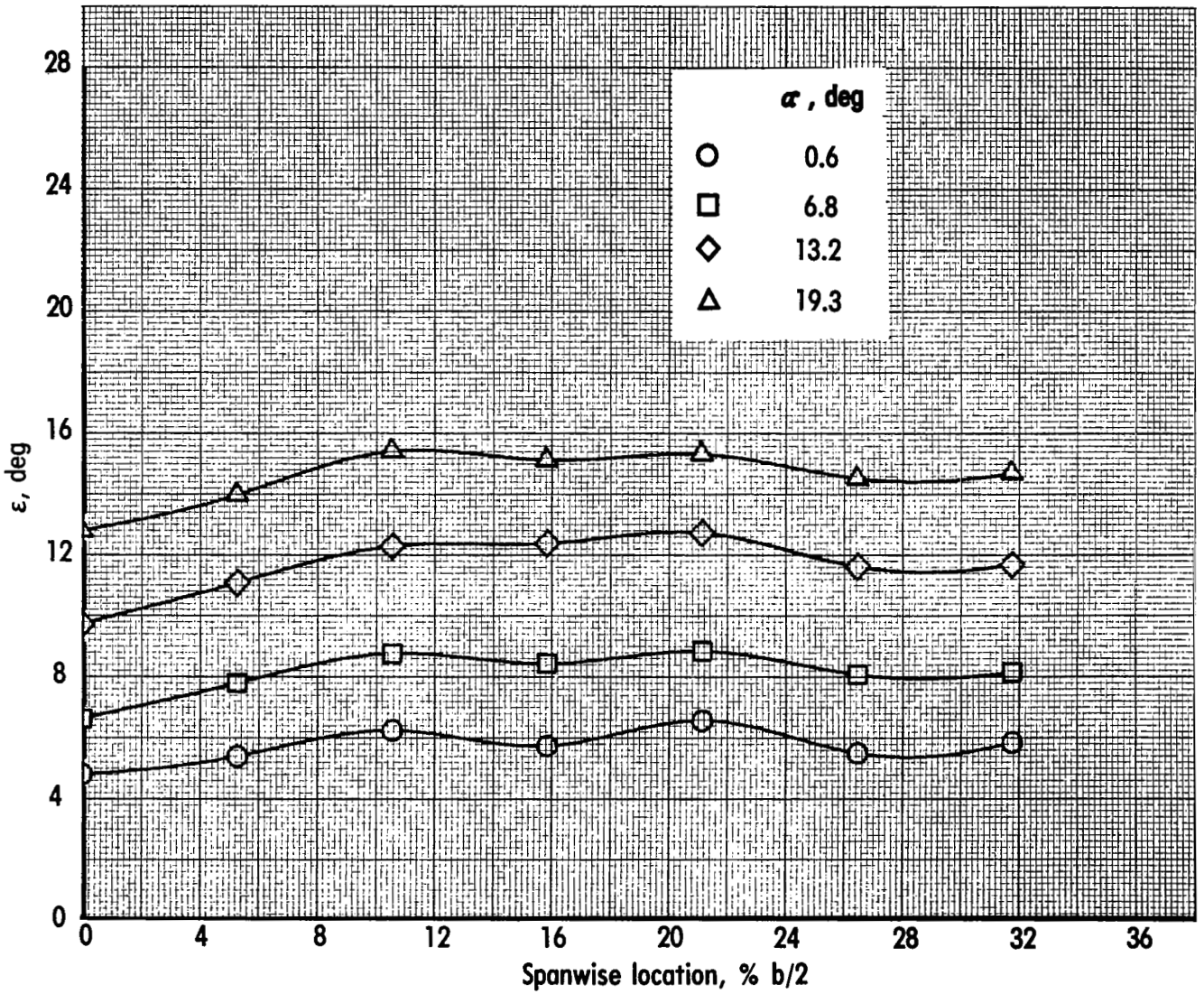

(b) C_μ = 1.01; inlets open.

Figure 69.- Continued.

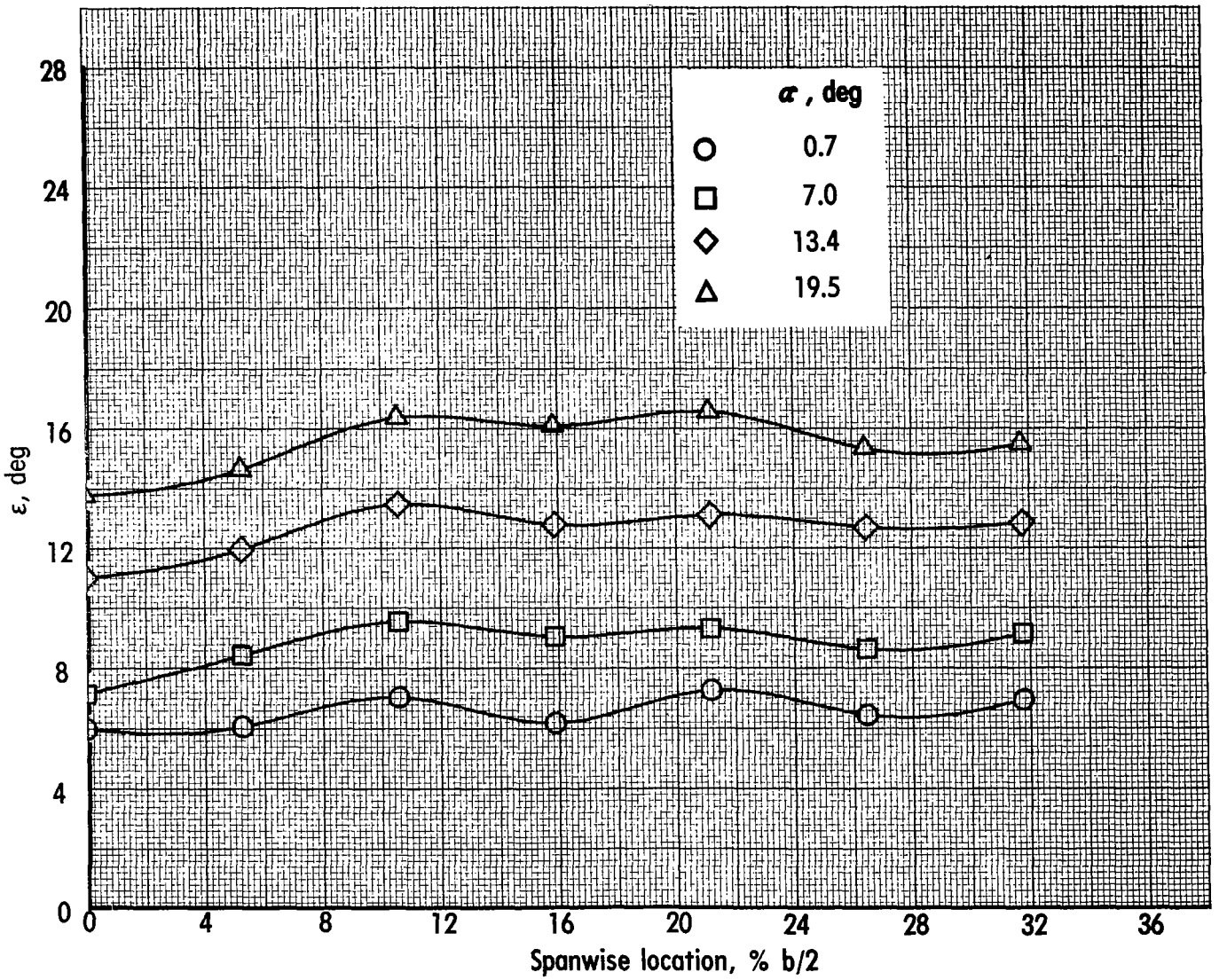

(c) C_μ = 2.02; inlets open.

Figure 69.- Continued.

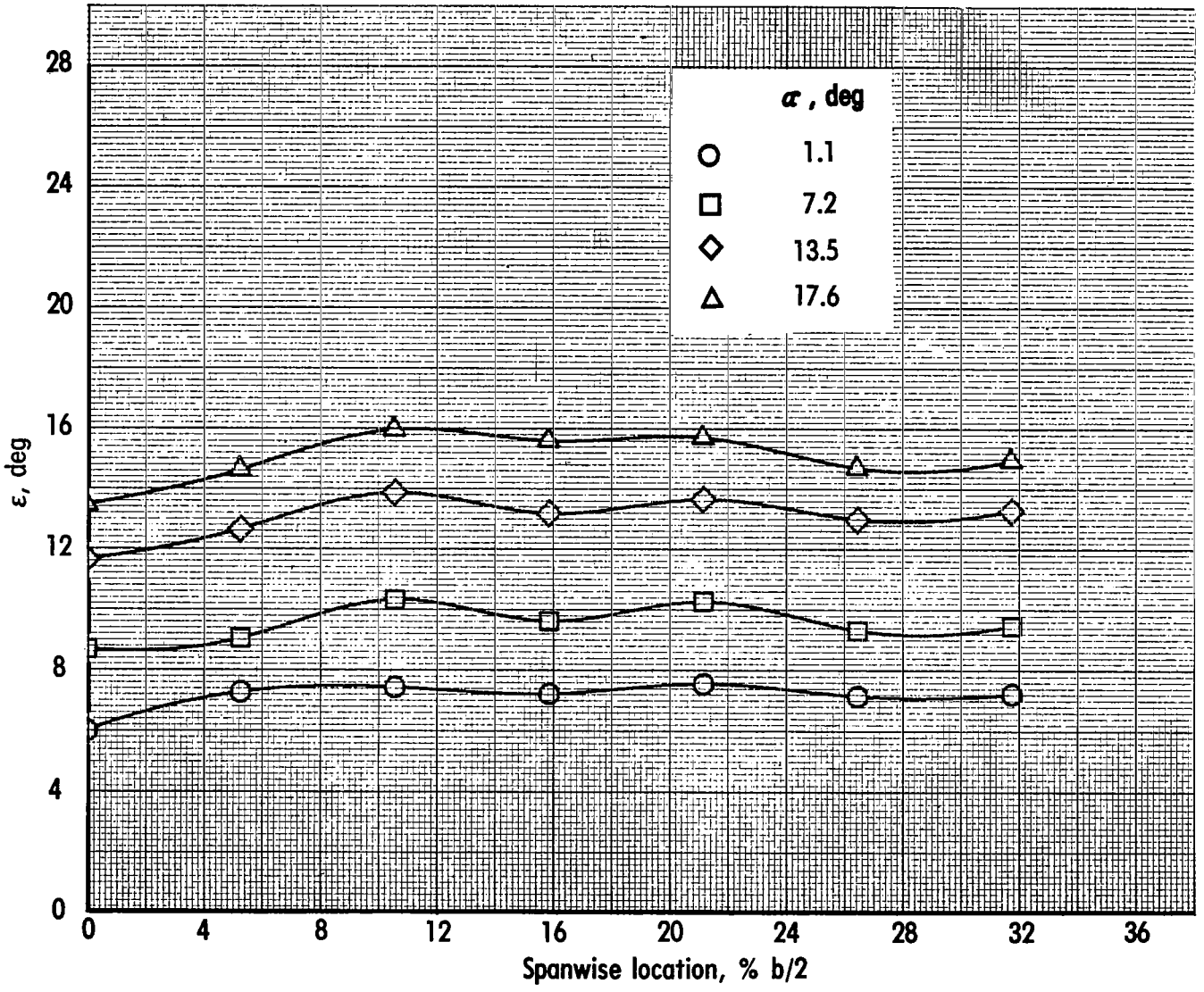

(d) C_μ = 3.05; inlets open.

Figure 69.- Continued.

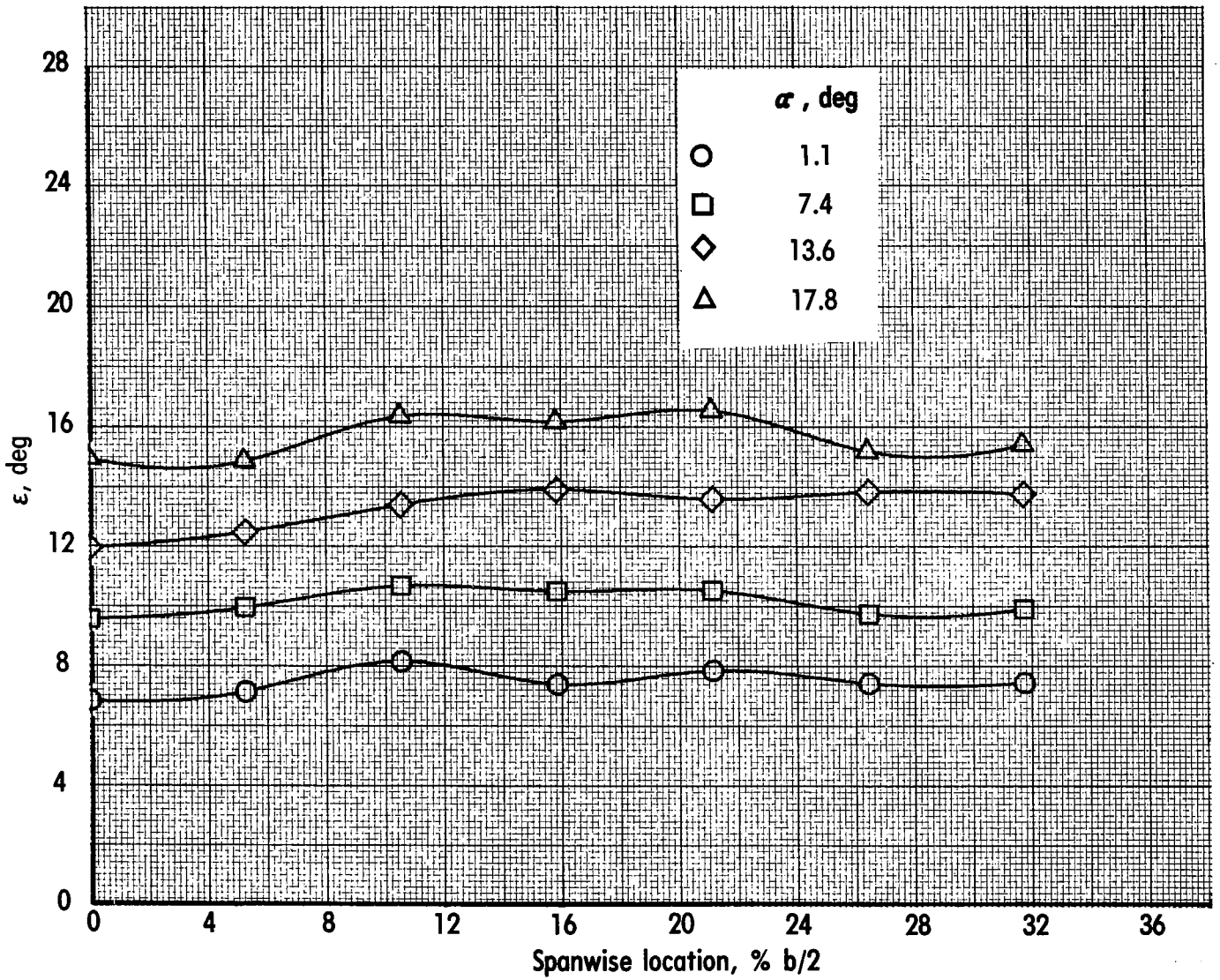

(e) C_μ = 4.10; inlets open.

Figure 69.- Concluded.

*U.S. GOVERNMENT PRINTING OFFICE: 1975 - 635-275/42

945 001 C1 U A 750926 S00903DS
DEPT OF THE AIR FORCE
AF WEAPONS LABORATORY
ATTN: TECHNICAL LIBRARY (SUL)
KIRTLAND AFB NM 87117

"The aeronautical and space activities of the United States shall be conducted so as to contribute . . . to the expansion of human knowledge of phenomena in the atmosphere and space. The Administration shall provide for the widest practicable and appropriate dissemination of information concerning its activities and the results thereof."

—NATIONAL AERONAUTICS AND SPACE ACT OF 1958

NASA SCIENTIFIC AND TECHNICAL PUBLICATIONS

TECHNICAL REPORTS: Scientific and technical information considered important, complete, and a lasting contribution to existing knowledge.

TECHNICAL NOTES: Information less broad in scope but nevertheless of importance as a contribution to existing knowledge.

TECHNICAL MEMORANDUMS: Information receiving limited distribution because of preliminary data, security classification, or other reasons. Also includes conference proceedings with either limited or unlimited distribution.

CONTRACTOR REPORTS: Scientific and technical information generated under a NASA contract or grant and considered an important contribution to existing knowledge.

TECHNICAL TRANSLATIONS: Information published in a foreign language considered to merit NASA distribution in English.

SPECIAL PUBLICATIONS: Information derived from or of value to NASA activities. Publications include final reports of major projects, monographs, data compilations, handbooks, sourcebooks, and special bibliographies.

TECHNOLOGY UTILIZATION PUBLICATIONS: Information on technology used by NASA that may be of particular interest in commercial and other non-aerospace applications. Publications include Tech Briefs, Technology Utilization Reports and Technology Surveys.

Details on the availability of these publications may be obtained from:

SCIENTIFIC AND TECHNICAL INFORMATION OFFICE

NATIONAL AERONAUTICS AND SPACE ADMINISTRATION

Washington, D.C. 20546